NOVEL INSIGHTS INTO OBESITY-RELATED DISEASES

EDITED BY: Sanyuan Hu, Yanmin Wang, Richard Young, Tongzhi Wu and Xiang Zhang

PUBLISHED IN: Frontiers in Physiology

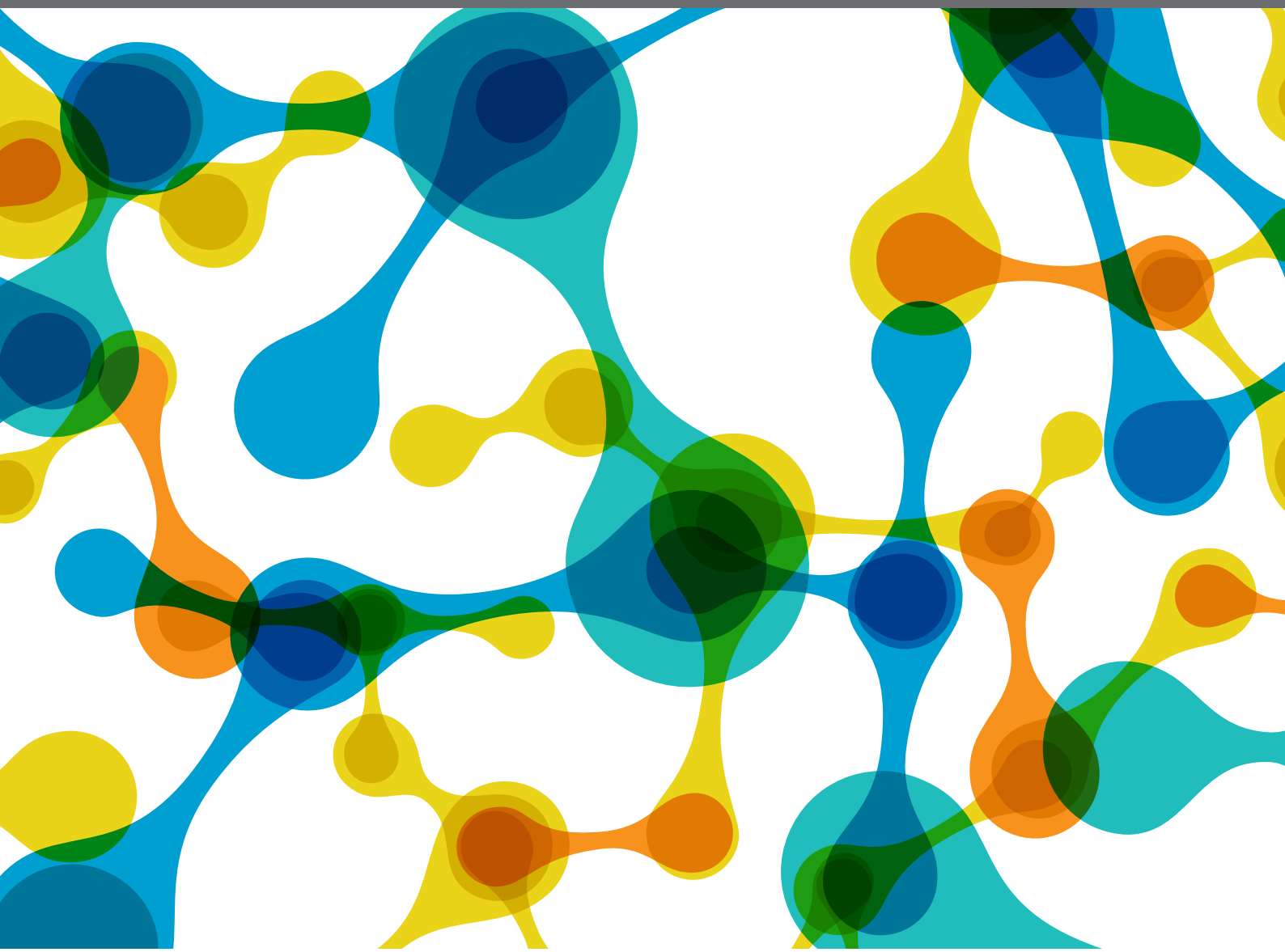

frontiers Research Topics

frontiers

ISSN 1664-8714
ISBN 978-2-88976-602-4
DOI 10.3389/978-2-88976-602-4

About Frontiers

Frontiers is more than just an open-access publisher of scholarly articles: it is a pioneering approach to the world of academia, radically improving the way scholarly research is managed. The grand vision of Frontiers is a world where all people have an equal opportunity to seek, share and generate knowledge. Frontiers provides immediate and permanent online open access to all its publications, but this alone is not enough to realize our grand goals.

Frontiers Journal Series

The Frontiers Journal Series is a multi-tier and interdisciplinary set of open-access, online journals, promising a paradigm shift from the current review, selection and dissemination processes in academic publishing. All Frontiers journals are driven by researchers for researchers; therefore, they constitute a service to the scholarly community. At the same time, the Frontiers Journal Series operates on a revolutionary invention, the tiered publishing system, initially addressing specific communities of scholars, and gradually climbing up to broader public understanding, thus serving the interests of the lay society, too.

Dedication to Quality

Each Frontiers article is a landmark of the highest quality, thanks to genuinely collaborative interactions between authors and review editors, who include some of the world's best academicians. Research must be certified by peers before entering a stream of knowledge that may eventually reach the public - and shape society; therefore, Frontiers only applies the most rigorous and unbiased reviews.
Frontiers revolutionizes research publishing by freely delivering the most outstanding research, evaluated with no bias from both the academic and social point of view. By applying the most advanced information technologies, Frontiers is catapulting scholarly publishing into a new generation.

What are Frontiers Research Topics?

Frontiers Research Topics are very popular trademarks of the Frontiers Journals Series: they are collections of at least ten articles, all centered on a particular subject. With their unique mix of varied contributions from Original Research to Review Articles, Frontiers Research Topics unify the most influential researchers, the latest key findings and historical advances in a hot research area! Find out more on how to host your own Frontiers Research Topic or contribute to one as an author by contacting the Frontiers Editorial Office: frontiersin.org/about/contact

NOVEL INSIGHTS INTO OBESITY-RELATED DISEASES

Topic Editors:
Sanyuan Hu, Shandong University, China
Yanmin Wang, California Medical Innovations Institute, United States
Richard Young, University of Adelaide, Australia
Tongzhi Wu, University of Adelaide, Australia
Xiang Zhang, Shandong University, China

Citation: Hu, S., Wang, Y., Young, R., Wu, T., Zhang, X., eds. (2022). Novel Insights into Obesity-Related Diseases. Lausanne: Frontiers Media SA.
doi: 10.3389/978-2-88976-602-4

Table of Contents

05 ***Editorial: Novel Insights Into Obesity-Related Diseases***
Xiang Zhang, anmin Wang and Sanyuan Hu

08 ***L-Leucine Improves Metabolic Disorders in Mice With* in-utero *Cigarette Smoke Exposure***
Yunxin Zeng, Taida Huang, Nan Wang, Yi Xu, Chunhui Sun, Min Huang, Chun Chen, Brian G. Oliver, Chenju Yi and Hui Chen

17 ***Lactate and Myocardiac Energy Metabolism***
Shuohui Dong, Linhui Qian, Zhiqiang Cheng, Chang Chen, Kexin Wang, Sanyuan Hu, Xiang Zhang and Tongzhi Wu

29 ***Corrigendum: Lactate and Myocardiac Energy Metabolism***
Shuohui Dong, Linhui Qian, Zhiqiang Cheng, Chang Chen, Kexin Wang, Sanyuan Hu, Xiang Zhang and Tongzhi Wu

30 ***Metabolic Changes of Hepatocytes in NAFLD***
Qianrang Lu, Xinyao Tian, Hao Wu, Jiacheng Huang, Mengxia Li, Zhibin Mei, Lin Zhou, Haiyang Xie and Shusen Zheng

40 ***Efficacy and Mechanisms of Gastric Volume-Restriction Bariatric Devices***
Yanmin Wang and Ghassan S. Kassab

48 ***Insulin Resistance Remission Following Laparoscopic Roux-en-Y Gastric Bypass and Laparoscopic Sleeve Gastrectomy in Chinese Type 2 Diabetes Mellitus Patients With a Body Mass Index of 27.5–32.5 kg/m²***
Ping Luo, Yaoquan Cao, Pengzhou Li, Guohui Wang, Zhi Song, Weizheng Li, Zhihong Su, Hui Zhou, Xianhao Yi, Zhibing Fu, Xulong Sun, Haibo Tang, Beibei Cui, Qianqian Yu, Liyong Zhu and Shaihong Zhu

55 ***Sleeve Gastrectomy Ameliorates Diabetes-Induced Cardiac Hypertrophy Correlates With the MAPK Signaling Pathway***
Qian Xu, Huanxin Ding, Songhan Li, Shuohui Dong, Linchuan Li, Bowen Shi, Mingwei Zhong and Guangyong Zhang

69 ***Electroacupuncture Combined With Diet Treatment Has a Therapeutic Effect on Perimenopausal Patients With Abdominal Obesity by Improving the Community Structure of Intestinal Flora***
Jili Sheng, Geyao Yang, Xiaoqing Jin, Caijuan Si, Yuan'an Huang, Zhouxiao Luo, Tao Liu and Jianfang Zhu

80 ***Corrigendum: Electroacupuncture Combined With Diet Treatment Has a Therapeutic Effect on Perimenopausal Patients With Abdominal Obesity by Improving the Community Structure of Intestinal Flora***
Jili Sheng, Geyao Yang, Xiaoqing Jin, Caijuan Si, Yuan'an Huang, Zhouxiao Luo, Tao Liu and Jianfang Zhu

81 ***Sleeve Gastrectomy-Induced AMPK Activation Attenuates Diabetic Cardiomyopathy by Maintaining Mitochondrial Homeostasis* via *NR4A1 Suppression in Rats***
Songhan Li, Shuohui Dong, Qian Xu, Bowen Shi, Linchuan Li, Wenjie Zhang, Jiankang Zhu, Yugang Cheng, Guangyong Zhang and Mingwei Zhong

95 ***Bile Acid Detection Techniques and Bile Acid-Related Diseases***
Xiang Zhao, Zitian Liu, Fuyun Sun, Lunjin Yao, Guangwei Yang and Kexin Wang

111 *The Gut Microbiota in Liver Transplantation Recipients During the Perioperative Period*
Zhiyong Lai, Zongkun Chen, Anhong Zhang, Zhiqiang Niu, Meng Cheng, Chenda Huo and Jun Xu

126 *Alteration of Ileal lncRNAs After Duodenal–Jejunal Bypass Is Associated With Regulation of Lipid and Amino Acid Metabolism*
Yongjun Liang, Minghua Yu, Yueqian Wang, Mengyi Li, Zhongtao Zhang, Zhengdong Qiao and Peng Zhang

frontiers | Frontiers in Physiology

EDITORIAL
published: 23 June 2022
doi: 10.3389/fphys.2022.952682

Editorial: Novel Insights Into Obesity-Related Diseases

Xiang Zhang[1]*, *Yanmin Wang*[2] and *Sanyuan Hu*[3,4]*

[1]Department of General Surgery, Qilu Hospital of Shandong University, Jinan, China, [2]California Medical Innovations Institute, San Diego, CA, United States, [3]First Affiliated Hospital of Shandong First Medical University, Jinan, China, [4]Shandong University, Jinan, China

Keywords: obesity, diabetes, cardiomyopathy, bariatric surgery, bile acids

Editorial on the Research Topic

Novel Insights Into Obesity-Related Diseases

Obesity is a chronic disease with an excessive amount of or ectopically distributed body fat, which leads to unfavorable cosmetic concern as well as increased risks of type 2 diabetes, cardiovascular diseases, nonalcoholic fatty liver disease (NAFLD) and so forth, which could be named as obesity-related diseases. Both obesity and the related diseases have reached epidemic proportions globally, being a major health, economic and social problem worldwide. It has been estimated that global obesity rates have almost tripled since 1975, and now over 671 million adult individuals are living with obesity (Collaborators et al., 2017; NCD Risk Factor Collaboration, 2017; The Lancet Diabetes and Endocrinology, 2021). Due to large population base, China has the largest number of obese worldwide, with approximately 46% of adults and 15% of children being affected (Wang et al., 2017). Therefore, a comprehensive understanding of the pathogenesis, along with the attempt to prevent or treat obesity and comorbidities is of great importance. In this Research Topic named "*Novel Insights into obesity-related diseases*", we aimed to gather the latest knowledge from basic research to clinical trials relating to pathogenesis and treatment of obesity and related disorders, in order to shed light on novel strategies for obesity management.

OPEN ACCESS

Edited and reviewed by:
John D. Imig,
Medical College of Wisconsin, Milwaukee, United States

***Correspondence:**
Xiang Zhang
xiang.zhang02@hotmail.com
Sanyuan Hu
husanyuan1962@hotmail.com

Specialty section:
This article was submitted to Integrative Physiology, a section of the journal Frontiers in Physiology

Received: *25 May 2022*
Accepted: *08 June 2022*
Published: *23 June 2022*

Citation:
Zhang X, Wang Y and Hu S (2022) Editorial: Novel Insights Into Obesity-Related Diseases. Front. Physiol. 13:952682. doi: 10.3389/fphys.2022.952682

BARIATRIC SURGERY

Currently, bariatric surgery still stands for the most effective interventions for long-term weight loss and alleviation of obesity-related diseases. Sleeve gastrectomy (SG) and Roux-en-Y gastric bypass (RYGB) are the most commonly performed bariatric surgeries worldwide, accounting for 45.9% and 39.6%, respectively (Angrisani et al., 2017; Pucci and Batterham, 2019). Bariatric surgery is usually recommended for people with a body mass index (BMI) > 35 kg/m^2 or 30–35 kg/m^2 with uncontrolled conditions (Zimmet et al., 2011). For Asian people with type 2 diabetes, the criterion should be reduced by 2.5 kg/m^2 (Dixon et al., 2011). In this Research Topic, the study by Luo et al. focused on Chinese diabetic patients with BMI of 27.5–32.5 kg/m^2, and reported a good insulin resistance remission at 6 months after laparoscopic SG and RYGB; Compared to SG, RYGB achieved a better diabetes remission (56.23% vs. 29.41%), which is consistent with the prevailing viewpoint that RYGB is more efficient in improving metabolic disorders (Padwal et al., 2011; Puzziferri et al., 2014) while SG has the advantage of low risk in the perioperative period and less long-term complications (Frezza et al., 2009; Dick et al., 2010). It seems to be the first report regarding diabetes control in Chinese patients undergoing SG and RYGB with relatively low BMI. Although bariatric surgery has been listed in a variety of obesity management guidelines, some people are not willing to undertake the surgery. In the US, only 1–2% of the eligible candidates undergo bariatric surgery for obesity each year (Gasoyan et al., 2019). Therefore, some gastric restrictive bariatric devices have been proposed (Vargas et al., 2018) as less invasive

alternatives. Wang et al. gave the first detailed review on this topic by introducing efficacy and mechanisms of gastric band, gastric sleeve implant, intragastric balloons and so forth. This review also pointed out that the purely "restrictive" devices may take effect beyond just mechanical restriction, which may be taken into consideration for future device design.

Despite sustained clinical therapeutic effects of bariatric surgery, the underlying mechanisms have not been fully elucidated. Diabetic cardiomyopathy, defined as a distinct disease entity that occurs in diabetic patients independent of primary cardiovascular disease (Jia et al., 2018), can be partially attenuated by SG (Leung et al., 2016). Two studies from the First Affiliated Hospital of Shandong First Medical University in China focused on the mechanisms underlying and found that both AMPK and MAPK signaling pathways were involved in the diabetic cardiomyopathy amelioration after SG based on a rodent model. These findings provide possible approaches to combat diabetic cardiomyopathy in patients. Bile acids are thought to be important mediators for metabolic benefits after bariatric surgery, as they were universally increased in the serum postoperatively (except purely restrictive procedures) (Wang et al., 2019). In the field of bile acid research, the technique for bile acid subtype detection is a necessity as different bile acid subtypes have distinct effects on metabolism. Zhao et al. reviewed most of the popular techniques for bile acid subtype detection, which helped researchers choose the most suitable technique based on research models, diseases as well as economic development and geographical factors. Apart from bile acids, long noncoding RNAs (lncRNAs) are also involved in metabolic improvements following bariatric surgery. Liang et al. previously reported duodenal and jejunal lncRNA alterations after duodenal-jejunal bypass (DJB) (Liang et al., 2017; Liang et al., 2018). In this Research Topic, Liang et al. have extended their work to the ileum, and found that dysregulated ileal lncRNAs were associated with lipid and amino acid metabolism and might contribute to postoperative energy homeostasis reestablishment. Instead of focusing on one single mechanism, the series of studies by Liang et al. used transcriptome analysis, which is a fundamental and powerful tool, to understand the microscopic functional alteration of certain organs after bariatric surgery. This methodology highlights the importance of omics technologies and represents future research direction in the modern era.

NOVEL THERAPIES

Compared to surgery, less invasive interventions are more acceptable. Electroacupuncture is a combination of traditional Chinese acupuncture and modern electrical treatment. The study by Sheng et al. reported that electroacupuncture plus diet control improved the community structure of intestinal flora and generated a therapeutic effect for perimenopausal females with abdominal obesity. The results were interesting and were promising for potential self-treatment at home in the future. Maternal cigarette smoke exposure is a severe issue and may cause preterm birth, low birth weight, and catch-up growth in childhood (Collaco et al., 2017). The study by Zeng et al. provided a potential strategy for reducing metabolic disorders in offspring by adding L-leucine supplement based on rodent models. This represents a novel discovery and worth further clinical verification.

PATHOPHYSIOLOGY OF OBESITY RELATED DISORDERS

Obesity also causes alterations in cardiac metabolism, which make ATP production less efficient, producing cardiac dysfunction (Alpert et al., 2018; Elagizi et al., 2018; Nakamura and Sadoshima, 2020). Adaptations to obesity-related metabolic disturbances induce changes in cardiac energy substrate preference. Recent studies have suggested lactate may represent an important fuel for the myocardium during exercise or myocadiac stress (Murashige et al., 2020; Cluntun et al., 2021). Dong et al. summarized the role of lactate in cardiac metabolism and its relevance to the progression and management of heart diseases, including acute myocardial ischemia and heart failure, and in diabetic state. The new perspective has prompted the research for understanding the role of lactate in cardiac metabolism under both normal physiological and pathological conditions. The effect of NAFLD on the whole system has been well reviewed before. The review by Lu et al., for the first time, concentrated on the metabolic changes within the hepatocytes and gave a detailed description of the pathogenesis and outcomes of the disease. As the ultimate cure for NAFLD, liver transplantation is widely performed. The study by Lai et al. reported an altered microbial composition in liver transplantation patients by using 16S rRNA sequencing of fecal samples. This study emphasized the importance of "gut-liver" axis in maintaining metabolic integrity and suggested that manipulation of gut microbiota may help postoperative recovery.

Obesity and related diseases have been an important health problem in the world. Fortunately, researchers never give up and keep exploring in this field. In this Research Topic, most of the studies concentrate on bariatric surgery including SG, RYGB, DJB, and device implant, aiming to investigate the mechanisms underlying and potential therapeutic targets. Electroacupuncture and L-leucine supplementation, have been reported as new therapies in perimenopausal patients with abdominal obesity and maternal cigarette smoke exposure induced metabolic disorder, respectively. Pathophysiology in heart diseases, NAFLD, and after liver transplantation were also investigated; Lactate and intestinal microbial composition are potential targets for manipulation. In summary, articles in this Research Topic have broadened our horizons and added novel insights into obesity-related diseases.

AUTHOR CONTRIBUTIONS

All authors listed have made a substantial, direct and intellectual contribution to the work, and approved it for publication.

FUNDING

This work was supported by National Natural Science Foundation of China (Project ID: 81700708/H0712, 82070869/H0712). The funders had no roles in the design of the study and collection, analysis, and interpretation of data or in writing the manuscript.

REFERENCES

Alpert, M. A., Karthikeyan, K., Abdullah, O., and Ghadban, R. (2018). Obesity and Cardiac Remodeling in Adults: Mechanisms and Clinical Implications. *Prog. Cardiovasc. Dis.* 61 (2), 114–123. Epub 20180707PubMed PMID: 29990533. doi:10.1016/j.pcad.2018.07.012

Angrisani, L., Santonicola, A., Iovino, P., Vitiello, A., Zundel, N., Buchwald, H., et al. (2017). Bariatric Surgery and Endoluminal Procedures: IFSO Worldwide Survey 2014. *Obes. Surg.* 27 (9), 2279–2289. PubMed PMID: 28405878; PubMed Central PMCID: PMCPMC5562777. doi:10.1007/s11695-017-2666-x

Cluntun, A. A., Badolia, R., Lettlova, S., Parnell, K. M., Shankar, T. S., Diakos, N. A., et al. (2021). The Pyruvate-Lactate axis Modulates Cardiac Hypertrophy and Heart Failure. *Cell. Metab.* 33 (3), 629–648. e10. Epub 20201216PubMed PMID: 33333007; PubMed Central PMCID: PMCPMC7933116. doi:10.1016/j.cmet.2020.12.003

Collaborators, G. B. D. O., Afshin, A., Forouzanfar, M. H., Reitsma, M. B., Sur, P., Estep, K., et al. (2017). Health Effects of Overweight and Obesity in 195 Countries over 25 Years. *N. Engl. J. Med.* 377 (1), 13–27. Epub 20170612PubMed PMID: 28604169; PubMed Central PMCID: PMCPMC5477817. doi:10.1056/NEJMoa1614362

Collaco, J. M., Wilson, K. M., and McGrath-Morrow, S. A. (2017). More Evidence Linking Smoke-free Legislation and Lower Risk of Prematurity and Low Birth Weight. *Pediatrics* 139 (6). Epub 20170517PubMed PMID: 28562293. doi:10.1542/peds.2017-0795

Dick, A., Byrne, T. K., Baker, M., Budak, A., and Morgan, K. (2010). Gastrointestinal Bleeding after Gastric Bypass Surgery: Nuisance or Catastrophe? *Surg. Obes. Relat. Dis.* 6 (6), 643–647. Epub 20100916PubMed PMID: 21111381. doi:10.1016/j.soard.2010.07.016

Dixon, J. B., Zimmet, P., Alberti, K. G., and Rubino, F.International Diabetes Federation Taskforce on E, Prevention (2011). Bariatric Surgery: an IDF Statement for Obese Type 2 Diabetes. *Surg. Obes. Relat. Dis.* 7 (4), 433–447. Epub 20110601PubMed PMID: 21782137. doi:10.1016/j.soard.2011.05.013

Elagizi, A., Kachur, S., Lavie, C. J., Carbone, S., Pandey, A., Ortega, F. B., et al. (2018). An Overview and Update on Obesity and the Obesity Paradox in Cardiovascular Diseases. *Prog. Cardiovasc. Dis.* 61 (2), 142–150. Epub 20180705PubMed PMID: 29981771. doi:10.1016/j.pcad.2018.07.003

Frezza, E. E., Reddy, S., Gee, L. L., and Wachtel, M. S. (2009). Complications after Sleeve Gastrectomy for Morbid Obesity. *Obes. Surg.* 19 (6), 684–687. Epub 20081016PubMed PMID: 18923879. doi:10.1007/s11695-008-9677-6

Gasoyan, H., Halpern, M. T., Tajeu, G., and Sarwer, D. B. (2019). Impact of Insurance Plan Design on Bariatric Surgery Utilization. *Surg. Obes. Relat. Dis.* 15 (10), 1812–1818. Epub 20190805PubMed PMID: 31515131; PubMed Central PMCID: PMCPMC6834903. doi:10.1016/j.soard.2019.07.022

Jia, G., Hill, M. A., and Sowers, J. R. (2018). Diabetic Cardiomyopathy. *Circ. Res.* 122 (4), 624–638. PubMed PMID: 29449364; PubMed Central PMCID: PMCPMC5819359. doi:10.1161/CIRCRESAHA.117.311586

Leung, M., Xie, M., Durmush, E., Leung, D. Y., and Wong, V. W. (2016). Weight Loss with Sleeve Gastrectomy in Obese Type 2 Diabetes Mellitus: Impact on Cardiac Function. *Obes. Surg.* 26 (2), 321–326. PubMed PMID: 26091811; PubMed Central PMCID: PMCPMC4709364. doi:10.1007/s11695-015-1748-x

Liang, Y., Yu, B., Wang, Y., Qiao, Z., Cao, T., and Zhang, P. (2017). Duodenal Long Noncoding RNAs Are Associated with Glycemic Control after Bariatric Surgery in High-Fat Diet-Induced Diabetic Mice. *Surg. Obes. Relat. Dis.* 13 (7), 1212–1226. Epub 20170220PubMed PMID: 28366671. doi:10.1016/j.soard.2017.02.010

Liang, Y., Yu, B., Wang, Y., Qiao, Z., Cao, T., and Zhang, P. (2018). Jejunal Long Noncoding RNAs Are Associated with Glycemic Control via Gut-Brain axis after Bariatric Surgery in Diabetic Mice. *Surg. Obes. Relat. Dis.* 14 (6), 821–832. Epub 20180309PubMed PMID: 29631984. doi:10.1016/j.soard.2018.03.006

Murashige, D., Jang, C., Neinast, M., Edwards, J. J., Cowan, A., Hyman, M. C., et al. (2020). Comprehensive Quantification of Fuel Use by the Failing and Nonfailing Human Heart. *Science* 370 (6514), 364–368. PubMed PMID: 33060364; PubMed Central PMCID: PMCPMC7871704. doi:10.1126/science.abc8861

Nakamura, M., and Sadoshima, J. (2020). Cardiomyopathy in Obesity, Insulin Resistance and Diabetes. *J. Physiol.* 598 (14), 2977–2993. Epub 20190403PubMed PMID: 30869158. doi:10.1113/JP276747

NCD Risk Factor Collaboration (2017). Worldwide Trends in Body-Mass Index, Underweight, Overweight, and Obesity from 1975 to 2016: a Pooled Analysis of 2416 Population-Based Measurement Studies in 128·9 Million Children, Adolescents, and Adults. *Lancet* 390 (10113), 2627–2642. PubMed PMID: 29029897. doi:10.1016/S0140-6736(17)32129-3

Padwal, R., Klarenbach, S., Wiebe, N., Birch, D., Karmali, S., Manns, B., et al. (2011). Bariatric Surgery: a Systematic Review and Network Meta-Analysis of Randomized Trials. *Obes. Rev.* 12 (8), 602–621. Epub 20110328PubMed PMID: 21438991. doi:10.1111/j.1467-789X.2011.00866.x

Pucci, A., and Batterham, R. L. (2019). Mechanisms Underlying the Weight Loss Effects of RYGB and SG: Similar, yet Different. *J. Endocrinol. Invest.* 42 (2), 117–128. Epub 20180505PubMed PMID: 29730732; PubMed Central PMCID: PMCPMC6394763. doi:10.1007/s40618-018-0892-2

Puzziferri, N., Roshek, T. B., 3rd, Mayo, H. G., Gallagher, R., Belle, S. H., and Livingston, E. H. (2014). Long-term Follow-Up after Bariatric Surgery. *JAMA* 312 (9), 934–942. PubMed PMID: 25182102; PubMed Central PMCID: PMCPMC4409000. doi:10.1001/jama.2014.10706

The Lancet Diabetes and Endocrinology (2021). Obesity in China: Time to Act. *Lancet Diabetes & Endocrinol.* 9 (7), 407. Epub 20210604PubMed PMID: 34097870. doi:10.1016/S2213-8587(21)00150-9

Vargas, E. J., Rizk, M., Bazerbachi, F., and Abu Dayyeh, B. K. (2018). Medical Devices for Obesity Treatment. *Med. Clin. N. Am.* 102 (1), 149–163. PubMed PMID: 29156183. doi:10.1016/j.mcna.2017.08.013

Wang, Y., Wang, L., and Qu, W. (2017). New National Data Show Alarming Increase in Obesity and Noncommunicable Chronic Diseases in China. *Eur. J. Clin. Nutr.* 71 (1), 149–150. Epub 20161005PubMed PMID: 27703162. doi:10.1038/ejcn.2016.171

Wang, W., Cheng, Z., Wang, Y., Dai, Y., Zhang, X., and Hu, S. (2019). Role of Bile Acids in Bariatric Surgery. *Front. Physiol.* 10, 374. Epub 20190402PubMed PMID: 31001146; PubMed Central PMCID: PMCPMC6454391. doi:10.3389/fphys.2019.00374

Zimmet, P., Alberti, K. G. M., Rubino, F., and Dixon, J. B. (2011). IDF's View of Bariatric Surgery in Type 2 Diabetes. *Lancet* 378 (9786), 108–110. PubMed PMID: 21742162. doi:10.1016/S0140-6736(11)61027-1

Conflict of Interest: The authors declare that the research was conducted in the absence of any commercial or financial relationships that could be construed as a potential conflict of interest.

frontiers in Physiology

ORIGINAL RESEARCH
published: 01 July 2021
doi: 10.3389/fphys.2021.700246

L-Leucine Improves Metabolic Disorders in Mice With *in-utero* Cigarette Smoke Exposure

Yunxin Zeng[1†], Taida Huang[1†], Nan Wang[1], Yi Xu[1], Chunhui Sun[1], Min Huang[1], Chun Chen[1], Brian G. Oliver[2,3], Chenju Yi[1*‡] and Hui Chen[2‡]*

[1] Research Center, The Seventh Affiliated Hospital of Sun Yat-sen University, Shenzhen, China, [2] Faculty of Science, School of Life Sciences, University of Technology Sydney, NSW, Australia, [3] Respiratory Cellular and Molecular Biology, Woolcock Institute of Medical Research, Sydney, NSW, Australia

Objectives: Maternal cigarette smoke exposure (SE) causes intrauterine undernutrition, resulting in increased risk for metabolic disorders and type 2 diabetes in the offspring without sex differences. L-leucine supplementation has been shown to reduce body weight and improve glucose metabolism in both obese animals and humans. In this study, we aimed to determine whether postnatal L-leucine supplementation in female offspring can ameliorate the detrimental impact of maternal SE.

Methods: Female Balb/c mice (6-week) were exposed to cigarette smoke (SE, 2 cigarettes/day) prior to mating for 5 weeks until the pups weaned. Sham dams were exposed to air during the same period. Half of the female offspring from the SE and SHAM dams were supplied with L-leucine via drinking water (1.5% w/w) after weaning (21-day) for 10 weeks and sacrificed at 13 weeks (adulthood).

Results: Maternal SE during pregnancy resulted in smaller body weight and glucose intolerance in the offspring. L-leucine supplement in Sham offspring reduced body weight, fat mass, and fasting blood glucose levels compared with their untreated littermates; however somatic growth was not changed. L-leucine supplement in SE offspring improved glucose tolerance and reduced fat mass compared with untreated littermates.

Conclusions: Postnatal L-leucine supplement could reduce fat accumulation and ameliorate glucose metabolic disorder caused by maternal SE. The application of leucine may provide a potential strategy for reducing metabolic disorders in offspring from mothers who continued to smoke during pregnancy.

Keywords: maternal smoking, glucose intolerance, insulin, fat mass, leucine

OPEN ACCESS

Edited by:
Ryan Ceddia, Vanderbilt University Medical Center, United States

Reviewed by:
Kamal Rahmouni, The University of Iowa, United States
Michael Zemel, NuSirt Biopharma, Inc, United States

***Correspondence:**
Chun Chen
chenchun69@126.com
Chenju Yi
yichj@mail.sysu.edu.cn

[†] These authors have contributed equally to this work

[‡] These authors share senior authorship

Specialty section:
This article was submitted to Metabolic Physiology, a section of the journal Frontiers in Physiology

Received: *25 April 2021*
Accepted: *04 June 2021*
Published: *01 July 2021*

Citation:
Zeng Y, Huang T, Wang N, Xu Y, Sun C, Huang M, Chen C, Oliver BG, Yi C and Chen H (2021) L-Leucine Improves Metabolic Disorders in Mice With in-utero Cigarette Smoke Exposure. Front. Physiol. 12:700246. doi: 10.3389/fphys.2021.700246

INTRODUCTION

Tobacco smoking is a global public health risk. According to the WHO, in 2016, the smoking rate in females over 15 years old was 20.7% in Europe, 12.4% in America, and 1.9% in China, while the second-hand smoking rate in females was as high as 46.9% in China (Ding et al., 2016; World Health Organization, 2019). Maternal cigarette smoke exposure (SE), including direct and second-hand smoking during pregnancy, is a major cause of intrauterine undernutrition resulting in

several adverse health outcomes, including preterm birth, low birth weight, and catch-up growth in childhood (Collaco et al., 2017; Wagijo et al., 2017). In addition to these short-term adverse effects, offspring from mothers exposed to cigarette smoke during pregnancy are also more likely to develop metabolic disorders in adulthood, such as glucose intolerance, type 2 diabetes, fatty liver changes, dyslipidemia, and cardiovascular disease (Mendez et al., 2008; Gorog et al., 2011; La Merrill et al., 2015).

Around 463 million people suffering from diabetes, which is one of the greatest public health challenges in both developed and developing countries (Saeedi et al., 2019). The incapability of pancreatic β-cells to produce adequate insulin or reduced insulin response in glucose deposit tissues leads to a chronic increase in blood glucose level followed by vascular damages which are the prime cause of death in diabetic patients (Bennett et al., 2018; Zheng et al., 2018). Previous studies in rodent models have shown that maternal nicotine treatment interrupts β-cell functions in offspring, and maternal SE induced intrauterine undernutrition is also associated with overconsumption in offspring, increasing the risk of insulin resistance and glucose intolerance (Holloway et al., 2005; Bruin et al., 2008, 2010; Sullivan et al., 2014). Therefore, to reduce the risk of metabolic disorder and diabetes, it is crucial to find effective preventive strategies to ameliorate the adverse impacts of maternal SE on offspring.

In the study of diabetes prevention, a high-protein diet has been proven to produce better glycemic control, fat loss, and preservation of muscle mass than a carbohydrate-rich diet with the same caloric intake (Skov et al., 1999; Parker et al., 2002; Layman et al., 2003). During this process, branch chain amino acids, especially L-leucine, have been suggested to play a critical role. Leucine is an essential amino acid and can only be obtained from the diet. In the brain, L-leucine activates the mammalian target of rapamycin in the hypothalamus (Cota et al., 2006), resulting in its beneficial effects of inducing weight loss, and improving glucose homeostasis in mouse models of obesity and diabetes (Arakawa et al., 2011; Chen et al., 2012; Westerterp-Plantenga et al., 2014). This evidence suggests that leucine supplement can be a potential strategy to prevent glucose disorders due to maternal SE.

The regulatory network for energy homeostasis has been widely studied in the hypothalamus where the neurons produce the appetite stimulator neuropeptide Y (NPY), and appetite suppressor α-melanocyte stimulating hormone cleaved from proopiomelanocortin (POMC) (Morton et al., 2006). Chemicals in cigarette smoke can inhibit hypothalamic NPY level and the same can happen in fetal brain and suckling pups when they continuously receive the chemicals from breastmilk. When the suckling pups are weaned, it can induce quitting smoking type of rebound response of NPY to cause overeating in childhood, similar to what happens to smokers when they quit smoking (Grove et al., 2001). In contrast, an intracerebroventricular administration of L-leucine, could reduce food intake and body weight in chow-fed animals, due to its suppression of hypothalamic NPY expression (Cota et al., 2006). Dietary leucine can pass the blood-brain barrier to access the brain (Chen et al., 2012); however, in the situation of high fat diet consumption, oral leucine supplement was not able to affect the adiposity but still can improve glycemic control (Chen et al., 2012).

While it is increasingly recognized the importance of the fetal environment on the susceptibility to future metabolic disorders, it is also important to look for effective early interventions to prevent adverse maternal impact in the offspring. Therefore, we hypothesized that in offspring from dams exposed to cigarette smoke during pregnancy, postnatal L-leucine supplement in drinking water will prevent excess fat accumulation and benefit glycemic control in adulthood. To address this hypothesis, we used our published mouse model of maternal SE (Huang et al., 2021) and supplied L-leucine in the drinking water to the female offspring from weaning for 10 weeks until they reached adulthood. As there is no sexual difference in metabolic disorders due to maternal SE, we only studied females. We aimed to investigate the effects of maternal SE and postnatal leucine supplement on body weight, adiposity, glucose tolerance, and the gene expression of metabolic markers in the hypothalamus and fat tissues.

MATERIALS AND METHODS

Animal Experiments

According to the previous publication on the strain dependence of the response to cigarette smoke exposure (Vlahos et al., 2006), female Balb/C mice (6-week-age) were used. They were housed at 20 ± 2°C and maintained on a 12:12 h light/dark cycle (lights on 6:00 a.m.) with *ad libitum* access to standard rodent chow and water. All the animal experiments were approved by the Animal Ethics Committee of the San Yet-sun University (SYSU-IACUC-2020-81060) and followed the guidelines for animal care and use for scientific research by the National Institute of Health, USA.

After acclimatization, mice with similar body weight were randomly assigned to two groups, sham exposure (SHAM) and SE. The SE group was exposed to smoke produced by 2 cigarettes (Double Happiness; Tar: 8 mg; nicotine: 0.7 mg; CO: 12 mg) inside a perspex box (18 liters) in the fume hood, twice a day for 5 weeks before mating and during the gestation and lactation periods following a published protocol as we have previously published (Huang et al., 2021). The breeders in the SHAM group were treated identically except for the exposure to the air. After 5 weeks of preconditioning, females were placed with male mice to mate (ratio 3:1). All breeders continuously received the same treatments until pups were weaned. The pups and male breeders remained in their home cages when the females were treated and not subjected to any exposure.

Post-weaning L-Leucine Supplement in Female Offspring

One day after birth, litter sizes were adjusted to 4–6 pups (sex ratio 1:1) to minimize the impact of milk competition. The pups were weaned at 21 days of age. Since there is no sexual difference in the metabolic disorders due to maternal SE, only

female offspring were used in the present study (males were subjected to a different study). Within each litter, half of the pups were supplied with L-leucine (Sigma, St Louis, MO, USA) via drinking water (1.5% w/w) for 10 weeks. Normal drinking water was provided to the other half of the litter. This yielded four experimental groups, SHAM, SHAM-leucine, SE, and SE-leucine. Water intake was measured 1 week before the endpoint by recording the difference between the weight of the water bottle at a 24 h interval.

Intraperitoneal Glucose Tolerance Test (IPGTT)

IPGTT was performed in the offspring at 12 weeks of age as previously described (Nguyen et al., 2015). In brief, after 5 h of fasting, the baseline of glucose level was measured in blood samples collected from the tail tip (T_0) by Accu-Chek® glucose meter (Roche, Germany). After glucose injection (2 g/kg, ip), the same measurement was performed again at 15, 30, 60, and 90 min to calculate the area under the curve (AUC) for each mouse.

Sample Collection

Female offspring were deeply anesthetized (ketamine/xylazine 180/32 mg/kg) at 13 weeks after overnight fasting. Blood glucose levels were immediately measured by Accu-Chek® glucose meter after blood collection. Plasma was stored at −20°C for the measurement of insulin levels using a commercially available ELISA kit following the manufacture's instruction (Abnova, Taiwan). The Homeostatic Model Assessment of Insulin Resistance (HOMA-IR) was calculated according to the formula: insulin (μU/mL) × glucose (mM)/22.5. Thereafter, mice were subsequently sacrificed by decapitation. The tissues including the hypothalamus, body fat (brown fat, epididymal, retroperitoneal, and visceral fat), organs (liver, kidney, and heart), as well as skeletal muscle (soleus, extensor digitorum longus (EDL), and quadratus lumborum) were dissected and weighed. Hypothalamus, retroperitoneal fat, and brown fat were stored at −80°C for subsequent measurement of mRNA expression of metabolic markers.

Quantitative Real-Time PCR Assays

Total RNA was isolated from individual samples by TriZol Reagent following the manufacture's protocol [Invitrogen, United State of America (USA)]. The purified total RNA was used for First-strand cDNA generation with a synthesis kit (One-step gDNA Removal, TransGen Biotech, China). TaqMan probe/primers were pre-optimized and validated by the manufacturer (Thermo Fisher Scientific, USA) were used for quantitative real-time PCR (CFX96, Bio-Rad, USA). Target metabolic marker genes included neuropeptide Y (Npy: Mm00445771_m1), neuropeptide Y1 receptor (Npy1r: Mm00445771_m1), proopiomelanocortin (Pomc: Mm00435874_m1), melanocortin-4 receptor: (Mc4r: Mm00457483_s1), single minded gene 1 (Sim1: Mm00441390_m1), monocarboxylic acid transporters 2 (Mct2: Mm00441442_m1), monocarboxylic acid transporters 4 (Mct4: Mm01246824_g1), lactate dehydrogenase B (Ldhb: Mm05874166_g1) in hypothalamus and carnitine palmitoyl-transferase 1 alpha (Cpt1α:Mm00550438_m1), tumor necrosis factor alpha (Tnfα: Mm00443259_g1), adipose triglyceride lipase (Atgl: Mm01275939_g1), as well as uncoupling protein 1 (Ucp1: Mm00494069_m1) in BAT.

Statistical Analysis

All the data are presented as mean ± SEM. Differences between the groups were analyzed using two-way ANOVA, except for

TABLE 1 | Effects of maternal se and postnatal leucine supplement in female offspring.

Offspring treatments	SHAM ($n = 18$)	SHAM-leucine ($n = 18$)	SE ($n = 16$)	SE-leucine ($n = 16$)
Body weight (g)	20.0 ± 0.3	19.3 ± 0.2$^{\Psi}$	18.6 ± 0.3*	18.4 ± 0.3*
Food intake (kJ/mouse/24 h)	34.9 ± 1.30	31.9 ± 1.76	36.7 ± 1.68	33.2 ± 1.93
HOMA	10.8 ± 1.21	9.07 ± 0.86	9.25 ± 0.93	10.5 ± 1.21
Naso-anal length (cm)	9.24 ± 0.08	9.17 ± 0.04	9.37 ± 0.37	8.96 ± 0.07
Liver (mg)	809 ± 14	712 ± 34$^{\Psi}$	745 ± 14	752 ± 21
Kidney (mg)	110 ± 2	107 ± 1	101 ± 3*	103 ± 2*
Heart (mg)	102 ± 3	99 ± 2	86 ± 3*	91 ± 2*
Brown fat (mg)	66.9 ± 2.5	62.7 ± 1.8	60.1 ± 3.0*	60.2 ± 1.8
Retroperitoneal fat (mg)	95.3 ± 7.6	76.3 ± 5.1$^{\Psi}$	80.9 ± 6.2	70.7 ± 5.6
Epididymal fat (mg)	521 ± 33	491 ± 22	507 ± 25	481 ± 36
Visceral fat (mg)	447 ± 16	428 ± 8	427 ± 14	403 ± 11
EDL (mg)	18.9 ± 0.6	18.7 ± 0.7	17.6 ± 0.4	16.8 ± 0.7*
Soleus (mg)	10.6 ±0.2	10.4 ± 0.2	9.8 ± 0.3*	9.9 ± 0.3
Quadra (mg)	253 ± 4	239 ± 7	242 ± 6	228 ± 8

*Results are expressed as mean ± SEM, and analyzed by two-way ANOVA, followed by post hoc LSD tests. *$P < 0.05$, maternal SE effect; $^{\Psi}P < 0.05$, leucine effect. EDL, extensor digitorum longus; Quadra, quadratus lumborum muscle; SE, smoke exposure.*

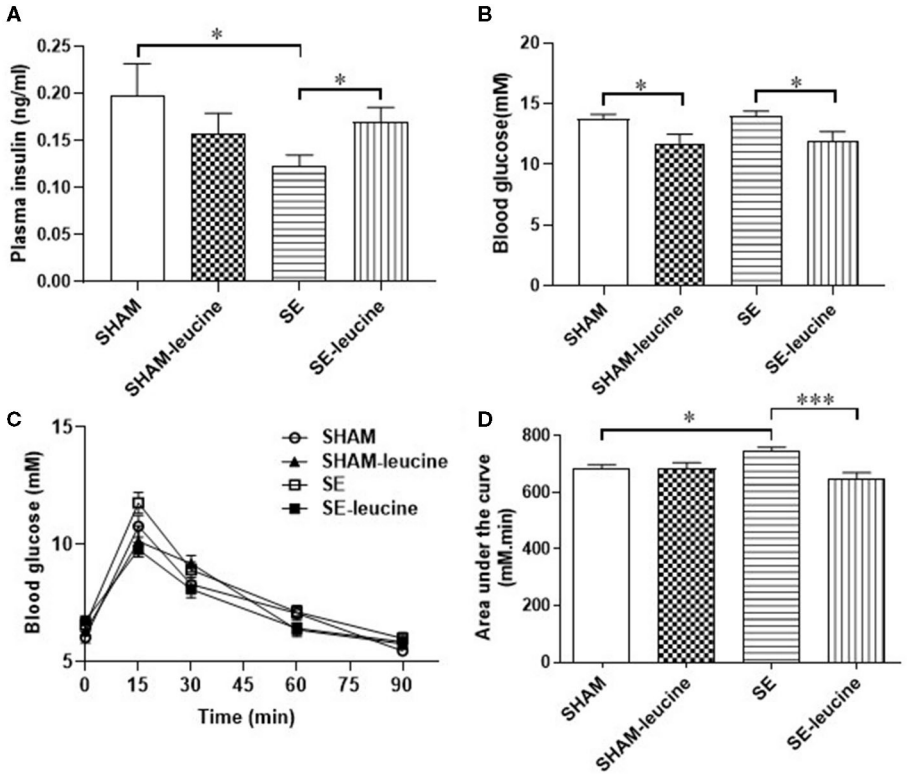

FIGURE 1 | Blood glucose metabolic profile in female offspring. Plasma insulin **(A)** and blood glucose **(B)** level in female offspring at 13 weeks. Blood glucose levels during Intraperitoneal glucose tolerance test (IPGTT, **C**) and the area under the curve **(D)** at 12 weeks. Results are expressed as the mean ± SEM ($n = 8$), and analyzed by two-way ANOVA, followed by *post-hoc* LSD tests. *$P < 0.05$, ***$P < 0.001$.

glucose level during IPGTT which were analyzed by multi-factor ANOVA, followed by *post-hoc* LSD tests, if the data were normally distributed. If not, data were log-transformed to achieve normality of distribution before they were analyzed. $P < 0.05$ was considered statistically significant.

RESULTS

Effects of Maternal SE and Postnatal L-Leucine Supplement on Anthropometry

At 13 weeks, mice in the SE groups showed smaller body weight than those in the SHAM group ($P < 0.05$, **Table 1**), consistent with the literature (Chan et al., 2016). Maternal SE also significantly reduced the weights of vital organs and skeletal muscle soleus ($P < 0.05$, SHAM vs. SE, **Table 1**). Although white fat masses also appeared smaller in the SE offspring, they did not reach statistical significance.

L-leucine supplement only significantly reduced body weight, liver weight, and retroperitoneal white fat mass in the SHAM offspring (P<0.05, SHAM-leucine vs. SHAM, **Table 1**). Such treatment did not significantly affect any of the anthropometric markers in the SE offspring, albeit smaller white fat mass (**Table 1**).

Neither maternal SE nor post-weaning L-leucine supplement affected food intake and somatic growth reflected by naso-anal length (**Table 1**). The water intake was similar between SHAM-leucine (3.62 ± 0.02 ml/mouse/day) and SE-leucine (3.17 ± 0.47 ml/mouse/day) groups in adulthood. This equivalent to a leucine intake of 54.3mg/mouse/day and 47.6mg/mouse/day at this time point.

Leucine Supplement Normalized the Glucose Intolerance Caused by Maternal SE

At 13 weeks, plasma insulin level was significantly decreased in the SE group than that in the SHAM group ($P < 0.05$, SHAM vs. SE, **Figure 1A**), although fasting blood glucose levels were similar between the groups (**Figure 1B**). In addition, adult SE offspring exhibited impaired ability to clear blood glucose during IPGTT compared with the SHAM offspring, reflected by the higher AUC values ($P < 0.05$, SHAM vs. SE, **Figures 1C,D**).

The supplement of leucine normalized plasma insulin level in the SE offspring ($P < 0.05$, SE-leucine vs), reduced fasting blood glucose in both SHAM and SE offspring ($P < 0.05$ vs. untreated littermates, **Figure 1B**). Moreover, leucine supplement effectively normalized glucose tolerance in the SE offspring ($P < 0.001$, SE vs. SE-leucine, **Figure 1D**). However, systematic glucose metabolism seems not to be related to insulin resistance, as HOMA index was not significantly changed by maternal SE or leucine supplement (**Table 1**).

L-Leucine Supplement Restored *Pomc* Expression in the Hypothalamus of SE Offspring

To evaluate the effects of the maternal SE and post-weaning leucine supplement on the feeding regulators, we measured food intake and analyzed the mRNA expression of classical genes involved in appetite regulation in the hypothalamus. There was no difference in food intake among the groups (**Table 1**). In the SE offspring, the levels of hypothalamic *Npy* and *Npy1r* mRNA expression were similar to those in the SHAM offspring (**Figures 2A,B**), whereas the *Pomc* expression was markedly downregulated ($P < 0.05$, SHAM vs. SE, **Figure 2C**). However, the expression of *Mc4r*, which is the dominant anorexigenic receptor for Pomc derived α-melanocyte-stimulating hormone, its downstream signaling *Sim1*, as well as lactate transports *Mct2* and *Mc4* and *Ldhd* (involved in lipid metabolism) was not affected by maternal SE (**Figures 2D–H**), in line with unchanged food intake.

Postweaning supplement of L-leucine only normalized *Pomc* expression in SE-leucine group ($p < 0.01$, SE vs. SE-leucine, **Figure 2C**). It did not significantly change any of the other metabolic regulators in the hypothalamus measured in this study, although there is a trend in increased *Mct4* in both SHAM and SE offspring (∼50% increase compared with their untreated littermates, **Figure 2G**). However, food intake was not significantly changed by leucine supplement (**Table 1**).

Effects on the Substrate Metabolic in the Fat in Female Offspring

In the SE group, the expression of the thermogenesis markers *Ucp1* was downregulated by maternal SE ($P < 0.05$, **Figure 3A**). There was a trend decrease in the expression of *Atgl* in retroperitoneal fat by maternal, but the difference was not statistically significant (**Figure 3B**). The expression of *Cpt1*α, a rate-limiting regulator for fatty acid β-oxidation in mitochondria, and inflammatory marker *Tnfα* was not affected by maternal SE (**Figures 3C,D**).

L-leucine supplement reduced *Ucp1* expression only in the SHAM offspring ($P < 0.05$, SHAM-leucine vs. SHAM), and increased *Atgl* expression only in the SE offspring ($P < 0.01$, **Figure 3B**). Interestingly, although leucine showed no impact on *Cpt1*α expression in either SHAM or SE offspring, its level was significantly lower in SE-leucine mice compared to SHAM-leucine group ($P < 0.05$, SHAM-leucine vs. SE-leucine, **Figure 3A**). The expression of *Tnfα* was not affected by L-leucine supplement (**Figure 3D**).

DISCUSSION

The smoking cessation rate among pregnant women is quite low (Coleman et al., 2015). This possesses a significant health risk in their offspring later in life. Finding a non-invasive and effective prophylactic strategy to protect such offspring can significantly improve their quality of life in the long term. The novel approach of this study is the introduction of post-weaning leucine supplement in the offspring to ameliorate the adverse impact of maternal SE. We found that leucine supplement normalized glucose metabolic disorders and insulin insufficiency caused by maternal SE in adult offspring. Even in the SHAM offspring, leucine supplement reduced their fat mass and lowered fasting blood glucose without affecting somatic growth, suggesting its benefit to metabolic profile in general.

In this study, we demonstrated the detrimental effect of maternal SE during pregnancy, which led to smaller body weight, glucose intolerance, and lower plasma insulin level in adult offspring. This is consistent with the literature (Saad et al., 2018; Li et al., 2019). Our study also showed long-lasting effects of maternal SE during pregnancy on reduced lean body mass, including the vital organs (e.g., liver) and skeletal muscle soleus. Tobacco smoke contains over 5000 harmful chemicals (Talhout et al., 2011). The nicotine in cigarette smoke was found to reduce the uteroplacental blood flow leading to inefficient nutrition supplement for the growing fetus. Nicotine can also cross the blood-placental barrier to enter the fetal circulation to concentrate higher nicotine level than that in smoking mother, which further disrupted normal development of the endocrine, neurologic, respiratory, and cardiovascular systems (Lisboa et al., 2012; Holbrook, 2016; Jamshed et al., 2020). In addition, CO inhibits oxygen delivery to the cells and cause *in utero* hypoxia due to a great affinity to hemoglobin and increases carboxyhemoglobin levels in umbilical arteries (Ko et al., 2014). In the present study, fetal underdevelopment was not corrected by so called "catch-up growth" after birth in humans (Al Mamun et al., 2006; Darendeliler, 2019). This may be due to the diet in the animal study, which is standard rodent chow with balanced nutrition; whereas in humans, smoking mothers are more likely to consume foods high in sugar and saturated fat which they also feed to their children (Al Mamun et al., 2006). This dietary choice would encourage the development of obesity in such offspring. Future studies can introduce the second insult of high fat diet consumption in the offspring to further study the mechanism underlying metabolic disorders in this population.

Furthermore, we also observed that maternal SE would induce glucose intolerance together with reduced plasma insulin level, which is consistent with the previous study in both human and mouse models (Henkin et al., 1999; Chen et al., 2011). In rodent models of nicotine exposure during lactation, pancreatic β-cells depletion with subsequent impaired glucose homeostasis was observed, suggesting the toxic effect of nicotine on β-cell function (Bruin et al., 2010; Primo et al., 2013). In addition, in the major glucose deposition organ fat tissue, the pro-inflammatory cytokine TNFα can directly block the insulin receptor signaling pathway to cause insulin resistance and glucose intolerance (Montgomery and Ekbom, 2002; Vuguin et al., 2004). However, in this study, the expression of fat *Tnfα* was not changed by maternal SE, in line with HOMA index ruling out the involvement of insulin resistance, suggesting insufficient insulin production may be the major driver of glucose metabolism disorder in the offspring with *in-utero* SE exposure. In humans, maternal smoking is linked to an increased risk of type 2 diabetes independent of diet choices (Jaddoe et al., 2014).

In the SE offspring, the fat mass of all pads collected in this study was reduced although without statistical significance. This

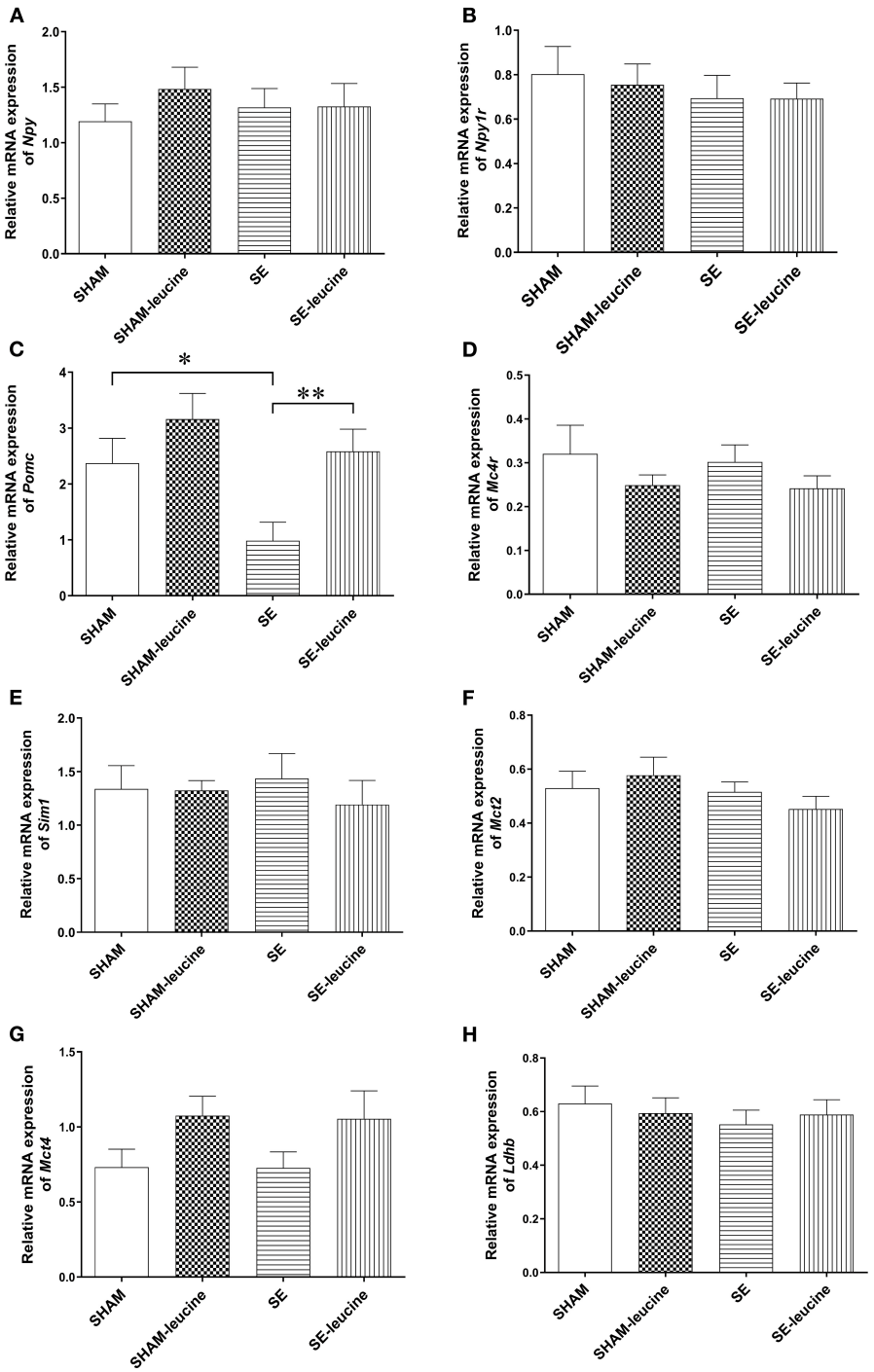

FIGURE 2 | Expression of metabolic regulators in the hypothalamus. The mRNA expression of *Npy* **(A)**, *Npy1r* **(B)**, *Pomc* **(C)**, *Mc4R* **(D)**, *Sim1* **(E)**, *Mct2* **(F)**, *Mct4* **(G)**, and *Ldhb* **(H)** in the hypothalamus of female offspring at 13 weeks ($n = 8$). Results are expressed as mean ± SEM and analyzed by two-way ANOVA, followed by *post hoc* LSD tests. $^{*}P < 0.05$, $^{**}P < 0.01$.

may lead to the adaptive reduction in *Ucp1* expression. UCP1 mediate non-shivering thermogenesis and basal metabolic rate in brown fat (Cannon and Nedergaard, 2004). Fasting or chronic food restriction can downregulate *Ucp1* expression (Cannon and Nedergaard, 2004; Oelkrug et al., 2015; Peixoto et al., 2020). It is unclear the contribution of downregulated hypothalamic *Pomc* expression as none of its downstream signaling elements in the regulation of metabolic homeostasis was changed accordingly,

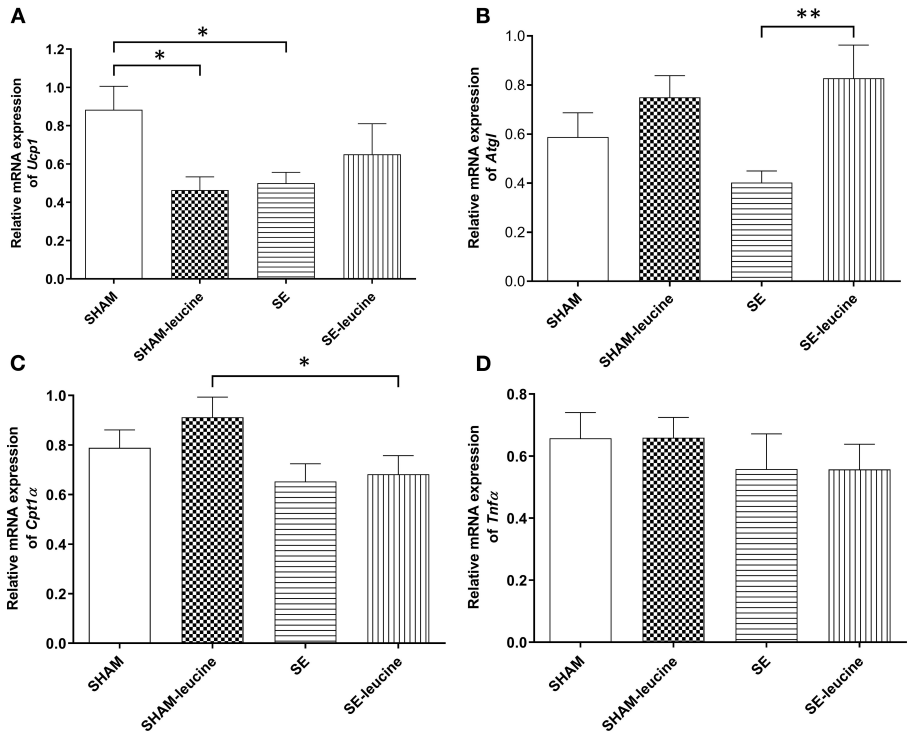

FIGURE 3 | Expression of lipid metabolic markers in the retroperitoneal white fat tissue. mRNA expression of uncoupling protein (Ucp)1 in the brown fat **(A)**, *Atgl* **(B)**, *Cpt1α* **(C)**, and *Tnfα* **(D)** in the retroperitoneal fat, in female offspring at 13 weeks ($n = 8$). Results are expressed as mean ± SEM. Data were analyzed by two-way ANOVA, followed by *post-hoc* LSD tests. $^{*}P < 0.05$, $^{**}P < 0.01$.

which requires investigations into other functions of *Pomc*. It may also be an adaptive response to reduced fat mass.

L-leucine supplements have been shown to improve glucose metabolism and insulin sensitivity even in obese rats (Bassil et al., 2007; Berry-Kravis et al., 2007; Chen et al., 2012). Indeed, the most prominent benefit of leucine supplement is perhaps the normalized glucose metabolism in the SE offspring. Since HOMA index was not significantly affected, the mechanism of improved glucose metabolism may not be related to insulin sensitivity, but driven by significantly increased blood insulin levels. This observation is supported by previous studies showing the beneficial effect of leucine on β-cell function and metabolism (Yang et al., 2010). L-leucine is an essential amino acid that is normally obtained via diet. Considering the independent risk of type 2 diabetes by maternal smoking, human trials can be considered to implement such prophylactic treatment.

Furthermore, in the SHAM offspring, L-leucine administration reduced their body weight and fat mass. As a result, *Ucp1* is downregulated to prevent excessive energy expenditure. Previous studies in mice demonstrated that leucine promotes fat loss by increasing fatty acid utilization in adipocytes (Gual et al., 2005; Sun and Zemel, 2007; Zhang et al., 2007). Atgl is an essential enzyme to break down triglycerides into free fatty acids and glycerol and CPT1α is the rate limiting step for β-oxidation of fatty acids into ATP in the mitochondria. With L-leucine supplement, both markers were non-significantly increased in the SHAM offspring. It raised the question of whether a statistical significance is required to exert physiological function. Nevertheless, the administration of leucine upregulated *Atgl* expression, in the face of some reduction in fat mass. In the SE offspring, fat loss was not as prominent as the SHAM offspring. This may be due to the need for a minimum amount of fat tissue to maintain normal metabolic function. Leucine did not show a measurable impact on the key metabolic regulators in the hypothalamus, which is somewhat consistent with our previous study using long-term leucine supplement (Chen et al., 2012). This suggests that peripheral tissues may be the primary targets in such setting. Future studies can also investigate whether this alteration can protect the SE offspring from high fat diet consumption induced obesity.

We need to acknowledge the limitations of this study. We only trialed one dose of L-leucine according to our previous study (Chen et al., 2012) in the female offspring to prove the concept. Previously, leucine supplement was shown to improve glucose metabolic disorders due to maternal obesity in male offspring (Chen et al., 2012; Saad et al., 2018). As this study was only performed on female mice, the positive outcome on glucose metabolism may not happen in the male offspring, who also showed similar metabolic disorders in our previous studies on the same model (Nguyen et al., 2015; Saad et al., 2018; Li et al., 2019; Huang et al., 2021). Future studies can investigate a dose-response curve of such treatment in both male and

female offspring. In this study, we only measured the classical metabolic regulators, which were not affected by a combination of a nutritional balanced diet and leucine. This may be due to glucose intolerance as the only measurable abnormality in this model. Future studies can induce more severe metabolic disorders by introducing additional risk factors.

CONCLUSION

L-leucine supplement can reduce fat mass potentially by increasing lipid breakdown and/or metabolism in the fat tissue in both SHAM and SE offspring. Importantly, our study also suggests the benefits of postnatal L-leucine supplement to improve glucose tolerance in SE offspring by improving their blood insulin levels, which may potentially reduce the risk of type 2 diabetes. Future studies can employ additional high fat diet feeding in the SE offspring to confirm the prophylactic effects of L-leucine supplement on the development of obesity and type 2 diabetes.

DATA AVAILABILITY STATEMENT

The raw data supporting the conclusions of this article will be made available by the authors, with valid justification.

ETHICS STATEMENT

The animal study was reviewed and approved by Animal Experimentation Ethics Committee of the San Yet-sun University (number: SYSU-IACUC-2020-81060).

AUTHOR CONTRIBUTIONS

YZ: methodology, investigation, and writing—original draft. TH: investigation and editing. NW, YX, CS, and MH: investigation. BO: conceptualization, supervision, and review. CY: conceptualization, supervision, writing, and editing. HC: conceptualization, supervision, writing, and review. All authors contributed to the article and approved the submitted version.

FUNDING

This study was supported by research grants from the National Nature Science Foundation of China (NSFC 81971309), Guangdong Basic and Applied Basic Research Foundation (2019A1515011333), Fundamental Research Funds for the Central Universities (19ykzd04), and the Shenzhen Fundamental Research Program (JCYJ20190809161405495, JCYJ20190809190601671 and RCYX20200714114644167).

REFERENCES

Al Mamun, A., Lawlor, D. A., Alati, R., O'callaghan, M. J., Williams, G. M., and Najman, J. M. (2006). Does maternal smoking during pregnancy have a direct effect on future offspring obesity? Evidence from a prospective birth cohort study. *Am. J. Epidemiol.* 164, 317–325. doi: 10.1093/aje/kwj209

Arakawa, M., Masaki, T., Nishimura, J., Seike, M., and Yoshimatsu, H. (2011). The effects of branched-chain amino acid granules on the accumulation of tissue triglycerides and uncoupling proteins in diet-induced obese mice. *Endo. J.* 58, 161–170. doi: 10.1507/endocrj.K10E-221

Bassil, M. S., Hwalla, N., and Obeid, O. A. (2007). Meal pattern of male rats maintained on histidine-, leucine-, or tyrosine-supplemented diet. *Obesity* 15, 616–623. doi: 10.1038/oby.2007.565

Bennett, J. E., Stevens, G. A., Mathers, C. D., Bonita, R., Rehm, J., Kruk, M. E., et al. (2018). NCD Countdown 2030: worldwide trends in non-communicable disease mortality and progress towards sustainable development goal target 3.4. *Lancet* 392, 1072–1088. doi: 10.1016/S0140-6736(18)31992-5

Berry-Kravis, E., Abrams, L., Coffey, S. M., Hall, D. A., Greco, C., Gane, L. W., et al. (2007). Fragile X-associated tremor/ataxia syndrome: clinical features, genetics, and testing guidelines. *Mov. Disord.* 22, 2018–2030. doi: 10.1002/mds.21493

Bruin, J. E., Gerstein, H. C., and Holloway, A. C. (2010). Long-term consequences of fetal and neonatal nicotine exposure: a critical review. *Toxicol. Sci.* 116, 364–374. doi: 10.1093/toxsci/kfq103

Bruin, J. E., Petre, M. A., Lehman, M. A., Raha, S., Gerstein, H. C., Morrison, K. M., et al. (2008). Maternal nicotine exposure increases oxidative stress in the offspring. *Free. Radical. Bio. Med.* 44, 1919–1925. doi: 10.1016/j.freeradbiomed.2008.02.010

Cannon, B., and Nedergaard, J. (2004). Brown adipose tissue: function and physiological significance. *Physiol. Rev.* 84, 277–359. doi: 10.1152/physrev.00015.2003

Chan, Y. L., Saad, S., Al-Odat, I., Zaky, A. A., Oliver, B., Pollock, C., et al. (2016). Impact of maternal cigarette smoke exposure on brain and kidney health outcomes in female offspring. *Clin. Exp. Pharmacol. Physiol.* 43, 1168–1176. doi: 10.1111/1440-1681.12659

Chen, H., Iglesias, M. A., Caruso, V., and Morris, M. J. (2011). Maternal cigarette smoke exposure contributes to glucose intolerance and decreased brain insulin action in mice offspring independent of maternal diet. *PLoS ONE* 6:e27260. doi: 10.1371/journal.pone.0027260

Chen, H., Simar, D., Ting, J. H. Y., Erkelens, J. R. S., and Morris, M. J. (2012). Leucine improves glucose and lipid status in offspring from obese dams, dependent on diet type, but not caloric intake. *J. Neuroendocrinol.* 24, 1356–1364. doi: 10.1111/j.1365-2826.2012.02339.x

Coleman, T., Chamberlain, C., Davey, M. A., Cooper, S. E., and Leonardi-Bee, J. (2015). Pharmacological interventions for promoting smoking cessation during pregnancy. *Cochrane. Database. Syst. Rev.* 12:CD010078. doi: 10.1002/14651858.CD010078.pub2

Collaco, J. M., Wilson, K. M., and Mcgrath-Morrow, S. A. (2017). More evidence linking smoke-free legislation and lower risk of prematurity and low birth weight. *Pediatrics* 139:e20170795. doi: 10.1542/peds.2017-0795

Cota, D., Proulx, K., Smith, K. A. B., Kozma, S., Thomas, G., Woods, S., et al. (2006). Hypothalamic mTOR signaling regulates food intake. *Science* 312, 927–930. doi: 10.1126/science.1124147

Darendeliler, F. (2019). IUGR: Genetic influences, metabolic problems, environmental associations/triggers, current and future management. *Best. Pract. Res. Clin. Endocrinol. Metab.* 33:101260. doi: 10.1016/j.beem.2019.01.001

Ding, R., Wang, P., Ma, L., and Tian, Y. (2016). A meta-analysis on the prevalence of secondhand smoke among Chinese mainland female residents. *Prev. Med.* 28, 671–676. Available online at: http://www.zjyfyxzz.com/CN/Y2016/V28/I7/671

Gorog, K., Pattenden, S., Antova, T., Niciu, E., Rudnai, P., Scholtens, S., et al. (2011). Maternal smoking during pregnancy and childhood obesity: results from the CESAR study. *Matern. Child. Health. J.* 15, 985–992. doi: 10.1007/s10995-009-0543-5

Grove, K. L., Sekhon, H. S., Brogan, R. S., Keller, J. A., Smith, M. S., and Spindel, E. R. (2001). Chronic maternal nicotine exposure alters neuronal systems in the arcuate nucleus that regulate feeding behavior in the newborn rhesus macaque. *J. Clin. Endocrinol. Metab.* 86, 5420–5426. doi: 10.1210/jcem.86.11.8033

Gual, P., Le, M.-B. Y., and Tanti, J. F. (2005). Positive and negative regulation of insulin signaling through IRS-1 phosphorylation. *Biochimie* 87, 99–109. doi: 10.1016/j.biochi.2004.10.019

Henkin, L., Zaccaro, D., Haffner, S., Karter, A., Rewers, M., Sholinsky, P., et al. (1999). Cigarette smoking, environmental tobacco smoke exposure and insulin

sensitivity: the Insulin resistance atherosclerosis study. *Ann. Epidemiol.* 9, 290–296. doi: 10.1016/S1047-2797(99)00003-4

Holbrook, B. D. (2016). The effects of nicotine on human fetal development. *Birth. Defects. Res. C. Embryo. Today.* 108, 181–192. doi: 10.1002/bdrc.21128

Holloway, A. C., Lim, G. E., Petrik, J. J., Foster, W. G., Morrison, K. M., and Gerstein, H. C. (2005). Fetal and neonatal exposure to nicotine in Wistar rats results in increased beta cell apoptosis at birth and postnatal endocrine and metabolic changes associated with type 2 diabetes. *Diabetologia* 48, 2661–2666. doi: 10.1007/s00125-005-0022-5

Huang, T., Yang, M., Zeng, Y., Huang, X., Wang, N., Chen, Y., et al. (2021). Maternal high fat diet consumption exaggerates metabolic disorders in mice with cigarette-smoking induced intrauterine undernutrition. *Front. Nutr.* 8:638576. doi: 10.3389/fnut.2021.638576

Jaddoe, V. W., De Jonge, L. L., Van Dam, R. M., Willett, W. C., Harris, H., Stampfer, M. J., et al. (2014). Fetal exposure to parental smoking and the risk of type 2 diabetes in adult women. *Diabetes Care* 37, 2966–2973. doi: 10.2337/dc13-1679

Jamshed, L., Perono, G. A., Jamshed, S., and Holloway, A. C. (2020). Early life exposure to nicotine: postnatal metabolic, neurobehavioral and respiratory outcomes and the development of childhood cancers. *Toxicol. Sci.* 178, 3–15. doi: 10.1093/toxsci/kfaa127

Ko, T. J., Tsai, L. Y., Chu, L. C., Yeh, S. J., Leung, C., Chen, C. Y., et al. (2014). Parental smoking during pregnancy and its association with low birth weight, small for gestational age, and preterm birth offspring: a birth cohort study. *Pediatr. Neonatol.* 55, 20–27. doi: 10.1016/j.pedneo.2013.05.005

La Merrill, M. A., Cirillo, P. M., Krigbaum, N. Y., and Cohn, B. A. (2015). The impact of prenatal parental tobacco smoking on risk of diabetes mellitus in middle-aged women. *J. Dev. Orig. Health. Dis.* 6, 242–249. doi: 10.1017/S2040174415000045

Layman, D. K., Shiue, H., Sather, C., Erickson, D. J., and Baum, J. (2003). Increased dietary protein modifies glucose and insulin homeostasis in adult women during weight loss. *J. Nutr.* 133, 405–410. doi: 10.1093/jn/133.2.405

Li, G., Chan, Y. L., Sukjamnong, S., Anwer, A. G., Vindin, H., Padula, M., et al. (2019). A mitochondrial specific antioxidant reverses metabolic dysfunction and fatty liver induced by maternal cigarette smoke in mice. *Nutrients* 11:1669. doi: 10.3390/nu11071669

Lisboa, P. C., De Oliveira, E., and De Moura, E. G. (2012). Obesity and endocrine dysfunction programmed by maternal smoking in pregnancy and lactation. *Front Physiol* 3:437. doi: 10.3389/fphys.2012.00437

Mendez, M. A., Maties, T., Carlos, F., Nuria, R. F., and Jordi, S. (2008). Maternal smoking very early in pregnancy is related to child overweight at age 5–7 y. *Am J. Clin. Nutr.* 87, 1906–1913. doi: 10.1093/ajcn/87.6.1906

Montgomery, S. M., and Ekbom, A. (2002). Smoking during pregnancy and diabetes mellitus in a British longitudinal birth cohort. *BMJ* 324:26. doi: 10.1136/bmj.324.7328.26

Morton, G., J., Cummings, D., E., Baskin, D., G., and Barsh (2006). Central nervous system control of food intake and body weight. *Nature* 443, 289–295. doi: 10.1038/nature05026

Nguyen, L. T., Stangenberg, S., Chen, H., Al-Odat, I., Chan, Y. L., Gosnell, M. E., et al. (2015). L-Carnitine reverses maternal cigarette smoke exposure-induced renal oxidative stress and mitochondrial dysfunction in mouse offspring. *Am. J. Physiol. Renal. Physiol.* 308, F689–F696. doi: 10.1152/ajprenal.00417.2014

Oelkrug, R., Polymeropoulos, E. T., and Jastroch, M. (2015). Brown adipose tissue: physiological function and evolutionary significance. *J. Comp. Physiol. B.* 185, 587–606. doi: 10.1007/s00360-015-0907-7

Parker, B., Noakes, M., Luscombe, N., and Clifton, P. (2002). Effect of a high-protein, high-monounsaturated fat weight loss diet on glycemic control and lipid levels in type 2 diabetes. *Diabetes Care* 25, 425–430. doi: 10.2337/diacare.25.3.425

Peixoto, T. C., Moura, E. G., Soares, P. N., Bertasso, I. M., Pietrobon, C. B., Caramez, F., et al. (2020). Nicotine exposure during breastfeeding reduces sympathetic activity in brown adipose tissue and increases in white adipose tissue in adult rats: sex-related differences. *Food. Chem. Toxicol.* 140:111328. doi: 10.1016/j.fct.2020.111328

Primo, C. C., Ruela, P. B., Brotto, L. D., Garcia, T. R., and Lima Ede, F. (2013). Effects of maternal nicotine on breastfeeding infants. *Rev. Paul. Pediatr.* 31, 392–397. doi: 10.1590/S0103-05822013000300018

Saad, S., Al-Odat, I., Chan, Y. L., Mcgrath, K. C., Pollock, C. A., Oliver, B. G., et al. (2018). Maternal L-carnitine supplementation improves glucose and lipid profiles in female offspring of dams exposed to cigarette smoke. *Clin. Exp. Pharmacol. Physiol.* 45, 694–703. doi: 10.1111/1440-1681.12921

Saeedi, P., Petersohn, I., Salpea, P., Malanda, B., Karuranga, S., Unwin, N., et al. (2019). Global and regional diabetes prevalence estimates for 2019 and projections for 2030 and 2045: Results from the International Diabetes Federation Diabetes Atlas, 9(th) edition. *Diabetes. Res. Clin. Pract.* 157:107843. doi: 10.1016/j.diabres.2019.107843

Skov, A. R., Toubro, S., Rønn, B., Holm, L., and Astrup, A. (1999). Randomized trial on protein vs carbohydrate in ad libitum fat reduced diet for the treatment of obesity. *Int. J. Obes. Relat. Metab. Disord.* 23, 528–536. doi: 10.1038/sj.ijo.0800867

Sullivan, E. L., Nousen, E. K., and Chamlou, K. A. (2014). Maternal high fat diet consumption during the perinatal period programs offspring behavior. *Physiol. Behav.* 123, 236–242. doi: 10.1016/j.physbeh.2012.07.014

Sun, X., and Zemel, M. B. (2007). Leucine and calcium regulate fat metabolism and energy partitioning in murine adipocytes and muscle cells. *Lipids* 42, 297–305. doi: 10.1007/s11745-007-3029-5

Talhout, R., Schulz, T., Florek, E., Van Benthem, J., Wester, P., and Opperhuizen, A. (2011). Hazardous compounds in tobacco smoke. *Int. J. Environ. Res. Public. Health.* 8, 613–628. doi: 10.3390/ijerph8020613

Vlahos, R., Bozinovski, S., Jones, J. E., Powell, J., Gras, J., Lilja, A., et al. (2006). Differential protease, innate immunity and NF kappa B induction profiles during lung inflammation induced by sub-chronic cigarette smoke exposure in mice. *Am. J. Physiol. Lung. Cell. Mol. Physiol.* 290, L931–L945. doi: 10.1152/ajplung.00201.2005

Vuguin, P., Raab, E., Liu, B., Barzilai, N., and Simmons, R. (2004). Hepatic insulin resistance precedes the development of diabetes in a model of intrauterine growth retardation. *Diabetes* 53, 2617–2622. doi: 10.2337/diabetes.53.10.2617

Wagijo, M. A., Sheikh, A., Duijts, L., and Been, J. V. (2017). Reducing tobacco smoking and smoke exposure to prevent preterm birth and its complications. *Paediatr. Respir. Rev.* 22, 3–10. doi: 10.1016/j.prrv.2015.09.002

Westerterp-Plantenga, M. S., Nieuwenhuizen, A., Tom,é, D., Soenen, S., and Westerterp, K. R. (2014). Dietary protein, weight loss, and weight maintenance. *Curr. Opin. Clin. Nutr. Metab. Care.* 17, 75–79. doi: 10.1146/annurev-nutr-080508-141056

World Health Organization (2019). *WHO Global Report on Trends in Prevalence of Tobacco Use 2000-2025, 3rd Edn.* Available online at: https://www.who.int/news/item/19-12-2019-who-launches-new-report-on-global-tobacco-use-trends

Yang, J., Chi, Y., Burkhardt, B. R., Guan, Y., and Wolf, B. A. (2010). Leucine metabolism in regulation of insulin secretion from pancreatic beta cells. *Nutr. Rev.* 68, 270–279. doi: 10.1111/j.1753-4887.2010.00282.x

Zhang, Y., Guo, K., Leblanc, R. E., Loh, D., Schwartz, G. J., and Yu, Y. H. (2007). Increasing dietary leucine intake reduces diet-induced obesity and improves glucose and cholesterol metabolism in mice via multimechanisms. *Diabetes* 56, 1647–1654. doi: 10.2337/db07-0123

Zheng, Y., Ley, S. H., and Hu, F. B. (2018). Global aetiology and epidemiology of type 2 diabetes mellitus and its complications. *Nat. Rev. Endocrinol.* 14, 88–89. doi: 10.1038/nrendo.2017.151

Conflict of Interest: The authors declare that the research was conducted in the absence of any commercial or financial relationships that could be construed as a potential conflict of interest.

frontiers in Physiology

REVIEW
published: 17 August 2021
doi: 10.3389/fphys.2021.715081

Lactate and Myocardiac Energy Metabolism

Shuohui Dong[1], Linhui Qian[2], Zhiqiang Cheng[1], Chang Chen[1], Kexin Wang[1], Sanyuan Hu[3], Xiang Zhang[1] and Tongzhi Wu[4,5]*

[1] Department of General Surgery, Qilu Hospital of Shandong University, Jinan, China, [2] Department of Colorectal and Anal Surgery, Feicheng Hospital Affiliated to Shandong First Medical University, Feicheng, China, [3] Department of General Surgery, The First Affiliated Hospital of Shandong First Medical University, Jinan, China, [4] Adelaide Medical School and Centre of Research Excellence in Translating Nutritional Science to Good Health, The University of Adelaide, Adelaide, SA, Australia, [5] Endocrine and Metabolic Unit, Royal Adelaide Hospital, Adelaide, SA, Australia

The myocardium is capable of utilizing different energy substrates, which is referred to as "metabolic flexibility." This process assures ATP production from fatty acids, glucose, lactate, amino acids, and ketones, in the face of varying metabolic contexts. In the normal physiological state, the oxidation of fatty acids contributes to approximately 60% of energy required, and the oxidation of other substrates provides the rest. The accumulation of lactate in ischemic and hypoxic tissues has traditionally be considered as a by-product, and of little utility. However, recent evidence suggests that lactate may represent an important fuel for the myocardium during exercise or myocadiac stress. This new paradigm drives increasing interest in understanding its role in cardiac metabolism under both physiological and pathological conditions. In recent years, blood lactate has been regarded as a signal of stress in cardiac disease, linking to prognosis in patients with myocardial ischemia or heart failure. In this review, we discuss the importance of lactate as an energy source and its relevance to the progression and management of heart diseases.

Keywords: myocardium, cardiac metabolism, energy substrate, lactate, lactate shuttle theory, myocardial ischemia, heart failure, diabetic cardiomyopathy

OPEN ACCESS

Edited by:
Alex Rafacho, Federal University of Santa Catarina, Brazil

Reviewed by:
Alexandra Latini, Federal University of Santa Catarina, Brazil
Henver Simionato Brunetta, State University of Campinas, Brazil

****Correspondence:***
Xiang Zhang
xiang.zhang02@hotmail.com

Specialty section:
This article was submitted to Metabolic Physiology, a section of the journal Frontiers in Physiology

Received: *26 May 2021*
Accepted: *29 July 2021*
Published: *17 August 2021*

Citation:
Dong S, Qian L, Cheng Z, Chen C, Wang K, Hu S, Zhang X and Wu T (2021) Lactate and Myocardiac Energy Metabolism. Front. Physiol. 12:715081. doi: 10.3389/fphys.2021.715081

INTRODUCTION

The heart is an efficient bio-pump of high energy demand. Adenosine triphosphate (ATP) is the direct source of energy that supports the contraction and relaxation of the myocardium. ATP can be derived through the processes of oxidation and fermentation, during which the intermediate pyruvate is transformed into lactate. The latter has long been considered to be a by-product of glucose metabolism. Over the last several decades, amounting research has demonstrated that lactate is a major energy substrate for skeletal muscle, heart and brain (Gertz et al., 1988; Bergman et al., 1999b; Glenn et al., 2015), as well as a main gluconeogenesis precursor (Bergman et al., 2000; Meyer et al., 2002a,b; Emhoff et al., 2013b) and a signaling molecule (Hashimoto et al., 2007). Increased levels of blood lactate are also associated with poor outcomes in critical systemic diseases, including severe trauma, hypoxemia, septic shock and so forth (Cerovic et al., 2003; Nguyen et al., 2004; Khosravani et al., 2009). However, the biochemical and clinical significance of lactate within the field of myocadiac metabolism remains under-appreciated, reflecting an incomplete understanding of its production, transport, metabolism and biological functions

(Garcia-Alvarez et al., 2014). Herein, we discuss myocardial energy metabolism, with an emphasis on the role of lactate metabolism and its relevance to the progression and management of heart diseases, including acute myocardial ischemia, and heart failure, and on diabetic state.

HISTORICAL VIEW ON MYOCARDIAL ENERGY METABOLISM

The initial understanding of cardiac function was first described by a Greek philosopher Aristotle. According to the latter, the heart produces necessary heat to maintain life, and cessation of the heartbeat means absence of life (Beloukas et al., 2013). This philosophy led to the recognition of energy metabolism being central to cardiac function and the capacity of cardiomyocyte to utilize various substrates to provide energy.

Oxygen was identified as a basic element of cardiac metabolism and function as early as in the 18th century (Gh, 2006). Subsequently, carbohydrate was described as an energy substrate during cardiac contraction (Locke and Rosenheim, 1907), but contributed no more than a third to the total cardiac energy demand (Evans, 1914). This observation stimulated the search of other energy substrates for myocadiac energy metabolism, which had been advanced rapidly since the introduction of coronary sinus catheterization technique (Bing et al., 1947). In this way, the oxygen extraction ratios can be computed to reflect the aerobic catabolism of different substrates. In 1954, Bing and his colleagues assessed the utilization of glucose, lactate, pyruvate, fatty acids, ketones and amino acids of the heart *in vivo* (Bing et al., 1947; Bing, 1954), and showed that fatty acids were the major energy substrate of the human heart, accounting for 67% of the total usage of oxygen. Surprisingly, lactate, formerly known as a metabolic waste product and fatigue agent, contributed 16.5% to the total usage of oxygen, in a comparable degree to glucose (17.9%) (Bing, 1954).

Subsequent studies concentrated on energy substrate usage of the heart under different circumstances. Keul et al. (1965a,b) found that, in humans during moderate intensity exercise, the contribution of fatty acids fell from 34 to 21%, while the contribution of lactate increased from 29 to 62%. In anesthetized dogs, the contribution of lactate to cardiac oxidative energy production increased to 87% when the arterial lactate concentration exceeded 4.5 mmol/L (Drake et al., 1980). These studies suggest that lactate competes with fatty acids for cardiac oxygen consumption. In recent years, the emergence of dual carbon-labeled carbohydrate isotope technique has allowed myocardial substrate utilization to be quantified precisely in humans. Based on this technique, it was observed that the myocardial isotopic lactate uptake increased from 34.9 μmol/min at rest to 120.4 μmol/min at 5 min of moderate intensity exercise in healthy male subjects (Gertz et al., 1988). This result further confirmed lactate as an important energy substrate for the heart, particularly under stress. It is now widely accepted that the heart uses various energy substrates to generate ATP, which is key to the maintenance of normal cardiac function under different circumstances.

MYOCARDIAL LACTATE METABOLISM

As discussed, in addition to fatty acids, carbon sources, including glucose and lactate, are important energy substrates of the myocardium. Traditionally, it has been thought that full oxidation of glucose to CO_2 provides most cells energy in human body, and lactate is only a product of incomplete oxidation in the face of urgent energy demands. However, if this was the case, whole-body glucose consumption would dominate over lactate consumption, and lactate production would be equivalent to its clearance (as a precursor of hepatic and renal gluconeogenesis). Rather, lactate has a circulatory turnover flux approximately twice that of glucose on a molar basis during fasting (Dunn et al., 1976; Katz et al., 1981; Stanley et al., 1986; Wolfe, 1990). Modern studies have proved that lactate could be produced continuously under aerobic conditions, and be used as an important energy source for the heart (Brooks, 2018). Accordingly, "lactate shuttle theory" was proposed to describe the transport and function of lactate within the body: lactate could act as the vehicle linking glycolysis and oxidative metabolism, and the linkages between lactate "producer" and "consumer" exist within and among cells, tissues, and organs (Brooks, 2018). In this section we will discuss the development of lactate shuttle theory in the context of myocardial energy metabolism.

Tissue-Tissue and Cell-Cell Lactate Transport

Benefiting from the development of differential arterio-venous metabolite analysis and radiotracer techniques, the whole process of circulating lactate production and disposal was characterized in several animal studies (Brooks et al., 1984). In rats, intravenous injection of ^{14}C-lactate resulted in exhaled breath gas containing $^{14}CO_2$, providing early evidence for the concept of circulating lactate in contributing to energy metabolism (Brooks et al., 1973; Brooks and Gaesser, 1980). To better explore the production and disposal of circulating lactate across diverse physiological states, Donovan CM and Brooks GA subsequently recorded rates of lactate disposal in rodent models both at rest and during exercise with radiotracer techniques (Brooks and White, 1978; Brooks and Donovan, 1983; Donovan and Brooks, 1983). By measuring the quantity and activity of O2, CO2, circulating carbon sources (glucose and lactate) and other metabolites during resting and exercise (Brooks et al., 1977), the authors observed in rats that the rates of lactate flux in circulating peripheral blood were unanticipatedly high in the resting state, although to a lesser extent when compared to glucose flux. However, during exercise, the rates of lactate flux in circulating blood were observed to increase above those of glucose flux.

These phenomena are likely to have reflected the breakdown of glycogen and an increase in the production of lactate during exercise. However, the latter was not necessarily accompanied by increased blood lactate concentrations (Brooks and Donovan, 1983; Donovan and Brooks, 1983), which can be attributed to the markedly increased lactate metabolic clearance rate during exercise. Hence, relatively stable blood lactate concentration during exercise can be explained by a greater

lactate metabolic clearance rate due to increased lactate oxidation and gluconeogenesis. Such adaption can avoid metabolic acidosis during exercise. As technology improves, non-invasive and non-radiating methods are available for evaluation of glucose and lactate metabolism in the human body, and the aforementioned effects of exercise on glucose and lactate flux rates have also been consistently replicated (Stanley et al., 1985; Mazzeo et al., 1986; Bergman et al., 1999a,b, 2000; Emhoff et al., 2013a,b). Fluctuations of lactate in the blood indicate that lactate transport between different tissues *via* the circulatory system. However, the main producers and consumers of blood lactate underlying these changes remain unknown.

In the following research, investigators attempted to assess tissue specificity of lactate metabolism (Katz et al., 1981; Stanley et al., 1986; Gertz et al., 1988; Bergman et al., 1999a,b). Two earlier studies in the 1970s found that lactate concentrations in red skeletal muscles in motion were lower than white skeletal muscles and their blood supplies (Mole et al., 1973; Hooker and Baldwin, 1979). Although these phenomena seemed unexplained at that time, this provided early evidence to suggest working skeletal muscles as a source of the circulating lactate. In 1988, the utilization of lactate released from working muscles by heart as a carbon source was observed (Gertz et al., 1988), which marked an important milestone for research in lactate metabolism. Subsequently, lactate transport between white and red skeletal muscles (Stanley et al., 1986; Bergman et al., 1999a), and between working skeletal muscles and heart were gradually identified (Katz et al., 1981; Gertz et al., 1988; Bergman et al., 2009). It is now well-documented that the beating heart takes up, and oxidizes lactate as a consumer in the process of the lactate transport.

The potential for lactate to transport across neighboring cells and tissues has been reported over two decades. It was initially found to occur in astrocytes-neurons in brain and fibroblasts-cancer cells in tumors (Lisanti et al., 2013; Magistretti and Allaman, 2015). Recently, mouse cardiomyocytes and fibroblasts co-culture models have shown the fibroblasts-cardiomyocytes lactate transport (Wisniewski et al., 2015; Gizak et al., 2020), supporting the concept that cardiomyocytes and fibroblasts form metabolic syncytia to share energy substrates, including lactate, and exchange molecular signals. Neighboring lactate transport improves energy metabolism efficiency and orchestrates substrate utilization in tissues. Such a metabolic architecture enables metabolic adaptability and plasticity. Nevertheless, accurate mechanisms of lactate transport between cardiomyocytes and fibroblasts are still unclear.

Transmembrane and Intracellular Lactate Transport

The increasing recognition of tissue-tissue and cell-cell lactate transport has provided a strong impetus to understand the metabolic fate of lactate transport and utilization within the cell. The discovery of membrane lactate transporters provided a plausible explanation of the transmembrane lactate transport. Lactate oxidation rates comply with Michaelis-Menten kinetics, suggesting that cellular uptake and release of lactate are facilitated by membrane transporters. The membrane lactate transporter was first observed on rat sarcolemmal vesicles in 1990 (Roth and Brooks, 1990), and subsequently named as monocarboxylate transport (MCT) (Garcia et al., 1994).

Hitherto, various isoforms of MCT have been identified to account for intracellular lactate transport, but how is lactate utilized in the cell, and the site at which the intracellular lactate utilization takes place remains debated. Previous studies on humans and various mammals demonstrated that intracellular lactate metabolism consumes oxygen (Depocas et al., 1969; Donovan and Brooks, 1983; Stanley et al., 1985; Mazzeo et al., 1986). Lactate oxidation for energy supply especially prominent when heart or muscle is in load condition (Gertz et al., 1981, 1988; Stanley et al., 1986; Bergman et al., 1999b). With this in mind, issues arose about exactly where lactate oxidation happened within a working cardiomyocyte. Given that lactate dehydrogenase (LDH), a key enzyme to catalyze the inter-conversion of lactate and pyruvate, is widely present in the cytosol, lactate oxidation was first considered to take place in the cytosol. However, the results from some studies were inconsistent (Laughlin et al., 1993; Chatham et al., 2001). In working muscles-beating heart lactate syncytium, increased rates of lactate flux were found to accompany by augmented blood flow and oxygen consumption. In addition, when ^{13}C-pyruvate was injected into myocardial blood circulation, the peaks of cytosolic ^{13}C-pyruvate and ^{13}C-lactate were observed. However, when ^{13}C-lactate was injected directly, ^{13}C-pyruvate was not detected in the cytosol (Chatham et al., 2001).

If not in the cytosol, where does intracellular lactate oxidation occur? Another candidate location for intracellular lactate oxidation is the mitochondria, the pivotal organelle for energy metabolism. Lactate oxidation was observed in several mitochondrial preparations (Kline et al., 1986; Brandt et al., 1987; De Bari et al., 2004; Passarella et al., 2014), of which mitochondrial preparations from human skeletal muscles provided the strongest evidence (Jacobs et al., 2013). Lactate oxidative capacity of muscle mitochondria was subsequently confirmed by magnetic resonance spectroscopy imaging (MRSI) (Park et al., 2015; Chen et al., 2016). However, some studies using the same experimental settings showed inconsistent results, challenging the lactate oxidative capacity in the mitochondria (Popinigis et al., 1991; Sahlin et al., 2002). This discrepancy might be related to the separation process of mitochondria (Kirkwood et al., 1986; Glancy et al., 2017), which is highly dependent on the isolated system and susceptible to be contamination and/or disturbance. Therefore, confirmation by more reliable experiments is still required due to its conceptual importance. More recently, identification of the mitochondrial lactate oxidation complex (mLOC) with techniques of organelle purification and magnetic resonance spectroscopy imaging has provided solid evidence on mitochondrial transmembrane transport of lactate mitochondria as a key site of intracellular lactate oxidation (**Figure 1**; Park et al., 2015; Chen et al., 2016). Components of the mLOC include the MCT1, CD147, LDH, terminal electron transport chain element cytochrome oxidase (COX), pyruvate dehydrogenase (PDH),

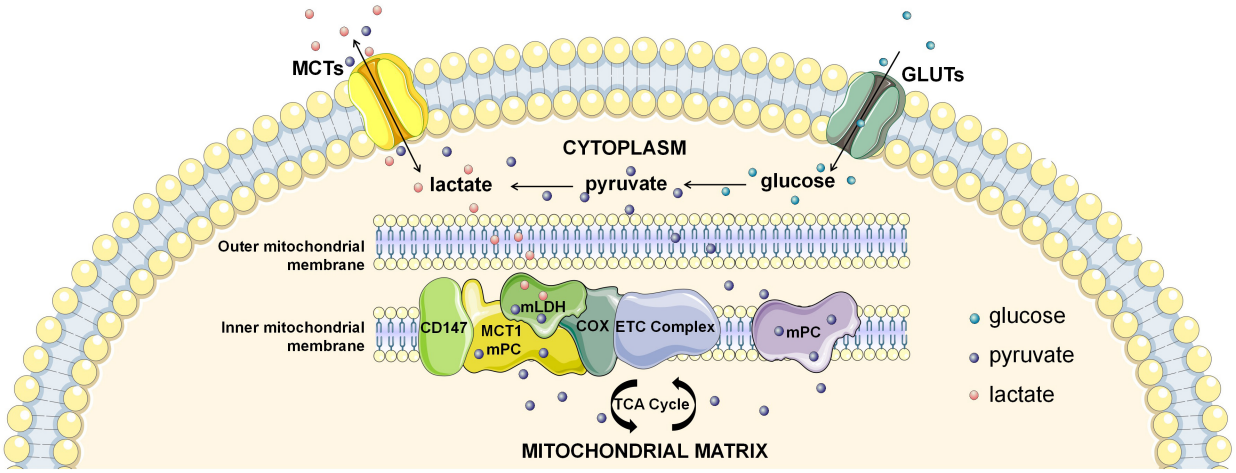

FIGURE 1 | The intracellular lactate shuttle. Both extracellular uptake and glycolytic production make up the cytosolic lactate pool. Intracellular lactate is shuttled from the cytoplasm to mitochondria for subsequent oxidization, facilitated by the mitochondrial lactate oxidation complex (mLOC). Monocarboxylate transporter 1 (MCT1) is inserted into the inner mitochondrial membrane, and CD147 is an indispensable chaperone protein of MCT1. Mitochondrial LDH (mLDH) is distributed on the surface of the inner mitochondrial membrane, and oxidizes lactate to pyruvate. In addition, terminal electron transport chain element cytochrome oxidase (COX) is responsible for the endergonic lactate oxidation. Mitochondrial pyruvate carrier (mPC) is distributed in the inner mitochondrial membrane, which is responsible for the mitochondrial transmembrane transport of pyruvate.

Krebs cycle related-enzymes, and mitochondrial respiratory chain (De Bari et al., 2004; Hashimoto et al., 2006, 2008; Atlante et al., 2007; Sonveaux et al., 2008; Passarella et al., 2014). Mitochondrial MCT1 is located in the inner membrane and is responsible for mitochondrial transmembrane transport of lactate, and CD147 is an indispensable chaperone protein of MCT1 (Park et al., 2015; Chen et al., 2016). Mitochondrial LDH was initially discovered in the sperm, but is now revealed to also exist in the liver, kidney and heart (Kline et al., 1986; Brandt et al., 1987; Tempia et al., 1988). Lactate oxidative capacity is strongly associated with the expression of mitochondrial LDH (Tempia et al., 1988), and is also associated with COX (Hashimoto et al., 2006). Finally, lactate is transformed to the end product (CO_2) by PDH, Krebs cycle related-enzymes, and mitochondrial respiratory chain catalysis. Future research in order to better define the mLOC is eagerly anticipated.

Another issue regarding intracellular lactate metabolism is why cells generate and consume lactate at the same time. For example, cardiomyocytes release glycolytically derived lactate and take up extracellular lactate simultaneously (Goodwin et al., 1998; Bartelds et al., 1999; Emhoff et al., 2013a). Although some studies indicated that glycolytically derived pyruvate is preferentially shifted to lactate rather than to acetyl-CoA, pyruvate derived from exogenous lactate tends to form acetyl-CoA (Barnard et al., 1971; Chatham et al., 1999). To account for these observations, one plausible explanation is that pathways of glycolytic lactate production and oxidation of exogenous lactate are functionally separate in the cardiomyocyte, i.e., compartmentation of intracellular lactate metabolism (Barnard et al., 1971; Mowbray and Ottaway, 1973; Sinniah, 1978; Lewandowski, 1992). LDH reversibly catalyzed the conversion of pyruvate to lactate or lactate to pyruvate. Given that the equilibrium constant for LDH is far in the direction of lactate and the change in free energy is large, glycolytically derived pyruvate can easily shift to lactate, rather than enter the TCA cycle (Barnard et al., 1971; Rabinowitz and Enerback, 2020). In addition, myocardial mitochondrial abundance is greatest at the subsarcolemmal surface (Palmer et al., 1977). Therefore, when exogenous lactate enters cardiomyocytes, it is expected to be readily transported into the mitochondria and enters the TCA cycle. This explanation reconciles *in vivo* and *in vitro* observations relating to myocardial lactate generation and consumption (Wisneski et al., 1985; Gertz et al., 1988; Mazer et al., 1990; Goodwin et al., 1998; Bartelds et al., 1999), and is in keeping with the lactate shuttle theory (Brooks et al., 1999; Brooks, 2000). It is recently proposed a hypothesis that characteristics of intracellular lactate metabolism enables the uncoupling of mitochondrial energy generation from glycolysis, and confers cells with increased metabolic flexibility (Rabinowitz and Enerback, 2020). Future studies of intracellular lactate metabolism are needed to investigate the regulation of lactate uptake and efflux and assess the exact value of the compartmentation of lactate metabolism.

LACTATE METABOLISM IN MYOCARDIAL DISEASES

In order to be compatible with complicated and volatile physiological and pathological states, the heart has evolved into an "omnivore" to consume different energy substrates in varying proportions. In myocardial diseases, there are universal disorders in energy substrate utilization and metabolic flexibility. While ATP production in the myocardium is often impaired in different pathological states, there is less consensus as to what actual switches in energy substrate preference occur. Traditionally,

lactate has been regarded as an undesirable metabolite and has, accordingly, been used to as a biomarker of myocardial injury. However, later studies suggests that lactate is of greater relevance than other metabolic substrates, to the maintenance of metabolic flexibility in the metabolically unhealthy heart (Hutter et al., 1984; Lopaschuk et al., 2010; Garcia-Alvarez et al., 2014), raising a fundamental question: *is lactate in heart disease a savior or a devil?* This section will discuss lactate oxidation in the context of acute myocardial ischemia, heart failure and diabetes.

Acute Myocardial Ischemia

Acute myocardial ischemia is a common feature of acute critical cardiac events including acute coronary syndrome, cardiogenic shock, and cardiac arrest. There is usually a clear etiology and the course of disease is often brief. Sudden heart attacks lead to drastic changes of cardiac metabolic environment within a short period of time. Myocardium death is mainly caused by deprivation of oxygen and energy substrates in acute myocardial ischemia (Ong et al., 2010). While fatty acids remain the main energy substrate in the ischemic myocardium (Stanley, 2001), respiration and oxidative phosphorylation functions of mitochondria are markedly impaired during ischemia. There is evidence that the number of mitochondria is augmented in acute myocardial ischemia (Ide et al., 2001), which might represent a compensatory response for acute ischemia and hypoxia. It has been proved that the most striking metabolic switch event in the ischemic myocardium relates to increased glycolysis (Trueblood et al., 2000; Askenasy, 2001; Russell et al., 2004; Carvajal et al., 2007). However, the raw materials for glycolysis in acute myocardial ischemia are in association with the extent of ischemia. During low-flow conditions, glucose uptake and lactate release may be maintained in ischemic myocardium, and increased glycolysis depends on higher influx of glucose and increased activity of glycolytic enzymes (King and Opie, 1998a,b; Horman et al., 2012; Herzig and Shaw, 2018). When blood flow is completely interrupted, glucose is replaced by glycogenolysis (Smeele et al., 2011; Wu et al., 2011). Despite profound differences in the sources of glycolytic substrates, activating or prolonging glycolysis has been shown to be beneficial for myocardial salvage in both conditions (Vanoverschelde et al., 1994; Lochner et al., 1996; Fiolet and Baartscheer, 2000; Trueblood et al., 2000; Askenasy, 2001; Russell et al., 2004; Carvajal et al., 2007; Kim et al., 2011; Smeele et al., 2011; Wu et al., 2011; Timmermans et al., 2014; Vanoverschelde et al., 1994; Lochner et al., 1996; King and Opie, 1998a,b; Fiolet and Baartscheer, 2000; Trueblood et al., 2000; Askenasy, 2001; Russell et al., 2004; Carvajal et al., 2007; Kim et al., 2011; Smeele et al., 2011; Wu et al., 2011; Horman et al., 2012; Timmermans et al., 2014; Herzig and Shaw, 2018).

The accumulation of lactate in the ischemic myocardium provides an important source of energy; both uptake and use of lactate by the myocardium increase significantly in the acute ischemic heart (Hutter et al., 1984; Lopaschuk et al., 2010). In animal shock models, lactate deprivation is related to increased mortality, while exogenous lactate infusion is associated with myocardial salvage (Barbee et al., 2000; Revelly et al., 2005; Levy et al., 2007).

Several observational studies have demonstrated that hyperlactatemia is associated with a poor prognosis in patients with acute coronary syndrome (Lazzeri et al., 2010; Vermeulen et al., 2010; Kossaify et al., 2013). In patients who received percutaneous coronary intervention, plasma lactate measured after percutaneous coronary intervention is a reliable predictor for mortality (Lazzeri et al., 2009; Valente et al., 2012). In cardiogenic shock, the prognostic value of lactate has been controversial. Some studies identified increased lactate as an independently prognostic factor (Weil and Afifi, 1970; Chiolero et al., 2000; Koreny et al., 2002; Attana et al., 2013b), however, others did not (Geppert et al., 2006). Moreover, elevated lactate levels are positively associated with mortality in cardiac arrest (Donnino et al., 2007; Nolan et al., 2008; Cocchi et al., 2011; Andersen et al., 2013). Accordingly, a large body of research is in support of lactate as a prognostic factor in acute myocardial ischemia. It is regrettable that there is yet no consensus about the cut-off values for lactate that would be associated with worse outcome. In some recent observational studies, serial measurements of lactate have been shown to be more efficient than a single measurement for outcome prediction in acute myocardial ischemia (Attana et al., 2013a).

Based upon the evidence to date, it appears that lactate has the potential to act both as an "energy substrate" and a "prognostic factor." Numerous studies have shown benefits in preserving the function of ischemic myocardium by modifying cardiac energy substrates and increasing ATP production (Dyck et al., 2004, 2006; Ussher and Lopaschuk, 2008; Lionetti et al., 2011). Both promoting the utilization of glucose and reducing the β-oxidation of fatty acids have been proposed as anti-ischemic strategies (Stanley et al., 2005; Dyck et al., 2006). However, there is a lack of clinical evidence to support treatment with lactate supplementation or deprivation in patients with acute cardiac events. It should also be noted that observational studies do not allow to conclude on the causal relationship between lactate and clinical outcomes.

Heart Failure

Heart failure is a complex disease which represents the end-stage outcome for many cardiac and systemic diseases (Savarese and Lund, 2017). Despite the heterogeneity of etiology (Jessup and Brozena, 2003), heart failure is associated with a marked reduction in the production of energy (Hearse, 1979; Neubauer et al., 1997; Neubauer, 2007). Impaired mitochondrial structure and oxidative function have been reported in the failing heart (Casademont and Miro, 2002; Neubauer, 2007; Aubert et al., 2013; Fukushima et al., 2015). Along with these changes, alterations of energy substrates were also detected (Krahe et al., 1993; Collins-Nakai et al., 1994; Lopaschuk et al., 2010). For example, decreasing ratio of fatty acids oxidation was observed in pressure overload-induced rat failing heart as well as mouse gene-knockout failing heart models (Allard et al., 1994; Casademont and Miro, 2002; Neubauer, 2007; Bugger et al., 2010), and ketone body was reported to be an alternative fuel in advanced human heart failure (Aubert et al., 2016; Bedi, Snyder et al., 2016). Although the myocardial glucose uptake is augmented, glucose oxidation and its contribution to ATP

production is markedly decreased (Paolisso et al., 1994; Moravec et al., 1996; Funada et al., 2009; Mori et al., 2013; Zhabyeyev et al., 2013; Zhang et al., 2013). *Where does the glucose go*? In both humans and animals, there is increased flux of glycolysis (Allard et al., 1994; Degens et al., 2006; Akki et al., 2008; Symons and Abel, 2013) and plasma concentrations of lactate during heart failure (Diakos et al., 2016; Fillmore et al., 2018). It is therefore apparent that mitochondrial oxidation shifts to glycolysis as a major metabolic reprogramming event in the failing heart.

Increased glycolysis is linked to augmented production of endogenous lactate. In addition, the intracellular lactate shuttle process is inhibited by impaired activity of mLOC, manifested by the progressive impairment of PDH (Funada et al., 2009; Zhabyeyev et al., 2013; Zhang et al., 2013; Dodd et al., 2014; Diakos et al., 2016; Fillmore et al., 2018) and low expression of MCT (Gupte et al., 2014). Taken together, these events would give rise to the accumulation of intracellular lactate in the myocardium. This however, does not allow to conclude whether high level of intracellular lactate is good or bad! On the one hand, it has been indicated that intracellular lactate overload is able to trigger the influx of Na^+ and Ca^{2+}, which can induce a decrease in the systolic function of myocardium (Fiolet and Baartscheer, 2000; Jaswal et al., 2011). On the other hand, both basic science and clinical evidence have pointed toward an important role of lactate as a key energy substrate in the failing heart (Schurr et al., 1997; Chiolero et al., 2000; Luptak et al., 2005). A recent study described heart metabolomics profiling of the uptake and release of metabolites in patients with or without heart failure. This study showed that the failing heart nearly doubled lactate consumption compared to the normal heart (Murashige et al., 2020). The mRNA expression of MCT4 (which mediates the transmembrane transport of lactate) increased 2.5–3.5 times higher of its original level during myocardial injury (Zhu et al., 2013; Gabriel-Costa et al., 2015). Promoting the lactate transport from cytoplasm to mitochondria improved energy deficiency in heart failure (Wilson et al., 1998; McClelland and Brooks, 2002; Zhu et al., 2013). Furthermore, inhibition of MCT4 and hence lactate export in a cell model of heart failure led to further accumulation of intracellular lactate and increased lactate transport for mitochondrial oxidization (Cluntun et al., 2021).

Hyperlactatemia and lactic acidosis reflect an unbalanced state of lactate production and disposal. In long-term clinical practice, lactate is regarded as a risk factor of heart failure. In patients who suffer from heart failure and have elevated blood lactate, many clinicians may empirically consider pharmacotherapeutic interventions with agents that may modulate lactate metabolism, and vasodilators or positive inotropic drugs. However, systemic lactate deprivation is disadvantageous to myocardial energy supply in pathological conditions (Levy et al., 2007). Given that lactate concentrations in capillary, arterial, and venous blood are insufficient to distinguish excess lactate production from impaired lactate clearance, it would be imprudent to treat abnormal blood lactate levels in patients with heart failure.

Lactate Metabolism in Diabetic State

Adaptations to long-term diabetic state induce changes in cardiac energy substrate preference. Rising circulating fatty acids (Reaven et al., 1988; Young et al., 2002; Atkinson et al., 2003), high myocardial uptake of fatty acids (Avogaro et al., 1990; Sampson et al., 2003; Bonen et al., 2004; Peterson et al., 2008), and increased myocardial fatty acid β-oxidation (Belke et al., 2000; Aasum et al., 2003; Carley and Severson, 2005; How et al., 2007; Bugger and Abel, 2014; Riehle and Abel, 2016; Kenny and Abel, 2019) are important metabolic characteristics in diabetes. In addition, there are studies reporting hyperketonemia and high myocardial ketone body utilization in poorly controlled diabetes (Lommi et al., 1996, 1997; Kodde et al., 2007). The so-called "ketone body metabolic pathway" doesn't really exist in the cell, because ketone bodies can cross the mitochondrial membrane and the cell membrane directly through the MCTs and enter the TCA cycle (Halestrap, 2013; Felmlee et al., 2020). The flow of ketone bodies into the TCA cycle is expected to inhibit mitochondrial oxidation of glucose and lactate in cardiomyocytes. Compared to studies on fatty acid and ketone body metabolism in heart, very few studies have assessed myocardial glucose and lactate utilization in the diabetic state. It is generally accepted that acceleration of fatty acid β-oxidation and insulin resistance are related to the reduction of glucose oxidation (Randle et al., 1963; Randle, 1995, 1998; Peterson et al., 2004). With regard to myocardial lactate metabolism, several studies observed the rate of lactate efflux was greater than lactate uptake under diabetic condition (Chatham et al., 2001). Given that MCT expression in cardiomyocytes is not influenced by diabetes in rat models (Chatham et al., 1999), decreased lactate uptake might be related to the increased cytosolic NADH/NAD^+ ratio in the diabetic state (Puckett and Reddy, 1979; Ramasamy et al., 1997; Trueblood and Ramasamy, 1998; Chatham et al., 1999). Taken together, myocardial glucose and lactate metabolism are impaired on diabetic state. Impaired insulin signaling was reported to impel the deterioration of cardiac function (Abel et al., 1999; Peterson et al., 2004; Zhang et al., 2013; Byrne et al., 2016). Patients with diabetes exhibited an increased risk of heart failure, and cardiac hypertrophy is the main pathologic change of the myocardial remodeling. As discussed, substrate switch of heart failure generally appeared as a decreased fatty acid oxidation and an increased uptake of glucose and lactate (Neubauer, 2007; Casademont and Miro; 2002, Allard et al., 1994; Krishnan et al., 2009; Bugger et al., 2010). By contrast, diabetic heart failure exhibits different substrate switch—an increase in fatty acid metabolism and a decrease in glucose and lactate metabolism (Bugger and Abel, 2014; Riehle and Abel, 2016; Kenny and Abel, 2019). It is also intriguing that these divergent cardiac energy substrate preferences result in similar myocardial remodeling.

Metformin is the most widely used oral agent for the management of type 2 diabetes. In the landmark UKPDS study, the use of metformin was reported to reduce the risk of myocardial infarction by 39% (No Authors listed., 1998). Metformin is associated with a modest increase plasma lactate levels, but the risk of lactate acidosis is rare (Abbasi et al., 2000; Liu et al., 2009; Shen et al., 2012; Koren et al., 2017). Metformin does not appear to affect myocardial lactate utilization, but has been shown to reduce the intracellular lactate shuttle and increase lactate accumulation (Madiraju et al., 2014;

Duca et al., 2015; Lu et al., 2017). Given that metformin is associated with increased lactate production, and tissue hypoxia is always present during heart failure. Metformin has previously been believed to increase the risk of lactic acidosis in heart failure patients. However, in recent years, metformin has been exhibited to be safe and effective in patients with heart failure in several large retrospective studies (Misbin et al., 1998; Aguilar et al., 2011). Based on these studies, metformin has been recommended for patients with diabetes mellitus and chronic heart failure (Eurich et al., 2005, 2013). Taken together, the effects of metformin on lactate metabolism do not outweigh its the benefits in diabetic cardiomyopathy. But we have to pay more attention to metformin-associated lactic acidosis (MALA), a symptom that may occur in the clinic. The exact mechanism of MALA is still unknown, but it would be necessary to elevated blood metformin concentration and secondary obstacles of lactate production and clearance (Lucis, 1983; Owen et al., 2000; Almirall et al., 2008; Frid et al., 2010; Bridges et al., 2014). As these secondary events may be unpredictable and heterogeneous, current clinical application of metformin may be too conservative. Given that fatal consequence of MALA, metformin must be used with caution, particularly in patients with circulatory dysfunction (Buse et al., 2016).

CONCLUSION

In the pursuit of an understanding of myocardial metabolism, lactate was once considered as a metabolic waste, and the metamorphosis from "ugly duckling" to "white swan" was full of frustration and ordeals. Up to time now, it is apparent that lactate has multiple identities in myocardial metabolism, including energy substrate, metabolite, signal molecule, and prognostic factor. Cardiac lactate metabolism is a dynamic process that can rapidly shift to adapt to alterations in cardiac energy requirements or changing environment. Lactate is also very important as an energy substrate in acute myocardial ischemia, heart failure, and diabetic state, and abnormal myocardial lactate metabolism is closely related to diseases. Characterization of the lactate metabolic profile of myocardium in physiological and pathological conditions may help direct future pharmacological therapies to harmonize the metabolic flexibility of the heart.

AUTHOR CONTRIBUTIONS

SD, LQ, ZC, CC, KW, and XZ were involved in writing of the manuscript. SH, XZ, and TW involved in the conception. XZ and TW was involved in the conception, design, and the coordination of the study. SD, LQ, and ZC were involved in the picture drawing. SD, LQ, ZC, CC, KW, SH, XZ, and TW critically reviewed the manuscript and have approved the publication of this final version of the manuscript. XZ and TW are the guarantors of this work. All authors contributed to the article and approved the submitted version.

ACKNOWLEDGMENTS

The authors would like to thank all of the research participants, scholars, and funding agencies who have contributed to the research cited in this manuscript.

REFERENCES

Aasum, E., Hafstad, A. D., Severson, D. L., and Larsen, T. S. (2003). Age-dependent changes in metabolism, contractile function, and ischemic sensitivity in hearts from db/db mice. *Diabetes* 52, 434–441. doi: 10.2337/diabetes.52.2.434

Abbasi, A. A., Kasmikha, R., and Sotingeanu, D. G. (2000). Metformin-induced lacticacidemia in patients with type 2 diabetes mellitus. *Endocr. Pract.* 6, 442–446. doi: 10.4158/EP.6.6.442

Abel, E. D., Kaulbach, H. C., Tian, R., Hopkins, J. C., Duffy, J., Doetschman, T., et al. (1999). Cardiac hypertrophy with preserved contractile function after selective deletion of GLUT4 from the heart. *J. Clin. Invest.* 104, 1703–1714. doi: 10.1172/JCI7605

Aguilar, D., Chan, W., Bozkurt, B., Ramasubbu, K., and Deswal, A. (2011). Metformin use and mortality in ambulatory patients with diabetes and heart failure. *Circ. Heart Fail.* 4, 53–58. doi: 10.1161/CIRCHEARTFAILURE.110.952556

Akki, A., Smith, K., and Seymour, A. M. (2008). Compensated cardiac hypertrophy is characterised by a decline in palmitate oxidation. *Mol. Cell. Biochem.* 311, 215–224. doi: 10.1007/s11010-008-9711-y

Allard, M. F., Schonekess, B. O., Henning, S. L., English, D. R., and Lopaschuk, G. D. (1994). Contribution of oxidative metabolism and glycolysis to ATP production in hypertrophied hearts. *Am. J. Physiol.* 267, H742–H750. doi: 10.1152/ajpheart.1994.267.2.H742

Almirall, J., Briculle, M., and Gonzalez-Clemente, J. M. (2008). Metformin-associated lactic acidosis in type 2 diabetes mellitus: incidence and presentation in common clinical practice. *Nephrol. Dial. Transplant.* 23, 2436–2438. doi: 10.1093/ndt/gfn152

Andersen, L. W., Mackenhauer, J., Roberts, J. C., Berg, K. M., Cocchi, M. N., and Donnino, M. W. (2013). Etiology and therapeutic approach to elevated lactate levels. *Mayo Clin. Proc.* 88, 1127–1140. doi: 10.1016/j.mayocp.2013.06.012

Askenasy, N. (2001). Glycolysis protects sarcolemmal membrane integrity during total ischemia in the rat heart. *Basic Res. Cardiol.* 96, 612–622. doi: 10.1007/s003950170013

Atkinson, L. L., Kozak, R., Kelly, S. E., Onay Besikci, A., Russell, J. C., and Lopaschuk, G. D. (2003). Potential mechanisms and consequences of cardiac triacylglycerol accumulation in insulin-resistant rats. *Am. J. Physiol. Endocrinol. Metab.* 284, E923–E930. doi: 10.1152/ajpendo.00360.2002

Atlante, A., de Bari, L., Bobba, A., Marra, E., and Passarella, S. (2007). Transport and metabolism of L-lactate occur in mitochondria from cerebellar granule cells and are modified in cells undergoing low potassium dependent apoptosis. *Biochim. Biophys. Acta* 1767, 1285–1299. doi: 10.1016/j.bbabio.2007.08.003

Attana, P., Lazzeri, C., Chiostri, M., Gensini, G. F., and Valente, S. (2013a). Dynamic behavior of lactate values in venous-arterial extracorporeal membrane oxygenation for refractory cardiac arrest. *Resuscitation* 84, e145–6. doi: 10.1016/j.resuscitation.2013.07.007

Attana, P., Lazzeri, C., Chiostri, M., Picariello, C., Gensini, G. F., and Valente, S. (2013b). Strong-ion gap approach in patients with cardiogenic shock following ST-elevation myocardial infarction. *Acute Card. Care* 15, 58–62. doi: 10.3109/17482941.2013.776691

Aubert, G., Martin, O. J., Horton, J. L., Lai, L., Vega, R. B., Leone, T. C., et al. (2016). The Failing Heart Relies on Ketone Bodies as a Fuel. *Circulation* 133, 698–705. doi: 10.1161/CIRCULATIONAHA.115.017355

Aubert, G., Vega, R. B., and Kelly, D. P. (2013). Perturbations in the gene regulatory pathways controlling mitochondrial energy production in the failing heart. *Biochim. Biophys. Acta* 1833, 840–847. doi: 10.1016/j.bbamcr.2012.08.015

Avogaro, A., Nosadini, R., Doria, A., Fioretto, P., Velussi, M., Vigorito, C., et al. (1990). Myocardial metabolism in insulin-deficient diabetic humans without coronary artery disease. *Am. J. Physiol.* 258, E606–E618. doi: 10.1152/ajpendo.1990.258.4.E606

Barbee, R. W., Kline, J. A., and Watts, J. A. (2000). Depletion of lactate by dichloroacetate reduces cardiac efficiency after hemorrhagic shock. *Shock* 14, 208–214. doi: 10.1097/00024382-200014020-00022

Barnard, R. J., Edgerton, V. R., Furukawa, T., and Peter, J. B. (1971). Histochemical, biochemical, and contractile properties of red, white, and intermediate fibers. *Am. J. Physiol.* 220, 410–414. doi: 10.1152/ajplegacy.1971.220.2.410

Bartelds, B., Knoester, H., Beaufort-Krol, G. C., Smid, G. B., Takens, J., Zijlstra, W. G., et al. (1999). Myocardial lactate metabolism in fetal and newborn lambs. *Circulation* 99, 1892–1897. doi: 10.1161/01.cir.99.14.1892

Bedi, K. C. Jr., Snyder, N. W., Brandimarto, J., Aziz, M., Mesaros, C., Worth, A. J., et al. (2016). Evidence for Intramyocardial Disruption of Lipid Metabolism and Increased Myocardial Ketone Utilization in Advanced Human Heart Failure. *Circulation* 133, 706–716. doi: 10.1161/CIRCULATIONAHA.115.017545

Belke, D. D., Larsen, T. S., Gibbs, E. M., and Severson, D. L. (2000). Altered metabolism causes cardiac dysfunction in perfused hearts from diabetic (db/db) mice. *Am. J. Physiol. Endocrinol. Metab.* 279, E1104–E1113. doi: 10.1152/ajpendo.2000.279.5.E1104

Beloukas, A. I., Magiorkinis, E., Tsoumakas, T. L., Kosma, A. G., and Diamantis, A. (2013). Milestones in the history of research on cardiac energy metabolism. *Can. J. Cardiol.* 29, 1504–1511. doi: 10.1016/j.cjca.2012.10.008

Bergman, B. C., Butterfield, G. E., Wolfel, E. E., Lopaschuk, G. D., Casazza, G. A., Horning, M. A., et al. (1999a). Muscle net glucose uptake and glucose kinetics after endurance training in men. *Am. J. Physiol.* 277, E81–E92. doi: 10.1152/ajpendo.1999.277.1.E81

Bergman, B. C., Horning, M. A., Casazza, G. A., Wolfel, E. E., Butterfield, G. E., and Brooks, G. A. (2000). Endurance training increases gluconeogenesis during rest and exercise in men. *Am. J. Physiol. Endocrinol. Metab.* 278, E244–E251. doi: 10.1152/ajpendo.2000.278.2.E244

Bergman, B. C., Tsvetkova, T., Lowes, B., and Wolfel, E. E. (2009). Myocardial glucose and lactate metabolism during rest and atrial pacing in humans. *J. Physiol.* 587, 2087–2099. doi: 10.1113/jphysiol.2008.168286

Bergman, B. C., Wolfel, E. E., Butterfield, G. E., Lopaschuk, G. D., Casazza, G. A., Horning, M. A., et al. (1999b). Active muscle and whole body lactate kinetics after endurance training in men. *J. Appl. Physiol.* 87, 1684–1696. doi: 10.1152/jappl.1999.87.5.1684

Bing, R. J. (1954). The metabolism of the heart. *Harvey Lect.* 50, 27–70.

Bing, R. J., Vandam, L. D., Gregoire, F., Handelsman, J. C., Goodale, W. T., Eckenhoff, J. E., et al. (1947). Catheterization of the coronary sinus and the middle cardiac vein in man. *Proc. Soc. Exp. Biol. Med.* 66:239. doi: 10.3181/00379727-66-16049p

Bonen, A., Parolin, M. L., Steinberg, G. R., Calles-Escandon, J., Tandon, N. N., Glatz, J. F., et al. (2004). Triacylglycerol accumulation in human obesity and type 2 diabetes is associated with increased rates of skeletal muscle fatty acid transport and increased sarcolemmal FAT/CD36. *FASEB J.* 18, 1144–1146. doi: 10.1096/fj.03-1065fje

Brandt, R. B., Laux, J. E., Spainhour, S. E., and Kline, E. S. (1987). Lactate dehydrogenase in rat mitochondria. *Arch. Biochem. Biophys.* 259, 412–422. doi: 10.1016/0003-9861(87)90507-8

Bridges, H. R., Jones, A. J., Pollak, M. N., and Hirst, J. (2014). Effects of metformin and other biguanides on oxidative phosphorylation in mitochondria. *Biochem. J.* 462, 475–487. doi: 10.1042/BJ20140620

Brooks, G. A. (2000). Intra- and extra-cellular lactate shuttles. *Med. Sci. Sports Exerc.* 32, 790–799. doi: 10.1097/00005768-200004000-00011

Brooks, G. A. (2018). The Science and Translation of Lactate Shuttle Theory. *Cell. Metab.* 27, 757–785. doi: 10.1016/j.cmet.2018.03.008

Brooks, G. A., and Donovan, C. M. (1983). Effect of endurance training on glucose kinetics during exercise. *Am. J. Physiol.* 244, E505–E512. doi: 10.1152/ajpendo.1983.244.5.E505

Brooks, G. A., and Gaesser, G. A. (1980). End points of lactate and glucose metabolism after exhausting exercise. *J. Appl. Physiol. Respir. Environ. Exerc. Physiol.* 49, 1057–1069. doi: 10.1152/jappl.1980.49.6.1057

Brooks, G. A., and White, T. P. (1978). Determination of metabolic and heart rate responses of rats to treadmill exercise. *J. Appl. Physiol. Respir. Environ. Exerc. Physiol.* 45, 1009–1015. doi: 10.1152/jappl.1978.45.6.1009

Brooks, G. A., Bissell, M. J., and Bassham, J. A. (1977). Ion-retardation desalting of blood and other animal tissues for separation of soluble metabolites by two-dimensional chromatography. *Anal. Biochem.* 83, 580–588. doi: 10.1016/0003-2697(77)90061-6

Brooks, G. A., Brauner, K. E., and Cassens, R. G. (1973). Glycogen synthesis and metabolism of lactic acid after exercise. *Am. J. Physiol.* 224, 1162–1166. doi: 10.1152/ajplegacy.1973.224.5.1162

Brooks, G. A., Donovan, C. M., and White, T. P. (1984). Estimation of anaerobic energy production and efficiency in rats during exercise. *J. Appl. Physiol. Respir. Environ. Exerc. Physiol.* 56, 520–525. doi: 10.1152/jappl.1984.56.2.520

Brooks, G. A., Dubouchaud, H., Brown, M., Sicurello, J. P., and Butz, C. E. (1999). Role of mitochondrial lactate dehydrogenase and lactate oxidation in the intracellular lactate shuttle. *Proc. Natl. Acad. Sci. U. S. A.* 96, 1129–1134. doi: 10.1073/pnas.96.3.1129

Bugger, H., and Abel, E. D. (2014). Molecular mechanisms of diabetic cardiomyopathy. *Diabetologia* 57, 660–671. doi: 10.1007/s00125-014-3171-6

Bugger, H., Schwarzer, M., Chen, D., Schrepper, A., Amorim, P. A., Schoepe, M., et al. (2010). Proteomic remodelling of mitochondrial oxidative pathways in pressure overload-induced heart failure. *Cardiovasc. Res.* 85, 376–384. doi: 10.1093/cvr/cvp344

Buse, J. B., DeFronzo, R. A., Rosenstock, J., Kim, T., Burns, C., Skare, S., et al. (2016). The Primary Glucose-Lowering Effect of Metformin Resides in the Gut, Not the Circulation: results From Short-term Pharmacokinetic and 12-Week Dose-Ranging Studies. *Diabetes Care* 39, 198–205. doi: 10.2337/dc15-0488

Byrne, N. J., Levasseur, J., Sung, M. M., Masson, G., Boisvenue, J., Young, M. E., et al. (2016). Normalization of cardiac substrate utilization and left ventricular hypertrophy precede functional recovery in heart failure regression. *Cardiovasc. Res.* 110, 249–257. doi: 10.1093/cvr/cvw051

Carley, A. N., and Severson, D. L. (2005). Fatty acid metabolism is enhanced in type 2 diabetic hearts. *Biochim. Biophys. Acta* 1734, 112–126. doi: 10.1016/j.bbalip.2005.03.005

Carvajal, K., Zarrinpashneh, E., Szarszoi, O., Joubert, F., Athea, Y., Mateo, P., et al. (2007). Dual cardiac contractile effects of the alpha2-AMPK deletion in low-flow ischemia and reperfusion. *Am. J. Physiol. Heart Circ. Physiol.* 292, H3136–H3147. doi: 10.1152/ajpheart.00683.2006

Casademont, J., and Miro, O. (2002). Electron transport chain defects in heart failure. *Heart Fail. Rev.* 7, 131–139. doi: 10.1023/a:1015372407647

Cerovic, O., Golubovic, V., Spec-Marn, A., Kremzar, B., and Vidmar, G. (2003). Relationship between injury severity and lactate levels in severely injured patients. *Intensive Care Med.* 29, 1300–1305. doi: 10.1007/s00134-003-1753-8

Chatham, J. C., Des Rosiers, C., and Forder, J. R. (2001). Evidence of separate pathways for lactate uptake and release by the perfused rat heart. *Am. J. Physiol. Endocrinol. Metab.* 281, E794–E802. doi: 10.1152/ajpendo.2001.281.4.E794

Chatham, J. C., Gao, Z. P., Bonen, A., and Forder, J. R. (1999). Preferential inhibition of lactate oxidation relative to glucose oxidation in the rat heart following diabetes. *Cardiovasc. Res.* 43, 96–106. doi: 10.1016/s0008-6363(99)00056-5

Chen, Y. J., Mahieu, N. G., Huang, X., Singh, M., Crawford, P. A., Johnson, S. L., et al. (2016). Lactate metabolism is associated with mammalian mitochondria. *Nat. Chem. Biol.* 12, 937–943. doi: 10.1038/nchembio.2172

Chiolero, R. L., Revelly, J. P., Leverve, X., Gersbach, P., Cayeux, M. C., Berger, M. M., et al. (2000). Effects of cardiogenic shock on lactate and glucose metabolism after heart surgery. *Crit. Care Med.* 28, 3784–3791. doi: 10.1097/00003246-200012000-00002

Cluntun, A. A., Badolia, R., Lettlova, S., Parnell, K. M., Shankar, T. S., Diakos, N. A., et al. (2021). The pyruvate-lactate axis modulates cardiac hypertrophy and heart failure. *Cell Metab.* 33, 629–648.e10. doi: 10.1016/j.cmet.2020.12.003

Cocchi, M. N., Miller, J., Hunziker, S., Carney, E., Salciccioli, J., Farris, S., et al. (2011). The association of lactate and vasopressor need for mortality prediction in survivors of cardiac arrest. *Minerva. Anestesiol.* 77, 1063–1071.

Collins-Nakai, R. L., Noseworthy, D., and Lopaschuk, G. D. (1994). Epinephrine increases ATP production in hearts by preferentially increasing glucose metabolism. *Am. J. Physiol.* 267, H1862–H1871. doi: 10.1152/ajpheart.1994.267.5.H1862

De Bari, L., Atlante, A., Valenti, D., and Passarella, S. (2004). Partial reconstruction of in vitro gluconeogenesis arising from mitochondrial l-lactate uptake/metabolism and oxaloacetate export via novel L-lactate translocators. *Biochem. J.* 380, 231–242. doi: 10.1042/BJ20031981

Degens, H., de Brouwer, K. F., Gilde, A. J., Lindhout, M., Willemsen, P. H., Janssen, B. J., et al. (2006). Cardiac fatty acid metabolism is preserved in the compensated hypertrophic rat heart. *Basic Res. Cardiol.* 101, 17–26. doi: 10.1007/s00395-005-0549-0

Depocas, F., Minaire, Y., and Chatonnet, J. (1969). Rates of formation and oxidation of lactic acid in dogs at rest and during moderate exercise. *Can. J. Physiol. Pharmacol.* 47, 603–610. doi: 10.1139/y69-106

Diakos, N. A., Navankasattusas, S., Abel, E. D., Rutter, J., McCreath, L., Ferrin, P., et al. (2016). Evidence of Glycolysis Up-Regulation and Pyruvate Mitochondrial Oxidation Mismatch During Mechanical Unloading of the Failing Human Heart: implications for Cardiac Reloading and Conditioning. *JACC Basic Transl. Sci.* 1, 432–444. doi: 10.1016/j.jacbts.2016.06.009

Dodd, M. S., Atherton, H. J., Carr, C. A., Stuckey, D. J., West, J. A., Griffin, J. L., et al. (2014). Impaired in vivo mitochondrial Krebs cycle activity after myocardial infarction assessed using hyperpolarized magnetic resonance spectroscopy. *Circ. Cardiovasc. Imaging* 7, 895–904. doi: 10.1161/CIRCIMAGING.114.001857

Donnino, M. W., Miller, J., Goyal, N., Loomba, M., Sankey, S. S., Dolcourt, B., et al. (2007). Effective lactate clearance is associated with improved outcome in post-cardiac arrest patients. *Resuscitation* 75, 229–234. doi: 10.1016/j.resuscitation.2007.03.021

Donovan, C. M., and Brooks, G. A. (1983). Endurance training affects lactate clearance, not lactate production. *Am. J. Physiol.* 244, E83–E92. doi: 10.1152/ajpendo.1983.244.1.E83

Drake, A. J., Haines, J. R., and Noble, M. I. (1980). Preferential uptake of lactate by the normal myocardium in dogs. *Cardiovasc. Res.* 14, 65–72. doi: 10.1093/cvr/14.2.65

Duca, F. A., Cote, C. D., Rasmussen, B. A., Zadeh-Tahmasebi, M., Rutter, G. A., Filippi, B. M., et al. (2015). Metformin activates a duodenal Ampk-dependent pathway to lower hepatic glucose production in rats. *Nat. Med.* 21, 506–511. doi: 10.1038/nm.3787

Dunn, A., Katz, J., Golden, S., and Chenoweth, M. (1976). Estimation of glucose turnover and recycling in rabbits using various [3H, 14C]glucose labels. *Am. J. Physiol.* 230, 1159–1162. doi: 10.1152/ajplegacy.1976.230.4.1159

Dyck, J. R., Cheng, J. F., Stanley, W. C., Barr, R., Chandler, M. P., Brown, S., et al. (2004). Malonyl coenzyme a decarboxylase inhibition protects the ischemic heart by inhibiting fatty acid oxidation and stimulating glucose oxidation. *Circ. Res.* 94, e78–84. doi: 10.1161/01.RES.0000129255.19569.8f

Dyck, J. R., Hopkins, T. A., Bonnet, S., Michelakis, E. D., Young, M. E., Watanabe, M., et al. (2006). Absence of malonyl coenzyme A decarboxylase in mice increases cardiac glucose oxidation and protects the heart from ischemic injury. *Circulation* 114, 1721–1728. doi: 10.1161/CIRCULATIONAHA.106.642009

Emhoff, C. A., Messonnier, L. A., Horning, M. A., Fattor, J. A., Carlson, T. J., and Brooks, G. A. (2013b). Gluconeogenesis and hepatic glycogenolysis during exercise at the lactate threshold. *J. Appl. Physiol.* 114, 297–306. doi: 10.1152/japplphysiol.01202.2012

Emhoff, C. A., Messonnier, L. A., Horning, M. A., Fattor, J. A., Carlson, T. J., and Brooks, G. A. (2013a). Direct and indirect lactate oxidation in trained and untrained men. *J. Appl. Physiol.* 115, 829–838. doi: 10.1152/japplphysiol.00538.2013

Eurich, D. T., Majumdar, S. R., McAlister, F. A., Tsuyuki, R. T., and Johnson, J. A. (2005). Improved clinical outcomes associated with metformin in patients with diabetes and heart failure. *Diabetes Care* 28, 2345–2351. doi: 10.2337/diacare.28.10.2345

Eurich, D. T., Weir, D. L., Majumdar, S. R., Tsuyuki, R. T., Johnson, J. A., Tjosvold, L., et al. (2013). Comparative safety and effectiveness of metformin in patients with diabetes mellitus and heart failure: systematic review of observational studies involving 34,000 patients. *Circ. Heart Fail.* 6, 395–402. doi: 10.1161/CIRCHEARTFAILURE.112.000162

Evans, C. L. (1914). The effect of glucose on the gaseous metabolism of the isolated mammalian heart. *J. Physiol.* 47, 407–418. doi: 10.1113/jphysiol.1914.sp001633

Felmlee, M. A., Jones, R. S., Rodriguez-Cruz, V., Follman, K. E., and Morris, M. E. (2020). Monocarboxylate Transporters (SLC16): function, Regulation, and Role in Health and Disease. *Pharmacol. Rev.* 72, 466–485. doi: 10.1124/pr.119.018762

Fillmore, N., Levasseur, J. L., Fukushima, A., Wagg, C. S., Wang, W., Dyck, J. R. B., et al. (2018). Uncoupling of glycolysis from glucose oxidation accompanies the development of heart failure with preserved ejection fraction. *Mol. Med.* 24:3. doi: 10.1186/s10020-018-0005-x

Fiolet, J. W., and Baartscheer, A. (2000). Cellular calcium homeostasis during ischemia; a thermodynamic approach. *Cardiovasc. Res.* 45, 100–106. doi: 10.1016/s0008-6363(99)00294-1

Frid, A., Sterner, G. N., Londahl, M., Wiklander, C., Cato, A., Vinge, E., et al. (2010). Novel assay of metformin levels in patients with type 2 diabetes and varying levels of renal function: clinical recommendations. *Diabetes Care* 33, 1291–1293. doi: 10.2337/dc09-1284

Fukushima, A., Milner, K., Gupta, A., and Lopaschuk, G. D. (2015). Myocardial Energy Substrate Metabolism in Heart Failure : from Pathways to Therapeutic Targets. *Curr. Pharm. Des.* 21, 3654–3664. doi: 10.2174/1381612821666150710150445

Funada, J., Betts, T. R., Hodson, L., Humphreys, S. M., Timperley, J., Frayn, K. N., et al. (2009). Substrate utilization by the failing human heart by direct quantification using arterio-venous blood sampling. *PLoS One* 4:e7533. doi: 10.1371/journal.pone.0007533

Gabriel-Costa, D., da Cunha, T. F., Bechara, L. R., Fortunato, R. S., Bozi, L. H., Coelho Mde, A., et al. (2015). Lactate up-regulates the expression of lactate oxidation complex-related genes in left ventricular cardiac tissue of rats. *PLoS One* 10:e0127843. doi: 10.1371/journal.pone.0127843

Garcia, C. K., Goldstein, J. L., Pathak, R. K., Anderson, R. G., and Brown, M. S. (1994). Molecular characterization of a membrane transporter for lactate, pyruvate, and other monocarboxylates: implications for the Cori cycle. *Cell* 76, 865–873. doi: 10.1016/0092-8674(94)90361-1

Garcia-Alvarez, M., Marik, P., and Bellomo, R. (2014). Stress hyperlactataemia: present understanding and controversy. *Lancet Diabetes Endocrinol.* 2, 339–347. doi: 10.1016/S2213-8587(13)70154-2

Geppert, A., Dorninger, A., Delle-Karth, G., Zorn, G., Heinz, G., and Huber, K. (2006). Plasma concentrations of interleukin-6, organ failure, vasopressor support, and successful coronary revascularization in predicting 30-day mortality of patients with cardiogenic shock complicating acute myocardial infarction. *Crit. Care Med.* 34, 2035–2042. doi: 10.1097/01.CCM.0000228919.33620.D9

Gertz, E. W., Wisneski, J. A., Neese, R., Bristow, J. D., Searle, G. L., and Hanlon, J. T. (1981). Myocardial lactate metabolism: evidence of lactate release during net chemical extraction in man. *Circulation* 63, 1273–1279. doi: 10.1161/01.cir.63.6.1273

Gertz, E. W., Wisneski, J. A., Stanley, W. C., and Neese, R. A. (1988). Myocardial substrate utilization during exercise in humans. Dual carbon-labeled carbohydrate isotope experiments. *J. Clin. Invest.* 82, 2017–2025. doi: 10.1172/JCI113822

Gh, V. K. (2006). [The 100(th) anniversary of "The Conduction System of the Mammalian Heart" by Sunao Tawara]. *Herzschrittmacherther. Elektrophysiol.* 17, 140–145. doi: 10.1007/s00399-006-0525-x

Gizak, A., McCubrey, J. A., and Rakus, D. (2020). Cell-to-cell lactate shuttle operates in heart and is important in age-related heart failure. *Aging* 12, 3388–3406. doi: 10.18632/aging.102818

Glancy, B., Hartnell, L. M., Combs, C. A., Femnou, A., Sun, J., Murphy, E., et al. (2017). Power Grid Protection of the Muscle Mitochondrial Reticulum. *Cell. Rep.* 19, 487–496. doi: 10.1016/j.celrep.2017.03.063

Glenn, T. C., Martin, N. A., Horning, M. A., McArthur, D. L., Hovda, D. A., Vespa, P., et al. (2015). Lactate: brain fuel in human traumatic brain injury: a comparison with normal healthy control subjects. *J. Neurotrauma.* 32, 820–832. doi: 10.1089/neu.2014.3483

Goodwin, G. W., Taylor, C. S., and Taegtmeyer, H. (1998). Regulation of energy metabolism of the heart during acute increase in heart work. *J. Biol. Chem.* 273, 29530–29539. doi: 10.1074/jbc.273.45.29530

Gupte, A. A., Hamilton, D. J., Cordero-Reyes, A. M., Youker, K. A., Yin, Z., Estep, J. D., et al. (2014). Mechanical unloading promotes myocardial energy recovery in human heart failure. *Circ. Cardiovasc. Genet.* 7, 266–276. doi: 10.1161/CIRCGENETICS.113.000404

Halestrap, A. P. (2013). Monocarboxylic acid transport. *Compr. Physiol.* 3, 1611–1643. doi: 10.1002/cphy.c130008

Hashimoto, T., Hussien, R., and Brooks, G. A. (2006). Colocalization of MCT1, CD147, and LDH in mitochondrial inner membrane of L6 muscle cells: evidence of a mitochondrial lactate oxidation complex. *Am. J. Physiol. Endocrinol. Metab.* 290, E1237–E1244. doi: 10.1152/ajpendo.00594.2005

Hashimoto, T., Hussien, R., Cho, H. S., Kaufer, D., and Brooks, G. A. (2008). Evidence for the mitochondrial lactate oxidation complex in rat neurons: demonstration of an essential component of brain lactate shuttles. *PLoS One* 3:e2915. doi: 10.1371/journal.pone.0002915

Hashimoto, T., Hussien, R., Oommen, S., Gohil, K., and Brooks, G. A. (2007). Lactate sensitive transcription factor network in L6 cells: activation of MCT1 and mitochondrial biogenesis. *FASEB J.* 21, 2602–2612. doi: 10.1096/fj.07-8174com

Hearse, D. J. (1979). Oxygen deprivation and early myocardial contractile failure: a reassessment of the possible role of adenosine triphosphate. *Am. J. Cardiol.* 44, 1115–1121. doi: 10.1016/0002-9149(79)90177-2

Herzig, S., and Shaw, R. J. (2018). AMPK: guardian of metabolism and mitochondrial homeostasis. *Nat. Rev. Mol. Cell. Biol.* 19, 121–135. doi: 10.1038/nrm.2017.95

Hooker, A. M., and Baldwin, K. M. (1979). Substrate oxidation specificity in different types of mammalian muscle. *Am. J. Physiol.* 236, C66–C69. doi: 10.1152/ajpcell.1979.236.1.C66

Horman, S., Beauloye, C., Vanoverschelde, J. L., and Bertrand, L. (2012). AMP-activated protein kinase in the control of cardiac metabolism and remodeling. *Curr. Heart Fail. Rep.* 9, 164–173. doi: 10.1007/s11897-012-0102-z

How, O. J., Larsen, T. S., Hafstad, A. D., Khalid, A., Myhre, E. S., Murray, A. J., et al. (2007). Rosiglitazone treatment improves cardiac efficiency in hearts from diabetic mice. *Arch. Physiol. Biochem.* 113, 211–220. doi: 10.1080/13813450701783281

Hutter, J. F., Schweickhardt, C., Piper, H. M., and Spieckermann, P. G. (1984). Inhibition of fatty acid oxidation and decrease of oxygen consumption of working rat heart by 4-bromocrotonic acid. *J. Mol. Cell. Cardiol.* 16, 105–108. doi: 10.1016/s0022-2828(84)80718-x

Ide, T., Tsutsui, H., Hayashidani, S., Kang, D., Suematsu, N., Nakamura, K., et al. (2001). Mitochondrial DNA damage and dysfunction associated with oxidative stress in failing hearts after myocardial infarction. *Circ. Res.* 88, 529–535. doi: 10.1161/01.res.88.5.529

Jacobs, R. A., Meinild, A. K., Nordsborg, N. B., and Lundby, C. (2013). Lactate oxidation in human skeletal muscle mitochondria. *Am. J. Physiol. Endocrinol. Metab.* 304, E686–E694. doi: 10.1152/ajpendo.00476.2012

Jaswal, J. S., Keung, W., Wang, W., Ussher, J. R., and Lopaschuk, G. D. (2011). Targeting fatty acid and carbohydrate oxidation–a novel therapeutic intervention in the ischemic and failing heart. *Biochim. Biophys. Acta* 1813, 1333–1350. doi: 10.1016/j.bbamcr.2011.01.015

Jessup, M., and Brozena, S. (2003). Heart failure. *N. Engl. J. Med.* 348, 2007–2018. doi: 10.1056/NEJMra021498

Katz, J., Okajima, F., Chenoweth, M., and Dunn, A. (1981). The determination of lactate turnover in vivo with 3H- and 14C-labelled lactate. The significance of sites of tracer administration and sampling. *Biochem. J.* 194, 513–524. doi: 10.1042/bj1940513

Kenny, H. C., and Abel, E. D. (2019). Heart Failure in Type 2 Diabetes Mellitus. *Circ. Res.* 124, 121–141. doi: 10.1161/CIRCRESAHA.118.311371

Keul, J., Doll, E., Steim, H., Fleer, U., and Reindell, H. (1965a). [on Metabolism of the Human Heart. 3. Oxidative Metabolism of the Human Heart in Different Work Conditions]. *Pflugers Arch. Gesamte, Physiol. Menschen. Tiere.* 282, 43–53.

Keul, J., Doll, E., Steim, H., Homburger, H., Kern, H., and Reindell, H. (1965b). [on Metabolism of the Human Heart. I. Substrate Supply of the Healthy Human Heart during Rest, during and after Physical Work]. *Pflugers Arch. Gesamte. Physiol. Menschen. Tiere.* 282, 1–27.

Khosravani, H., Shahpori, R., Stelfox, H. T., Kirkpatrick, A. W., and Laupland, K. B. (2009). Occurrence and adverse effect on outcome of hyperlactatemia in the critically ill. *Crit. Care* 13:R90. doi: 10.1186/cc7918

Kim, A. S., Miller, E. J., Wright, T. M., Li, J., Qi, D., Atsina, K., et al. (2011). A small molecule AMPK activator protects the heart against ischemia-reperfusion injury. *J. Mol. Cell. Cardiol.* 51, 24–32. doi: 10.1016/j.yjmcc.2011.03.003

King, L. M., and Opie, L. H. (1998a). Glucose and glycogen utilisation in myocardial ischemia–changes in metabolism and consequences for the myocyte. *Mol. Cell. Biochem.* 180, 3–26. doi: 10.1007/978-1-4615-5687-9_1

King, L. M., and Opie, L. H. (1998b). Glucose delivery is a major determinant of glucose utilisation in the ischemic myocardium with a residual coronary flow. *Cardiovasc. Res.* 39, 381–392. doi: 10.1016/s0008-6363(98)00100-x

Kirkwood, S. P., Munn, E. A., and Brooks, G. A. (1986). Mitochondrial reticulum in limb skeletal muscle. *Am. J. Physiol.* 251, C395–C402. doi: 10.1152/ajpcell.1986.251.3.C395

Kline, E. S., Brandt, R. B., Laux, J. E., Spainhour, S. E., Higgins, E. S., Rogers, K. S., et al. (1986). Localization of L-lactate dehydrogenase in mitochondria. *Arch. Biochem. Biophys.* 246, 673–680. doi: 10.1016/0003-9861(86)90323-1

Kodde, I. F., van der Stok, J., Smolenski, R. T., and de Jong, J. W. (2007). Metabolic and genetic regulation of cardiac energy substrate preference. *Comp. Biochem. Physiol. A Mol. Integr. Physiol.* 146, 26–39. doi: 10.1016/j.cbpa.2006.09.014

Koren, S., Zilberman-Itskovich, S., Koren, R., Doenyas-Barak, K., and Golik, A. (2017). Metformin Does Not Induce Hyperlactatemia in Patients Admitted to Internal Medicine Ward. *Isr. Med. Assoc. J.* 19, 300–303.

Koreny, M., Karth, G. D., Geppert, A., Neunteufl, T., Priglinger, U., Heinz, G., et al. (2002). Prognosis of patients who develop acute renal failure during the first 24 hours of cardiogenic shock after myocardial infarction. *Am. J. Med.* 112, 115–119. doi: 10.1016/s0002-9343(01)01070-1

Kossaify, A., Garcia, A., Succar, S., Ibrahim, A., Moussallem, N., Kossaify, M., et al. (2013). Perspectives on the value of biomarkers in acute cardiac care and implications for strategic management. *Biomark Insights* 8, 115–126. doi: 10.4137/BMI.S12703

Krahe, T., Schindler, R., Neubauer, S., Ertl, G., Horn, M., and Lackner, K. (1993). [31P-cardio-MR-spectroscopy in myocardial insufficiency]. *Rofo* 159, 64–70. doi: 10.1055/s-2008-1032723

Krishnan, J., Suter, M., Windak, R., Krebs, T., Felley, A., Montessuit, C., et al. (2009). Activation of a HIF1alpha-PPARgamma axis underlies the integration of glycolytic and lipid anabolic pathways in pathologic cardiac hypertrophy. *Cell. Metab.* 9, 512–524. doi: 10.1016/j.cmet.2009.05.005

Laughlin, M. R., Taylor, J., Chesnick, A. S., DeGroot, M., and Balaban, R. S. (1993). Pyruvate and lactate metabolism in the in vivo dog heart. *Am. J. Physiol.* 264, H2068–H2079. doi: 10.1152/ajpheart.1993.264.6.H2068

Lazzeri, C., Sori, A., Chiostri, M., Gensini, G. F., and Valente, S. (2009). Prognostic role of insulin resistance as assessed by homeostatic model assessment index in the acute phase of myocardial infarction in nondiabetic patients submitted to percutaneous coronary intervention. *Eur. J. Anaesthesiol.* 26, 856–862. doi: 10.1097/EJA.0b013e32832a235c

Lazzeri, C., Valente, S., Chiostri, M., Picariello, C., and Gensini, G. F. (2010). Evaluation of acid-base balance in ST-elevation myocardial infarction in the early phase: a prognostic tool? *Coron. Artery Dis.* 21, 266–272. doi: 10.1097/mca.0b013e32833b20c6

Levy, B., Mansart, A., Montemont, C., Gibot, S., Mallie, J. P., Regnault, V., et al. (2007). Myocardial lactate deprivation is associated with decreased cardiovascular performance, decreased myocardial energetics, and early death in endotoxic shock. *Intensive Care Med.* 33, 495–502. doi: 10.1007/s00134-006-0523-9

Lewandowski, E. D. (1992). Metabolic heterogeneity of carbon substrate utilization in mammalian heart: nMR determinations of mitochondrial versus cytosolic compartmentation. *Biochemistry* 31, 8916–8923. doi: 10.1021/bi00152a031

Lionetti, V., Stanley, W. C., and Recchia, F. A. (2011). Modulating fatty acid oxidation in heart failure. *Cardiovasc. Res.* 90, 202–209. doi: 10.1093/cvr/cvr038

Lisanti, M. P., Martinez-Outschoorn, U. E., and Sotgia, F. (2013). Oncogenes induce the cancer-associated fibroblast phenotype: metabolic symbiosis and "fibroblast addiction" are new therapeutic targets for drug discovery. *Cell Cycle* 12, 2723–2732. doi: 10.4161/cc.25695

Liu, F., Lu, J. X., Tang, J. L., Li, L., Lu, H. J., Hou, X. H., et al. (2009). Relationship of plasma creatinine and lactic acid in type 2 diabetic patients without renal dysfunction. *Chin. Med. J.* 122, 2547–2553.

Lochner, A., Pentz, A., Williams, K., Tromp, E., and Harper, I. S. (1996). Substrate effects on sarcolemmal permeability in the normoxic and hypoxic perfused rat heart. *Basic Res. Cardiol.* 91, 64–78. doi: 10.1007/BF00788867

Locke, F. S., and Rosenheim, O. (1907). Contributions to the physiology of the isolated heart: the consumption of dextrose by mammalian cardiac muscle. *J. Physiol.* 36, 205–220. doi: 10.1113/jphysiol.1907.sp001229

Lommi, J., Koskinen, P., Naveri, H., Harkonen, M., and Kupari, M. (1997). Heart failure ketosis. *J. Intern. Med.* 242, 231–238. doi: 10.1046/j.1365-2796.1997.00187.x

Lommi, J., Kupari, M., Koskinen, P., Naveri, H., Leinonen, H., Pulkki, K., et al. (1996). Blood ketone bodies in congestive heart failure. *J. Am. Coll. Cardiol.* 28, 665–672. doi: 10.1016/0735-1097(96)00214-8

Lopaschuk, G. D., Ussher, J. R., Folmes, C. D., Jaswal, J. S., and Stanley, W. C. (2010). Myocardial fatty acid metabolism in health and disease. *Physiol. Rev.* 90, 207–258. doi: 10.1152/physrev.00015.2009

Lu, L., Ye, S., Scalzo, R. L., Reusch, J. E. B., Greyson, C. R., and Schwartz, G. G. (2017). Metformin prevents ischaemic ventricular fibrillation in metabolically normal pigs. *Diabetologia* 60, 1550–1558. doi: 10.1007/s00125-017-4287-2

Lucis, O. J. (1983). The status of metformin in Canada. *Can. Med. Assoc. J.* 128, 24–26.

Luptak, I., Balschi, J. A., Xing, Y., Leone, T. C., Kelly, D. P., and Tian, R. (2005). Decreased contractile and metabolic reserve in peroxisome proliferator-activated receptor-alpha-null hearts can be rescued by increasing glucose transport and utilization. *Circulation* 112, 2339–2346. doi: 10.1161/CIRCULATIONAHA.105.534594

Madiraju, A. K., Erion, D. M., Rahimi, Y., Zhang, X. M., Braddock, D. T., Albright, R. A., et al. (2014). Metformin suppresses gluconeogenesis by inhibiting mitochondrial glycerophosphate dehydrogenase. *Nature* 510, 542–546. doi: 10.1038/nature13270

Magistretti, P. J., and Allaman, I. (2015). A cellular perspective on brain energy metabolism and functional imaging. *Neuron* 86, 883–901. doi: 10.1016/j.neuron.2015.03.035

Mazer, C. D., Stanley, W. C., Hickey, R. F., Neese, R. A., Cason, B. A., Demas, K. A., et al. (1990). Myocardial metabolism during hypoxia: maintained lactate oxidation during increased glycolysis. *Metabolism* 39, 913–918. doi: 10.1016/0026-0495(90)90300-2

Mazzeo, R. S., Brooks, G. A., Schoeller, D. A., and Budinger, T. F. (1986). Disposal of blood [1-13C]lactate in humans during rest and exercise. *J. Appl. Physiol.* 60, 232–241. doi: 10.1152/jappl.1986.60.1.232

McClelland, G. B., and Brooks, G. A. (2002). Changes in MCT 1, MCT 4, and LDH expression are tissue specific in rats after long-term hypobaric hypoxia. *J. Appl. Physiol.* 92, 1573–1584. doi: 10.1152/japplphysiol.01069.2001

Meyer, C., Dostou, J. M., Welle, S. L., and Gerich, J. E. (2002a). Role of human liver, kidney, and skeletal muscle in postprandial glucose homeostasis. *Am. J. Physiol. Endocrinol. Metab.* 282, E419–E427. doi: 10.1152/ajpendo.00032.2001

Meyer, C., Stumvoll, M., Dostou, J., Welle, S., Haymond, M., and Gerich, J. (2002b). Renal substrate exchange and gluconeogenesis in normal postabsorptive humans. *Am. J. Physiol. Endocrinol. Metab.* 282, E428–E434. doi: 10.1152/ajpendo.00116.2001

Misbin, R. I., Green, L., Stadel, B. V., Gueriguian, J. L., Gubbi, A., and Fleming, G. A. (1998). Lactic acidosis in patients with diabetes treated with metformin. *N. Engl. J. Med.* 338, 265–266. doi: 10.1056/NEJM199801223380415

Mole, P. A., Baldwin, K. M., Terjung, R. L., and Holloszy, J. O. (1973). Enzymatic pathways of pyruvate metabolism in skeletal muscle: adaptations to exercise. *Am. J. Physiol.* 224, 50–54. doi: 10.1152/ajplegacy.1973.224.1.50

Moravec, J., El, Alaoui-Talibi Z, Moravec, M., and Guendouz, A. (1996). Control of oxidative metabolism in volume-overloaded rat hearts: effect of pretreatment with propionyl-L-carnitine. *Adv. Exp. Med. Biol.* 388, 205–212. doi: 10.1007/978-1-4613-0333-6_25

Mori, J., Alrob, O. A., Wagg, C. S., Harris, R. A., Lopaschuk, G. D., and Oudit, G. Y. (2013). ANG II causes insulin resistance and induces cardiac metabolic switch and inefficiency: a critical role of PDK4. *Am. J. Physiol. Heart Circ. Physiol.* 304, H1103–H1113. doi: 10.1152/ajpheart.00636.2012

Mowbray, J., and Ottaway, J. H. (1973). The effect of insulin and growth hormone on the flux of tracer from labelled lactate in perfused rat heart. *Eur. J. Biochem.* 36, 369–379. doi: 10.1111/j.1432-1033.1973.tb02921.x

Murashige, D., Jang, C., Neinast, M., Edwards, J. J., Cowan, A., Hyman, M. C., et al. (2020). Comprehensive quantification of fuel use by the failing and nonfailing human heart. *Science* 370, 364–368. doi: 10.1126/science.abc8861

Neubauer, S. (2007). The failing heart–an engine out of fuel. *N. Engl. J. Med.* 356, 1140–1151. doi: 10.1056/NEJMra063052

Neubauer, S., Horn, M., Cramer, M., Harre, K., Newell, J. B., Peters, W., et al. (1997). Myocardial phosphocreatine-to-ATP ratio is a predictor of mortality in patients with dilated cardiomyopathy. *Circulation* 96, 2190–2196. doi: 10.1161/01.cir.96.7.2190

Nguyen, H. B., Rivers, E. P., Knoblich, B. P., Jacobsen, G., Muzzin, A., Ressler, J. A., et al. (2004). Early lactate clearance is associated with improved outcome in severe sepsis and septic shock. *Crit. Care Med.* 32, 1637–1642. doi: 10.1097/01.ccm.0000132904.35713.a7

No Authors listed. (1998). Intensive blood-glucose control with sulphonylureas or insulin compared with conventional treatment and risk of complications in patients with type 2 diabetes (UKPDS 33). UK Prospective Diabetes Study (UKPDS) Group. *Lancet* 352, 837–853. doi: 10.1016/s0140-6736(98)07019-6

Nolan, J. P., Neumar, R. W., Adrie, C., Aibiki, M., Berg, R. A., Bottiger, B. W., et al. (2008). Post-cardiac arrest syndrome: epidemiology, pathophysiology, treatment, and prognostication. A Scientific Statement from the International Liaison Committee on Resuscitation; the American Heart Association Emergency Cardiovascular Care Committee; the Council on Cardiovascular Surgery and Anesthesia; the Council on Cardiopulmonary, Perioperative, and Critical Care; the Council on Clinical Cardiology; the Council on Stroke. *Resuscitation* 79, 350–379. doi: 10.1016/j.resuscitation.2008.09.017

Ong, S. B., Subrayan, S., Lim, S. Y., Yellon, D. M., Davidson, S. M., and Hausenloy, D. J. (2010). Inhibiting mitochondrial fission protects the heart against ischemia/reperfusion injury. *Circulation* 121, 2012–2022. doi: 10.1161/CIRCULATIONAHA.109.906610

Owen, M. R., Doran, E., and Halestrap, A. P. (2000). Evidence that metformin exerts its anti-diabetic effects through inhibition of complex 1 of the mitochondrial respiratory chain. *Biochem. J.* 348, 607–614. doi: 10.1042/0264-6021:3480607

Palmer, J. W., Tandler, B., and Hoppel, C. L. (1977). Biochemical properties of subsarcolemmal and interfibrillar mitochondria isolated from rat cardiac muscle. *J. Biol. Chem.* 252, 8731–8739. doi: 10.1016/s0021-9258(19)75283-1

Paolisso, G., Gambardella, A., Galzerano, D., D'Amore, A., Rubino, P., Verza, M., et al. (1994). Total-body and myocardial substrate oxidation in congestive heart failure. *Metabolism* 43, 174–179. doi: 10.1016/0026-0495(94)90241-0

Park, J. M., Josan, S., Mayer, D., Hurd, R. E., Chung, Y., Bendahan, D., et al. (2015). Hyperpolarized 13C NMR observation of lactate kinetics in skeletal muscle. *J. Exp. Biol.* 218, 3308–3318. doi: 10.1242/jeb.123141

Passarella, S., Paventi, G., and Pizzuto, R. (2014). The mitochondrial L-lactate dehydrogenase affair. *Front. Neurosci.* 8:407. doi: 10.3389/fnins.2014.00407

Peterson, L. R., Herrero, P., McGill, J., Schechtman, K. B., Kisrieva-Ware, Z., Lesniak, D., et al. (2008). Fatty acids and insulin modulate myocardial substrate metabolism in humans with type 1 diabetes. *Diabetes* 57, 32–40. doi: 10.2337/db07-1199

Peterson, L. R., Herrero, P., Schechtman, K. B., Racette, S. B., Waggoner, A. D., Kisrieva-Ware, Z., et al. (2004). Effect of obesity and insulin resistance on myocardial substrate metabolism and efficiency in young women. *Circulation* 109, 2191–2196. doi: 10.1161/01.CIR.0000127959.28627.F8

Popinigis, J., Antosiewicz, J., Crimi, M., Lenaz, G., and Wakabayashi, T. (1991). Human skeletal muscle: participation of different metabolic activities in oxidation of L-lactate. *Acta Biochim. Pol.* 38, 169–175.

Puckett, S. W., and Reddy, W. J. (1979). A decrease in the malate–aspartate shuttle and glutamate translocase activity in heart mitochondria from alloxan-diabetic rats. *J. Mol. Cell. Cardiol.* 11, 173–187. doi: 10.1016/0022-2828(79)90462-0

Rabinowitz, J. D., and Enerback, S. (2020). Lactate: the ugly duckling of energy metabolism. *Nat. Metab.* 2, 566–571. doi: 10.1038/s42255-020-0243-4

Ramasamy, R., Oates, P. J., and Schaefer, S. (1997). Aldose reductase inhibition protects diabetic and nondiabetic rat hearts from ischemic injury. *Diabetes* 46, 292–300. doi: 10.2337/diab.46.2.292

Randle, P. J. (1995). Metabolic fuel selection: general integration at the whole-body level. *Proc. Nutr. Soc.* 54, 317–327. doi: 10.1079/pns19950057

Randle, P. J. (1998). Regulatory interactions between lipids and carbohydrates: the glucose fatty acid cycle after 35 years. *Diabetes Metab. Rev.* 14, 263–283. doi: 10.1002/(sici)1099-0895(199812)14:4<263::aid-dmr233<3.0.co;2-c

Randle, P. J., Garland, P. B., Hales, C. N., and Newsholme, E. A. (1963). The glucose fatty-acid cycle. Its role in insulin sensitivity and the metabolic disturbances of diabetes mellitus. *Lancet* 1, 785–789. doi: 10.1016/s0140-6736(63)91500-9

Reaven, G. M., Hollenbeck, C., Jeng, C. Y., Wu, M. S., and Chen, Y. D. (1988). Measurement of plasma glucose, free fatty acid, lactate, and insulin for 24 h in patients with NIDDM. *Diabetes* 37, 1020–1024. doi: 10.2337/diab.37.8.1020

Revelly, J. P., Tappy, L., Martinez, A., Bollmann, M., Cayeux, M. C., Berger, M. M., et al. (2005). Lactate and glucose metabolism in severe sepsis and cardiogenic shock. *Crit. Care Med.* 33, 2235–2240. doi: 10.1097/01.ccm.0000181525.99295.8f

Riehle, C., and Abel, E. D. (2016). Insulin Signaling and Heart Failure. *Circ. Res.* 118, 1151–1169. doi: 10.1161/CIRCRESAHA.116.306206

Roth, D. A., and Brooks, G. A. (1990). Lactate and pyruvate transport is dominated by a pH gradient-sensitive carrier in rat skeletal muscle sarcolemmal vesicles. *Arch. Biochem. Biophys.* 279, 386–394. doi: 10.1016/0003-9861(90)90506-t

Russell, R. R. III, Li, J., Coven, D. L., Pypaert, M., Zechner, C., Palmeri, M., et al. (2004). AMP-activated protein kinase mediates ischemic glucose uptake and prevents postischemic cardiac dysfunction, apoptosis, and injury. *J. Clin. Invest.* 114, 495–503. doi: 10.1172/JCI19297

Sahlin, K., Fernstrom, M., Svensson, M., and Tonkonogi, M. (2002). No evidence of an intracellular lactate shuttle in rat skeletal muscle. *J. Physiol.* 541, 569–574. doi: 10.1113/jphysiol.2002.016683

Sampson, M. J., Davies, I. R., Braschi, S., Ivory, K., and Hughes, D. A. (2003). Increased expression of a scavenger receptor (CD36) in monocytes from subjects with Type 2 diabetes. *Atherosclerosis* 167, 129–134. doi: 10.1016/s0021-9150(02)00421-5

Savarese, G., and Lund, L. H. (2017). Global Public Health Burden of Heart Failure. *Card. Fail. Rev.* 3, 7–11. doi: 10.15420/cfr.2016:25:2

Schurr, A., Payne, R. S., Miller, J. J., and Rigor, B. M. (1997). Brain lactate is an obligatory aerobic energy substrate for functional recovery after hypoxia: further in vitro validation. *J. Neurochem.* 69, 423–426. doi: 10.1046/j.1471-4159.1997.69010423.x

Shen, Y., Liu, F., Li, Q., Tang, J., Zheng, T., Lu, F., et al. (2012). The gonadal hormone regulates the plasma lactate levels in type 2 diabetes treated with and without metformin. *Diabetes Technol. Ther.* 14, 469–474. doi: 10.1089/dia.2011.0275

Sinniah, B. (1978). Hymenolepis diminuta infection in a Malaysian oil palm estate worker–first case from Malaysia. *Southeast Asian J. Trop. Med. Public Health* 9, 453–454.

Smeele, K. M., Ter, Horst LH, Koeman, A., Heikkinen, S., Laakso, M., and Weber, N. C. (2011). The effect of standard chow and reduced hexokinase II on growth, cardiac and skeletal muscle hexokinase and low-flow cardiac ischaemia-reperfusion injury. *Lab. Anim.* 45, 160–166. doi: 10.1258/la.2011.010096

Sonveaux, P., Vegran, F., Schroeder, T., Wergin, M. C., Verrax, J., Rabbani, Z. N., et al. (2008). Targeting lactate-fueled respiration selectively kills hypoxic tumor cells in mice. *J. Clin. Invest.* 118, 3930–3942. doi: 10.1172/JCI36843

Stanley, W. C. (2001). Cardiac energetics during ischaemia and the rationale for metabolic interventions. *Coron. Artery Dis.* 12, S3–S7.

Stanley, W. C., Gertz, E. W., Wisneski, J. A., Morris, D. L., Neese, R. A., and Brooks, G. A. (1985). Systemic lactate kinetics during graded exercise in man. *Am. J. Physiol.* 249, E595–E602. doi: 10.1152/ajpendo.1985.249.6.E595

Stanley, W. C., Gertz, E. W., Wisneski, J. A., Neese, R. A., Morris, D. L., and Brooks, G. A. (1986). Lactate extraction during net lactate release in legs of humans during exercise. *J. Appl. Physiol.* 60, 1116–1120. doi: 10.1152/jappl.1986.60.4.1116

Stanley, W. C., Morgan, E. E., Huang, H., McElfresh, T. A., Sterk, J. P., Okere, I. C., et al. (2005). Malonyl-CoA decarboxylase inhibition suppresses fatty acid oxidation and reduces lactate production during demand-induced ischemia. *Am. J. Physiol. Heart Circ. Physiol.* 289, H2304–H2309. doi: 10.1152/ajpheart.00599.2005

Symons, J. D., and Abel, E. D. (2013). Lipotoxicity contributes to endothelial dysfunction: a focus on the contribution from ceramide. *Rev. Endocr. Metab. Disord.* 14, 59–68. doi: 10.1007/s11154-012-9235-3

Tempia, A., Fiore, G., Berardino, M., Aimone-Secat, M., Ballaris, M. A., and Pattono, R. (1988). [Use of 3 different anesthetic mixtures in peridural anesthesia for extracorporeal shockwave lithotripsy (ESWL)]. *Minerva. Anestesiol.* 54, 315–320.

Timmermans, A. D., Balteau, M., Gelinas, R., Renguet, E., Ginion, A., de Meester, C., et al. (2014). A-769662 potentiates the effect of other AMP-activated protein kinase activators on cardiac glucose uptake. *Am. J. Physiol. Heart Circ. Physiol.* 306, H1619–H1630. doi: 10.1152/ajpheart.00965.2013

Trueblood, N. A., Ramasamy, R., Wang, L. F., and Schaefer, S. (2000). Niacin protects the isolated heart from ischemia-reperfusion injury. *Am. J. Physiol. Heart Circ. Physiol.* 279, H764–H771. doi: 10.1152/ajpheart.2000.279.2.H764

Trueblood, N., and Ramasamy, R. (1998). Aldose reductase inhibition improves altered glucose metabolism of isolated diabetic rat hearts. *Am. J. Physiol.* 275, H75–H83. doi: 10.1152/ajpheart.1998.275.1.H75

Ussher, J. R., and Lopaschuk, G. D. (2008). The malonyl CoA axis as a potential target for treating ischaemic heart disease. *Cardiovasc. Res.* 79, 259–268. doi: 10.1093/cvr/cvn130

Valente, S., Lazzeri, C., Crudeli, E., Chiostri, M., Giglioli, C., Bernardo, P., et al. (2012). Intraaortic balloon pump: incidence and predictors of complications in the Florence registry. *Clin. Cardiol.* 35, 200–204. doi: 10.1002/clc.20975

Vanoverschelde, J. L., Janier, M. F., Bakke, J. E., Marshall, D. R., and Bergmann, S. R. (1994). Rate of glycolysis during ischemia determines extent of ischemic injury and functional recovery after reperfusion. *Am. J. Physiol.* 267, H1785–H1794. doi: 10.1152/ajpheart.1994.267.5.H1785

Vermeulen, R. P., Hoekstra, M., Nijsten, M. W., van der Horst, I. C., van Pelt, L. J., Jessurun, G. A., et al. (2010). Clinical correlates of arterial lactate levels in patients with ST-segment elevation myocardial infarction at admission: a descriptive study. *Crit. Care* 14, R164. doi: 10.1186/cc9253

Weil, M. H., and Afifi, A. A. (1970). Experimental and clinical studies on lactate and pyruvate as indicators of the severity of acute circulatory failure (shock). *Circulation* 41, 989–1001. doi: 10.1161/01.cir.41.6.989

Wilson, M. C., Jackson, V. N., Heddle, C., Price, N. T., Pilegaard, H., Juel, C., et al. (1998). Lactic acid efflux from white skeletal muscle is catalyzed by the monocarboxylate transporter isoform MCT3. *J. Biol. Chem.* 273, 15920–15926. doi: 10.1074/jbc.273.26.15920

Wisneski, J. A., Gertz, E. W., Neese, R. A., Gruenke, L. D., Morris, D. L., and Craig, J. C. (1985). Metabolic fate of extracted glucose in normal human myocardium. *J. Clin. Invest.* 76, 1819–1827. doi: 10.1172/JCI112174

Wisniewski, J. R., Gizak, A., and Rakus, D. (2015). Integrating Proteomics and Enzyme Kinetics Reveals Tissue-Specific Types of the Glycolytic and Gluconeogenic Pathways. *J. Proteome. Res.* 14, 3263–3273. doi: 10.1021/acs.jproteome.5b00276

Wolfe, R. R. (1990). Isotopic measurement of glucose and lactate kinetics. *Ann. Med.* 22, 163–170. doi: 10.3109/07853899009147263

Wu, R., Smeele, K. M., Wyatt, E., Ichikawa, Y., Eerbeek, O., Sun, L., et al. (2011). Reduction in hexokinase II levels results in decreased cardiac function and altered remodeling after ischemia/reperfusion injury. *Circ. Res.* 108, 60–69. doi: 10.1161/CIRCRESAHA.110.223115

Young, M. E., Guthrie, P. H., Razeghi, P., Leighton, B., Abbasi, S., Patil, S., et al. (2002). Impaired long-chain fatty acid oxidation and contractile dysfunction in the obese Zucker rat heart. *Diabetes* 51, 2587–2595. doi: 10.2337/diabetes.51.8.2587

Zhabyeyev, P., Gandhi, M., Mori, J., Basu, R., Kassiri, Z., Clanachan, A., et al. (2013). Pressure-overload-induced heart failure induces a selective reduction in glucose oxidation at physiological afterload. *Cardiovasc. Res.* 97, 676–685. doi: 10.1093/cvr/cvs424

Zhang, L., Jaswal, J. S., Ussher, J. R., Sankaralingam, S., Wagg, C., Zaugg, M., et al. (2013). Cardiac insulin-resistance and decreased mitochondrial energy production precede the development of systolic heart failure after pressure-overload hypertrophy. *Circ. Heart Fail.* 6, 1039–1048. doi: 10.1161/CIRCHEARTFAILURE.112.000228

Zhu, Y., Wu, J., and Yuan, S. Y. (2013). MCT1 and MCT4 expression during myocardial ischemic-reperfusion injury in the isolated rat heart. *Cell. Physiol. Biochem.* 32, 663–674. doi: 10.1159/000354470

Conflict of Interest: The authors declare that the research was conducted in the absence of any commercial or financial relationships that could be construed as a potential conflict of interest.

Publisher's Note: All claims expressed in this article are solely those of the authors and do not necessarily represent those of their affiliated organizations, or those of the publisher, the editors and the reviewers. Any product that may be evaluated in this article, or claim that may be made by its manufacturer, is not guaranteed or endorsed by the publisher.

frontiers | Frontiers in Physiology

CORRECTION
published: 09 June 2022
doi: 10.3389/fphys.2022.947253

Corrigendum: Lactate and Myocardiac Energy Metabolism

Shuohui Dong[1], Linhui Qian[2], Zhiqiang Cheng[1], Chang Chen[1], Kexin Wang[1], Sanyuan Hu[3], Xiang Zhang[1] and Tongzhi Wu[4,5]*

[1]Department of General Surgery, Qilu Hospital of Shandong University, Jinan, China, [2]Department of Colorectal and Anal Surgery, Feicheng Hospital Affiliated to Shandong First Medical University, Feicheng, China, [3]Department of General Surgery, The First Affiliated Hospital of Shandong First Medical University, Jinan, China, [4]Adelaide Medical School and Centre of Research Excellence in Translating Nutritional Science to Good Health, The University of Adelaide, Adelaide, SA, Australia, [5]Endocrine and Metabolic Unit, Royal Adelaide Hospital, Adelaide, SA, Australia

Keywords: myocardium, cardiac metabolism, energy substrate, lactate, lactate shuttle theory, myocardial ischemia, heart failure, diabetic cardiomyopathy

OPEN ACCESS

Approved by:
Frontiers Editorial Office, Frontiers Media SA, Switzerland

****Correspondence:***
Xiang Zhang
xiang.zhang02@hotmail.com

Specialty section:
This article was submitted to Metabolic Physiology, a section of the journal Frontiers in Physiology

Received: *18 May 2022*
Accepted: *19 May 2022*
Published: *09 June 2022*

Citation:
Dong S, Qian L, Cheng Z, Chen C, Wang K, Hu S, Zhang X and Wu T (2022) Corrigendum: Lactate and Myocardiac Energy Metabolism. Front. Physiol. 13:947253. doi: 10.3389/fphys.2022.947253

A Corrigendum on

Lactate and Myocardiac Energy Metabolism

by Dong S, Qian L, Cheng Z, Chen C, Wang K, Hu S, Zhang X and Wu T (2021). Front. Physiol. 12: 715081. doi: 10.3389/fphys.2021.715081

In the published article, there was an error in the article title. Instead of "Lactate and Myocadiac Energy Metabolism", it should be "Lactate and Myocardiac Energy Metabolism".

The authors apologize for this error and state that this does not change the scientific conclusions of the article in any way. The original article has been updated.

frontiers in Physiology

REVIEW
published: 30 August 2021
doi: 10.3389/fphys.2021.710420

Metabolic Changes of Hepatocytes in NAFLD

*Qianrang Lu[1,2], Xinyao Tian[1,2], Hao Wu[1,2], Jiacheng Huang[1,2], Mengxia Li[1,2], Zhibin Mei[1,2], Lin Zhou[1,2], Haiyang Xie[1,2] and Shusen Zheng[1,2,3]**

[1] Division of Hepatobiliary and Pancreatic Surgery, Department of Surgery, The First Affiliated Hospital, Zhejiang University School of Medicine, Hangzhou, China, [2] NHC Key Laboratory of Combined Multi-organ Transplantation, Hangzhou, China, [3] Department of Hepatobiliary and Pancreatic Surgery & Liver Transplantation, Shulan (Hangzhou) Hospital, Hangzhou, China

Nonalcoholic fatty liver disease (NAFLD) is often accompanied by systemic metabolic disorders such as hyperglycemia, insulin resistance, and obesity. The relationship between NAFLD and systemic metabolic disorders has been well reviewed before, however, the metabolic changes that occur in hepatocyte itself have not been discussed. In NAFLD, many metabolic pathways have undergone significant changes in hepatocyte, such as enhanced glycolysis, gluconeogenesis, lactate production, tricarboxylic acid (TCA) cycle, and decreased ketone body production, mitochondrial respiration, and adenosine triphosphate (ATP) synthesis, which play a role in compensating or exacerbating disease progression, and there is close and complex interaction existed between these metabolic pathways. Among them, some metabolic pathways can be the potential therapeutic targets for NAFLD. A detailed summary of the metabolic characteristics of hepatocytes in the context of NAFLD helps us better understand the pathogenesis and outcomes of the disease.

Keywords: WARBURG effect, NAFLD, Mitochondrial dysfunction, Insulin resistance, Metabolism

OPEN ACCESS

Edited by:
Xiang Zhang,
Qilu Hospital, Shandong University, China

Reviewed by:
Sonia Michael Najjar,
Heritage College of Osteopathic Medicine, Ohio University, United States
Carmen De Miguel,
University of Alabama at Birmingham, United States

***Correspondence:**
Shusen Zheng
shusenzheng@zju.edu.cn

Specialty section:
This article was submitted to Metabolic Physiology, a section of the journal Frontiers in Physiology

Received: *16 May 2021*
Accepted: *04 August 2021*
Published: *30 August 2021*

Citation:
Lu Q, Tian X, Wu H, Huang J, Li M, Mei Z, Zhou L, Xie H and Zheng S (2021) Metabolic Changes of Hepatocytes in NAFLD. Front. Physiol. 12:710420. doi: 10.3389/fphys.2021.710420

INTRODUCTION

The liver is the hub of the metabolism of glucose, fat, protein, vitamin, hormone, etc., and play a major part in metabolic homeostasis. All kinds of metabolic processes such as glycolysis, gluconeogenesis, lipogenesis, glycogen production can be conducted in liver. Therefore, nonalcoholic fatty liver disease (NAFLD) is often accompanied by systemic metabolic disorders (Byrne and Targher, 2015; Tilg et al., 2017; Khan et al., 2019). In view of the importance and complexity of liver metabolism, it is meaningful to study the metabolic characteristics of the liver under healthy as well as pathological conditions.

Nonalcoholic fatty liver disease, a continuum of liver abnormalities including nonalcoholic fatty liver (NAFL) and nonalcoholic steatohepatitis (NASH), and can progress to liver cirrhosis and hepatocellular carcinoma (Friedman et al., 2018). NAFL, also named hepatic steatosis, is the benign stage of NAFLD which is characterized by excessive lipid stored within the cytosol of hepatocytes. Patients in the state of NAFL take a lower risk of deleterious outcomes, while NASH can progress to cirrhosis, liver failure and even hepatic carcinoma (Singh et al., 2015). The presence of NASH means the existence of liver inflammation and injury, accompanied with elevated aminotransferases. Biopsy is the main method of diagnosis which is characterized by various degrees of fat accumulation, hepatocellular ballooning, lobular inflammation and fibrosis (Brunt et al., 2020).

Nowadays NAFLD accounts for the major part of liver disease worldwide. With the decreased incidence of hepatitis and increased obesity (Fan et al., 2017; Wu et al., 2020), the primary cause of end-stage liver disease will be replaced by NAFLD in the next few decades (Younossi et al., 2018). Currently, the worldwide prevalence of NAFLD is nearly 24% (2015) (Younossi et al., 2016). Therefore there is an increasing interest in studying NAFLD. To understand the pathogenesis of NAFLD, a useful conceptual framework is that the excess energy metabolic substrates, fatty acids (FAs), and carbohydrates, exceed the liver's processing capacity, resulting in the exacerbated formation of reactive oxygen species (ROS), by-products and lipid peroxidation, which will induce hepatocellular injury, inflammation and death (Friedman et al., 2018). In this review, we will discuss the hepatic metabolism changes and their effect in NAFLD.

CARBOHYDRATE METABOLISM

Glycolysis

Glycolysis refers to the process that one molecule of glucose is metabolized through a ten-step process in the cytoplasm to finally generate two molecules of pyruvate, providing with two molecules of NADH and two adenosine triphosphate (ATP). The glycolysis rate is mainly controlled by several rate-limiting enzymes, hexokinase (HK), phosphofructokinase (PFKM), and pyruvate kinase (PK), which are controlled by allosteric and hormonal regulation. In liver, the major isoform of hexokinase is hexokinase IV, glucokinase, which is primarily regulated by insulin but not inhibited by its product. Therefore, it is of great importance in the modulation of postprandial blood glucose. Insulin is the main hormone that regulates blood glucose. It bound to the insulin receptor (INSR) of target cells on the plasma membrane, then act through IRS(insulin receptor substrate)/PI3K(phosphoinositide 3-kinase)/AKT(protein kinase B) axis to regulate glucose metabolism (Haeusler et al., 2018; Petersen and Shulman, 2018). Phosphatase and tensin homolog (PTEN) catalyzed the reverse reaction of P13K and antagonize insulin function, but its activity is inhibited by insulin (Hodakoski et al., 2014).

Changes in glycolysis are found in many diseases. The WARBURG effect, known widely in tumor cells, is characterized by enhanced aerobic glycolysis and lactate production (Vander Heiden et al., 2009; Koppenol et al., 2011). It used to be misread that the damaged respiration is accounted for increased glucose fermentation in cancers. Actually, the tumor cells exhibit the WARBURG effect and meanwhile retain normal or even enhanced mitochondrial respiration (Koppenol et al., 2011; Lu et al., 2015). Recently, the similar metabolic change has also been found in many benign diseases, such as pulmonary hypertension, idiopathic pulmonary fibrosis (IPF), tuberculosis, failing heart (Chen et al., 2018), liver cirrhosis (Trivedi et al., 2021), etc., which indicate that WARBURG effect may not be unique to malignant tumor.

In the hepatocytes of fatty liver, similar metabolic changes also exist. Compared with regular chow (RC)-fed mice, the mRNA levels of key glycolysis related enzymes (HK2, PFKm, and PKm) were increased in the liver of high-fat diet (HFD)-fed mice (Liu et al., 2018). In the PTEN-null mice, HK2, PKM2, and other glycolytic enzymes are overexpressed via P13K/AKT2/PPARγ axis, which partially account for the susceptibility to fatty liver and hepatocellular carcinoma of PTEN-null mice (Horie et al., 2004). Moreover adenoviral-mediated overexpression of HK2 and PKM2 promotes liver growth and liver steatosis (Panasyuk et al., 2012), which may bridge the enhanced glycolysis with carcinogenesis in fatty liver. Using PET/CT to monitor the phosphorylation rate of liver glucose, which represents the activity of hexokinase, proved that the rate of phosphorylation of liver hexose is higher in patients with steatohepatitis (Keramida et al., 2016). Seahorse analysis also showed that the rate of extracellular acidification in HFD-fed mice increased suggesting enhanced glycolysis (Liu et al., 2018). Since NAFLD always accomplished by insulin resistance, hyperinsulinemia may be one of the reasons for enhanced glycolysis.

Recent studies have found that knocking down NOD-like receptor (NLR)X1 NLRX1 can inhibit glycolysis and enhance fat oxidation to reduce liver steatosis (Kors et al., 2018). Liver specific knockdown of SIRT6 will lead to the deacetylation of histone H3 lysine 9 (H3K9) in the promoter of glycolytic genes and elevated the expression of these genes, which consequently cause fatty liver dependent on enhancing glycolysis (Kim et al., 2010). Knockdown of Geranylgeranyl diphosphate synthase (GGPPS) can induce strengthened glycolysis through the LKB1–AMPK pathway, and lead to an increase in the inflammatory factors secreted in mouse primary hepatocytes. Furthermore, using 2-dexoy-D-glucose to inhibit glycolysis dramatically alleviates liver inflammation, injury and fibrosis due to the deletion of GGPPS in HFD mice (Liu et al., 2018). However, the pathway that glycolysis contributes to liver injury is unclear and deserves further study.

The product of glycolysis, pyruvate, will be dehydrogenated by lactate dehydrogenase to lactate or decarboxylated to acetyl-coenzyme A by pyruvate dehydrogenase complex (PDC) in mitochondria which thereby connects the glycolysis with the tricarboxylic acid (TCA) cycle (Zhou et al., 2001). The activity of the complex is regulated by pyruvate dehydrogenase phosphatase (PDP) and pyruvate dehydrogenase kinase (PDK1-4) through reversible dephosphorylation and phosphorylation. Phosphorylation is the inactive state of PDC (Bowker-Kinley et al., 1998).

The activity of PDC in hepatocytes of fatty liver is still controversial. Bajotto et al. (2006) and Go et al. (2016) found that the activity of pyruvate dehydrogenase complex in the liver of OLETF mice and HFD C57BL/6J mice was significantly lower than that of control group, which will consequently reduce the TCA cycle flux of pyruvate. Moreover, the activity, abundance and mRNA level of PDK2 and PDK4 are consistently increased, and positively related to plasma free fatty acid (FFA) concentrations (Bajotto et al., 2006; Go et al., 2016). Consistently, in the NAFLD patients and obese mice, the serum pyruvate concentration and liver pyruvate content are significantly higher than those of the control group (Fletcher et al., 2019; Wang et al., 2020; Shannon et al., 2021), though there is no evidence that it is caused by inactivity of PDC.

A current study by Shannon et al. (2021) revealed a contradictory result that in obese mice, the activity of PDC is enhanced accompanied by the reduced activity of PDK4 and enhanced activity of PDP2. The insulin sensitizer Metformin can normalize the activity of PDC and mitigated the flow of TCA derived from pyruvate (Shannon et al., 2021). However, given that the acetyl-CoA produced by pyruvate only accounts for 5% of the liver TCA cycle (Cappel et al., 2019), the effect of pyruvate oxidative decarboxylation by PDC may not directly participate the pathological process of fatty liver.

Lactate Production

The alternative metabolic pathway of pyruvate is lactate production. Under physiological conditions, lactate is mainly used by the heart, skeletal muscle and brain as an energy source (Gladden, 2004). The hepatocyte can convert excessive plasma lactate into glucose then bring back to plasma (Brooks, 2018). Lactate dehydrogenase(LDH) is composed of two subunits, H and M, with five isoenzymes: LDH1, LDH2, LHD3, LDH4, and LDH5 (Adeva-Andany et al., 2014). LDH-M, also known as LDHA, is more inclined to convert pyruvate into lactate; while LDH-H, also known as LDHB, is more inclined to convert lactate to pyruvate to dispose lactate (Dawson et al., 1964).

The production of lactate in fatty liver is significantly higher than normal (Liu et al., 2018; Wang et al., 2020), which is another feature of WARBURG effect (de la Cruz-López et al., 2019). P300/CBP-associated factor (PCAF)-mediated high acetylation level of LDH-B is one of the main causes in the accumulation of lactate in NAFLD. The activity of acetylated LDH-B is reduced, which hinders the ability of hepatocyte to dispose of lactate and results in the lactate accumulation (Wang et al., 2020). The increased lactate can not only worsen the hepatic steatosis, but also increase the acetylation of histone H3K9 by reducing the activity of nuclear histone deacetylase (HDAC), and therefore increase the expression of genes involved in lipogenesis and FA uptake (Wang et al., 2020).

Liver Gluconeogenesis

Gluconeogenesis refers to the conversion of non-glucose compounds (glycerol, glycogen-producing amino acids, lactic acid, etc.) into glucose (Hers and Hue, 1983). Hepatic gluconeogenesis occurs during prolonged fasting episodes after depletion of hepatic glycogen, and is primarily in response to the insulin and glucagon. After an overnight fasting, about the half of the total hepatic glucose production is attributed to gluconeogenesis (Rothman et al., 1991). In order to achieve gluconeogenesis, the key is to bypass the three irreversible reactions in glycolysis that the conversion of glucose to glucose-6-phosphate by HK, fructose-6-phosphate to fructose-1,6-diphosphate by PFK and phosphoenolpyruvate to pyruvate via PK (Petersen et al., 2017). Conversion of pyruvate to phosphoenolpyruvate is the first reverse reaction in gluconeogenesis catalyzed by pyruvate carboxylase (PC) and phosphoenolpyruvate carboxykinase (PEPCK). The production of pyruvate carboxylation catalyzed by PC, oxaloacetate, is the intermediates of TCA cycle, and such flux is also named anaplerosis. Then oxaloacetate is converted to phosphoenolpyruvate, which is called cataplerosis (Owen et al., 2002). Thus, a close link exists between gluconeogenesis and TCA cycle. The enzymes that catalyze the other two reverse reactions are fructose diphosphatase-1 and glucose-6-phosphatase.

In the individuals with high intrahepatic triglycerides (IHTG), the endogenous glucose is higher than that in normal people, among which derived from gluconeogenesis is increased by 25%, consistent with the flow of anaplerosis increased by 50% (Sunny et al., 2011). The same trend also appears on mice supplied with excessive lipid, either by HFD or by exogenously perfused. Moreover, the increasement of anaplerosis/cataplerosis is linked to enhanced oxidative metabolism and subsequently oxidative stress and inflammation (Satapati et al., 2016). Inhibition of anaplerotic/cataplerotic flux can attenuates gluconeogenesis and TCA cycle and consequently alleviates oxidative stress and hepatic steatosis (Go et al., 2016; Satapati et al., 2016; Yuan et al., 2016). The presumable mechanism could be that, first, the raise of allosteric activation of PK, acetyl-COA, due to enhanced FA oxidation may partially contribute to the enhanced gluconeogenesis. Second, as mentioned before, the increased content of pyruvate in the liver increases the substrate for gluconeogenesis. Third the increased TCA cycle flux that we will discuss later facilitates gluconeogenesis from TCA cycle cataplerosis.

LIPID METABOLISM

De novo Lipogenesis

Hepatic *de novo* lipogenesis (DNL) includes FAs synthesized from acetyl-CoA and then esterified with 3-phosphoglycerol to generate triglycerides (TG). Acetyl-CoA carboxylase (ACC) is the rate-limiting enzyme of FA synthesis, which carboxylate the acetyl-CoA to produce malonyl-CoA. Acetyl-CoA and citric acid are main allosteric activators of ACC. The expression and activity of the enzymes involved in DNL also modulated by various transcription factors like sterol regulatory element-binding protein 1C (SREBP1C) and carbohydrate-responsive element-binding protein (ChREBP; Shimomura et al., 1999; Dentin et al., 2005; Wang et al., 2015). Under physiological conditions, the TG synthesized in liver will not be stored in it, and will be exported in the form of very low density lipoproteins (VLDL; Kawano and Cohen, 2013).

The major feature of NAFLD is the lipid accumulation in hepatocytes. Under fasting conditions, the proportion of TG stored in liver of NAFLD patients are 26.1 $\pm$ 6.7% from DNL, 59.0 $\pm$ 9.9% from plasma free FAs and 14.9 $\pm$ 7.0% from dietary FAs, which is similar to the composition of VLDL-TG (Donnelly et al., 2005), and secretion rate of VLDL-TG is linearly related to the content of IHTG when IHTG content was $\leq$10% but reached a plateau in subjects with high IHTG (Fabbrini et al., 2008). Since NAFLD is often accompanied by insulin resistance (Watt et al., 2019), the lipolysis of peripheral adipose tissue increased, leading to an elevated in plasma FFA (Fabbrini et al., 2008; Samuel and Shulman, 2016). However, when compared to the individuals with low IHTG, no significant difference has been found in VLDL-TG derived from adipose tissue or diet in patients

with high IHTG. Only the VLDL-TG derived from DNL was significantly increased to the three times of low IHTG group. The percentage of newly-synthesized palmitate in VLDL-TG was two times higher in high IHTG group, indicating that it was the increased DNL that contributed to the accumulation of liver fat (Lambert et al., 2014). Fabbrini et al. (2008) also proved that the increase in VLDL-TG secretion was primarily attributed to the FAs derived from DNL and lipolysis of abdominal and hepatic lipid, other than lipolysis of subcutaneous fat.

Moreover, the expression of lipogenic regulatory factors and enzymes, such as SREBP1c, fatty acid synthase (FAS), liver X receptor α (LXRα), ChREBP, and ACC1, is higher in fatty liver (Kohjima et al., 2007; Higuchi et al., 2008). LXRs are classified as the nuclear hormone receptor superfamily, which can be activated by oxysterols due to elevated intracellular cholesterol concentration. LXR is widely involved in the regulation of many metabolic processes including cholesterol, glucose and lipid metabolism (Hiebl et al., 2018). LXRα can promote lipogenic gene transcription by activating SREBP1c (Repa et al., 2000). The expression level of LXR in NAFLD patients was four times that of the control group, and it was significantly related with the expression of SREBP-1c (Higuchi et al., 2008). Moreover The expression of SREBP1c can also be induced by tumor necrosis factor-alpha (TNF-α) (Endo et al., 2007) and the mRNA level of TNF-α is related to the severity of NASH (Crespo et al., 2001). ChREBP is also found to overexpress in hepatic steatosis patient and indicate the severity of hepatic steatosis but is negatively correlated with insulin resistance in NASH patients. Overexpression of ChREBP induce the hepatic steatosis but increase the insulin sensitivity (Benhamed et al., 2012). In addition, due to the systemic insulin resistance, the high levels of insulin will contribute to DNL (Mansouri et al., 2018).

Fatty Acid Oxidation

Fatty acids oxidation (FAO) is conducted in mitochondria, endoplasmic reticulum (ER) and peroxisomes which can produce abundant acetyl-CoA. The first step is activation of FAs to fatty acyl-CoA by acyl-CoA synthase in the outer mitochondrial membrane or ER. Mitochondria are the main site of FAs β-oxidation. The long-chain FAs rely on the assistance of carnitine palmitoyltransferase-1 (CPT1) to shuttled across the membrane while medium - and short-chain FAs do not. CPT1 is the key enzyme for β-oxidation, and malonyl-CoA, the intermediates of DNL, is a potent allosteric inhibitor of CPT (Bonnefont et al., 2004). Some transcription factors such as peroxisome proliferator-activated receptor α (PPARα) and its coactivator peroxisome proliferator-activated receptor gamma coactivator 1 α (PGC1α), can enhance the expression of CPT1 and other genes related to FAO (Bougarne et al., 2018). In the context of diabetes or FA overload, a part of FAs will be disposed through ω-oxidation in the endoplasmic reticulum which deteriorate ROS production and lipid peroxidation (Reddy, 2001; Wanders et al., 2011).

Theoretically increased DNL should inhibit the FA oxidation for the intermediate malonyl-CoA. However, in the patient with NASH or obesity, mitochondrial β-oxidation is still enhanced to coordinate with the excess FFA load, which has been proved by 13C-octanoate breath test and positron emission tomography and is correlated with systemic insulin resistance (Miele et al., 2003; Iozzo et al., 2010). In 12-week and 32-week HFD mice, the respiratory exchange ratio (ERE) value of the mice decreased and the oxygen consumption rate increased, suggesting increased FAO (Liu et al., 2018; Pittala et al., 2019). As the upregulation of fatty acid translocase (CD36/FAT), the uptake of FFA from plasma to hepatocytes also increased (Bechmann et al., 2010). CD36/FAT is one of the FA transport proteins which facilitates the uptake and utilization of FFAs in hepatocytes (Silverstein and Febbraio, 2009). Its expression is associated with serum FFAs and apoptosis mediators (Bechmann et al., 2010). The increased FFAs in hepatocytes could enhance the FAO consequently (Mansouri et al., 2018).

In fatty liver mouse model and NAFLD patients, the expression of genes involved in hepatic mitochondrial beta-oxidation such as PPARα, PGC1α and CPT1a is elevated as expected (Kohjima et al., 2007; Liu et al., 2018; Pittala et al., 2019). However, some research has shown that compared high-trans-fat high-fructose diet (TFD)-8 weeks-induced simple steatosis mice with NASH mice by 24 weeks, the expression of genes related beta-oxidation was decreased in liver with onset of NASH (Patterson et al., 2016). That may indicate that the ability of FAO may alter in different stages of NAFLD progression.

In addition, ω-oxidation conducted in the ER and β-oxidation in peroxisomes are upregulated in NASH as compensation (Robertson et al., 2001; Kohjima et al., 2007). However, it may lead to an increasement of ROS (Wanders et al., 2011; Del Río and López-Huertas, 2016). In addition, the increasement of the by-products of fat metabolism such as Cer and DAGs indicated that fat metabolism is insufficient during NSAH (Patterson et al., 2016), and these by-products will hinder insulin signaling pathway and result in insulin resistance (Samuel et al., 2010).

Ketogenesis

There are three major flux for acetyl-CoA pool produced from FAO and glycolysis that ketogenesis, TCA cycle and DNL in liver. Ketone bodies are mainly synthesized by hepatocyte using acetyl-CoA derived from FAO. However, they cannot be used in liver for lack of enzymes that can utilize ketone bodies, and have to be exported to extrahepatic tissues for terminal oxidation (Puchalska and Crawford, 2017). This physiological process provides an alternative energy source which is enhanced when glucose is unavailable (Robinson and Williamson, 1980). Primary regulators of ketogenesis include the rate of mitochondrial β-oxidation, CPT1 activity, TCA cycle flux and its intermediate concentrations, and the hormones such as glucagon and insulin. When content of acetyl-CoA was elevated due to increased β-oxidation or impaired glycolysis reduced the oxaloacetate derived from anaplerosis, ketogenesis will strengthen as consequence.

Under physiological conditions, in terms of the ratio of TCA cycle and ketogenesis, 86 ± 2% of acetyl-CoA is used for ketone body production, while in patients with NAFLD, only 77 ± 2% of acetyl-CoA with $P = 0.003$ enters ketogenesis after a 24-h fast, and the serum β-hydroxybutyric acid concentration was 30% lower than that of the control group (Fletcher et al., 2019), even though

there was no significant difference in the production of ketone bodies after overnight fasting (Sunny et al., 2011). In addition, the serum β-hydroxybutyric acid concentration was negatively correlated with the fat content in the liver (Fletcher et al., 2019). Compared with HFD-fed mice, ketogenic insufficiency aggravates the hepatic inflammation and injury in HDF-fed 3-hydroxymethylglutaryl CoA synthase (HMGCS2) antisense oligonucleotide (ASO)-treated mice. In addition, ketogenic insufficiency will increase DNL since more the acetyl-CoA will be catalyzed by citrate synthase to citrate (Cotter et al., 2014).

MITOCHONDRIAL METABOLISM

TCA Cycle

Another metabolic pathway of acetyl-CoA is TCA cycle. The TCA cycle is a series of closed loop reactions. One molecule of acetyl-CoA that go through TCA cycle will produce 3 molecules of NADH, 1 molecule of FADH2, 2 molecules of C02 and 1 molecule of guanosine triphosphate GTP but the carbon does not directly drive from acetyl-CoA. Then NADH and FADH2 will be further oxidized by mitochondrial respiratory chain (MRC) and provide abundant ATP. The TCA cycle serves as the center of cell catabolism because no matter FA, protein or glucose, the terminal decomposition products are all acetyl-CoA. The regulation of TCA cycle mainly depends on allosteric regulation of the substrates, ATP, NADH, etc., but hardly by hormones (Martínez-Reyes and Chandel, 2020).

Under the fasting condition for 12 and 24 h, the acetyl-CoA flow into the TCA cycle in the liver of NAFLD patients was 2 and 1.4 times of normal people, respectively. which is also positively correlated with the liver triglyceride content, the rate of gluconeogenesis, and the blood glucose concentration (Sunny et al., 2011; Fletcher et al., 2019), although there is mitochondrial damage in term of morphology (Sanyal et al., 2001). Combined with attenuated ketogenesis we discussed before, we can draw the conclusion that the excess acetyl-CoA in hepatocytes of NAFLD patients was prone to be catabolized through the TCA cycle rather than ketogenesis, which reduced the fat consumption. Given that activity of TCA cycle is seldom controlled by hormones, and expression of related enzymes is constitutive. Therefore, the increased fat oxidation should be the main reason for TCA enhancement. The enhanced gluconeogenesis accompanied by enrichment of oxaloacetate that is able to activate pyruvate carboxylase may also contribute to overactive TCA cycle. Moreover the mitochondrial TCA cycle flux parallels to the ROS production and consequently cause oxidative stress (Satapati et al., 2012), thereby participate in the progression from liver steatosis to steatohepatitis (Browning and Horton, 2004). By inhibiting anaplerotic/cataplerotic flow, mitochondrial TCA flow and oxidative metabolism was reduced, and thereby mitigating inflammation and oxidative stress (Satapati et al., 2016). The enhancement of the TCA cycle increases the intermediates, citrate. It not only allosterically activates acetyl-CoA carboxylase, but also provides acetyl-CoA for DNL through the citrate pyruvate cycle.

Mitochondrial Respiratory Chain

Embedded in the inner mitochondrial membrane, four kinds of protein complexes that complex I, II, III, IV make up the MRC which can transfer proton and electrons from NADH and FADH2. Then the oxygen molecules eventually accept electrons and hydrogen ions to produce water. During the delivery of electrons, protons are transported from the mitochondrial matrix at CI, CIII, and CIV and create proton-motive force (PMF).Then PMF is used to drive ATP generation by CV, coupling the MRC with ATP synthesis (Rich and Maréchal, 2010). As a consequence of normal mitochondrial respiratory, mitochondria generate ROS in a physiological range. Most of the electrons delivered to the MRC are correctly accepted by oxygen and then form water with protons catalyzed by cytochrome c oxidase (CIV). However, a small part of the electrons directly combined with oxygen to form superoxide anion radical (O_2^-) and other ROS, which usually happens in complex I and complex III (Willems et al., 2015; Mansouri et al., 2018). ROS in physiological level can activate various signaling pathways involved in cell proliferation, inflammation and etc. However, excessive ROS will attack intracellular macromolecular compound such as proteins, nucleic acids, lipids and lead to cell death or induce apoptosis (Zorov et al., 2014).

The efficiency of MRC also alters in NAFLD. In patients with obesity or simple fatty liver, hepatic mitochondrial respiration increased compared with healthy people. However, in patients with steatohepatitis, 31–40% of patients have lower hepatic mitochondrial respiratory levels than obese patients. It indicates that in the early stage of fatty liver, the respiration rate of mitochondria increases as compensation. When it progresses to the stage of steatohepatitis, the respiration of mitochondria begins to decrease, and this adaptive change disappears (Koliaki et al., 2015), and the activity of various complexes in the MRC of NASH patients is decreased consistently (Pérez-Carreras et al., 2003). As attenuated mitochondrial respiration is inadequate to the increased TCA cycle, which means the excess electrons cannot be captured by oxygen appropriately, NASH is always accompanied with more ROS production, DNA damage, inflammation and liver injury (Serviddio et al., 2008; Koliaki et al., 2015).

Moreover, in NASH patients and ob/ob mice, the expression of the uncoupling protein-2 (UCP-2) elevated, which aggravated the mitochondrial uncoupling and proton leakage of liver mitochondria, and reduced the efficiency of liver ATP synthesis (Chavin et al., 1999; Serviddio et al., 2008), All this leads to impaired ATP synthesis which has been validated in obesity and NAFLD patients. by nuclear magnetic resonance spectroscopy (Nair et al., 2003). Interestingly, uncoupling of liver mitochondria seems to play a protective role in the progress of fatty liver working by accelerating energy expenditure. Using adenine nucleotide translocase (ANT) inhibitor, carboxyatractyloside, can alleviate fatty liver and insulin resistance in mice by enhancing uncoupling (Cho et al., 2017).

THERAPEUTIC STRATEGIES TARGETED ON HEPATOCYTE METABOLISM

The treatment for NAFLD targeted on hepatocyte metabolism has demonstrated positive efficacy in some clinical trials. PPARα is one of the PPAR isotypes that mainly expressed in the liver, which can regulate liver FA uptake and the expression of FAO-related enzymes. Fibrates, PPARAα agonist, is mainly used to treat hyperlipidemia (Dubois et al., 2017). However, no obvious effect has been achieved in several clinical trials for the treatment of NAFLD. Nevertheless, several dual PPAR agonists have shown promising efficacy in recent clinical trials on the treatment of NAFLD. Saroglitazar, a dual PPAR α/γ agonist, has achieved a promising effect in the treatment of NAFLD in a phase 2 study(NCT03061721) (Gawrieh et al., 2021). Elafibranor, a dual PPARα/δ agonist, demonstrated the improvement of liver function tests and NASH resolution without worsening of fibrosis in a phase II study based on a post-hoc analysis(NCT01694849) (Ratziu et al., 2016). However, a phase III trial about it was terminated for not meeting the predefined primary surrogate efficacy endpoint (NCT02704403). FGF21 (fibroblast growth factor 21) is one of the target genes of PPARα, which mainly plays a role in the liver, such as enhancing FAO and reducing FA production (Kharitonenkov et al., 2005). Accordingly, Pegbelfermin, a FGF21 analogue, significantly reduced the hepatic fat fraction in patients with NASH determined by MRI-PDFF (magnetic resonance imaging-proton density fat fraction) in a phase 2a trial (NCT02413372) (Sanyal et al., 2019).

ACC is a key enzyme for lipogenesis. Therefore, it is reasonable to speculate that ACC inhibitors are able to reduce fatty liver. In a Phase 2 trial, GS-0976 (firsocostat), an ACC inhibitor, can significantly reduce DNL and ameliorate hepatic steatosis and markers of liver injury (NCT02856555) (Lawitz et al., 2018; Loomba et al., 2018). When combined with cilofexor (Farnesoid X Receptor agonist), firsocostat displayed greater improvement in hepatic steatosis and fibrosis of patients with advanced fibrosis caused by NASH defined by histology and clinically relevant biomarkers (NCT03449446) (Loomba et al., 2021).

Lifestyle intervention and weight loss are also effective methods to treat NAFLD. Among them, the ketogenic diet that increases the hepatic ketone production is popular in weight loss and is also helpful for NAFLD (Thoma et al., 2012; Saeed et al., 2019). In a clinical trial, 10 overweight/obese participants, who were restricted in carbohydrate intake while the intake of

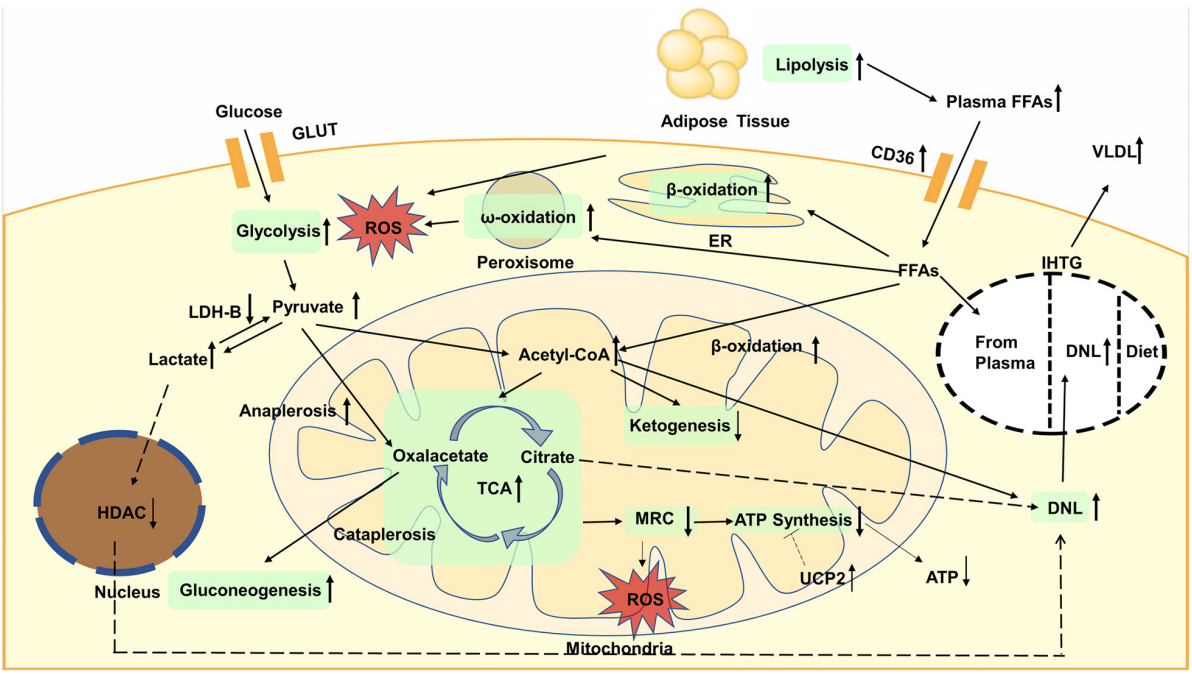

FIGURE 1 | Glycolysis is enhanced, resulting in the increased content of pyruvate in plasma and liver. Then pyruvate is converted to oxaloacetate through anaplerosis or to lactate, both of which are enhanced in NAFLD. Increased lactate will elevate the expression of lipogenic enzymes dependent on decreased activity of nuclear HDAC. Gluconeogenesis is increased and contribute to TCA cycle. Lipolysis is increased, leading to elevated plasma FFAs. accumulation of TAGs is mainly caused by increased DNL. The oxidation of fatty acids is also enhanced, not only in the mitochondria, but also in the endoplasmic reticulum and peroxisomes. The oxidation that occurs in the latter can lead to more production of ROS that causes inflammation and liver damage. Increased glycolysis and fatty acid oxidation will elevate acetyl-CoA and enhance the TCA cycle whereas ketogenesis is reduced. The activity of MRC is reduced, resulting in more ROS generation. The expression of UCP2 increased in fatty liver, which impaired efficiency of ATP synthesis and decreased ATP content. GLUT, glucose transporter; FFAs, plasma free fatty acids; CD36, cluster of designation 36; ROS, reactive oxygen species; ER, endoplasmic reticulum; VLDL, very low density lipoproteins; IHTG, intrahepatic triglycerides; DNL, *de novo* lipogenesis; LDH, lactate dehydrogenase; HDAC, histone deacetylase; TCA, tricarboxylic acid; MRC, mitochondrial respiratory chain; ATP, adenosine triphosphate; UCP, uncoupling protein.

fat and protein remained unchanged, demonstrated decreased IHTG content and improved insulin sensitivity, despite increased circulating FFA (Luukkonen et al., 2020).

There is no FDA-approved drug for NAFLD treatment so far. Therefore, it is of great interest to explore novel targets for NAFLD treatment. In animal models, changes in glycolysis, lactate production, and mitochondrial uncoupling can affect the progression of NAFLD, which can be the potential pharmacological targets for NAFLD.

CONCLUSION

Although the metabolism of liver is generally regulated by insulin and glucagon, NALFD is often accompanied by systemic insulin resistance and the insulin resistance is selective (Brown and Goldstein, 2008), which makes the actual metabolic state hard to predict. In this review we found that the changes in DNL, glycolysis, and ketogenesis is in accord with insulin effect, whereas gluconeogenesis and FAO is less inhibited by insulin.

Therefore, it is meaningful to study the specific changes in metabolism and their role in the pathogenesis of NAFLD. In this review, we mainly discussed changes in lipid and glucose metabolism. Glycolysis is significantly enhanced in the hepatocytes of fatty liver, resulting in the increased content of pyruvate in plasma and liver. Enhanced glycolysis can cause liver inflammation, but the specific pathway is still unclear. PDC is the main enzyme that controls the flux of pyruvate into the TCA cycle. The alteration of its activity in fatty liver is still controversial. Pyruvate can also be converted to oxaloacetate through anaplerosis that provides intermediates for TCA, or to lactate, both of which are enhanced in NAFLD. Increased lactate will elevate the expression of lipogenic enzymes dependent on acetylation of H3K9, and aggravate NAFLD.

Excessive accumulation of fat in hepatocyte is the fundamental feature of NAFLD, accompanied by an increase in VLDL secretion, which is mainly derived from strengthened DNL. Meanwhile, the FAs oxidation is also enhanced in the mitochondria as well as the peroxisomes and ER. The oxidation that occurs in the latter can lead to more production of ROS that causes inflammation and liver damage.

Increased glycolysis and FAO will elevate acetyl-CoA and enhance the TCA cycle, which will increase liver mitochondrial burden. However, the production of ketone bodies is reduced, indicating that the acetyl-CoA is more inclined to enter the flux of TCA cycle. Nevertheless, the activity of MRC is reduced, which cannot match the enhanced TCA cycle, resulting in more ROS generation. Moreover, the expression of UCP2 also increased in fatty liver, which impaired efficiency of ATP synthesis. The global metabolic changes are shown in **Figure 1**.

AUTHOR CONTRIBUTIONS

QL, XT, LZ, and SZ: conception. QL, XT, HW, JH, ML, and ZM: drafting manuscript. XT, HX, LZ, and SZ: revising manuscript. All authors contributed to the article and approved the submitted version.

FUNDING

This work was supported by Innovative Research Groups of National Natural Science Foundation of China (No. 81721091).

ACKNOWLEDGMENTS

Thanks to Innovative Research Groups of National Natural Science Foundation of China for financial support.

REFERENCES

Adeva-Andany, M., López-Ojén, M., Funcasta-Calderón, R., Ameneiros-Rodríguez, E., Donapetry-García, C., Vila-Altesor, M., et al. (2014). Comprehensive review on lactate metabolism in human health. *Mitochondrion* 17, 76–100. doi: 10.1016/j.mito.2014.05.007

Bajotto, G., Murakami, T., Nagasaki, M., Qin, B., Matsuo, Y., Maeda, K., et al. (2006). Increased expression of hepatic pyruvate dehydrogenase kinases 2 and 4 in young and middle-aged Otsuka Long-Evans Tokushima Fatty rats: induction by elevated levels of free fatty acids. *Metabolism* 55, 317–323. doi: 10.1016/j.metabol.2005.09.014

Bechmann, L. P., Gieseler, R. K., Sowa, J. P., Kahraman, A., Erhard, J., Wedemeyer, I., et al. (2010). Apoptosis is associated with CD36/fatty acid translocase upregulation in non-alcoholic steatohepatitis. *Liver Int.* 30, 850–859. doi: 10.1111/j.1478-3231.2010.02248.x

Benhamed, F., Denechaud, P. D., Lemoine, M., Robichon, C., Moldes, M., Bertrand-Michel, J., et al. (2012). The lipogenic transcription factor ChREBP dissociates hepatic steatosis from insulin resistance in mice and humans. *J. Clin. Invest.* 122, 2176–2194. doi: 10.1172/jci41636

Bonnefont, J. P., Djouadi, F., Prip-Buus, C., Gobin, S., Munnich, A., and Bastin, J. (2004). Carnitine palmitoyltransferases 1 and 2: biochemical, molecular and medical aspects. *Mol. Aspects Med.* 25, 495–520. doi: 10.1016/j.mam.2004.06.004

Bougarne, N., Weyers, B., Desmet, S. J., Deckers, J., Ray, D. W., Staels, B., et al. (2018). Molecular actions of PPARα in lipid metabolism and inflammation. *Endocr. Rev.* 39, 760–802. doi: 10.1210/er.2018-00064

Bowker-Kinley, M. M., Davis, W. I., Wu, P., Harris, R. A., and Popov, K. M. (1998). Evidence for existence of tissue-specific regulation of the mammalian pyruvate dehydrogenase complex. *Biochem. J.* 329(Pt 1), 191–196. doi: 10.1042/bj3290191

Brooks, G. A. (2018). The science and translation of lactate shuttle theory. *Cell Metab.* 27, 757–785. doi: 10.1016/j.cmet.2018.03.008

Brown, M. S., and Goldstein, J. L. (2008). Selective versus total insulin resistance: a pathogenic paradox. *Cell Metab.* 7, 95–96. doi: 10.1016/j.cmet.2007.12.009

Browning, J. D., and Horton, J. D. (2004). Molecular mediators of hepatic steatosis and liver injury. *J. Clin. Invest.* 114, 147–152. doi: 10.1172/jci22422

Brunt, E. M., Kleiner, D. E., Carpenter, D. H., Rinella, M., Harrison, S. A., Loomba, R., et al. (2020). Nonalcoholic fatty liver disease: reporting histologic findings in clinical practice. *Hepatology* 73, 2028–2038. doi: 10.1002/hep.31599

Byrne, C. D., and Targher, G. (2015). NAFLD: a multisystem disease. *J. Hepatol.* 62(Suppl_1), S47–S64. doi: 10.1016/j.jhep.2014.12.012

Cappel, D. A., Deja, S., Duarte, J. A. G., Kucejova, B., Iñigo, M., Fletcher, J. A., et al. (2019). Pyruvate-carboxylase-mediated anaplerosis promotes antioxidant capacity by sustaining TCA cycle and redox metabolism in liver. *Cell Metab.* 29, 1291–1305.e8. doi: 10.1016/j.cmet.2019.03.014

Chavin, K. D., Yang, S., Lin, H. Z., Chatham, J., Chacko, V. P., Hoek, J. B., et al. (1999). Obesity induces expression of uncoupling protein-2 in hepatocytes and promotes liver ATP depletion. *J. Biol. Chem.* 274, 5692–5700. doi: 10.1074/jbc.274.9.5692

Chen, Z., Liu, M., Li, L., and Chen, L. (2018). Involvement of the Warburg effect in non-tumor diseases processes. *J. Cell. Physiol.* 233, 2839–2849. doi: 10.1002/jcp.25998

Cho, J., Zhang, Y., Park, S. Y., Joseph, A. M., Han, C., Park, H. J., et al. (2017). Mitochondrial ATP transporter depletion protects mice against liver steatosis and insulin resistance. *Nat. Commun.* 8:14477. doi: 10.1038/ncomms14477

Cotter, D. G., Ercal, B., Huang, X., Leid, J. M., D'Avignon, D. A., Graham, M. J., et al. (2014). Ketogenesis prevents diet-induced fatty liver injury and hyperglycemia. *J. Clin. Invest.* 124, 5175–5190. doi: 10.1172/jci76388

Crespo, J., Cayón, A., Fernández-Gil, P., Hernández-Guerra, M., Mayorga, M., Domínguez-Díez, A., et al. (2001). Gene expression of tumor necrosis factor alpha and TNF-receptors, p55 and p75, in nonalcoholic steatohepatitis patients. *Hepatology* 34, 1158–1163. doi: 10.1053/jhep.2001.29628

Dawson, D. M., Goodfriend, T. L., and Kaplan, N. O. (1964). Lactic dehydrogenases: functions of the two types rates of synthesis of the two major forms can be correlated with metabolic differentiation. *Science* 143, 929–933. doi: 10.1126/science.143.3609.929

de la Cruz-López, K. G., Castro-Muñoz, L. J., Reyes-Hernández, D. O., García-Carrancá, A., and Manzo-Merino, J. (2019). Lactate in the regulation of tumor microenvironment and therapeutic approaches. *Front. Oncol.* 9:1143. doi: 10.3389/fonc.2019.01143

Del Río, L. A., and López-Huertas, E. (2016). ROS generation in peroxisomes and its role in cell signaling. *Plant Cell Physiol.* 57, 1364–1376. doi: 10.1093/pcp/pcw076

Dentin, R., Girard, J., and Postic, C. (2005). Carbohydrate responsive element binding protein (ChREBP) and sterol regulatory element binding protein-1c (SREBP-1c): two key regulators of glucose metabolism and lipid synthesis in liver. *Biochimie* 87, 81–86. doi: 10.1016/j.biochi.2004.11.008

Donnelly, K. L., Smith, C. I., Schwarzenberg, S. J., Jessurun, J., Boldt, M. D., and Parks, E. J. (2005). Sources of fatty acids stored in liver and secreted via lipoproteins in patients with nonalcoholic fatty liver disease. *J. Clin. Invest.* 115, 1343–1351. doi: 10.1172/jci23621

Dubois, V., Eeckhoute, J., Lefebvre, P., and Staels, B. (2017). Distinct but complementary contributions of PPAR isotypes to energy homeostasis. *J. Clin. Invest.* 127, 1202–1214. doi: 10.1172/jci88894

Endo, M., Masaki, T., Seike, M., and Yoshimatsu, H. (2007). TNF-alpha induces hepatic steatosis in mice by enhancing gene expression of sterol regulatory element binding protein-1c (SREBP-1c). *Exp. Biol. Med.* 232, 614–621.

Fabbrini, E., Mohammed, B. S., Magkos, F., Korenblat, K. M., Patterson, B. W., and Klein, S. (2008). Alterations in adipose tissue and hepatic lipid kinetics in obese men and women with nonalcoholic fatty liver disease. *Gastroenterology* 134, 424–431. doi: 10.1053/j.gastro.2007.11.038

Fan, J. G., Kim, S. U., and Wong, V. W. (2017). New trends on obesity and NAFLD in Asia. *J. Hepatol.* 67, 862–873. doi: 10.1016/j.jhep.2017.06.003

Fletcher, J. A., Deja, S., Satapati, S., Fu, X., Burgess, S. C., and Browning, J. D. (2019). Impaired ketogenesis and increased acetyl-CoA oxidation promote hyperglycemia in human fatty liver. *JCI Insight* 5:e127737. doi: 10.1172/jci.insight.127737

Friedman, S. L., Neuschwander-Tetri, B. A., Rinella, M., and Sanyal, A. J. (2018). Mechanisms of NAFLD development and therapeutic strategies. *Nat. Med.* 24, 908–922. doi: 10.1038/s41591-018-0104-9

Gawrieh, S., Noureddin, M., Loo, N., Mohseni, R., Awasty, V., Cusi, K., et al. (2021). Saroglitazar, a PPAR-α/γ agonist, for treatment of NAFLD: a randomized controlled double-blind phase 2 trial. *Hepatology*. doi: 10.1002/hep.31843 [Epub ahead of print].

Gladden, L. B. (2004). Lactate metabolism: a new paradigm for the third millennium. *J. Physiol.* 558(Pt 1), 5–30. doi: 10.1113/jphysiol.2003.058701

Go, Y., Jeong, J. Y., Jeoung, N. H., Jeon, J. H., Park, B. Y., Kang, H. J., et al. (2016). Inhibition of pyruvate dehydrogenase kinase 2 protects against hepatic steatosis through modulation of tricarboxylic acid cycle anaplerosis and ketogenesis. *Diabetes* 65, 2876–2887. doi: 10.2337/db16-0223

Haeusler, R. A., McGraw, T. E., and Accili, D. (2018). Biochemical and cellular properties of insulin receptor signalling. *Nat. Rev. Mol. Cell Biol.* 19, 31–44. doi: 10.1038/nrm.2017.89

Hers, H. G., and Hue, L. (1983). Gluconeogenesis and related aspects of glycolysis. *Annu. Rev. Biochem.* 52, 617–653. doi: 10.1146/annurev.bi.52.070183.003153

Hiebl, V., Ladurner, A., Latkolik, S., and Dirsch, V. M. (2018). Natural products as modulators of the nuclear receptors and metabolic sensors LXR, FXR and RXR. *Biotechnol. Adv.* 36, 1657–1698. doi: 10.1016/j.biotechadv.2018.03.003

Higuchi, N., Kato, M., Shundo, Y., Tajiri, H., Tanaka, M., Yamashita, N., et al. (2008). Liver X receptor in cooperation with SREBP-1c is a major lipid synthesis regulator in nonalcoholic fatty liver disease. *Hepatol. Res.* 38, 1122–1129. doi: 10.1111/j.1872-034X.2008.00382.x

Hodakoski, C., Hopkins, B. D., Barrows, D., Mense, S. M., Keniry, M., Anderson, K. E., et al. (2014). Regulation of PTEN inhibition by the pleckstrin homology domain of P-REX2 during insulin signaling and glucose homeostasis. *Proc. Natl. Acad. Sci. U.S.A.* 111, 155–160. doi: 10.1073/pnas.1213773111

Horie, Y., Suzuki, A., Kataoka, E., Sasaki, T., Hamada, K., Sasaki, J., et al. (2004). Hepatocyte-specific Pten deficiency results in steatohepatitis and hepatocellular carcinomas. *J. Clin. Invest.* 113, 1774–1783. doi: 10.1172/jci20513

Iozzo, P., Bucci, M., Roivainen, A., Någren, K., Järvisalo, M. J., Kiss, J., et al. (2010). Fatty acid metabolism in the liver, measured by positron emission tomography, is increased in obese individuals. *Gastroenterology* 139, 846–856.e6. doi: 10.1053/j.gastro.2010.05.039

Kawano, Y., and Cohen, D. E. (2013). Mechanisms of hepatic triglyceride accumulation in non-alcoholic fatty liver disease. *J. Gastroenterol.* 48, 434–441. doi: 10.1007/s00535-013-0758-5

Keramida, G., Hunter, J., and Peters, A. M. (2016). Hepatic glucose utilization in hepatic steatosis and obesity. *Biosci. Rep.* 36:e00402. doi: 10.1042/bsr20160381

Khan, R. S., Bril, F., Cusi, K., and Newsome, P. N. (2019). Modulation of insulin resistance in nonalcoholic fatty liver disease. *Hepatology* 70, 711–724. doi: 10.1002/hep.30429

Kharitonenkov, A., Shiyanova, T. L., Koester, A., Ford, A. M., Micanovic, R., Galbreath, E. J., et al. (2005). FGF-21 as a novel metabolic regulator. *J. Clin. Invest.* 115, 1627–1635. doi: 10.1172/jci23606

Kim, H. S., Xiao, C., Wang, R. H., Lahusen, T., Xu, X., Vassilopoulos, A., et al. (2010). Hepatic-specific disruption of SIRT6 in mice results in fatty liver formation due to enhanced glycolysis and triglyceride synthesis. *Cell Metab.* 12, 224–236. doi: 10.1016/j.cmet.2010.06.009

Kohjima, M., Enjoji, M., Higuchi, N., Kato, M., Kotoh, K., Yoshimoto, T., et al. (2007). Re-evaluation of fatty acid metabolism-related gene expression in nonalcoholic fatty liver disease. *Int. J. Mol. Med.* 20, 351–358.

Koliaki, C., Szendroedi, J., Kaul, K., Jelenik, T., Nowotny, P., Jankowiak, F., et al. (2015). Adaptation of hepatic mitochondrial function in humans with non-alcoholic fatty liver is lost in steatohepatitis. *Cell Metab.* 21, 739–746. doi: 10.1016/j.cmet.2015.04.004

Koppenol, W. H., Bounds, P. L., and Dang, C. V. (2011). Otto Warburg's contributions to current concepts of cancer metabolism. *Nat. Rev. Cancer* 11, 325–337. doi: 10.1038/nrc3038

Kors, L., Rampanelli, E., Stokman, G., Butter, L. M., Held, N. M., Claessen, N., et al. (2018). Deletion of NLRX1 increases fatty acid metabolism and prevents diet-induced hepatic steatosis and metabolic syndrome. *Biochim. Biophys. Acta Mol. Basis Dis.* 1864(5 Pt A), 1883–1895. doi: 10.1016/j.bbadis.2018.03.003

Lambert, J. E., Ramos-Roman, M. A., Browning, J. D., and Parks, E. J. (2014). Increased de novo lipogenesis is a distinct characteristic of individuals with nonalcoholic fatty liver disease. *Gastroenterology* 146, 726–735. doi: 10.1053/j.gastro.2013.11.049

Lawitz, E. J., Coste, A., Poordad, F., Alkhouri, N., Loo, N., McColgan, B. J., et al. (2018). Acetyl-CoA carboxylase inhibitor GS-0976 for 12 weeks reduces hepatic de novo lipogenesis and steatosis in patients with nonalcoholic steatohepatitis. *Clin. Gastroenterol. Hepatol.* 16, 1983–1991.e3. doi: 10.1016/j.cgh.2018.04.042

Liu, J., Jiang, S., Zhao, Y., Sun, Q., Zhang, J., Shen, D., et al. (2018). Geranylgeranyl diphosphate synthase (GGPPS) regulates non-alcoholic fatty liver disease (NAFLD)-fibrosis progression by determining hepatic glucose/fatty acid preference under high-fat diet conditions. *J. Pathol.* 246, 277–288. doi: 10.1002/path.5131

Loomba, R., Kayali, Z., Noureddin, M., Ruane, P., Lawitz, E. J., Bennett, M., et al. (2018). GS-0976 reduces hepatic steatosis and fibrosis markers in patients

with nonalcoholic fatty liver disease. *Gastroenterology* 155, 1463–1473.e6. doi: 10.1053/j.gastro.2018.07.027

Loomba, R., Noureddin, M., Kowdley, K. V., Kohli, A., Sheikh, A., Neff, G., et al. (2021). Combination therapies including cilofexor and firsocostat for bridging fibrosis and cirrhosis attributable to NASH. *Hepatology* 73, 625–643. doi: 10.1002/hep.31622

Lu, J., Tan, M., and Cai, Q. (2015). The Warburg effect in tumor progression: mitochondrial oxidative metabolism as an anti-metastasis mechanism. *Cancer Lett.* 356(2 Pt A), 156–164. doi: 10.1016/j.canlet.2014.04.001

Luukkonen, P. K., Dufour, S., Lyu, K., Zhang, X. M., Hakkarainen, A., Lehtimäki, T. E., et al. (2020). Effect of a ketogenic diet on hepatic steatosis and hepatic mitochondrial metabolism in nonalcoholic fatty liver disease. *Proc. Natl. Acad. Sci. U.S.A.* 117, 7347–7354. doi: 10.1073/pnas.1922344117

Mansouri, A., Gattolliat, C. H., and Asselah, T. (2018). Mitochondrial dysfunction and signaling in chronic liver diseases. *Gastroenterology* 155, 629–647. doi: 10.1053/j.gastro.2018.06.083

Martínez-Reyes, I., and Chandel, N. S. (2020). Mitochondrial TCA cycle metabolites control physiology and disease. *Nat. Commun.* 11:102. doi: 10.1038/s41467-019-13668-3

Miele, L., Grieco, A., Armuzzi, A., Candelli, M., Forgione, A., Gasbarrini, A., et al. (2003). Hepatic mitochondrial beta-oxidation in patients with nonalcoholic steatohepatitis assessed by 13C-octanoate breath test. *Am. J. Gastroenterol.* 98, 2335–2336. doi: 10.1111/j.1572-0241.2003.07725.x

Nair, S., Pc, V., Arnold, C., and Diehl, A. M. (2003). Hepatic ATP reserve and efficiency of replenishing: comparison between obese and nonobese normal individuals. *Am. J. Gastroenterol.* 98, 466–470. doi: 10.1111/j.1572-0241.2003.07221.x

Owen, O. E., Kalhan, S. C., and Hanson, R. W. (2002). The key role of anaplerosis and cataplerosis for citric acid cycle function. *J. Biol. Chem.* 277, 30409–30412. doi: 10.1074/jbc.R200006200

Panasyuk, G., Espeillac, C., Chauvin, C., Pradelli, L. A., Horie, Y., Suzuki, A., et al. (2012). PPARγ contributes to PKM2 and HK2 expression in fatty liver. *Nat. Commun.* 3:672. doi: 10.1038/ncomms1667

Patterson, R. E., Kalavalapalli, S., Williams, C. M., Nautiyal, M., Mathew, J. T., Martinez, J., et al. (2016). Lipotoxicity in steatohepatitis occurs despite an increase in tricarboxylic acid cycle activity. *Am. J. Physiol. Endocrinol. Metab.* 310, E484–E494. doi: 10.1152/ajpendo.00492.2015

Pérez-Carreras, M., Del Hoyo, P., Martín, M. A., Rubio, J. C., Martín, A., Castellano, G., et al. (2003). Defective hepatic mitochondrial respiratory chain in patients with nonalcoholic steatohepatitis. *Hepatology* 38, 999–1007. doi: 10.1053/jhep.2003.50398

Petersen, M. C., and Shulman, G. I. (2018). Mechanisms of insulin action and insulin resistance. *Physiol. Rev.* 98, 2133–2223. doi: 10.1152/physrev.00063.2017

Petersen, M. C., Vatner, D. F., and Shulman, G. I. (2017). Regulation of hepatic glucose metabolism in health and disease. *Nat. Rev. Endocrinol.* 13, 572–587. doi: 10.1038/nrendo.2017.80

Pittala, S., Krelin, Y., Kuperman, Y., and Shoshan-Barmatz, V. (2019). A mitochondrial VDAC1-based peptide greatly suppresses steatosis and NASH-associated pathologies in a mouse model. *Mol. Ther.* 27, 1848–1862. doi: 10.1016/j.ymthe.2019.06.017

Puchalska, P., and Crawford, P. A. (2017). Multi-dimensional roles of ketone bodies in fuel metabolism, signaling, and therapeutics. *Cell Metab.* 25, 262–284. doi: 10.1016/j.cmet.2016.12.022

Ratziu, V., Harrison, S. A., Francque, S., Bedossa, P., Lehert, P., Serfaty, L., et al. (2016). Elafibranor, an agonist of the peroxisome proliferator-activated receptor-α and -δ, induces resolution of nonalcoholic steatohepatitis without fibrosis worsening. *Gastroenterology* 150, 1147–1159.e5. doi: 10.1053/j.gastro.2016.01.038

Reddy, J. K. (2001). Nonalcoholic steatosis and steatohepatitis. III. Peroxisomal beta-oxidation, PPAR alpha, and steatohepatitis. *Am. J. Physiol. Gastrointest. Liver Physiol.* 281, G1333–G1339. doi: 10.1152/ajpgi.2001.281.6.G1333

Repa, J. J., Liang, G., Ou, J., Bashmakov, Y., Lobaccaro, J. M., Shimomura, I., et al. (2000). Regulation of mouse sterol regulatory element-binding protein-1c gene (SREBP-1c) by oxysterol receptors, LXRalpha and LXRbeta. *Genes Dev.* 14, 2819–2830. doi: 10.1101/gad.844900

Rich, P. R., and Maréchal, A. (2010). The mitochondrial respiratory chain. *Essays Biochem.* 47, 1–23. doi: 10.1042/bse0470001

Robertson, G., Leclercq, I., and Farrell, G. C. (2001). Nonalcoholic steatosis and steatohepatitis. II. Cytochrome P-450 enzymes and oxidative stress. *Am. J. Physiol Gastrointest. Liver Physiol.* 281, G1135–G1139. doi: 10.1152/ajpgi.2001.281.5.G1135

Robinson, A. M., and Williamson, D. H. (1980). Physiological roles of ketone bodies as substrates and signals in mammalian tissues. *Physiol. Rev.* 60, 143–187. doi: 10.1152/physrev.1980.60.1.143

Rothman, D. L., Magnusson, I., Katz, L. D., Shulman, R. G., and Shulman, G. I. (1991). Quantitation of hepatic glycogenolysis and gluconeogenesis in fasting humans with 13C NMR. *Science* 254, 573–576. doi: 10.1126/science.1948033

Saeed, N., Nadeau, B., Shannon, C., and Tincopa, M. (2019). Evaluation of dietary approaches for the treatment of non-alcoholic fatty liver disease: a systematic review. *Nutrients* 11:3064. doi: 10.3390/nu11123064

Samuel, V. T., Petersen, K. F., and Shulman, G. I. (2010). Lipid-induced insulin resistance: unravelling the mechanism. *Lancet* 375, 2267–2277. doi: 10.1016/s0140-6736(10)60408-4

Samuel, V. T., and Shulman, G. I. (2016). The pathogenesis of insulin resistance: integrating signaling pathways and substrate flux. *J. Clin. Invest.* 126, 12–22. doi: 10.1172/jci77812

Sanyal, A., Charles, E. D., Neuschwander-Tetri, B. A., Loomba, R., Harrison, S. A., Abdelmalek, M. F., et al. (2019). Pegbelfermin (BMS-986036), a PEGylated fibroblast growth factor 21 analogue, in patients with non-alcoholic steatohepatitis: a randomised, double-blind, placebo-controlled, phase 2a trial. *Lancet* 392, 2705–2717. doi: 10.1016/s0140-6736(18)31785-9

Sanyal, A. J., Campbell-Sargent, C., Mirshahi, F., Rizzo, W. B., Contos, M. J., Sterling, R. K., et al. (2001). Nonalcoholic steatohepatitis: association of insulin resistance and mitochondrial abnormalities. *Gastroenterology* 120, 1183–1192. doi: 10.1053/gast.2001.23256

Satapati, S., Kucejova, B., Duarte, J. A., Fletcher, J. A., Reynolds, L., Sunny, N. E., et al. (2016). Mitochondrial metabolism mediates oxidative stress and inflammation in fatty liver. *J. Clin. Invest.* 126:1605. doi: 10.1172/jci86695

Satapati, S., Sunny, N. E., Kucejova, B., Fu, X., He, T. T., Méndez-Lucas, A., et al. (2012). Elevated TCA cycle function in the pathology of diet-induced hepatic insulin resistance and fatty liver. *J. Lipid Res.* 53, 1080–1092. doi: 10.1194/jlr.M023382

Serviddio, G., Bellanti, F., Tamborra, R., Rollo, T., Capitanio, N., Romano, A. D., et al. (2008). Uncoupling protein-2 (UCP2) induces mitochondrial proton leak and increases susceptibility of non-alcoholic steatohepatitis (NASH) liver to ischaemia-reperfusion injury. *Gut* 57, 957–965. doi: 10.1136/gut.2007.147496

Shannon, C. E., Ragavan, M., Palavicini, J. P., Fourcaudot, M., Bakewell, T. M., Valdez, I. A., et al. (2021). Insulin resistance is mechanistically linked to hepatic mitochondrial remodeling in non-alcoholic fatty liver disease. *Mol. Metab.* 45:101154. doi: 10.1016/j.molmet.2020.101154

Shimomura, I., Bashmakov, Y., and Horton, J. D. (1999). Increased levels of nuclear SREBP-1c associated with fatty livers in two mouse models of diabetes mellitus. *J. Biol. Chem.* 274, 30028–30032. doi: 10.1074/jbc.274.42.30028

Silverstein, R. L., and Febbraio, M. (2009). CD36, a scavenger receptor involved in immunity, metabolism, angiogenesis, and behavior. *Sci. Signal.* 2:re3. doi: 10.1126/scisignal.272re3

Singh, S., Allen, A. M., Wang, Z., Prokop, L. J., Murad, M. H., and Loomba, R. (2015). Fibrosis progression in nonalcoholic fatty liver vs nonalcoholic steatohepatitis: a systematic review and meta-analysis of paired-biopsy studies. *Clin. Gastroenterol. Hepatol.* 13, 643–654.e1-9; quiz e39–e40. doi: 10.1016/j.cgh.2014.04.014

Sunny, N. E., Parks, E. J., Browning, J. D., and Burgess, S. C. (2011). Excessive hepatic mitochondrial TCA cycle and gluconeogenesis in humans with nonalcoholic fatty liver disease. *Cell Metab.* 14, 804–810. doi: 10.1016/j.cmet.2011.11.004

Thoma, C., Day, C. P., and Trenell, M. I. (2012). Lifestyle interventions for the treatment of non-alcoholic fatty liver disease in adults: a systematic review. *J. Hepatol.* 56, 255–266. doi: 10.1016/j.jhep.2011.06.010

Tilg, H., Moschen, A. R., and Roden, M. (2017). NAFLD and diabetes mellitus. *Nat. Rev. Gastroenterol. Hepatol.* 14, 32–42. doi: 10.1038/nrgastro.2016.147

Trivedi, P., Wang, S., and Friedman, S. L. (2021). The power of plasticity-metabolic regulation of hepatic stellate cells. *Cell Metab.* 33, 242–257. doi: 10.1016/j.cmet.2020.10.026

Vander Heiden, M. G., Cantley, L. C., and Thompson, C. B. (2009). Understanding the Warburg effect: the metabolic requirements of cell proliferation. *Science* 324, 1029–1033. doi: 10.1126/science.1160809

Wanders, R. J., Komen, J., and Kemp, S. (2011). Fatty acid omega-oxidation as a rescue pathway for fatty acid oxidation disorders in humans. *FEBS J.* 278, 182–194. doi: 10.1111/j.1742-4658.2010.07947.x

Wang, T., Chen, K., Yao, W., Zheng, R., He, Q., Xia, J., et al. (2020). Acetylation of lactate dehydrogenase B drives NAFLD progression by impairing lactate clearance. *J. Hepatol.* 74, 1038–1052. doi: 10.1016/j.jhep.2020.11.028

Wang, Y., Viscarra, J., Kim, S. J., and Sul, H. S. (2015). Transcriptional regulation of hepatic lipogenesis. *Nat. Rev. Mol. Cell Biol.* 16, 678–689. doi: 10.1038/nrm4074

Watt, M. J., Miotto, P. M., De Nardo, W., and Montgomery, M. K. (2019). The liver as an endocrine organ-linking NAFLD and insulin resistance. *Endocr. Rev.* 40, 1367–1393. doi: 10.1210/er.2019-00034

Willems, P. H., Rossignol, R., Dieteren, C. E., Murphy, M. P., and Koopman, W. J. (2015). Redox homeostasis and mitochondrial dynamics. *Cell Metab.* 22, 207–218. doi: 10.1016/j.cmet.2015.06.006

Wu, L. M., He, H., Chen, G., Kuang, Y., Lin, B. Y., Chen, X. H., et al. (2020). Associations between obesity and metabolic health with nonalcoholic fatty liver disease in elderly Chinese. *Hepatobiliary Pancreat. Dis. Int.* 19, 252–257. doi: 10.1016/j.hbpd.2020.02.010

Younossi, Z., Anstee, Q. M., Marietti, M., Hardy, T., Henry, L., Eslam, M., et al. (2018). Global burden of NAFLD and NASH: trends, predictions, risk factors and prevention. *Nat. Rev. Gastroenterol. Hepatol.* 15, 11–20. doi: 10.1038/nrgastro.2017.109

Younossi, Z. M., Koenig, A. B., Abdelatif, D., Fazel, Y., Henry, L., and Wymer, M. (2016). Global epidemiology of nonalcoholic fatty liver disease-meta-analytic assessment of prevalence, incidence, and outcomes. *Hepatology* 64, 73–84. doi: 10.1002/hep.28431

Yuan, X., Li, H., Bai, H., Zhao, X., Zhang, C., Liu, H., et al. (2016). The 11β-hydroxysteroid dehydrogenase type 1 inhibitor protects against the insulin resistance and hepatic steatosis in db/db mice. *Eur. J. Pharmacol.* 788, 140–151. doi: 10.1016/j.ejphar.2016.05.034

Zhou, Z. H., McCarthy, D. B., O'Connor, C. M., Reed, L. J., and Stoops, J. K. (2001). The remarkable structural and functional organization of the eukaryotic pyruvate dehydrogenase complexes. *Proc. Natl. Acad. Sci. U.S.A.* 98, 14802–14807. doi: 10.1073/pnas.011597698

Zorov, D. B., Juhaszova, M., and Sollott, S. J. (2014). Mitochondrial reactive oxygen species (ROS) and ROS-induced ROS release. *Physiol. Rev.* 94, 909–950. doi: 10.1152/physrev.00026.2013

Conflict of Interest: The authors declare that the research was conducted in the absence of any commercial or financial relationships that could be construed as a potential conflict of interest.

Publisher's Note: All claims expressed in this article are solely those of the authors and do not necessarily represent those of their affiliated organizations, or those of the publisher, the editors and the reviewers. Any product that may be evaluated in this article, or claim that may be made by its manufacturer, is not guaranteed or endorsed by the publisher.

frontiers in Physiology

MINI REVIEW
published: 28 October 2021
doi: 10.3389/fphys.2021.761481

Efficacy and Mechanisms of Gastric Volume-Restriction Bariatric Devices

*Yanmin Wang and Ghassan S. Kassab**

California Medical Innovations Institute, San Diego, CA, United States

Obesity is a chronic disease that affects over 795 million people worldwide. Bariatric surgery is an effective therapy to combat the epidemic of clinically severe obesity, but it is only performed in a very small proportion of patients because of the limited surgical indications, the irreversibility of the procedure, and the potential postoperative complications. As an alternative to bariatric surgery, numerous medical devices have been developed for the treatment of morbid obesity and obesity-related disorders. Most devices target restriction of the stomach, but the mechanism of action is likely more than just mechanical restriction. The objective of this review is to integrate the underlying mechanisms of gastric restrictive bariatric devices in obesity and comorbidities. We call attention to the need for future studies on potential mechanisms to shed light on how current gastric volume-restriction bariatric devices function and how future devices and treatments can be further improved to combat the epidemic of obesity.

Keywords: obesity, weight loss, medical device, restrictive procedure, review

OPEN ACCESS

Edited by:
Kathleen S. Curtis,
Oklahoma State University Center for Health Sciences, United States

Reviewed by:
Carmen De Miguel,
University of Alabama at Birmingham, United States
Zhi Yi Ong,
University of New South Wales, Australia

***Correspondence:**
Ghassan S. Kassab
gkassab@calmi2.org

Specialty section:
This article was submitted to Metabolic Physiology, a section of the journal Frontiers in Physiology

Received: *19 August 2021*
Accepted: *07 October 2021*
Published: *28 October 2021*

Citation:
Wang Y and Kassab GS (2021) Efficacy and Mechanisms of Gastric Volume-Restriction Bariatric Devices. Front. Physiol. 12:761481. doi: 10.3389/fphys.2021.761481

INTRODUCTION

Obesity is a consequence of caloric imbalance and excessive fat accumulation. The World Health Organization (WHO) defined obesity as body mass index (BMI) over 30, while 25–30 is considered overweight. Obesity is a major public health problem in the developed world, which significantly increases the risk of multiple diseases and disorders such as type 2 diabetes mellitus, hypertension, heart disease, and cancer. The prevalence of obesity has greatly increased in the past decades. It was estimated that in 2016, the number of children/adolescents and adults that suffered from obesity worldwide were 124 and 671 million, respectively (Bentham et al., 2017). In addition, 213 million children/adolescents and 1.3 billion adults were in the range of overweight (Bentham et al., 2017). In the US, the prevalence of obesity in adults and children ages 6–11 old has reached over 35% (Flegal et al., 2012) and 17% (Ogden et al., 2016).

In various countries and regions, bariatric surgery has been listed in obesity management guidelines as the most effective way to treat morbid obesity and the related disorders (Jensen et al., 2014; Yumuk et al., 2015; Wharton et al., 2020). The most popular procedures (American Society for Metabolic and Bariatric Surgery, 2021) gastric bypass and sleeve gastrectomy are, however, not readily accepted by many patients because both include removal of some part of the stomach, and this gastrectomy may induce severe complications. Only 1–2% of the eligible candidates undergo bariatric surgery for obesity each year in the US (Gasoyan et al., 2019). Furthermore, based on Western guidelines, patients whose BMI is lower than 35 (or 40 without adiposity-related disease) are beyond the indications of bariatric surgery and thus lack effective treatments.

As less invasive alternatives, many gastric restrictive bariatric devices such as gastric band, intragastric balloons, and so on, have been used for combating obesity and some achieve

comparable efficacy to surgeries (Vargas et al., 2018). Although most of the devices are intended to restrict the stomach to decrease calorie intake, the mechanisms of action for the considerable weight loss following gastric volume-restricted bariatric devices are not fully appreciated. This review aims to integrate the potential mechanisms through which restrictive bariatric devices induce weight loss and metabolic improvements. To the best of our knowledge, this is the first review on this topic.

Gastric Band

In the adjustable gastric banding (AGB) procedure, an adjustable silicone band is placed around the stomach below the gastro esophageal junction to restrict the dilation of the gastric pouch as shown in **Figure 1A**. AGB is the most well-known gastric restrictive device: first implanted in 1983 (Kuzmak, 1991), it gained popularity in early twenty-first century (Favretti et al., 2009; Ibrahim et al., 2017). A meta-analysis (Garb et al., 2009) found that the excess weight loss (weight loss/pre-operative excess body weight × 100%) post-AGB was 42.6% at 1 year, 50.3% at 2 years, and 55.2% at over 3 years. Another meta-analysis (Golzarand et al., 2017) showed that AGB induced nearly 48% excess weight loss at either 5 or 10 years postoperatively. According to data from 20 years follow-up in patients with obesity, AGB was associated with significantly lower incidence of diabetes, cardiovascular diseases, cancer, and renal diseases (Pontiroli et al., 2018). The cost for AGB is significantly lower than that for Roux-en-Y gastric bypass or sleeve gastrectomy (SG) (Doble et al., 2019). Some studies, however, reported that AGB failed to maintain reduced body weight or control obesity-related morbidities (Pournaras et al., 2010; Chang et al., 2014; Park et al., 2019). Worse still, additional studies showed that patients who underwent AGB may need a second surgery due to band migration or erosion, pouch dilatation, achalasia or megaesophagus, stomach obstruction, or other severe complications (Arias et al., 2009; Chang et al., 2014; Kodner and Hartman, 2014; Tsai et al., 2019). The reported reoperation rate was up to 82.7% in 15-year follow-up (Tsai et al., 2019). As a result, the popularity of AGB has been dramatically decreased in the past decade. In recent years, several improved AGB devices and systems (Billy et al., 2014; Edelman et al., 2014; Ponce et al., 2014) have been developed, but the long-term effects remain unclear. In 2019, AGB only accounted for 0.9% of bariatric procedures in the US (American Society for Metabolic and Bariatric Surgery, 2021).

There have been numerous studies focused on the potential mechanism of AGB in weight control and metabolic amelioration induced by the placement of the band. AGB is considered to improve eating behavior such as alleviating binge eating disorders and decreasing emotional eating and night eating in the short term (Opozda et al., 2016; Hindle et al., 2020), whereas long-term results are inconsistent (Opozda et al., 2016; Smith et al., 2019). Monteiro et al. (2007) compared AGB rats and pair-fed rats, observing that AGB rats were leaner. This study suggests that additional factors beyond restriction exist. It seems that gastric motility, neural activity, ghrelin level, concentrations of gut hormones, energy expenditure, bile acids metabolism, and gut microbial diversity play important roles; however, the conclusions varied significantly (Wang et al., 2019). For example, Aron-Wisnewsky et al. (2019) observed that gut microbial gene abundance increased after AGB whereas Lee et al. (2019) reported an opposite result. Another example is that ghrelin levels were found to be unchanged (Sysko et al., 2013), increased (Kawasaki et al., 2015), or decreased (Leonetti et al., 2003) following AGB. We assume that the variations are not only partly due to the differences in techniques of the procedures and baseline conditions of the subjects, but also because the underlying factors are complex (i.e., multiple mediators work together and interact with each other).

In addition to AGB in which the stomach is restricted horizontally, vertical banded gastroplasty (VBG) used banding above the crow's foot of Latarjet's nerve along with vertical staple line toward the angle of His to restrict the stomach. In the early 1980s, Mason (1982) reported that VBG caused more weight loss and less complications when compared with other surgical procedures. Kellum et al. (1990) reported that at 6 months after VBG, excess weight loss in patients with morbid obesity was 41.8%. Brolin et al. (1994) found that patients underwent VBG preferred to eat high-caloric food, resulting in postoperative weight regain. Olbers et al. (2006) obtained similar results, showing that VBG patients consumed more sweet foods and less vegetables and fruits. One study (Amsalem et al., 2014) revealed that VGB (specifically the silastic ring vertical gastroplasty) as well as AGB significantly lower the risk of pregnancy complications such as gestational diabetes mellitus and hypertension. This suggests that some metabolic factors exist in these restrictive procedures, which requires further research. In Kellum et al. (1990)'s study, glucose, insulin, enteroglucagon, serotonin, vasoactive intestinal polypeptide, and cholecystokinin (CCK) responses to meals were not changed after VBG. Tremaroli et al. (2015) suggested that VBG has long-term positive effects on gut microbiota and bile acids. The resting energy expenditure was reported to be decreased after VBG, but it seemed a reflection of weight loss instead of the reason (Olbers et al., 2006). Similar to AGB, however, long-term studies (Balsiger et al., 2000; van Wezenbeek et al., 2015; Froylich et al., 2020) revealed that the weight reduction after VBG was not sustained and complications such as pouch dilatation, staple-line disruptions, and outlet stenosis were frequent. Therefore, VBG lost popularity and is no longer practiced.

Gastric Sleeve Implant and Gastric Clip

Since so-called restrictive procedures are technically simple, there have been several devices designed to treat obesity by reducing gastric volume, apart from traditional gastric banding devices, in either laboratory or clinical settings. Our group developed a restrictive device (referred to as Gastric Sleeve Implant, GSI), which is designed to be laparoscopically implantable and removable (Guo et al., 2011, 2014) as shown in **Figure 1B**. When placed loosely on the outside (serosa) of the stomach, the device generates a sleeve-shaped pouch similar to sleeve gastrectomy (SG) but avoids the irreversibility of the SG because it does not require stapling or gastrectomy. When the stomach is empty, GSI does not compress the stomach, which reduces the risk of device migration or tissue necrosis. GSI also has two C-rings to

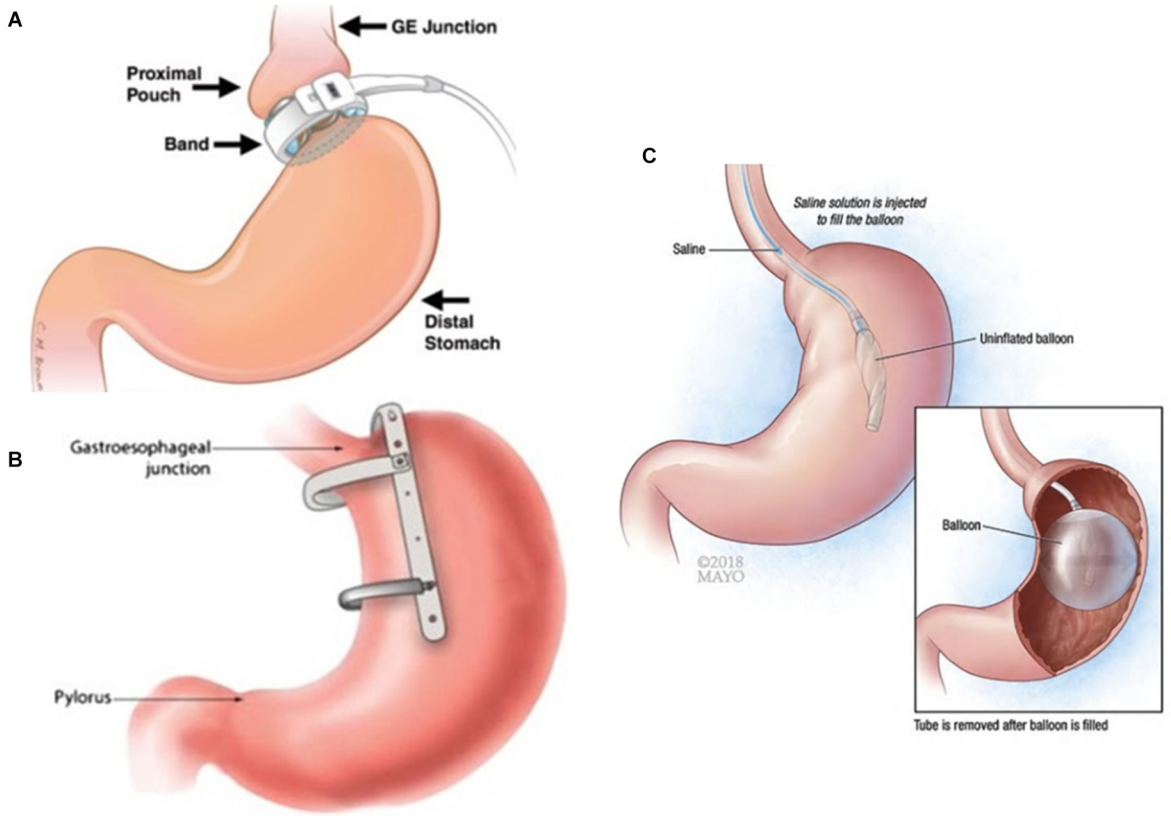

FIGURE 1 | Schematic of gastric restrictive bariatric devices. **(A)** Adjustable gastric banding (AGB). Used with permission of the Radiological Society of North America (RSNA®) (Sonavane et al., 2012). The band is planted around the stomach below gastroesophageal (GE) junction. **(B)** Gastric sleeve implant (GSI). Reprinted by permission from Springer Nature, *Obesity Surgery*, Efficacy of a Laparoscopic Gastric Restrictive Device in an Obese Canine Model, Guo et al. (2014) COPYRIGHT 2013. The device is mounted on the lesser curvature and creates a vertical sleeve food track. **(C)** Intragastric balloons (IGB). Used with permission of Mayo Foundation for Medical Education and Research, all rights reserved (https://www.mayoclinic.org/medical-professionals/endocrinology/news/intragastric-balloon-a-re-emerging-approach-for-obesity/mac-20430245). The inflated balloon occupies some intragastric space.

prevent the distension of the sleeve (Guo et al., 2011, 2014). The GSI is safe, effective and has been proven removable in animals (Guo et al., 2011, 2014). In a canine model, the excess weight loss reached 75% at 12 weeks after procedure but returned to 22% at 6 months after the removal of the device (Guo et al., 2014). To explore the underlying mechanism, our canine and rat studies (Guo et al., 2012) showed an elevated level of ghrelin and a reduced concentration of leptin after the implantation of GSI, which returned to normal levels after GSI removal. We assume that GSI induces an adaptive or compensatory increase in ghrelin secretion at early stages after surgery due to the integrity of stomach, which would counteract additional weight loss and cause the corresponding body weight recovery after its removal (Guo et al., 2012). The lower leptin level induced by GSI is highly correlated with weight loss. It is probably secondary to weight loss as serum leptin concentration reflects the total amount of fat mass in the body (Guo et al., 2012). The Glucagon-like peptide-1 (GLP-1) concentration was found to be unchanged.

Subsequently, a device with similar principle, the vertical gastric clip (Jacobs et al., 2017; Noel et al., 2018) or BariClip (Noel et al., 2020), was used in patients. Parallel to the lesser curvature, the device separates a medial lumen from an excluded lateral gastric pouch (Jacobs et al., 2017). The reduction of BMI and % excess weight loss were 12.7 and 66.7, respectively, at 2 years after the operation (Jacobs et al., 2017). In addition, the quality of life was improved in more than 90% of patients (Noel et al., 2018). A simpler device named Gastric Clip (Chao et al., 2019) was also used in clinics. The gastric clip creates a transverse gastric partition when obliquely applied to the upper fundus (Chao et al., 2019). One year after surgery, BMI was significantly reduced from 44 to 37 kg/m^2, and the total weight loss (weight loss/pre-operative body weight × 100%) was 23.5%. Diabetes and hyperlipidemia were effectively alleviated as well (Chao et al., 2019), and the effects were much better when combined with a proximal jejunal bypass. The possible mechanisms underlying clip-induced weight change require further studies. The long-term benefits of these devices are currently lacking, however, and some patients were reported to suffer from gastric obstruction or insufficient weight loss after such procedures and thus underwent clip removal or revisional surgery (de la Plaza Llamas et al., 2020;

TABLE 1 | Parameter changes after gastric volume-restriction bariatric devices.

	Adjustable gastric banding (AGB)	Vertical banded gastroplasty (VBG)	Gastric sleeve implant (GSI)	Intragastric balloons (IGB)	Endoscopic sleeve gastroplasty (ESG)	Articulating circular endoscopic (ACE)
Gastric emptying	↔ ↓			↓	↓	
Energy expenditure	↑ ↔ ↓	↓		↓		
Ghrelin level	↑ ↔ ↓		↑	↑ ↔ ↓	↔ ↓	↓
Glucagon-like peptide 1 level	↔ ↓		↔		↔	
Peptide YY level	↑ ↔			↔	↔	
Cholecystokinin level		↔		↓		
Leptin level			↓	↓	↔ ↓	
Adiponectin level				↔	↔	↑
Bile acids	↑ ↓	↑				
Gut microbiota	Gene richness ↑ ↓; Proteobacteria ↑	E. Coli ↑; Eubacterium rectale ↓; Roseburia intestinalis ↓				
Eating habit	Binge eating ↔ ↓; emotional eating ↔ ↓; night eating ↓; grazing ↑	High-caloric food ↑; sweet food ↑; vegetable↓; fruit ↓		Grazing ↓; emotional eating ↓; sweet food ↓; after-dinner grazing ↓		

↑, increased; ↔, unchanged; ↓, decreased. More than one arrow indicates inconsistent data; blank means unknown data.

Chang et al., 2021). Furthermore, gastric clip has been used to assist with SG, but a gastrectomy was still performed to achieve metabolic improvements in mice (Schlager et al., 2011; Wei et al., 2020). This implies that a simple gastric clip may not be a reliable bariatric device as a stand-alone. More follow-up data is needed.

Intragastric Balloons

Intragastric balloons (IGB) have been used to occupy the gastric space by endoscopic placement as shown in **Figure 1C**. The FDA has approved three IGBs (Vyas et al., 2017; Vargas et al., 2018), i.e., Orbera, Obalon, and ReShape Duo [no longer available (FDA, 2020)] to combat obesity with BMI 30–40 kg/m^2. In addition, there have been some other IGBs (such as Elipse, Medsil, Spatz3, and so on) (Bužga et al., 2014; Ramai et al., 2020; Badurdeen et al., 2021) awaiting for validation or approval. As a result, reducing gastric capacity via endoscopically implanted IGBs has emerged as a viable option to alleviate morbid obesity. A retrospective study of 5,874 patients (Fittipaldi-Fernandez et al., 2020) showed that the incidence of gastric perforation and digestive bleeding were only 0.07 and 0.05% in the first half year after IGB implant. According to the American Society for Metabolic and Bariatric Surgery (2021), in 2015, balloons were used only in 0.3% cases of bariatric procedures in the US, while in 2019 the number increased to 1.8%.

Generally, the balloons are placed endoscopically into stomach for no more than 6 months (in some techniques the time is longer), after which they are removed. A meta-analysis including 5,668 subjects (Popov et al., 2017) reported that patients had 28% excess weight loss and 4.8 kg/m^2 BMI decrease at 6 months after IGBs removal, although some weight regain was observed at balloon removal. Some investigators showed that after 6-month implantation, the total weight loss of the IGBs is 6.8–13.2% (Vargas et al., 2018); at 12 months, i.e., 6 months following balloon removal, the weight loss is still satisfactory, albeit modest at 7.6–11.3% total weight loss (Vargas et al., 2018). This indicates that the weight reduction outcome after IGBs is not dependent on gastric restriction. Genco et al. (2013) reported that IGB placement improves eating habits, reducing frequent food consuming, preference of sweet foods, emotional eating, and after-dinner grazing in patients with obesity. Some IGBs are reported to alter gastric motility and hormone levels in addition to reducing gastric volume. Mion et al. (2005) found that balloon placement leads to suppression of gastric emptying and ghrelin production, but the subsequent weight reduction is not associated with gastric emptying. Another study (Mathus-Vliegen and de Groot, 2013) reported a decrease of CCK after IGBs, which may correlate with delayed gastric emptying. In these studies, the variations of ghrelin and CCK are likely to be the results of weight loss rather than the causes. Fuller's group (Fuller et al., 2013) performed a randomized controlled trial for IGB evaluation. In their study, ghrelin was increased and leptin was decreased when the device was implanted, but both concentrations recovered to baseline after the removal of the balloon. In addition, fasting levels of adiponectin or Peptide YY (PYY) were not affected by weight loss associated with the IGBs treatment. Similarly, Bužga et al. (2014) observed that serum ghrelin was increased while leptin and fibroblast growth factor 21 levels were decreased at 6 months after balloon insertion in patients with BMI of 43 kg/m^2, but longer-term results were

not assessed. Another study (Mathus-Vliegen and Eichenberger, 2014) also indicated that fasting and postprandial ghrelin levels remained stable at 13 and 26 weeks after IGBs, despite sustained weight loss. A study (Badurdeen et al., 2021) showed that 9-month administration of Liraglutide (GLP-1 agonist) after IGB removal was effective in preventing weight regain and reducing fat mass. It indicates that GLP-1 concentration is potentially an important factor of IGB-induced weight loss, which needs further verification.

Aside from the potential changes in gastrointestinal motility and hormones, IGB therapy reduces fat mass and resting metabolic rate (Gaździńska et al., 2020), which are associated with weight decrease. IGBs are also reported to improve obesity related disorders such as hypertension (Popov et al., 2017), hyperglycemia (Popov et al., 2017), dyslipidemia (Ramai et al., 2020), and non-alcoholic fatty liver disease (Chandan et al., 2021). More studies are needed to reveal deeper mechanisms.

Endoscopic Gastroplasty and Gastroplication

Endoscopic Sleeve Gastroplasty (ESG) is also an emerging endoluminal method to manage obesity. First used in patients a decade ago, it has been improved in recent years (Kumar et al., 2018). Using endoscopic suturing devices, ESG procedure places a series of sutures from the antrum to the fundus, creating a banana-shape stomach pouch like SG does. Similar devices to mimic SG or gastroplasty include Apollo OverStitch, EndoCinch, Incisionless Operating Platform, amongst others (Kumar, 2015).

In comparison of laparoscopic SG and AGB, although SG achieved the greatest weight reduction, ESG is thought to be the safest and most viable choice with lower morbidity and shorter stay in hospital (Novikov et al., 2018). Jain et al. (2017) summarized nine single center prospective human studies treating obesity by ESG technique. In these studies, no intra-procedure complication was reported, while 2.3% of the patients experienced major but not fatal postoperative complications such as perigastric leakage. Although the detailed techniques were different, the % excess weight loss was reported to be 30–57 (Jain et al., 2017). An international multicenter study (Barrichello et al., 2019) showed that at 12-month after ESG, the total and excess weight loss were 15.1 and 59.4%, and adipose tissue was significantly lowered. Lopez-Nava and coworkers retrospectively analyzed 248 patients, indicating that at 6 and 24 months after ESG, the total weight loss was 15.2 and 18.6%, respectively (Lopez-Nava et al., 2017). In another study with a smaller group of patients, they found that at 1 year after ESG, BMI loss was 7.3 kg/m^2, while total and excess weight loss were 18.7 and 54.6% (Lopez-Nava et al., 2016). Alqahtani et al. (2019) provided similar data, showing 13.7, 15, and 14.8% total weight loss at 6, 12, 18 months, respectively. In this study, ESG also resulted in satisfactory remissions of diabetes, hypertension, and dyslipidemia (Alqahtani et al., 2019). Sharaiha et al. (2017) studied 91 consecutive patients who underwent ESG. At 1 year after procedure, the patients not only lost 14.4% body weight, but also showed significantly improved levels of hemoglobin A1c, systolic blood pressure, alanine aminotransferase, and serum triglycerides (Sharaiha et al., 2017).

There have been some studies exploring the underlying contributors of weight loss and metabolic improvements beyond restriction following ESG. Lopez-Nava et al. (2020) found a reduced levels of leptin and an improved insulin secretory pattern in patients at 6 months after ESG, while ghrelin, GLP-1, PYY, and adiponectin remained stable. These changes differed from those following SG, which is likely because of the different post-operatively anatomical structures between the two procedures. The researchers concluded that hormonal variations play little role in weight loss and metabolic improvements (Lopez-Nava et al., 2020). In contrast, Abu Dayyeh et al. (2017) revealed that insulin sensitivity was improved after ESG, with decreased (not significantly) ghrelin levels and unchanged leptin, GLP-1, and PYY. Moreover, they reported that ESG delays gastric emptying, thus producing early satiation and decreasing caloric consumption to reach maximum fullness in patients, but the sample size was to be increased (Abu Dayyeh et al., 2017). This finding is in support of the above-mentioned Lopez-Nava et al.'s conclusion, although the gut hormone changes in the two papers were not comparable. The variation may mainly be due to different follow-up duration as well as baseline conditions of the subjects.

The articulating circular endoscopic (ACE) stapler is a transoral bariatric device for endoscopic gastroplication which has identical principle to ESG. Paulus et al. (2020) reported that in subjects whose BMI was 38.3 kg/m^2 at baseline, BMI decreased to 33.9 kg/m^2 at 1 year postoperatively. After the procedure, patients had a downregulated ghrelin gene expression as well as its activating enzyme in the upper gastrointestinal tract and increased level of plasma adiponectin (van der Wielen et al., 2017). Trans-oral endoscopic restrictive implant system (De Jong et al., 2010; Verlaan et al., 2016) is another similar device. At 6 months after using the device, total and excess weight loss were 15.1 and 30.1%, but the longer-term effects were not reported yet and the biological mediators were to be explored.

Other Bariatric Technologies

It should be noted that there are other bariatric devices than we could include in the rapidly developing field, and every technique has both the pros and cons. Our current review mainly focuses on mechanisms behind the gastric volume restricted devices. Understanding the possible mechanisms beyond restriction will help us better understand the pathophysiology of obesity and provide the potential to develop more effective approaches to combat the epidemic of obesity. **Table 1** summarizes the factors that may contribute to weight control with device implants.

CONCLUSION

Although many gastric volume-restriction bariatric devices have been developed for laboratory or clinical use, the underlying mechanism of the devices in alleviating morbid obesity and comorbidities is still not fully understood. Despite the fact that

the "restrictive" devices physically limit or reduce gastric capacity, mechanical restriction may not have the key role in achieving the beneficial outcomes. Gastric motility and hormone responses may also contribute to the efficacy of the procedures. Changes in hormone levels provide some indication as to how these bariatric devices work; however, they do not necessarily provide a mechanism for the weight loss effects. Instead, these changes could be compensatory, rather than mediators. Further studies are required to determine whether these changes in hormone levels are in fact causal to weight loss. Studies regarding other factors that contribute to bariatric surgeries (Madsbad et al., 2014; Wang et al., 2019) such as vagal and hypothalamic activity, role of bile acids, and gut flora alterations are lacking. More studies are encouraged to elucidate the detailed mechanisms of weight and energy regulation and glucose metabolism after use of gastric bariatric devices.

AUTHOR CONTRIBUTIONS

YW searched and arranged literatures. GK engaged in the conception, design, and coordination of the work. Both authors participated in drafting and revising the manuscript.

REFERENCES

Abu Dayyeh, B. K., Acosta, A., Camilleri, M., Mundi, M. S., Rajan, E., Topazian, M. D., et al. (2017). Endoscopic sleeve gastroplasty alters gastric physiology and induces loss of body weight in obese individuals. *Clin. Gastroenterol. Hepatol.* 15, 37–43.e1. doi: 10.1016/j.cgh.2015.12.030

Alqahtani, A., Al-Darwish, A., Mahmoud, A. E., Alqahtani, Y. A., and Elahmedi, M. (2019). Short-term outcomes of endoscopic sleeve gastroplasty in 1000 consecutive patients. *Gastrointest. Endosc.* 89, 1132–1138. doi: 10.1016/j.gie.2018.12.012

American Society for Metabolic and Bariatric Surgery (2021). *Estimate of Bariatric Surgery Numbers, 2011-2019*. Available Online at: https://asmbs.org/resources/estimate-of-bariatric-surgery-numbers (accessed March 30, 2021).

Amsalem, D., Aricha-Tamir, B., Levi, I., Shai, D., and Sheiner, E. (2014). Obstetric outcomes after restrictive bariatric surgery: what happens after 2 consecutive pregnancies? *Surg. Obes. Relat. Dis.* 10, 445–449. doi: 10.1016/j.soard.2013.08.016

Arias, I. E., Radulescu, M., Stiegeler, R., Singh, J. P., Martinez, P., Ramirez, A., et al. (2009). Diagnosis and treatment of megaesophagus after adjustable gastric banding for morbid obesity. *Surg. Obes. Relat. Dis.* 5, 156–159. doi: 10.1016/j.soard.2008.11.007

Aron-Wisnewsky, J., Prifti, E., Belda, E., Ichou, F., Kayser, B. D., Dao, M. C., et al. (2019). Major microbiota dysbiosis in severe obesity: fate after bariatric surgery. *Gut* 68, 70–82. doi: 10.1136/gutjnl-2018-316103

Badurdeen, D., Hoff, A. C., Barrichello, S., Hedjoudje, A., Itani, M. I., Farha, J., et al. (2021). Efficacy of liraglutide to prevent weight regain after retrieval of an adjustable intra-gastric balloon—a case-matched study. *Obes. Surg.* 31, 1204–1213. doi: 10.1007/s11695-020-05117-8

Balsiger, B. M., Poggio, J. L., Mai, J., Kelly, K. A., and Sarr, M. G. (2000). Ten and more years after vertical banded gastroplasty as primary operation for morbid obesity. *J. Gastrointest. Surg.* 4, 598–605. doi: 10.1016/S1091-255X(00)80108-0

Barrichello, S., Hourneaux, de Moura, D. T., Hourneaux de Moura, E. G., Jirapinyo, P., Hoff, A. C., et al. (2019). Endoscopic sleeve gastroplasty in the management of overweight and obesity: an international multicenter study. *Gastrointest. Endosc.* 90, 770–780. doi: 10.1016/j.gie.2019.06.013

Bentham, J., Di Cesare, M., Bilano, V., Bixby, H., Zhou, B., Stevens, G. A., et al. (2017). Worldwide trends in body-mass index, underweight, overweight, and obesity from 1975 to 2016: a pooled analysis of 2416 population-based measurement studies in 128·9 million children, adolescents, and adults. *Lancet* 390, 2627–2642. doi: 10.1016/S0140-6736(17)32129-3

Billy, H. T., Sarwer, D. B., Ponce, J., Ng-Mak, D. S., Shi, R., Cornell, C., et al. (2014). Quality of life after laparoscopic adjustable gastric banding (LAP-BAND): APEX interim 3-year analysis. *Postgrad. Med.* 126, 131–140. doi: 10.3810/pgm.2014.07.2791

Brolin, R. E., Robertson, L. B., Kenler, H. A., and Cody, R. P. (1994). Weight loss and dietary intake after vertical banded gastroplasty and Roux-en-Y gastric bypass. *Ann. Surg.* 220, 782–790. doi: 10.1097/00000658-199412000-00012

Bužga, M., Machytka, E., Klvaňa, P., Kupka, T., Zavadilová, V., Zonča, P., et al. (2014). Effects of the intragastric balloon Medsil® on weight loss, fat tissue, lipid metabolism, and hormones involved in energy balance. *Obes. Surg.* 24, 909–915. doi: 10.1007/s11695-014-1191-4

Chandan, S., Mohan, B. P., Khan, S. R., Facciorusso, A., Ramai, D., Kassab, L. L., et al. (2021). Efficacy and safety of intragastric balloon (IGB) in non-alcoholic fatty liver disease (NAFLD): a comprehensive review and meta-analysis. *Obes. Surg.* 31, 1271–1279. doi: 10.1007/s11695-020-05084-0

Chang, P.-C., Chen, K.-H., Huang, I. Y.-W., Huang, C.-K., Chen, C.-Y., Wang, M.-Y., et al. (2021). Laparoscopic revision for gastric clipping: a single center experience and taiwan database review. *Obes. Surg.* 31, 3653–3659. doi: 10.1007/s11695-021-05466-y

Chang, S.-H., Stoll, C. R. T., Song, J., Varela, J. E., Eagon, C. J., and Colditz, G. A. (2014). The effectiveness and risks of bariatric surgery: an updated systematic review and meta-analysis, 2003-2012. *JAMA Surg.* 149, 275–287. doi: 10.1001/jamasurg.2013.3654

Chao, S. H., Lin, C. L., Lee, W. J., Chen, J. C., and Chou, J. J. (2019). Proximal jejunal bypass improves the outcome of gastric clip in patients with obesity and type 2 diabetes mellitus. *Obes. Surg.* 29, 1148–1153. doi: 10.1007/s11695-018-3607-z

De Jong, K., Mathus-Vliegen, E. M. H., Veldhuyzen, E. A. M. L., Eshuis, J. H., and Fockens, P. (2010). Short-term safety and efficacy of the trans-oral endoscopic restrictive implant system for the treatment of obesity. *Gastrointest. Endosc.* 72, 497–504. doi: 10.1016/j.gie.2010.02.053

de la Plaza Llamas, R., Díaz Candelas, D. A., and Ramia, J. M. (2020). Laparoscopic removal of a displaced vertical gastric clip causing gastric outlet obstruction. *Obes. Surg.* 30, 2856–2857. doi: 10.1007/s11695-020-04606-0

Doble, B., Welbourn, R., Carter, N., Byrne, J., Rogers, C. A., Blazeby, J. M., et al. (2019). Multi-Centre micro-costing of Roux-En-Y gastric bypass, sleeve gastrectomy and adjustable gastric banding procedures for the treatment of severe, complex obesity. *Obes. Surg.* 29, 474–484. doi: 10.1007/s11695-018-3553-9

Edelman, S., Ng-Mak, D. S., Fusco, M., Ashton, D., Okerson, T., Liu, Q., et al. (2014). Control of type 2 diabetes after 1 year of laparoscopic adjustable gastric banding in the helping evaluate reduction in obesity (HERO) study. *Diabetes, Obes. Metab.* 16, 1009–1015. doi: 10.1111/dom.12313

Favretti, F., Ashton, D., Busetto, L., Segato, G., and De Luca, M. (2009). The gastric band: first-choice procedure for obesity surgery. *World J. Surg.* 33, 2039–2048. doi: 10.1007/s00268-009-0091-6

FDA (2020). *UPDATE: Potential Risks with Liquid-filled Intragastric Balloons - Letter to Health Care Providers | FDA*. Available Online at: https://www.fda.gov/medical-devices/letters-health-care-providers/update-potential-risks-liquid-filled-intragastric-balloons-letter-health-care-providers-0 (accessed March 22, 2021).

Fittipaldi-Fernandez, R. J., Zotarelli-Filho, I. J., Diestel, C. F., Klein, M. R. S. T., de Santana, M. F., de Lima, J. H. F., et al. (2020). Intragastric balloon: a retrospective evaluation of 5874 patients on tolerance, complications, and efficacy in different degrees of overweight. *Obes. Surg.* 30, 4892–4898. doi: 10.1007/s11695-020-04985-4

Flegal, K. M., Carroll, M. D., Kit, B. K., and Ogden, C. L. (2012). Prevalence of obesity and trends in the distribution of body mass index among US adults, 1999-2010. *JAMA* 307, 491–497. doi: 10.1001/jama.2012.39

Froylich, D., Abramovich, T. S., Fuchs, S., Zippel, D., and Hazzan, D. (2020). Long-term (over 13 years) follow-up of vertical band gastroplasty. *Obes. Surg.* 30, 1808–1813. doi: 10.1007/s11695-020-04448-w

Fuller, N. R., Lau, N. S., Denyer, G., and Caterson, I. D. (2013). An intragastric balloon produces large weight losses in the absence of a change in ghrelin or peptide YY. *Clin. Obes.* 3, 172–179. doi: 10.1111/cob.12030

Garb, J., Welch, G., Zagarins, S., Kuhn, J., and Romanelli, J. (2009). Bariatric surgery for the treatment of morbid obesity: a meta-analysis of weight loss outcomes for laparoscopic adjustable gastric banding and laparoscopic gastric bypass. *Obes. Surg.* 19, 1447–1455. doi: 10.1007/s11695-009-9927-2

Gasoyan, H., Tajeu, G., Halpern, M. T., and Sarwer, D. B. (2019). Reasons for underutilization of bariatric surgery: the role of insurance benefit design. *Surg. Obes. Relat. Dis.* 15, 146–151. doi: 10.1016/j.soard.2018.10.005

Gaździńska, A. P., Mojkowska, A., Zieliński, P., and Gazdzinski, S. P. (2020). Changes in resting metabolic rate and body composition due to intragastric balloon therapy. *Surg. Obes. Relat. Dis.* 16, 34–39. doi: 10.1016/j.soard.2019.10.011

Genco, A., Maselli, R., Frangella, F., Cipriano, M., Paone, E., Meuti, V., et al. (2013). Effect of consecutive intragastric balloon (BIB®) plus diet versus single BIB® plus diet on eating disorders not otherwise specified (EDNOS) in obese patients. *Obes. Surg.* 23, 2075–2079. doi: 10.1007/s11695-013-1028-6

Golzarand, M., Toolabi, K., and Farid, R. (2017). The bariatric surgery and weight losing: a meta-analysis in the long- and very long-term effects of laparoscopic adjustable gastric banding, laparoscopic Roux-en-Y gastric bypass and laparoscopic sleeve gastrectomy on weight loss in adults. *Surg. Endosc.* 31, 4331–4345. doi: 10.1007/s00464-017-5505-1

Guo, X., Mattar, S. G., Mimms, S. E., Navia, J. A., and Kassab, G. S. (2014). Efficacy of a laparoscopic gastric restrictive device in an obese canine model. *Obes. Surg.* 24, 159–166. doi: 10.1007/s11695-013-1127-4

Guo, X., Mattar, S. G., Navia, J. A., and Kassab, G. S. (2012). Response of gut hormones after implantation of a reversible gastric restrictive device in different animal models. *J. Surg. Res.* 178, 165–171. doi: 10.1016/j.jss.2012.02.032

Guo, X., Zheng, H., Mattar, S. G., Lu, X., Sandusky, G., Navia, J. A., et al. (2011). Reversible gastric restriction implant: safety and efficacy in a canine model. *Obes. Surg.* 21, 1444–1450. doi: 10.1007/s11695-010-0299-4

Hindle, A., Garcia, X. D. P., Hayden, M., O'Brien, P. E., and Brennan, L. (2020). Pre-operative restraint and post-operative hunger, disinhibition and emotional eating predict weight loss at 2 Years post-laparoscopic adjustable gastric banding. *Obes. Surg.* 30, 1347–1359. doi: 10.1007/s11695-019-04274-9

Ibrahim, A. M., Thumma, J. R., and Dimick, J. B. (2017). Reoperation and medicare expenditures after laparoscopic gastric band surgery. *JAMA Surg.* 152, 835–842. doi: 10.1001/jamasurg.2017.1093

Jacobs, M., Zundel, N., Plasencia, G., Rodriguez-Pumarol, P., Gomez, E., and Leithead, J. (2017). A vertically placed clip for weight loss: a 39-month pilot study. *Obes. Surg.* 27, 1174–1181. doi: 10.1007/s11695-016-2432-5

Jain, D., Bhandari, B. S., Arora, A., and Singhal, S. (2017). Endoscopic sleeve gastroplasty - a New tool to manage obesity. *Clin. Endosc.* 50, 552–561. doi: 10.5946/ce.2017.032

Jensen, M. D., Ryan, D. H., Apovian, C. M., Ard, J. D., Comuzzie, A. G., Donato, K. A., et al. (2014). 2013 AHA/ACC/TOS guideline for the management of overweight and obesity in adults: a report of the American college of cardiology/American heart association task force on practice guidelines and the obesity society. *J. Am. Coll. Cardiol.* 63, 2985–3023. doi: 10.1016/j.jacc.2013.11.004

Kawasaki, T., Ohta, M., Kawano, Y., Masuda, T., Gotoh, K., Inomata, M., et al. (2015). Effects of sleeve gastrectomy and gastric banding on the hypothalamic feeding center in an obese rat model. *Surg. Today* 45, 1560–1566. doi: 10.1007/s00595-015-1135-1

Kellum, J. M., Kuemmerle, J. F., O'Dorisio, T. M., Rayford, P., Martin, D., Engle, K., et al. (1990). Gastrointestinal hormone responses to meals before and after gastric bypass and vertical banded gastroplasty. *Ann. Surg.* 211, 763–771. doi: 10.1097/00000658-199006000-00016

Kodner, C., and Hartman, D. R. (2014). Complications of adjustable gastric banding surgery for obesity. *Am. Fam. Physician* 89, 813–818.

Kumar, N. (2015). Endoscopic therapy for weight loss: gastroplasty, duodenal sleeves, intragastric balloons, and aspiration. *World J. Gastrointest. Endosc.* 7, 847–859. doi: 10.4253/wjge.v7.i9.847

Kumar, N., Abu Dayyeh, B. K., Lopez-Nava Breviere, G., Galvao Neto, M. P., Sahdala, N. P., Shaikh, S. N., et al. (2018). Endoscopic sutured gastroplasty: procedure evolution from first-in-man cases through current technique. *Surg. Endosc.* 32, 2159–2164. doi: 10.1007/s00464-017-5869-2

Kuzmak, L. I. (1991). A review of seven years' experience with silicone gastric banding. *Obes. Surg. Incl. Laparosc. Allied Care* 1, 403–408. doi: 10.1381/096089291765560809

Lee, C. J., Florea, L., Sears, C. L., Maruthur, N., Potter, J. J., Schweitzer, M., et al. (2019). Changes in gut microbiome after bariatric surgery versus medical weight loss in a pilot randomized trial. *Obes. Surg.* 29, 3239–3245. doi: 10.1007/s11695-019-03976-4

Leonetti, F., Silecchia, G., Iacobellis, G., Ribaudo, M. C., Zappaterreno, A., Tiberti, C., et al. (2003). Different plasma ghrelin levels after laparoscopic gastric bypass and adjustable gastric banding in morbid obese subjects. *J. Clin. Endocrinol. Metab.* 88, 4227–4231. doi: 10.1210/jc.2003-030133

Lopez-Nava, G., Galvao, M., Bautista-Castaño, I., Fernandez-Corbelle, J., and Trell, M. (2016). Endoscopic sleeve gastroplasty with 1-year follow-up: factors predictive of success. *Endosc. Int. Open* 04, E222–E227. doi: 10.1055/s-0041-110771

Lopez-Nava, G., Negi, A., Bautista-Castaño, I., Rubio, M. A., and Asokkumar, R. (2020). Gut and metabolic hormones changes after endoscopic sleeve gastroplasty (ESG) vs. laparoscopic sleeve gastrectomy (LSG). *Obes. Surg.* 30, 2642–2651. doi: 10.1007/s11695-020-04541-0

Lopez-Nava, G., Sharaiha, R. Z., Vargas, E. J., Bazerbachi, F., Manoel, G. N., Bautista-Castaño, I., et al. (2017). Endoscopic sleeve gastroplasty for obesity: a multicenter study of 248 patients with 24 months follow-up. *Obes. Surg.* 27, 2649–2655. doi: 10.1007/s11695-017-2693-7

Madsbad, S., Dirksen, C., and Holst, J. J. (2014). Mechanisms of changes in glucose metabolism and bodyweight after bariatric surgery. lancet. *Diabetes Endocrinol.* 2, 152–164. doi: 10.1016/S2213-8587(13)70218-3

Mason, E. E. (1982). Vertical banded gastroplasty for obesity. *Arch. Surg.* 117, 701–706. doi: 10.1001/archsurg.1982.01380290147026

Mathus-Vliegen, E. M. H., and de Groot, G. H. (2013). Fasting and meal-induced CCK and PP secretion following intragastric balloon treatment for obesity. *Obes. Surg.* 23, 622–633. doi: 10.1007/s11695-012-0834-6

Mathus-Vliegen, E. M. H., and Eichenberger, R. I. (2014). Fasting and meal-suppressed ghrelin levels before and after intragastric balloons and balloon-induced weight loss. *Obes. Surg.* 24, 85–94. doi: 10.1007/s11695-013-1053-5

Mion, F., Napoléon, B., Roman, S., Malvoisin, E., Trepo, F., Pujol, B., et al. (2005). Effects of intragastric balloon on gastric emptying and plasma ghrelin levels in non-morbid obese patients. *Obes. Surg.* 15, 510–516. doi: 10.1381/0960892053723411

Monteiro, M. P., Ribeiro, A. H., Nunes, A. F., Sousa, M. M., Monteiro, J. D., Águas, A. P., et al. (2007). Increase in ghrelin levels after weight loss in obese Zucker rats is prevented by gastric banding. *Obes. Surg.* 17, 1599–1607. doi: 10.1007/s11695-007-9324-7

Noel, P., Eddbali, I., and Nedelcu, M. (2020). Laparoscopic clip gastroplasty with the BariClip. *Obes. Surg.* 30, 5182–5183. doi: 10.1007/s11695-020-04803-x

Noel, P., Nedelcu, A. M., Eddbali, I., and Zundel, N. (2018). Laparoscopic vertical clip gastroplasty - quality of life. *Surg. Obes. Relat. Dis.* 14, 1587–1593. doi: 10.1016/j.soard.2018.07.013

Novikov, A. A., Afaneh, C., Saumoy, M., Parra, V., Shukla, A., Dakin, G. F., et al. (2018). Endoscopic sleeve gastroplasty, laparoscopic sleeve gastrectomy, and laparoscopic band for weight loss: how do they compare? *J. Gastrointest. Surg.* 22, 267–273. doi: 10.1007/s11605-017-3615-7

Ogden, C. L., Carroll, M. D., Lawman, H. G., Fryar, C. D., Kruszon-Moran, D., Kit, B. K., et al. (2016). Trends in obesity prevalence among children and adolescents in the United States, 1988-1994 through 2013-2014. *JAMA* 315, 2292–2299. doi: 10.1001/jama.2016.6361

Olbers, T., Björkman, S., Lindroos, A., Maleckas, A., Lönn, L., Sjöström, L., et al. (2006). Body composition, dietary intake, and energy expenditure after laparoscopic Roux-en-Y gastric bypass and laparoscopic vertical banded gastroplasty: a randomized clinical trial. *Ann. Surg.* 244, 715–722. doi: 10.1097/01.sla.0000218085.25902.f8

Opozda, M., Chur-Hansen, A., and Wittert, G. (2016). Changes in problematic and disordered eating after gastric bypass, adjustable gastric banding and vertical sleeve gastrectomy: a systematic review of pre-post studies. *Obes. Rev.* 17, 770–792. doi: 10.1111/obr.12425

Park, C. H., Nam, S.-J., Choi, H. S., Kim, K. O., Kim, D. H., Kim, J.-W., et al. (2019). Comparative efficacy of bariatric surgery in the treatment of morbid obesity and

diabetes mellitus: a systematic review and network meta-analysis. *Obes. Surg.* 29, 2180–2190. doi: 10.1007/s11695-019-03831-6

Paulus, G. F., van Avesaat, M., Crijnen, J. A. W., Ernest, van Heurn, L. W., Westerterp-Plantenga, M. S., et al. (2020). Preliminary evidence that endoscopic gastroplication reduces food reward. *Appetite* 150:104632. doi: 10.1016/j.appet.2020.104632

Ponce, J., Taheri, S., Lusco, V., Cornell, C., Ng-Mak, D. S., Shi, R., et al. (2014). Efficacy and safety of the adjustable gastric band-pooled interim analysis of the APEX and HERO studies at 48 weeks. *Curr. Med. Res. Opin.* 30, 841–848. doi: 10.1185/03007995.2013.874992

Pontiroli, A. E., Zakaria, A. S., Fanchini, M., Osio, C., Tagliabue, E., Micheletto, G., et al. (2018). A 23-year study of mortality and development of co-morbidities in patients with obesity undergoing bariatric surgery (laparoscopic gastric banding) in comparison with medical treatment of obesity. *Cardiovasc. Diabetol.* 17:161. doi: 10.1186/s12933-018-0801-1

Popov, V. B., Ou, A., Schulman, A. R., and Thompson, C. C. (2017). The impact of intragastric balloons on obesity-related co-morbidities: a systematic review and meta-analysis. *Am. J. Gastroenterol.* 112, 429–439. doi: 10.1038/ajg.2016.530

Pournaras, D. J., Osborne, A., Hawkins, S. C., Vincent, R. P., Mahon, D., Ewings, P., et al. (2010). Remission of type 2 diabetes after gastric bypass and banding: mechanisms and 2 year outcomes. *Ann. Surg.* 252, 966–971. doi: 10.1097/SLA.0b013e3181efc49a

Ramai, D., Singh, J., Mohan, B. P., Madedor, O., Brooks, O. W., Barakat, M., et al. (2020). Influence of the elipse intragastric balloon on obesity and metabolic profile: a systematic review and meta-analysis. *J. Clin. Gastroenterol.* online ahead of print. doi: 10.1097/MCG.0000000000001484

Schlager, A., Khalaileh, A., Mintz, Y., Gazala, M. A., Globerman, A., Ilani, N., et al. (2011). A mouse model for sleeve gastrectomy: applications for diabetes research. *Microsurgery* 31, 66–71. doi: 10.1002/micr.20797

Sharaiha, R. Z., Kumta, N. A., Saumoy, M., Desai, A. P., Sarkisian, A. M., Benevenuto, A., et al. (2017). Endoscopic sleeve gastroplasty significantly reduces body mass index and metabolic complications in obese patients. *Clin. Gastroenterol. Hepatol.* 15, 504–510. doi: 10.1016/j.cgh.2016.12.012

Smith, K. E., Orcutt, M., Steffen, K. J., Crosby, R. D., Cao, L., Garcia, L., et al. (2019). Loss of control eating and binge eating in the 7 years following bariatric surgery. *Obes. Surg.* 29, 1773–1780. doi: 10.1007/s11695-019-03791-x

Sonavane, S. K., Menias, C. O., Kantawala, K. P., Shanbhogue, A. K., Prasad, S. R., Eagon, J. C., et al. (2012). Laparoscopic adjustable gastric banding: what radiologists need to know. *Radiographics* 32, 1161–1178. doi: 10.1148/rg.324115177

Sysko, R., Devlin, M. J., Schebendach, J., Tanofsky-Kraff, M., Zimmerli, E., Korner, J., et al. (2013). Hormonal responses and test meal intake among obese teenagers before and after laparoscopic adjustable gastric banding. *Am. J. Clin. Nutr.* 98, 1151–1161. doi: 10.3945/ajcn.113.061762

Tremaroli, V., Karlsson, F., Werling, M., Ståhlman, M., Kovatcheva-Datchary, P., Olbers, T., et al. (2015). Roux-en-Y gastric bypass and vertical banded gastroplasty induce long-Term changes on the human gut microbiome contributing to fat mass regulation. *Cell Metab.* 22, 228–238. doi: 10.1016/j.cmet.2015.07.009

Tsai, C., Zehetner, J., Beel, J., and Steffen, R. (2019). Long-term outcomes and frequency of reoperative bariatric surgery beyond 15 years after gastric banding: a high band failure rate with safe revisions. *Surg. Obes. Relat. Dis.* 15, 900–907. doi: 10.1016/j.soard.2019.03.017

van der Wielen, N., Paulus, G., van Avesaat, M., Masclee, A., Meijerink, J., and Bouvy, N. (2017). Effect of endoscopic gastroplication on the genome-wide transcriptome in the upper gastrointestinal tract. *Obes. Surg.* 27, 740–748. doi: 10.1007/s11695-016-2356-0

van Wezenbeek, M. R., Smulders, J. F., de Zoete, J. P. J. G. M., Luyer, M. D., van Montfort, G., and Nienhuijs, S. W. (2015). Long-term results of primary vertical banded gastroplasty. *Obes. Surg.* 25, 1425–1430. doi: 10.1007/s11695-014-1543-0

Vargas, E. J., Rizk, M., Bazerbachi, F., and Abu Dayyeh, B. K. (2018). Medical devices for obesity treatment: endoscopic bariatric therapies. *Med. Clin. North Am.* 102, 149–163. doi: 10.1016/j.mcna.2017.08.013

Verlaan, T., de Jong, K., de la Mar-Ploem, E. D., Veldhuyzen, E. A., Mathus-Vliegen, E. M., and Fockens, P. (2016). Trans-oral endoscopic restrictive implant system: endoscopic treatment of obesity? *Surg. Obes. Relat. Dis.* 12, 1711–1718. doi: 10.1016/j.soard.2016.02.027

Vyas, D., Deshpande, K., and Pandya, Y. (2017). Advances in endoscopic balloon therapy for weight loss and its limitations. *World J. Gastroenterol.* 23, 7813–7817. doi: 10.3748/wjg.v23.i44.7813

Wang, Y., Guo, X., Lu, X., Mattar, S., and Kassab, G. (2019). Mechanisms of weight loss after sleeve gastrectomy and adjustable gastric banding: far more than just restriction. *Obesity* 27, 1776–1783. doi: 10.1002/oby.22623

Wei, J.-H., Yeh, C.-H., Lee, W.-J., Lin, S.-J., and Huang, P.-H. (2020). Sleeve gastrectomy in mice using surgical clips. *J. Vis. Exp.*, e60719. doi: 10.3791/60719

Wharton, S., Lau, D. C. W., Vallis, E. M., Sharma, A. M., Biertho, L., Campbell-Scherer, D., et al. (2020). Obesity in adults: a clinical practice guideline. *CMAJ* 192, E875–E891. doi: 10.1503/cmaj.191707

Yumuk, V., Tsigos, C., Fried, M., Schindler, K., Busetto, L., Micic, D., et al. (2015). European guidelines for obesity management in adults. *Obes. Facts* 8, 402–424. doi: 10.1159/000442721

Conflict of Interest: The authors declare that the research was conducted in the absence of any commercial or financial relationships that could be construed as a potential conflict of interest.

frontiers in Physiology

ORIGINAL RESEARCH
published: 08 November 2021
doi: 10.3389/fphys.2021.772577

Insulin Resistance Remission Following Laparoscopic Roux-en-Y Gastric Bypass and Laparoscopic Sleeve Gastrectomy in Chinese Type 2 Diabetes Mellitus Patients With a Body Mass Index of 27.5–32.5 kg/m^2

Ping Luo†, Yaoquan Cao†, Pengzhou Li, Guohui Wang, Zhi Song, Weizheng Li, Zhihong Su, Hui Zhou, Xianhao Yi, Zhibing Fu, Xulong Sun, Haibo Tang, Beibei Cui, Qianqian Yu, Liyong Zhu and Shaihong Zhu**

Department of General Surgery, Third Xiangya Hospital, Central South University, Changsha, China

OPEN ACCESS

Edited by:
Sanyuan Hu,
Shandong University, China

Reviewed by:
Mingwei Zhong,
Shandong University, China
Ruizhi Feng,
Nanjing Medical University, China
Xiaomei Guo,
California Medical Innovations Institute, United States

***Correspondence:**
Liyong Zhu
zly8128@126.com
Shaihong Zhu
shaihongzhu@126.com

†These authors have contributed equally to this work and share first authorship

Specialty section:
This article was submitted to Metabolic Physiology, a section of the journal Frontiers in Physiology

Received: *08 September 2021*
Accepted: *11 October 2021*
Published: *08 November 2021*

Citation:
Luo P, Cao Y, Li P, Wang G, Song Z, Li W, Su Z, Zhou H, Yi X, Fu Z, Sun X, Tang H, Cui B, Yu Q, Zhu L and Zhu S (2021) Insulin Resistance Remission Following Laparoscopic Roux-en-Y Gastric Bypass and Laparoscopic Sleeve Gastrectomy in Chinese Type 2 Diabetes Mellitus Patients With a Body Mass Index of 27.5–32.5 kg/m^2. Front. Physiol. 12:772577. doi: 10.3389/fphys.2021.772577

Background: Insulin resistance (IR) is closely associated with the pathogenesis of type 2 diabetes mellitus (T2DM). However, remission of insulin sensitivity after bariatric surgery in patients with T2DM and a body mass index (BMI) of 27.5–32.5 kg/m^2 has not been fully elucidated.

Methods: Thirty-six T2DM patients with a BMI of 27.5–32.5 kg/m^2 were prospectively consecutively recruited for laparoscopic Roux-en-Y gastric bypass (LRYGB) or laparoscopic sleeve gastrectomy (LSG). Hyperinsulinemic euglycemic clamp, oral glucose tolerance test (OGTT), and other indicators were tested at baseline and 6 months postoperative. Glucose disposal rate (GDR), time to reach euglycemia, homeostatic model assessment of IR, quantitative insulin sensitivity check index (QUICKI), triglyceride glucose (TyG) index, 30-min insulinogenic index (IGI30), and disposition index (DI) were calculated at baseline and 6 months after surgery. The criterion for remission in T2DM patients was the achievement of the triple composite endpoint.

Results: Anthropometric and glucolipid metabolism parameters significantly improved following surgery. The GDR increased significantly from baseline to 6 months after LRYGB (from 4.28 ± 1.70 mg/kg/min to 8.47 ± 1.89 mg/kg/min, $p < 0.0001$) and LSG (from 3.18 ± 1.36 mg/kg/min to 7.09 ± 1.69 mg/kg/min, $p < 0.001$). The TyG index decreased after surgery (RYGB group, from 9.93 ± 1.03 to 8.60 ± 0.43, $p < 0.0001$; LSG group, from 10.04 ± 0.79 to 8.72 ± 0.65, $p = 0.0002$). There was a significant reduction in the IGI30 (RYGB group, from 2.04 ± 2.12 to 0.83 ± 0.47, $p = 0.005$; LSG group, from 2.12 ± 1.73 to 0.92 ± 0.66, $p = 0.001$). The mean DI significantly increased from 1.14 ± 1.35 to 7.11 ± 4.93 in the RYGB group ($p = 0.0001$) and from 1.25 ± 1.78 to 5.60 ± 4.58 in the LSG group ($p = 0.003$). Compared with baseline, HOMR-IR, QUICKI, area under the curve-C-peptide release test (AUC-CRT), and AUC-OGTT were significantly changed at 6 months postoperative. Overall, 52.63% of patients

in the LRYGB group versus 29.41% of patients in the LSG group achieved the triple composite endpoint.

Conclusion: Both LRYGB and LSG effectively induced remission of IR in patients with T2DM and a BMI of 27.5–32.5 kg/m^2.

Keywords: type 2 diabetes mellitus, bariatric surgery, insulin resistance, hyperinsulinemic euglycemic clamp, oral glucose tolerance test

INTRODUCTION

China had the largest number of adults with diabetes in 2019, a population that is projected to increase to 147.2 million by 2045 (Saeedi et al., 2019). Laparoscopic Roux-en-Y gastric bypass (LRYGB) and laparoscopic sleeve gastrectomy (LSG) are the most commonly performed bariatric procedures and appropriate treatments for patients with type 2 diabetes mellitus (T2DM), especially for those with comorbidities (Zimmet et al., 2011). Bariatric surgery is among the most effective treatments for patients with T2DM and a body mass index (BMI) >35 kg/m^2 or 30–35 kg/m^2 with uncontrolled conditions (Zimmet et al., 2011). According to the International Diabetes Federation statement, the BMI threshold for Asian patients with T2DM should be reduced by 2.5 kg/m^2 (Dixon et al., 2011). Available evidence indicates that surgery is one option, along with lifestyle and medical interventions, for cure in Asian T2DM patients with a BMI <35 kg/m^2, and that the BMI cut-off point for surgery be lowered for Asian patients with T2DM (Lee and Aung, 2016).

It is well known that insulin resistance (IR) is closely associated with the pathogenesis of T2DM (DeFronzo, 2004). T2DM in the Chinese population is characterized by a low BMI, abdominal obesity, significant IR, and impairment of islet cell function in the early stages of diabetes (Chan et al., 2009). IR is reportedly significantly associated with incident diabetes compared with β-cell dysfunction in the Chinese population, especially in adults with obesity (Wang et al., 2020). Hence, it is critical to accurately assess the IR of patients with T2DM and obesity. The principal methods for evaluating IR in clinical practice are the homeostatic model assessment of IR (HOMA-IR), quantitative insulin sensitivity check index (QUICKI), oral glucose tolerance test (OGTT) with modeling, and hyperinsulinemic euglycemic clamp (Mingrone and Cummings, 2016). The HOMA-IR is the most popular but least accurate and varies among populations (Matthews et al., 1985). The QUICKI is a simple and accurate method for assessing insulin sensitivity in humans (Katz et al., 2000). The triglyceride glucose (TyG) index, as a reliable surrogate marker, has also been used to evaluate IR (Zhang et al., 2017). The clamp is considered the gold standard and is used to evaluate other indicators (Rabasa-Lhoret and Laville, 2001).

Beneficial effects of bariatric surgery on glucose metabolism are known, but the remission of insulin sensitivity after bariatric surgery in T2DM patients with a BMI of 27.5–32.5 kg/m^2 has not been fully elucidated. This prospective cohort study aimed to use the hyperinsulinemic euglycemic clamp and other indicators to evaluate the effect of LRYGB and LSG on insulin sensitivity for T2DM patients with a BMI in 27.5–32.5 kg/m^2.

MATERIALS AND METHODS

Study Design and Subjects

Thirty-six T2DM patients with a BMI of 27.5–32.5 kg/m^2 were prospectively consecutively recruited from July 2019 to June 2020 in the Department of General Surgery, Third Xiangya Hospital, Central South University (Changsha, China). Surgery was safely performed by the same surgical group and the procedure was performed as previously described (Yu et al., 2021). The protocol was approved by the Ethical Committee of our hospital (R19025). Informed consent was obtained from all patients before the study.

The inclusion criteria were as follows: (1) diagnosis of T2DM conforming to the guideline of (Diagnosis and classification of diabetes mellitus, American Diabetes Association, 2014); (2) BMI of 27.5–32.5 kg/m^2; (3) age 18–65 years; and (4) T2DM duration <15 years. The exclusion criteria were: (1) surgical contraindications to LSG and LRYGB; (2) severe T2DM comorbidities or organic diseases, such as myocardial infarction, renal failure, or stroke; (3) alcohol or medicine addiction; and (4) uncontrolled psychiatric disease.

Study Protocol and Data Collection

Insulin sensitivity was evaluated at baseline and at 6 months postoperative. Insulin sensitivity was measured using the hyperinsulinemic euglycemic clamp, HOMA-IR, QUICKI, and TyG index. The TyG index was calculated as ln [fasting triglyceride (mg/dL) × fasting glucose (mg/dL)/2]. HOMA-IR was calculated as fasting glucose (mmol/L) × fasting insulin (μU/mL)/22.5. QUICKI was calculated as 1/[log (fasting insulin) + log (fasting glucose)]. Insulin secretion and β-cell function were measured using OGTT modeling. T2DM remission was evaluated using the composite triple endpoint at a 6-month follow-up. The criterion for achieving the triple composite endpoint was a glycosylated hemoglobin A1c (HbA1c) <7.0%, low-density lipoprotein <2.59 mmol/L, and systolic blood pressure <130 mmHg (Ikramuddin et al., 2015).

Anthropometric and glucolipid metabolism parameters were collected at baseline and 6 months postoperative.

Hyperinsulinemic Euglycemic Clamp

All patients underwent hyperinsulinemic euglycemic clamp experiments at baseline and 6 months after surgery. Catheters were inserted into the antecubital vein for infusion and in the dorsal vein for blood sample collection. A heated box was used on the blood-taking arm to obtain arterialized venous blood. Insulin (Humulin R, Eli Lilly, United States) was administered

intravenously at a rate of 40 mU/kg/min for 150 min. Blood samples were drawn using an intravenous catheter in a heated vein, and glucose concentrations were measured at 5-min intervals. Dextrose 20% was infused at variable rates to maintain a glucose level of 5.0 mmol/L. The time taken to reach euglycemia was calculated from the beginning of the experiment to euglycemia. Glucose disposal rate (GDR) was measured during steady-state intervals (Zhao et al., 2017).

Oral Glucose Tolerance Test

All participants completed the OGTT at baseline and 6 months postoperative. All patients fasted for at least 10 h and ingested 250 mL of water (including 75 g of glucose) in 5 min. Blood samples were collected from the median cubital vein at 0, 30, and 120 min. Based on the OGTT data, we calculated the 30-min insulinogenic index (IGI30) as [C-peptide 30 min (ng/mL) – C-peptide 0 min (ng/mL)]/[glucose 30 min (mmol/L) – glucose 0 min (mmol/L)]. Insulin secretion was assessed using IGI30 and the area under the curve (AUC) for C-peptide release test (AUC-CRT). Disposition index (DI), calculated by multiplying the GDR by IGI30, was used to evaluate β-cell function (Lee et al., 2017; Lemieux et al., 2019).

Statistical Analysis

The data analysis was performed using SPSS software version 26 (SPSS Inc.). Continuous variables are expressed as mean ± standard deviation. Categorical variables are expressed as frequencies and percentages. The normality of the continuous variables was evaluated using the Shapiro–Wilk test. The normality distribution variables were compared using the Wilcoxon signed rank or Student's paired *t*-test for baseline and postoperative data. Non-normally distributed variables were compared using the non-parametric test. Categorical variables were compared using the chi-square test. Statistical significance was defined as p values < 0.05.

RESULTS

Subject Characteristics

A total of 36 patients (17 in the LSG group and 19 in the LRYGB group) with T2DM and a BMI of 27.5–32.5 kg/m^2 participated in this study. All participants completed the surgery and follow-up. Accordingly, data from 17 participants (12 men, five women) in the LSG group (mean age, 39.06 ± 13.66 years; mean duration of T2DM, 5.71 ± 4.21 years) and 19 participants (15 men, four women) in the LRYGB group (mean age, 42.53 ± 10.63 years; mean duration of T2DM, 5.68 ± 3.27 years) were analyzed before and 6 months following surgery. Five patients in the LSG group versus nine in the LRYGB group were using insulin. The mean duration of insulin infusion was 1.88 ± 3.41 years in the LSG group and 2.56 ± 3.70 years in the LRYGB group. Eleven patients with hypertension in the LSG group versus 12 patients with hypertension in the LRYGB group were included. In the LSG group, nine patients were treated with calcium channel blockers, and two did not take any antihypertensive medications. In the LRYGB group, eight patients were treated with calcium channel blockers, three with angiotensin-converting enzymes, and one with a calcium channel blocker plus angiotensin-converting enzyme. The other baseline characteristics are shown in **Table 1**. No significant intergroup differences were found in the characteristics of the subjects.

As shown in **Table 2**, BMI, waist-to-height ratio (WtHR), systolic blood pressure, diastolic blood pressure, and triglycerides (TG) decreased significantly at 6 months postoperative versus baseline. The mean fasting glucose decreased from 9.77 ± 3.39 mmol/L to 5.98 ± 1.58 mmol/L in the LSG group versus from 10.16 ± 4.73 mmol/L to 5.68 ± 1.55 mmol/L in the LRYGB group. The mean HbA1c decreased from 8.74 ± 1.77% to 6.02 ± 0.82% in the LSG group and from 8.81 ± 1.93% to 6.1 ± 0.87% in the LRYGB group.

Insulin Sensitivity, Insulin Secretion, and β-Cell Function

As shown in **Tables 2**, **3**, the GDR significantly increased at 6 months after LSG (from 3.18 ± 1.36 mg/kg/min to 7.09 ± 1.69 mg/kg/min) and LRYGB (from 4.28 ± 1.70 mg/kg/min to 8.47 ± 1.89 mg/kg/min). Time to reach euglycemia decreased remarkably from 126.0 ± 9.61 min to 106.7 ± 13.82 min in the LSG group and from 124.4 ± 9.44 min to 108.1 ± 13.13 min in the LRYGB group at 6 months postoperative. The mean QUICKI increased at 6 months after LSG (from 0.44 ± 0.06 to 0.54 ± 0.09) and LRYGB (from 0.52 ± 0.09 to 0.74 ± 0.17). The mean TyG index significantly decreased by 1.32 ± 1.15 in the LSG group and by 1.33 ± 1.11 in the LRYGB group at 6 months postoperative. Meanwhile, a significant change was observed in insulin secretion and β-cell function after bariatric surgery. The mean IGI30 decreased by 1.20 ± 1.14 in the LSG group and by 1.22 ± 1.68 in the LRYGB group. The mean DI increased by 4.29 ± 4.88 in the LSG group and by 5.97 ± 5.09 in the LRYGB group. The AUC-CRT significantly increased 6 months after surgery. Compared with the baseline, other indicators, including HOMR-IR and AUC-OGTT, significantly decreased postoperatively.

TABLE 1 | Comparison of clinical characteristics in the LRYGB and LSG group.

Characteristics	LRYGB (*n* = 19)	LSG (*n* = 17)	*P* value
Gender	19	17	0.5761
Men	15	12	
Female	4	5	
Age (year)	42.53 ± 10.63	39.0 ± 13.66	0.3987
Duration of T2DM (year)	5.68 ± 3.27	5.71 ± 4.21	0.9863
Metformin	15	10	0.2013
Duration (year)	4.58 ± 3.96	4.24 ± 4.84	0.8164
Insulin infusions	9	5	0.2830
Duration (year)	2.56 ± 3.70	1.88 ± 3.41	0.5623
Comorbidities			
Hypertension	12	11	0.9258
Non-alcoholic fatty liver	15	16	0.1994

TABLE 2 | Variables comparison of the LRYGB and LSG group at baseline and post-surgery.

	LRYGB (n = 19)			LSG (n = 17)		
	Basal	**Post-surgery**	***P* value**	**Basal**	**Post-surgery**	***P* value**
Body mass (kg)	79.47 ± 9.70	69.48 ± 11.52	< 0.0001****	89.61 ± 9.15	79.12 ± 10.71	< 0.0001****
BMI (kg/m^2)	28.77 ± 1.64	25.09 ± 3.02	< 0.0001****	31.25 ± 1.55	27.51 ± 2.74	< 0.0001****
Waist circumference (cm)	97.50 ± 6.47	83.63 ± 8.27	< 0.0001****	112.4 ± 15.37	92.97 ± 11.63	< 0.0001****
Hip circumference (cm)	99.97 ± 6.14	91.84 ± 5.73	< 0.0001****	110.8 ± 10.38	100.8 ± 8.05	< 0.0001****
WHR	0.98 ± 0.04	0.91 ± 0.05	< 0.0001****	1.01 ± 0.08	0.92 ± 0.08	0.0003
WtHR	0.59 ± 0.38	0.50 ± 0.04	< 0.0001****	0.67 ± 0.09	0.55 ± 0.07	< 0.0001****
SBP (mmHg)	134.8 ± 16.98	123 ± 21.04	0.0212*	135.4 ± 18.52	125.1 ± 17.41	0.0764**
DBP (mmHg)	86.47 ± 12.59	79.21 ± 13.55	0.0356*	92.94 ± 14.74	81.76 ± 7.46	0.0063**
ALT (U/L)	54.58 ± 51.54	27.84 ± 25.36	0.0556	52.88 ± 45.94	23.94 ± 19.86	0.0081**
AST (U/L)	31.58 ± 17.64	24.84 ± 9.51	0.1806	29.59 ± 18.81	19.88 ± 10.73	0.0418*
LDL (mmol/L)	2.49 ± 0.86	2.43 ± 0.38	0.7665	2.56 ± 0.96	3.02 ± 0.98	0.1055
HDL (mmol/L)	1.14 ± 0.24	1.21 ± 0.23	0.3035	1.01 ± 0.28	1.16 ± 0.20	0.0116*
TC (mmol/L)	5.15 ± 0.93	4.39 ± 0.60	< 0.0001****	5.27 ± 1.16	5.27 ± 0.90	0.9875
TG (mmol/L)	3.82 ± 4.10	1.28 ± 0.44	0.0096**	4.10 ± 4.23	1.56 ± 1.11	0.0219*
Fasting						
Glucose (mmol/L)	10.16 ± 4.73	5.68 ± 1.55	< 0.0001****	9.77 ± 3.39	5.98 ± 1.58	0.0003***
HbA1c (%)	8.81 ± 1.93	6.1 ± 0.87	< 0.0001****	8.74 ± 1.77	6.02 ± 0.82	< 0.0001****
Hyperinsulinemic clamp						
Glucose disposal rate (mg/kg/min)	4.28 ± 1.70	8.47 ± 1.89	< 0.0001****	3.18 ± 1.36	7.09 ± 1.69	< 0.0001****
Time to reach euglycemia (min)	124.4 ± 9.44	108.1 ± 13.13	< 0.0001****	126.0 ± 9.61	106.7 ± 13.82	< 0.0001****
OGTT (mmol/L)						
0 min	9.85 ± 4.69	5.54 ± 1.20	0.0008***	9.32 ± 2.63	6.21 ± 2.37	0.0041**
30 min	14.05 ± 3.55	13.62 ± 3.24	0.6828	13.65 ± 2.56	12.62 ± 3.94	0.4028
120 min	17.90 ± 4.29	7.70 ± 4.12	< 0.0001****	16.99 ± 3.22	9.25 ± 4.97	< 0.0001****
AUC (min × mmol/L)	1796 ± 443.9	1247 ± 347.9	< 0.0001****	1723 ± 307.0	1266 ± 417.4	0.0024**
OGTT-CRT (μg/L)						
0 min	2.63 ± 0.88	1.70 ± 0.46	< 0.0001****	3.51 ± 1.59	3.08 ± 1.34	0.2304
30 min	3.97 ± 1.25	7.82 ± 2.55	< 0.0001****	4.78 ± 2.49	9.30 ± 6.15	0.0040**
120 min	6.16 ± 2.28	7.40 ± 3.78	0.2187	8.15 ± 4.52	8.89 ± 3.49	0.5365
AUC (min × μg/L)	554.4 ± 166.7	827.3 ± 277.6	0.0017**	706.3 ± 362.6	1004 ± 493.3	0.0136*
HOMA-IR	5.48 ± 3.86	1.34 ± 0.72	< 0.0001****	10.98 ± 7.68	4.61 ± 3.19	0.0004***
IGI30	2.04 ± 2.12	0.83 ± 0.47	0.005**	2.12 ± 1.73	0.92 ± 0.66	0.001**
Disposition index	1.14 ± 1.35	7.11 ± 4.93	0.000****	1.25 ± 1.78	5.60 ± 4.58	0.004**
Triglyceride glucose index	9.93 ± 1.03	8.60 ± 0.43	< 0.0001*	10.04 ± 0.79	8.72 ± 0.65	0.0002***
QUICKI	0.52 ± 0.09	0.74 ± 0.17	< 0.0001****	0.44 ± 0.06	0.54 ± 0.09	< 0.0001****

**P < 0.05; **P < 0.01; ***P < 0.001; ****P < 0.0001.*

WHR, waist-hip ratio; WtHR, waist-to-height ratio; SBP, systolic blood pressure; DBP, diastolic blood pressure; LDL, low-density lipoprotein; HDL, high-density lipoprotein; TC, total cholesterol; TG, triglyceride; HbA1c, glycosylated hemoglobin A1c; OGTT, oral glucose tolerance test; AUC, area under the curve; CRT, C peptide release test; IGI30, 30-min insulinogenic index; QUICKI, quantitative insulin sensitivity check index.

Composite Triple Endpoint

As shown in **Table 4**, the proportion of composite triple endpoint remissions appeared higher in the LRYGB group than in the LSG group (52.63% vs. 29.41%), but the difference was not statistically significant [odds ratio, 0.3750; 95% confidence interval (CI), 0.09252–1.511; $p = 0.1922$].

DISCUSSION

Type 2 diabetes mellitus is a global problem, but more than 50% of patients are unable to achieve their therapeutic targets (Saydah et al., 2004). IR is an important factor in the pathophysiology of T2DM and it significantly increases the incidence of comorbidities (Way et al., 2016). Bariatric surgery likely contributes to antidiabetic effects through weight loss and other weight-independent mechanisms (Batterham and Cummings, 2016). Previous research has shown that LRYGB and LSG are effective at achieving IR normalization based on the data of patients with severe obesity (Benaiges et al., 2013). However, the data on bariatric surgery for IR remission are insufficient in patients with T2DM and a low BMI.

Here we investigated whether LSG and LRYGB improve insulin sensitivity in patients with T2DM and a BMI of 27.5–32.5 kg/m^2. No intergroup differences were observed in the baseline characteristics of the patients. To this end, we assessed

TABLE 3 | Comparison of variable differences of the LRYGB and LSG group between baseline and post-surgery.

	Bariatric surgery	
Variables	**LRYGB (*n* = 19)**	**LSG (*n* = 17)**
ΔBMI (kg/m^2)	−3.68 ± 2.05	−3.73 ± 1.88
ΔWHR	−0.07 ± 0.06	−0.09 ± 0.08
ΔWtHR	−0.09 ± 0.04	−0.12 ± 0.05
Fasting		
ΔGlucose (mmol/L)	−4.48 ± 3.93	−3.79 ± 3.41
ΔHbA1c (%)	−2.71 ± 1.78	−2.72 ± 1.97
Hyperinsulinemic clamp		
ΔGlucose disposal rate (mg/kg/min)	4.19 ± 1.94	3.90 ± 1.45
ΔTime to reach euglycemia (min)	−16.32 ± 11.88	−19.29 ± 10.61
OGTT		
ΔAUC-OGTT (min × mmol/L)	−549.6 ± 491.4	−456.7 ± 524.5
ΔAUC-CRT (min × μg/L)	272.8 ± 323.6	297.8 ± 442.8
ΔHOMA-IR	−4.14 ± 3.72	−6.37 ± 5.90
ΔIGI30	−1.22 ± 1.68	−1.20 ± 1.14
ΔDisposition index	5.97 ± 5.09	4.29 ± 4.88
ΔTriglyceride glucose index	−1.33 ± 1.11	−1.32 ± 1.15
ΔQUICKI	0.21 ± 0.18	0.09 ± 0.06

WHR, waist-hip ratio; WtHR, waist-to-height ratio; SBP, systolic blood pressure; DBP, diastolic blood pressure; LDL, low-density lipoprotein; HDL, high-density lipoprotein; TC, total cholesterol; TG, triglyceride; HbA1c, glycosylated hemoglobin A1c; OGTT, oral glucose tolerance test; AUC, area under the curve; CRT, C peptide release test; IGI30, 30-min insulinogenic index; QUICKI, quantitative insulin sensitivity check index.

the GDR, time to reach euglycemia, HOMR-IR, QUICKI, OGTT with modeling, and TyG index. Our data show that, after weight loss induced by LSG or LRYGB, there were significant improvements in the GDR, HOMR-IR, QUICKI, and TyG index. All of the indicators evaluating the IR significantly improved from baseline to 6 months postoperative. Our previous study also showed that IR significantly improved at 3 months following LRYGB in patients with T2DM and a BMI <32.5 kg/m^2 (Zhao et al., 2017). Similar to our study, a dramatic reduction in IR was observed in patients with T2DM and a BMI of 23–35 kg/m^2 after LRYGB (Lee et al., 2011). Lee et al. (2010) found that IR decreased in patients with T2DM and a BMI of 25–35 kg/m^2 following LSG.

A reduction in insulin secretion (Δinsulin/Δglucose in 30 min) and an increase in total insulin secretion (AUC for insulin) was observed at 6 months after bariatric surgery in T2DM patients with a BMI <35 kg/m^2 (Lee et al., 2011). Similar results for insulin secretion were found using IGI30 and AUC-CRT in our study population. An increase in β-cell mass through "nesidioblastosis" may account for the increase in insulin secretion (Kaiser, 2005). The increase in the insulin secretion rate response to the OGTT, together with the restoration of the first-phase insulin secretion, might explain the reversal of T2DM after LRYGB (Salinari et al., 2013). Early improvement of β-cell function was associated with T2DM remission after LSG (Mullally et al., 2019). Our data showed a significant increase in DI at 6 months postoperative in both the groups. This showed that LRYGB and LSG significantly improved β-cell function, which may be one of the mechanisms of diabetes remission after bariatric surgery.

TABLE 4 | Comparison of diabetes remission in the LRYGB and LSG group.

Diabetes remission	**LRYGB (*n* = 19)**	**LSG (*n* = 17)**	**Odds ratio (95% confidence interval)**	***P* value**
Composite triple endpoint	10 (52.8%)	5 (29.41%)	0.38 (0.09–1.51)	0.1993
Fail to composite triple endpoint	9 (47.37%)	12 (70.59%)		

Meanwhile, other indicators, including BMI, WtHR, blood pressure, TG, fasting glucose, and HbA1c, also significantly improved from baseline to 6 months postoperative in our study groups. Based on our data, we may conclude that LSG and LRYGB are also effective at alleviating IR in Chinese patients with T2DM and a BMI of 27.5–32.5 kg/m^2.

Both LSG and LRYGB are proven effective options for T2DM and comorbidities, especially in patients with a BMI >35 kg/m^2 (Zimmet et al., 2011). Our previous studies also demonstrated that weight, glycemic, and lipid profiles improved in T2DM patients with a BMI <32.5 kg/m^2 who underwent bariatric surgery (Ji et al., 2020). In the present study, anthropometric and glycolipid parameters improved from baseline to 6 months after LSG and LRYGB. This finding is consistent with the results of previous studies (Di et al., 2016; Du et al., 2017; Ji et al., 2020). Consequently, the two bariatric procedures were available for Chinese patients with T2DM and a BMI of 27.5–35 kg/m^2. Two randomized clinical trials (RCTs) showed no difference in remission of T2DM, quality of life, or individual burden for patients with surgical complications at 5 years postoperative in patients with a BMI >35 kg/m^2 (Peterli et al., 2017). Based on our results, the proportion of patients achieving composite triple endpoint remission in the LRYGB group seemed higher than that in the LSG group, but the difference was not statistically significant. This may indicate that LRYGB also has no short-term advantage in the improvement of the composite triple endpoint for Chinese patients with T2DM and a low BMI.

The present study had several limitations. First, its sample size was small. Second, the patients were not randomly assigned to the bariatric procedures. Third, the follow-up time was significantly insufficient, and the triple composite endpoint to evaluate the remission of T2DM was not ideal.

CONCLUSION

Both LRYGB and LSG effectively achieve remission of IR in patients with T2DM and a BMI of 27.5–37.5 kg/m^2. Larger sample and longer follow-up RCTs are required to validate our findings.

DATA AVAILABILITY STATEMENT

The raw data supporting the conclusions of this article will be made available by the authors, without undue reservation.

ETHICS STATEMENT

The studies involving human participants were reviewed and approved by the Human Ethics Committee of the Third Xiangya Hospital of Central South University. The patients/participants provided their written informed consent to participate in this study.

AUTHOR CONTRIBUTIONS

PL and YC contributed to study design and writing. PZL, GW, ZS, and WL contributed to surgery. ZHS, HZ, XY, ZF, XS, HT, BC, and QY contributed to data collections and data analysis. LZ and SZ contributed to guide. All authors contributed to the article and approved the submitted version.

FUNDING

This work was supported by the Natural Science Foundation of Hunan Province (Grant No. 2021JJ31039).

ACKNOWLEDGMENTS

We thank all the patients enrolled in this study for their cooperation and clinical staff for their responsible work.

REFERENCES

American Diabetes Association (2014). Diagnosis and classification of diabetes mellitus. *Diabetes Care* 37(Suppl. 1), S81–S90. doi: 10.2337/dc14-S081

Batterham, R. L., and Cummings, D. E. (2016). Mechanisms of diabetes improvement following bariatric/metabolic surgery. *Diabetes Care* 39, 893–901. doi: 10.2337/dc16-0145

Benaiges, D., Flores Le-Roux, J. A., Pedro-Botet, J., Chillarón, J. J., Renard, M., Parri, A., et al. (2013). Sleeve gastrectomy and Roux-en-Y gastric bypass are equally effective in correcting insulin resistance. *Int. J. Surg.* 11, 309–313. doi: 10.1016/j.ijsu.2013.02.007

Chan, J. C., Malik, V., Jia, W., Kadowaki, T., Yajnik, C. S., Yoon, K. H., et al. (2009). Diabetes in Asia: epidemiology, risk factors, and pathophysiology. *JAMA* 301, 2129–2140. doi: 10.1001/jama.2009.726

DeFronzo, R. A. (2004). Pathogenesis of type 2 diabetes mellitus. *Med. Clin. North Am.* 88, 787–835. doi: 10.1016/j.mcna.2004.04.013

Di, J., Zhang, H., Yu, H., Zhang, P., Wang, Z., and Jia, W. (2016). Effect of Roux-en-Y gastric bypass on the remission of type 2 diabetes: a 3-year study in Chinese patients with a BMI <30 kg/m(2). *Surg. Obes. Relat. Dis.* 12, 1357–1363. doi: 10.1016/j.soard.2016.02.007

Dixon, J. B., Zimmet, P., Alberti, K. G., and Rubino, F. (2011). Bariatric surgery: an IDF statement for obese Type 2 diabetes. *Surg. Obes. Relat. Dis.* 7, 433–447. doi: 10.1016/j.soard.2011.05.013

Du, X., Zhou, H. X., Zhang, S. Q., Tian, H. M., Zhou, Z. G., and Cheng, Z. (2017). A comparative study of the metabolic effects of LSG and LRYGB in Chinese diabetes patients with BMI<35 kg/m(2). *Surg. Obes. Relat. Dis.* 13, 189–197. doi: 10.1016/j.soard.2016.08.499

Ikramuddin, S., Billington, C. J., Lee, W. J., Bantle, J. P., Thomas, A. J., Connett, J. E., et al. (2015). Roux-en-Y gastric bypass for diabetes (the Diabetes Surgery Study): 2-year outcomes of a 5-year, randomised, controlled trial. *Lancet Diabetes Endocrinol.* 3, 413–422. doi: 10.1016/s2213-8587(15)00089-3

Ji, G., Li, W., Li, P., Tang, H., Yu, Z., Sun, X., et al. (2020). Effect of Roux-en-Y gastric bypass for patients with type 2 diabetes mellitus and a BMI?<?32.5 kg/m: a 6-year study in Chinese patients. *Obes. Surg.* 30, 2631–2636. doi: 10.1007/s11695-020-04534-z

Kaiser, A. M. (2005). Hyperinsulinemic hypoglycemia with nesidioblastosis after gastric-bypass surgery. *N. Engl. J. Med.* 353, 2192–2194.

Katz, A., Nambi, S. S., Mather, K., Baron, A. D., Follmann, D. A., Sullivan, G., et al. (2000). Quantitative insulin sensitivity check index: a simple, accurate method for assessing insulin sensitivity in humans. *J. Clin. Endocrinol. Metab.* 85, 2402–2410. doi: 10.1210/jcem.85.7.6661

Lee, D. Y., Yoo, M. G., Kim, H. J., Jang, H. B., Kim, J. H., Lee, H. J., et al. (2017). Association between alcohol consumption pattern and the incidence risk of type 2 diabetes in Korean men: a 12-years follow-up study. *Sci. Rep.* 7:7322. doi: 10.1038/s41598-017-07549-2

Lee, W. J., and Aung, L. (2016). Metabolic surgery for type 2 diabetes mellitus: experience from Asia. *Diabetes Metab. J.* 40, 433–443. doi: 10.4093/dmj.2016.40.6.433

Lee, W. J., Chong, K., Chen, C. Y., Chen, S. C., Lee, Y. C., Ser, K. H., et al. (2011). Diabetes remission and insulin secretion after gastric bypass in patients with body mass index <35 kg/m2. *Obes. Surg.* 21, 889–895. doi: 10.1007/s11695-011-0401-6

Lee, W. J., Ser, K. H., Chong, K., Lee, Y. C., Chen, S. C., Tsou, J. J., et al. (2010). Laparoscopic sleeve gastrectomy for diabetes treatment in nonmorbidly obese patients: efficacy and change of insulin secretion. *Surgery* 147, 664–669. doi: 10.1016/j.surg.2009.10.059

Lemieux, P., Weisnagel, S. J., Caron, A. Z., Julien, A. S., Morisset, A. S., Carreau, A. M., et al. (2019). Effects of 6-month vitamin D supplementation on insulin sensitivity and secretion: a randomised, placebo-controlled trial. *Eur. J. Endocrinol.* 181, 287–299. doi: 10.1530/eje-19-0156

Matthews, D. R., Hosker, J. P., Rudenski, A. S., Naylor, B. A., Treacher, D. F., and Turner, R. C. (1985). Homeostasis model assessment: insulin resistance and beta-cell function from fasting plasma glucose and insulin concentrations in man. *Diabetologia* 28, 412–419. doi: 10.1007/bf00280883

Mingrone, G., and Cummings, D. E. (2016). Changes of insulin sensitivity and secretion after bariatric/metabolic surgery. *Surg. Obes. Relat. Dis.* 12, 1199–1205. doi: 10.1016/j.soard.2016.05.013

Mullally, J. A., Febres, G. J., Bessler, M., and Korner, J. (2019). Sleeve gastrectomy and Roux-en-Y gastric bypass achieve similar early improvements in beta-cell function in obese patients with type 2 diabetes. *Sci. Rep.* 9:1880. doi: 10.1038/s41598-018-38283-y

Peterli, R., Wölnerhanssen, B. K., Vetter, D., Nett, P., Gass, M., Borbély, Y., et al. (2017). Laparoscopic sleeve gastrectomy versus Roux-Y-gastric bypass for morbid obesity-3-year outcomes of the prospective randomized Swiss Multicenter Bypass Or Sleeve Study (SM-BOSS). *Ann. Surg.* 265, 466–473. doi: 10.1097/sla.0000000000001929

Rabasa-Lhoret, R., and Laville, M. (2001). [How to measure insulin sensitivity in clinical practice?]. *Diabetes Metab.* 27, 201–208.

Saeedi, P., Petersohn, I., Salpea, P., Malanda, B., Karuranga, S., Unwin, N., et al. (2019). Global and regional diabetes prevalence estimates for 2019 and projections for 2030 and 2045: results from the International Diabetes Federation Diabetes Atlas, 9(th) edition. *Diabetes Res. Clin. Pract.* 157:107843. doi: 10.1016/j.diabres.2019.107843

Salinari, S., Bertuzzi, A., Guidone, C., Previti, E., Rubino, F., and Mingrone, G. (2013). Insulin sensitivity and secretion changes after gastric bypass in normotolerant and diabetic obese subjects. *Ann. Surg.* 257, 462–468. doi: 10.1097/SLA.0b013e318269cf5c

Saydah, S. H., Fradkin, J., and Cowie, C. C. (2004). Poor control of risk factors for vascular disease among adults with previously diagnosed diabetes. *JAMA* 291, 335–342. doi: 10.1001/jama.291.3.335

Wang, T., Lu, J., Shi, L., Chen, G., Xu, M., Xu, Y., et al. (2020). Association of insulin resistance and β-cell dysfunction with incident diabetes among adults in China: a nationwide, population-based, prospective cohort study. *Lancet Diabetes Endocrinol.* 8, 115–124. doi: 10.1016/s2213-8587(19)30425-5

Way, K. L., Hackett, D. A., Baker, M. K., and Johnson, N. A. (2016). The effect of regular exercise on insulin sensitivity in type 2 diabetes mellitus: a systematic

review and meta-analysis. *Diabetes Metab. J.* 40, 253–271. doi: 10.4093/dmj.2016.40.4.253

Yu, Z., Li, W., Sun, X., Tang, H., Li, P., Ji, G., et al. (2021). Predictors of type 2 diabetes mellitus remission after metabolic surgery in Asian patients with a BMI < 32.5 kg/m(2). *Obes. Surg.* 31, 4125–4133. doi: 10.1007/s11695-021-05544-1

Zhang, M., Wang, B., Liu, Y., Sun, X., Luo, X., Wang, C., et al. (2017). Cumulative increased risk of incident type 2 diabetes mellitus with increasing triglyceride glucose index in normal-weight people: the Rural Chinese Cohort Study. *Cardiovasc. Diabetol.* 16:30. doi: 10.1186/s12933-017-0514-x

Zhao, L., Zhu, L., Su, Z., Liu, Y., Li, P., Yang, X., et al. (2017). Using the hyperinsulinemic euglycemic clamp to assess insulin sensitivity at 3 months following Roux-en-Y gastric bypass surgery in type 2 diabetes patients with BMI <35 kg/m(2) in China. *Int. J. Surg.* 38, 90–94. doi: 10.1016/j.ijsu.2016.12.120

Zimmet, P., Alberti, K. G., Rubino, F., and Dixon, J. B. (2011). IDF's view of bariatric surgery in type 2 diabetes. *Lancet* 378, 108–110. doi: 10.1016/s0140-6736(11)61027-1

Conflict of Interest: The authors declare that the research was conducted in the absence of any commercial or financial relationships that could be construed as a potential conflict of interest.

Publisher's Note: All claims expressed in this article are solely those of the authors and do not necessarily represent those of their affiliated organizations, or those of the publisher, the editors and the reviewers. Any product that may be evaluated in this article, or claim that may be made by its manufacturer, is not guaranteed or endorsed by the publisher.

frontiers in Physiology

ORIGINAL RESEARCH
published: 11 November 2021
doi: 10.3389/fphys.2021.785799

Sleeve Gastrectomy Ameliorates Diabetes-Induced Cardiac Hypertrophy Correlates With the MAPK Signaling Pathway

*Qian Xu[1], Huanxin Ding[1], Songhan Li[1], Shuohui Dong[1], Linchuan Li[2], Bowen Shi[1], Mingwei Zhong[2] and Guangyong Zhang[1]**

[1]Department of General Surgery, Shandong Provincial Qianfoshan Hospital, Shandong University, Jinan, China, [2]Department of General Surgery, The First Affiliated Hospital of Shandong First Medical University, Jinan, China

OPEN ACCESS

Edited by:
Xiang Zhang,
Shandong University, China

Reviewed by:
Arun Prasath Lakshmanan,
Sidra Medicine, Qatar
Michinari Nakamura,
Rutgers University,
Newark, United States
Xiaofei Xu,
Beijing Hospital, China

***Correspondence:**
Guangyong Zhang
guangyongzhang@hotmail.com

Specialty section:
This article was submitted to Metabolic Physiology, a section of the journal Frontiers in Physiology

Received: *29 September 2021*
Accepted: *25 October 2021*
Published: *11 November 2021*

Citation:
Xu Q, Ding H, Li S, Dong S, Li L, Shi B, Zhong M and Zhang G (2021) Sleeve Gastrectomy Ameliorates Diabetes-Induced Cardiac Hypertrophy Correlates With the MAPK Signaling Pathway. Front. Physiol. 12:785799. doi: 10.3389/fphys.2021.785799

Background: Cardiac hypertrophy as a main pathological manifestation of diabetic cardiomyopathy (DCM), is a significant complication of diabetes. Bariatric surgery has been proven to relieve DCM; however, whether it can alleviate diabetes-induced cardiac hypertrophy is undefined.

Methods: Diabetic and obese rats were performed sleeve gastrectomy (SG) after having diabetes for 16 weeks. The rats were euthanized 8 weeks after SG. Metabolic parameters, heart function parameters, myocardial glucose uptake, morphometric and histological changes, and the expression level of mitogen-activated protein kinases (MAPKs) were determined and compared among the control group (CON group), diabetes mellitus group (DM group), sham operation group (SHAM group), and SG group.

Results: Compared with the SHAM group, the blood glucose, body weight, insulin resistance, and other metabolic parameters were significantly improved in the SG group. There was also a marked improvement in myocardial morphometric and histological parameters after SG. Furthermore, the myocardial glucose uptake and heart function were reversed after SG. Additionally, the phosphorylation of MAPKs was inhibited after SG, including p38 MAPKs, c-Jun N-terminal kinases (JNKs), and extracellular signal-regulated kinases 1/2 (ERK1/2). The expression of DUSP6, which dephosphorylates ERK1/2, was upregulated after SG. These findings suggest that SG ameliorated diabetes-induced cardiac hypertrophy correlates with the MAPK signaling pathway.

Conclusion: These results showed that diabetes-induced cardiac hypertrophy was ameliorated after SG was closely related to the inhibition of the MAPK signaling pathway and upregulation of DUSP6. Therefore, this study provides a novel strategy for treating diabetes-induced cardiac hypertrophy.

Keywords: diabetes-induced cardiac hypertrophy, sleeve gastrectomy, MAPK, ERK1/2, DUSP6

INTRODUCTION

During the past three decades, the number of people with diabetes mellitus has increased fourfold (Gibb and Hill, 2018). Diabetes and its complications, including diabetic cardiomyopathy (DCM), pose a serious threat to global health and place a great burden on global health care (Holman et al., 2015; Zimmet, 2017). DCM substantially increases a person's risk of heart failure (Kannel et al., 1974; de Simone et al., 2010); among hospitalized patients with heart failure, approximately 44% have diabetes mellitus (Echouffo-Tcheugui et al., 2016). Cardiac hypertrophy and myocardial fibrosis are the main pathological features of DCM, with a significant association with death in DCM patients (Kobayashi and Liang, 2015; Jia et al., 2018). Unfortunately, there is no reliable strategy for treating this disease.

Initially, bariatric surgery was only used to treat morbid obesity, but we have found that it also has some benefits for the treatment of type 2 diabetes mellitus (T2DM) and its complications (Affinati et al., 2019; Ruze et al., 2020). Presently, sleeve gastrectomy (SG) and Roux-en-Y gastric bypass (RYGB) are the most common bariatric surgeries undertaken globally, accounting for 45.9 and 39.6%, respectively (Angrisani et al., 2017; Pucci and Batterham, 2019). Nowadays, multiple studies have demonstrated that bariatric surgery improved hyperglycemia and reduced body weight (Affinati et al., 2019; Arterburn et al., 2020; Docherty and le Roux, 2020). Markedly, bariatric surgery significantly alleviates T2DM and improves its complications, compared with traditional medical treatment (Nguyen and Varela, 2017). Huang et al. have shown that the bariatric surgery improved DCM and diabetes-induced cardiac hypertrophy clearly (Huang et al., 2018), yet the specific mechanism is unclear.

The mitogen-activated protein kinase (MAPK) signaling pathway has been demonstrated to play a key role in pathological cardiac hypertrophy by multiple studies (Ba et al., 2019; Liao et al., 2019). As a highly conserved signaling pathway, this pathway is widely found in mammals (Cargnello and Roux, 2011). The conventional MAPK signaling family is mainly composed of three pathways, the p38 MAPKs, the c-Jun N-terminal kinases (JNKs), and the extracellular signal-regulated kinases 1/2 (ERK1/2; Siti et al., 2021). The biological responses of MAPKs depend on their phosphorylation level (Liu et al., 2016). Chang et al. (2011) and Shen et al. (2011) have reported that these three MAPKs were upregulated in glucose-induced cardiomyocytes and in streptozotocin (STZ)-induced diabetic rats. A strong link between MAPK signaling pathway and cardiac hypertrophy has been reported (Singh et al., 2017). Among these three MAPKs, JNK and p38 attenuate cardiac hypertrophy by regulating pro-inflammation and stress, whereas ERK1/2 regulates cell growth, differentiation, and proliferation (Mutlak and Kehat, 2021). The dephosphorylation of MAPKs is achieved *via* dual-specificity phosphatases (DUSPs; Liu and Molkentin, 2016). Currently, 13 DUSPs have been characterized, among them, DUSP1 has been reported to downregulate p38, JNK, and ERK1/2 in transgenic mice (Bueno et al., 2001; Liu et al., 2016). Consistently, a DUSP1 and DUSP4 double-null mutant led to enhancement of p38 phosphorylation, which in turn reduced the survival rate (Auger-Messier et al., 2013). DUSP6 has been reported to inhibit ERK1/2 to improve cardiac hypertrophy (Ramkissoon et al., 2019). Thus, we concluded that MAPK signaling pathways and DUSPs play a vital role in diabetes-induced cardiac hypertrophy.

Our previous study has demonstrated that cardiac hypertrophy was ameliorated after bariatric surgery in diabetic rats (Huang et al., 2019). However, whether the amelioration of cardiac hypertrophy by SG is related to MAPK signaling pathways and DUSPs is unknown. In this study, we explored this using a high-fat diet (HFD)-STZ-T2DM rat model.

MATERIALS AND METHODS

Animals

Eighty 4-week-old male Wistar rats (80–110 g; Vital River Laboratory Animal Technology Co., Ltd., Beijing, China) were housed in the animal laboratory of Shandong Provincial Qianfoshan Hospital of Shandong University in specific pathogen-free housing conditions at 20–26°C and 50–60% humidity. The animal study was reviewed and approved by approved by the Institutional Animal Care and Use Committee of Shandong Provincial Qianfoshan Hospital of Shandong University. All animals were adaptively fed a standard diet for 1 week (SD; 15% of the calories were fat, Laboratory Animal Center of Shandong University, Jinan, China) and then randomly divided into the following four groups (**Figure 1**):

(1) Control group (CON group; $n = 15$): fed a SD during the entire study. (2) Diabetes mellitus group (DM group; $n = 18$): received a single intraperitoneal STZ (Sigma-Aldrich, St. Louis, MO, United States) injection at 33 mg/kg body weight after a 4-week HFD (40% of the calories were fat; Jiangsu Xietong Pharmaceutical Bio-engineering Co., Ltd., Nanjing, China) followed by a 12-h fast. STZ was dissolved in 0.1 mol/L sodium citrate buffer (pH = 4.5; Beijing Solarbio Science & Technology Co., Ltd., Beijing, China) to 0.1 ml/mg. Three days after the STZ injection, the random blood glucose was measured three consecutive times ($\geq$ 16.7 mmol/L was considered a successful model of diabetic rats; Zhang et al., 2020). (3) Sham operation group (SHAM group, $n = 20$): treated like the DM group, but a sham operation was performed 16 weeks after the STZ injection. The rats continued to be fed an HFD for 8 weeks after the operation and were then euthanized. (4) Sleeve gastrectomy group (SG group, $n = 27$): treated like the DM group, but the SG was performed 16 weeks after the STZ injection. The rats continued to be fed an HFD for 8 weeks after the operation and were then euthanized.

After the experiments, all rats in the CON group survived, five rats in the DM group died of hyperglycemia, and two and six rats in the SHAM group died of hyperglycemia and infection, respectively. In the SG group, two rats died of hypoglycemia, four rats died of intestinal obstruction, three rats died of infection, and three rats died of gastric leakage. Namely, 15, 13, 12, and 15 rats survived in the CON, DM, SHAM, and SG groups, respectively. In addition, there were 2, 0, 2, and 2 rats in CON group, DM group, SHAM group, and SG group, respectively, which were defined as outliers by

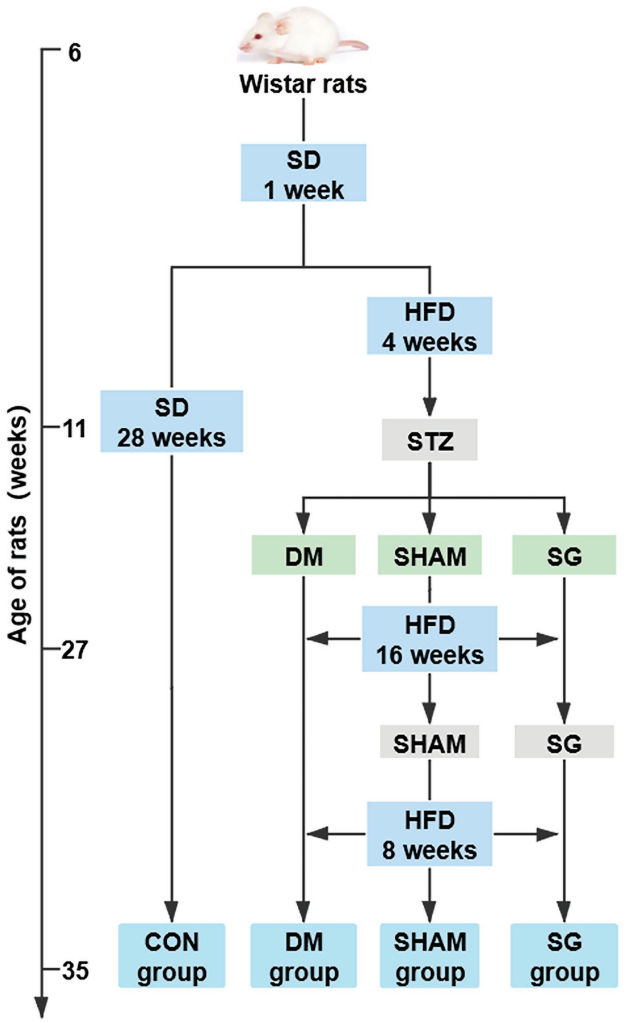

FIGURE 1 | The flow chart of animal experiments. $N = 10$ for per groups. SD, standard diet; HFD, high-fat diet; STZ, streptozotocin; CON, control; DM, diabetes mellitus; SHAM, sham operation; SG, sleeve gastrectomy.

Grubbs' test. Thus, 13, 13, 10, and 13 rats in the CON, DM, SHAM, and SG groups could be included in this study, respectively. To make the sample size of each group equal, 5, 3, 2, and 5 rats from the CON, DM, SHAM, and SG groups including outliers were randomly euthanatized by injecting an overdose of 10% chloral hydrate (6 ml/kg). Consequently, each group had 10 rats.

Surgical Procedures

Sleeve gastrectomy: SG was performed as previously reported (Bruinsma et al., 2015). All rats fasted for 12 h before operation and were then anesthetized with 2% isoflurane gas. First, a 4 cm incision in the middle of the upper abdomen was made. Then, the stomach was be dissociated until the gastric blood vessels and tissue structure were clearly distinguished. The blood vessels of the gastric fundus and the greater gastric curvature were ligated by 7–0 lines (Ningbo Cheng-He Microsurgical Instruments Factory, Ningbo, China) and then interrupted after successful ligation. Next, a 0.5 cm incision parallel to the greater gastric curvature was made at the gastric fundus to remove the stomach contents. The gastric fundus and a large portion of the gastric body on the greater gastric curvature were removed, and subsequently, the remaining stomach was sutured with a 5–0 line (Ningbo Cheng-He Microsurgical Instruments Factory). The anatomical position of the abdominal cavity was restored after confirming no active bleeding. Finally, the abdominal cavity was closed layer by layer with 3–0 lines (Ningbo Cheng-He Microsurgical Instruments Factory).

Sham operation: This operation was the same as the above SG procedure before blocking the gastric blood vessels. There were no other interventions, except for exposing abdominal organs, such as the stomach, small intestine, and liver. Additionally, to maintain the same degree of stress as the SG group, we prolonged the operative and anesthesia time in line with the SG group.

Physiological Parameters

The body weight of all the rats was measured before the operation and 2, 4, 6, and 8 weeks after the operation. The food intake was measured at the same time points as the body weight. After euthanasia, the heart weight (HW) and tibia length (TL) of the rats were measured and the HW/TL ratio was calculated and analyzed.

Blood Chemistry

The fasting blood glucose (FBG) was measured by a glucometer (Roche One Touch Ultra, Lifescan, Johnson & Johnson, Milpitas, CA, United States) after a 12-h fast at the same time points as the body weight was measured. Blood was collected from the tail vein of anesthetized rats and immediately centrifuged for 8 min at 3000 rpm, and then, the upper serum was collected and stored in a frozen tube at −80°C. The serum insulin was measured by an ELISA kit (EZRMI-13K, Millipore, Darmstadt, Germany). Finally, the homeostasis model assessment of insulin resistance (HOMA-IR) was calculated to estimate the degree of insulin resistance. The calculation formula was: HOMA-IR = fasting serum insulin (mIU/L) × FBG (mmol/L) /22.5.

Oral Glucose Tolerance Test and Insulin Tolerance Test

The oral glucose tolerance test (OGTT) was performed after a 12-h fast at the same time points as body weight was measured. Rats were administered with 1 g/kg glucose by oral gavage, and then, their blood glucose was measured after 0, 10, 30, 60, and 120 min. The area under the curve (AUC) of the OGTT (AUC_{OGTT}) was calculated by the trapezoidal method.

Two days after the OGTT, the insulin tolerance test (ITT) was performed after a 12-h fast. Rats were administered with 0.5 IU/kg insulin (Gansulin 40R, Tonghua Dongbao Pharmaceutical Co., Ltd., Tonghua, China) by intraperitoneal injection, and then, their blood glucose was measured after 0, 10, 30, 60, and 120 min. The AUC of the ITT (AUC_{ITT}) was calculated by the trapezoidal method.

Echocardiographic Evaluation

Echocardiography was performed after the 12-h fast and before the euthanasia of rats with a Vevo 2,100 imaging system (VisualSonics, Toronto, Canada). Rats were anesthetized with 2% isoflurane. Doppler mode and M-mode imaging were performed to evaluate the cardiac structure. Furthermore, left ventricular end-diastolic diameter, left ventricular end-systolic diameter, ejection fraction, and fractional shortening were analyzed to evaluate the function of the left ventricle.

Positron-Emission Tomography Scan and Image Processing

Positron-emission tomography (PET) scan was performed following a 12-h fast and before the euthanasia of rats, which were anesthetized with 2% isoflurane. After intravenous injection of 800 μCi (29.6 MBq) 18F-FDG, the entire rat body was continuously scanned with a PET scanner (Metis 1800, Madic Technology Co., Ltd., Linyi, China) for 60 min. The PET images recorded show three dimensions: coronal, sagittal, and transverse. Additionally, the average standard uptake value (SUV_{Mean}) was analyzed by PMOD 4.1 software (PMOD Technologies LLC., Zurich, Switzerland) to evaluate the myocardial glucose uptake of the rats.

Morphometric and Histological Analysis

The heart tissue was fixed with 4% paraformaldehyde, embedded in paraffin, and sectioned into 5 μm sections. The paraffin sections were stained with hematoxylin and eosin (H&E; G1003, Servicebio, Wuhan, China) to evaluate the heart structure. Furthermore, to determine collagen deposition, Sirius Red (G1018, Servicebio, Wuhan, China) and Masson (G1006, Servicebio, Wuhan, China) staining were performed on the 5 μm paraffin heart tissue sections. The collagen volume fraction (CVF) was calculated by ImageJ software (National Institutes of Health, Bethesda, MD, United States) and used as a quantitative measure of collagen deposition. To determine the area of cardiac myocytes (CMs), paraffin sections of transversely cut muscle fibers were stained with wheat germ agglutinin (WGA; L4895, Sigma-Aldrich, St. Louis, MO, United States). ImageJ software was used to calculate the CM area. Oil Red O staining assessed myocardial lipid accumulation. The fresh tissue frozen sections were reheated and dried and then fixed it in the fixative solution for15 min. Oil Red solution (G1016, Servicebio, Wuhan, China) was used to stain the frozen sections. And then immersed them into isopropanol for differentiation. After stained by hematoxylin (G1004, Servicebio, Wuhan, China), followed by three washes. Finally, the sections with glycerin gelatin. All the sections were made into digital sliders by a Pannoramic Digital Slide Scanners (Pannoramic DESK, P-MIDI, P250, and P1000, 3DHISTECH Ltd., Budapest, Hungary).

Quantitative Real-Time PCR

Total RNA was extracted from frozen heart tissue by TRIzol reagent (G3013, Servicebio, Wuhan, China). Single-strand complementary DNA (cDNA) was synthesized by ReverTra Ace qPCR RT Kit (FSQ-101, TOYOBO Co., Ltd., Osaka, Japan). For quantitative real-time PCR, the SYBR Green Realtime PCR Master Mix (QPK-201, TOYOBO Co., Ltd.) was used following the manufacturer's instructions. The total PCR reaction volume was 20 μl, containing 0.8 μl of each primer. The target-specific primers were designed by Sangon Biotech (Shanghai, China), and the specific sequences are listed in **Table 1**.

Immunohistochemistry

Paraffin-embedded heart tissue was sectioned into 5 μm sections. The paraffin sections were deparaffinized and rehydrated in xylol and alcohol. The antigen was retrieved in a microwave oven with citrate antigen retrieval solution (ZLI 9064, ZSGB-BIO, Beijing, China) after three washes with phosphate-buffered saline (PBS, G0002-2L, Servicebio). Sections were incubated overnight at 4°C with primary antibodies (Collagen I, 1:500, ab270993, Abcam, Cambridge, MA, United States; Collagen III, 1:200, ab7778, Abcam; DUSP6, 1:100, ET1602-18, Huabio, China; p-ERK1/2, 1:200, 4,370 T, Cell Signaling Technology, Danvers, MA, United States), followed by three washes with PBS. Sections were then incubated with a universal two-step detection kit (PV-9000, ZSGB-BIO) following the manufacturer's instructions. After three washes with PBS, the sections were stained with diamino-benzidine (DAB, ZLI-9018, ZSGB-BIO) and hematoxylin and then dehydrated, and transparency were performed. Finally, the sections were made into digital slides with Pannoramic Digital Slide Scanners (Pannoramic DESK, P-MIDI, P250, and P1000, 3DHISTECH Ltd.).

Western Blot Analysis

Total protein was extracted from frozen heart tissue using a Minute™ muscle tissue total protein extraction kit (SA-06-MS, Invent Biotechnologies, Inc., United States) following the manufacturer's instructions. Protein samples were quantified

TABLE 1 | Specific sequences of primers used in real-time PCR.

Gene	Primer sequence, 5′-3′	Gene ID
Anp	F: GAGCGAGCAGACCGATGAAGC R: TCCATCTCTCTGAGACGGGTTGAC	24602
β-mhc	F: CACCGCCTCCTCCACCTCTG R: CCAGAACACCAGCCTCATCAACC	29557
Col1a1	F: TGTTGGTCCTGCTGGCAAGAATG R: GTCACCTTGTTCGCCTGTCTCAC	29393
Col3a1	F: AGTCGGAGGAATGGGTGGCTATC R: CAGGAGATCCAGGATGTCCAGAGG	84032
Col4a5	F: CATACAAGGTGTGGCGGGAAATCC R: TCCTGGCTGGCTGATGGTCTG	363457
Col9a1	F: GAGCCAGGAAGACAAGGACACAAG R: CCAACTATGCCAGTGATGCCTCTC	305104
Dusp6	F: CGGTGACAGTGGCTTACCTTATGC R: TGAAGTTGAAGTTGGGAGAGATGTTGG	116663
β-actin	F: TGCTATGTTGCCCTAGACTTCG R: GTTGGCATAGAGGTCTTTACGG	81822

F, forward and R, reverse.

using a BCA Protein Assay Kit (E-BC-K318-M, Elabscience, Wuhan, China). Protein samples were resolved on 10% SDS-PAGE gels (PG212, EpiZyme, Shanghai, China) and transferred onto polyvinylidene fluoride membranes (Millipore, Burlington, MA, United States). The membranes were blocked with 5% fat-free milk and incubated overnight at 4°C with primary antibodies (ANP, 1:1000, ab209232, Abcam, United States; β-MHC, 1:1000, 22280-1-AP, Proteintech, China; p38, 1:1000, ET1702-65, Huabio, China; JNK, 1:1000, RT1550, Huabio, China; ERK1/2, 1:1000, 67170-1-Ig, Proteintech, China; p-p38, 1:1000, ER1903-01, Huabio, China; p-JNK, 1:1000, 4668S, Cell Signaling Technology, USA; p-ERK1/2, 1:1000, 4370T, Cell Signaling Technology, United States; DUSP 6, 1:1000, ET1602-18, Huabio, China; β-ACTIN, 1:1000, ab8226, Abcam, United States). Then, the membranes were washed and incubated with secondary antibodies (Goat anti-Mouse IgG, 1:10000, ab216776, Abcam; Goat Anti-Rabbit IgG, 1:10000, ab6721, Abcam). The protein bands were visualized by ECL (Millipore) and quantified using ImageJ software (National Institutes of Health).

Statistical Analysis

Data were analyzed using Graph Pad Prism 8.0 (GraphPad software, San Diego, CA, United States) and intergroup comparisons were performed with one-way ANOVA followed by Tukey's multiple comparisons test. Statistical outliers were determined using the Grubbs' test. $p < 0.05$ was considered statistically significant. Data are presented as the mean ± SEM.

RESULTS

SG Significantly Improves Metabolic Parameters in Diabetic Obese Rats

The metabolic abnormalities in diabetic obese rats were significantly improved in the SG group (**Figure 2**). The results showed that the body weight and food intake of the DM group were significantly higher than those of the CON group, whereas SG significantly reduced these parameters (**Figures 2A,B**). Furthermore, compared with the SHAM group, the SG group had a lower level of FBG from 2 weeks after the operation (**Figure 2C**). In addition to the change in FBG and the serum insulin level, we found that the insulin resistance of the SG group was significantly improved compared with that of the SHAM group as assessed by HOMA-IR (**Figures 2C–E**). Consistent with the above results, analysis of AUC_{OGTT} and AUC_{ITT} demonstrated a significant improvement in insulin resistance in the SG group (**Figures 2F,G**). All these data above collectively showed that SG can significantly improve the metabolic parameters of diabetic obese rats.

SG Significantly Reverses Heart Dysfunction in Diabetic Obese Rats

Cardiac hypertrophy was evidenced by increased HW/TL in the DM group compared with the CON group. However, the SG group had a lower HW/TL compared with the SHAM group (**Figure 3A**). Analyzing the mRNA level of collagen genes demonstrated that the expression of *Col1a1* and *Col3a1* in the DM group was higher than that in the CON group (**Figure 3B**). Notably, SG significantly reduced the expression of these genes compared with that in the SHAM group, yet there was no significant difference in the expression of *Col4a5* and *Col9a1* among these four groups (**Figure 3B**). Furthermore, immunohistochemistry showed that the expression intensity and distribution of collagen I and collagen III in the DM group were significantly higher than those in the CON group (**Figure 3C**). Furthermore, the SG group showed lower expression intensity and distribution of collagen I and collagen III compared with that in the SHAM group, but it did not decrease to the level of the CON group (**Figure 3C**). With respect to natriuretic peptide A (ANP) and cardiac muscle myosin heavy chain β isoform (β-MHC), the DM group had a higher expression of both, compared with the CON group (**Figures 3D,E**). Additionally, SG significantly decreased this expression, suggesting that the cardiac hypertrophy in the SG group was improved (**Figures 3D,E**). Similarly, the changes in the mRNA levels of *Anp* and *β-mhc* confirmed the above results (**Figure 3F**).

Moreover, echocardiography, an important method for evaluating heart function, showed that SG significantly improved the heart function and left ventricular wall thickness of diabetic obese rats (**Figure 4A**). The SG group showed smaller left ventricular end-diastolic diameter and left ventricular end-systolic diameter, approximately 2 mm and 1 mm reduction, respectively, compared with the SHAM group (**Figures 4B,C**). Furthermore, SG significantly elevated the ratio of ejection fraction and fractional shortening, by approximately 20 and 10%, respectively (**Figures 4D,E**).

All these results suggest that SG improved the degree of myocardial fibrosis and diabetes-induced cardiac hypertrophy, and it had a positive effect on the heart function impaired by DM.

SG Significantly Improves Myocardial Glucose Uptake in Diabetic Obese Rats

Multiple studies have shown that DM can result in obstruction of myocardial glucose uptake (Steneberg et al., 2018). Thus, we evaluated myocardial glucose uptake by PET scans (**Figure 4F**). The SUV_{Mean} of the CON group and SG group was significantly higher than that of the DM group and SHAM group, respectively; however, the SUV_{Mean} of the SG group did not reach the level of the CON group (**Figure 4G**). These results suggest that SG improved the diabetes-induced obstruction of myocardial glucose uptake.

SG Significantly Improves Myocardial Morphology and Histopathology

Many studies have reported that diabetes causes changes in myocardial histomorphology (Sassi et al., 2017; Pabel et al., 2018). Compared with the CON group, the CMs in the DM group were disordered, the myocardial fibers were fragmented and broken, and the cytoplasmic distribution was uneven. Notably, SG significantly ameliorated these changes (**Figure 5A**). To evaluate CM size, WGA staining was used to analyze the CM area. The results showed that DM led to larger CMs,

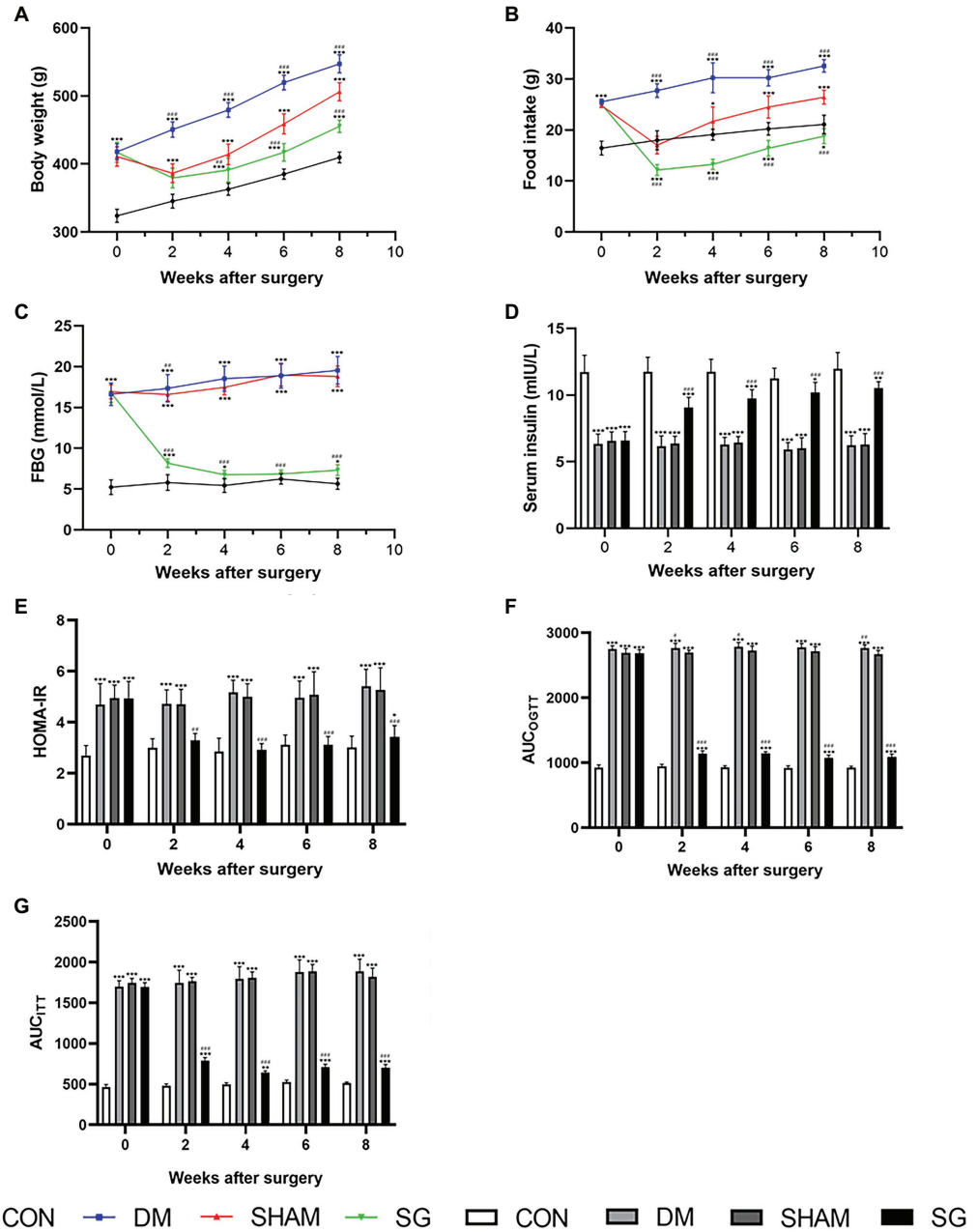

FIGURE 2 | The effect of SG on the metabolic parameters. **(A)** Body weight, **(B)** food intake, **(C)** FBG, **(D)** serum insulin, **(E)** HOMA-IR, **(F)** AUC_{OGTT}, **(G)** AUC_{ITT} before and after operation. Data are expressed as means ± SEM for $n = 10$ per groups. $^{*}p < 0.05$ vs. CON group, $^{**}p < 0.001$ vs. CON group, $^{***}p < 0.0001$ vs. CON group; $^{\#}p < 0.05$ vs. SHAM group, $^{\#\#}p < 0.001$ vs. SHAM group, $^{\#\#\#}p < 0.0001$ vs. SHAM group. FBG, fasting blood glucose; HOMA-IR, homeostasis model assessment of insulin resistance; AUC_{OGTT}, the area under the curve of the oral glucose tolerance test; AUC_{ITT}, the area under the curve of the insulin tolerance test; CON, control; DM, diabetes mellitus; SHAM, sham operation; SG, sleeve gastrectomy.

whereas in the SG group, the area of CMs was significantly smaller than that in the SHAM group (**Figures 5B,F**). Myocardial fibrosis, a significant feature of cardiac hypertrophy, was evaluated by the CVF, which was determined by Sirius Red staining and Masson staining (**Figures 5C,D**). The SG group showed a significantly reduction in CVF, compared with the SHAM group (**Figure 5G**). Oil Red O staining was performed to evaluate the lipid accumulation. As a result, compared with the SHAM group, SG group showed a significantly reduction in lipid accumulation (**Figure 5E**). Namely, SG reduced the size of CMs and improved their arrangement and the cytoplasmic distribution. Furthermore, it significantly improved myocardial lipid accumulation and fibrosis.

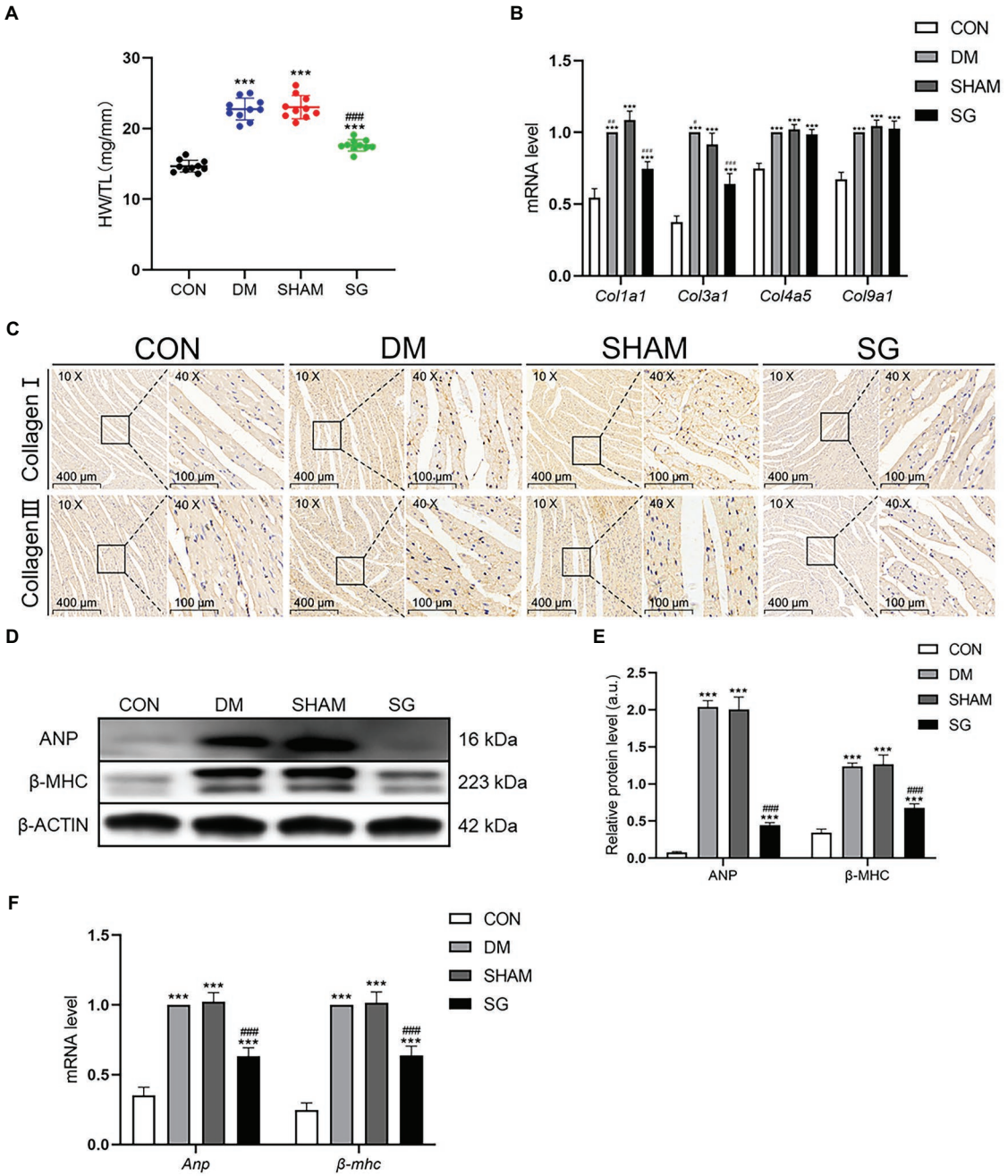

FIGURE 3 | The positive effect of SG on the heart basic parameters and the expression of collagen. **(A)** HW/TL was measured. **(B)** Heart mRNA levels of *Col1a1*, *Col3a1*, *Col4a5*, and *Col9a1* were measured. **(C)** The representative immunohistochemical staining of collagen I and collagen III (magnification 10×, scale bars represent 400 μm; magnification 40×, scale bars represent 100 μm). Brown staining is considered positive. **(D)** The representative bands of ANP and β-MHC and **(E)** relative protein level of ANP and β-MHC were quantitatively analyzed. **(F)** Heart mRNA levels of *Anp* and *β-mhc* were measured. Data are expressed as means ± SEM for $n = 10$ per groups. $^{*}p < 0.05$ vs. CON group, $^{**}p < 0.001$ vs. CON group, $^{***}p < 0.0001$ vs. CON group; $^{\#}p < 0.05$ vs. SHAM group, $^{\#\#}p < 0.001$ vs. SHAM group, $^{\#\#\#}p < 0.0001$ vs. SHAM group. HW/TL, heart weight/tibial length; CON, control; DM, diabetes mellitus; SHAM, sham operation; SG, sleeve gastrectomy.

Effects of SG on MAPK Signaling Pathways

Based on previous studies showing that the activation of MAPK signaling pathways resulted in cardiac hypertrophy (Singh et al., 2017), we investigated the effect of SG on these pathways. Western blot was performed to analyze the expression of MAPKs. The myocardial expression of p-p38, p-JNK, and p-ERK1/2 was significantly higher in the DM group and SHAM

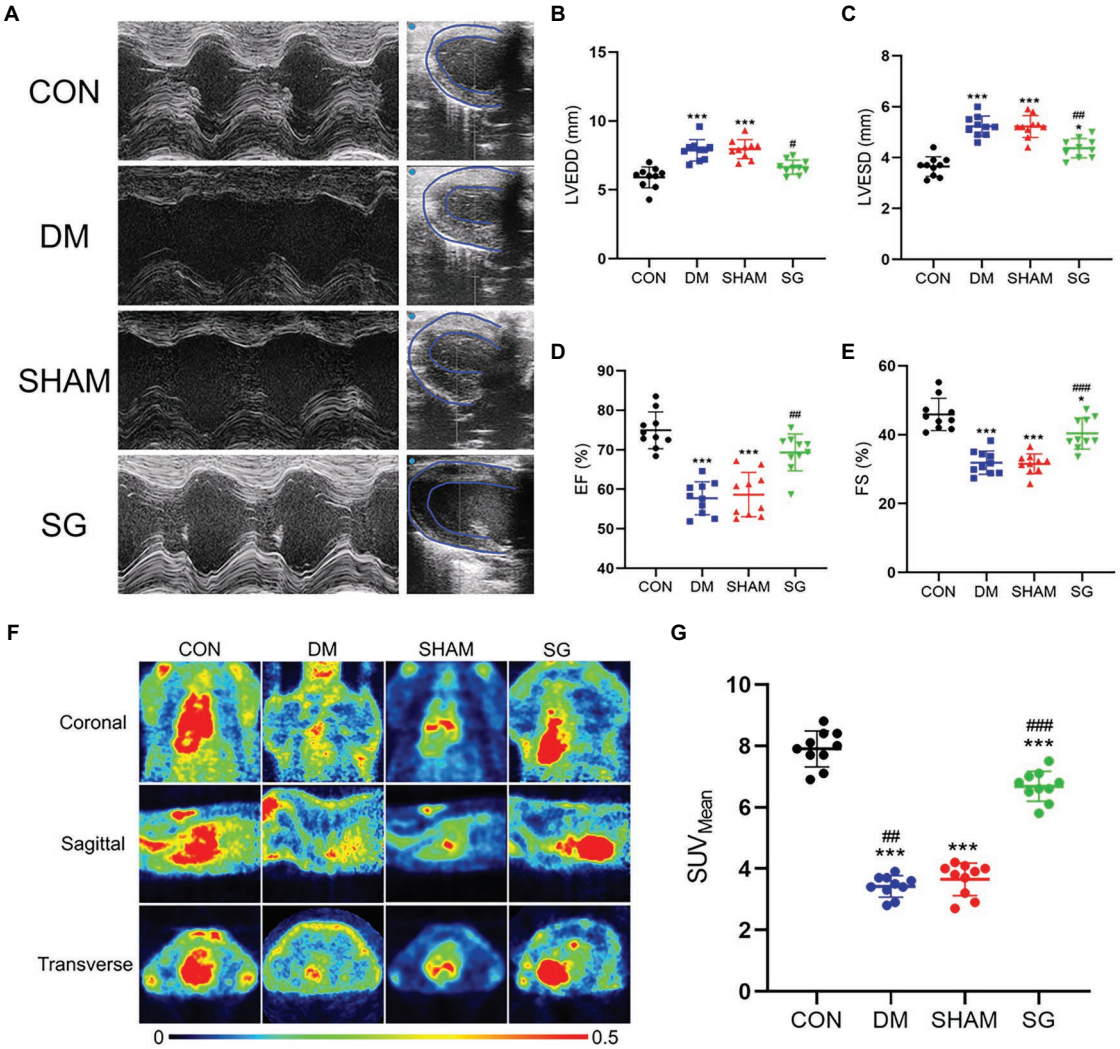

FIGURE 4 | The beneficial effect of SG on the heart function and myocardial glucose uptake. **(A)** The representative images of echocardiography, and the **(B)** LVEDD, **(C)** LVESD, **(D)** EF, **(E)** FS were measured and analyzed. **(F)** The representative heart PET images of the rats and **(G)** comparisons of the myocardial glucose uptake through SUV_{Mean}. Data are expressed as means ± SEM for $n = 10$ per groups. $^{*}p < 0.05$ vs. CON group, $^{**}p < 0.001$ vs. CON group, $^{***}p < 0.0001$ vs. CON group; $^{\#}p < 0.05$ vs. SHAM group, $^{\#\#}p < 0.001$ vs. SHAM group, $^{\#\#\#}p < 0.0001$ vs. SHAM group. PET, positron-emission tomography; LVEDD, left ventricular end-diastolic diameter; LVESD, left ventricular end-systolic diameter; EF, ejection fraction; FS, fractional shortening; SUV_{Mean}, the average standard uptake value; CON, control; DM, diabetes mellitus; SHAM, sham operation; SG, sleeve gastrectomy.

group, compared with the CON group, but these three MAPKs were significantly downregulated after SG (**Figures 6A,B**). The results of the ratio of p-p38 to total p38, p-JNK to total JNK, and p-ERK1/2 to total ERK1/2 were consistent with the above result (**Figures 6C–E**). Taken together, we deduced that SG ameliorated diabetes-induced cardiac hypertrophy, at least partly, associated with inhibition of MAPK signaling pathways.

Effects of SG on the Expression of DUSP6

DUSPs specifically dephosphorylate and inactivate MAPKs (Liu and Molkentin, 2016). ERK1/2 plays a key role in cell growth, differentiation, and proliferation (Mutlak and Kehat, 2021). Previous study has reported that DUSP6 may inhibit ERK1/2 (Ramkissoon et al., 2019). Based on these theories, we investigated the myocardial expression of DUSP6. As we speculated, Western blot showed that the DUSP6 expression in the DM group was significantly lower than that in the CON group, whereas it was significantly upregulated after SG (**Figures 6F,G**). The real-time PCR results were consistent with the protein expression results (**Figure 6H**). These data suggest that the upregulation of DUSP6 may correlate with SG.

DUSP6 Promotes ERK1/2 Dephosphorylation

To determine the effect of DUSP6 on ERK1/2 dephosphorylation, immunohistochemistry and quantitative analysis were performed. Two consecutive paraffin-embedded heart tissue sections were incubated with primary antibodies for DUSP6 and p-ERK1/2.

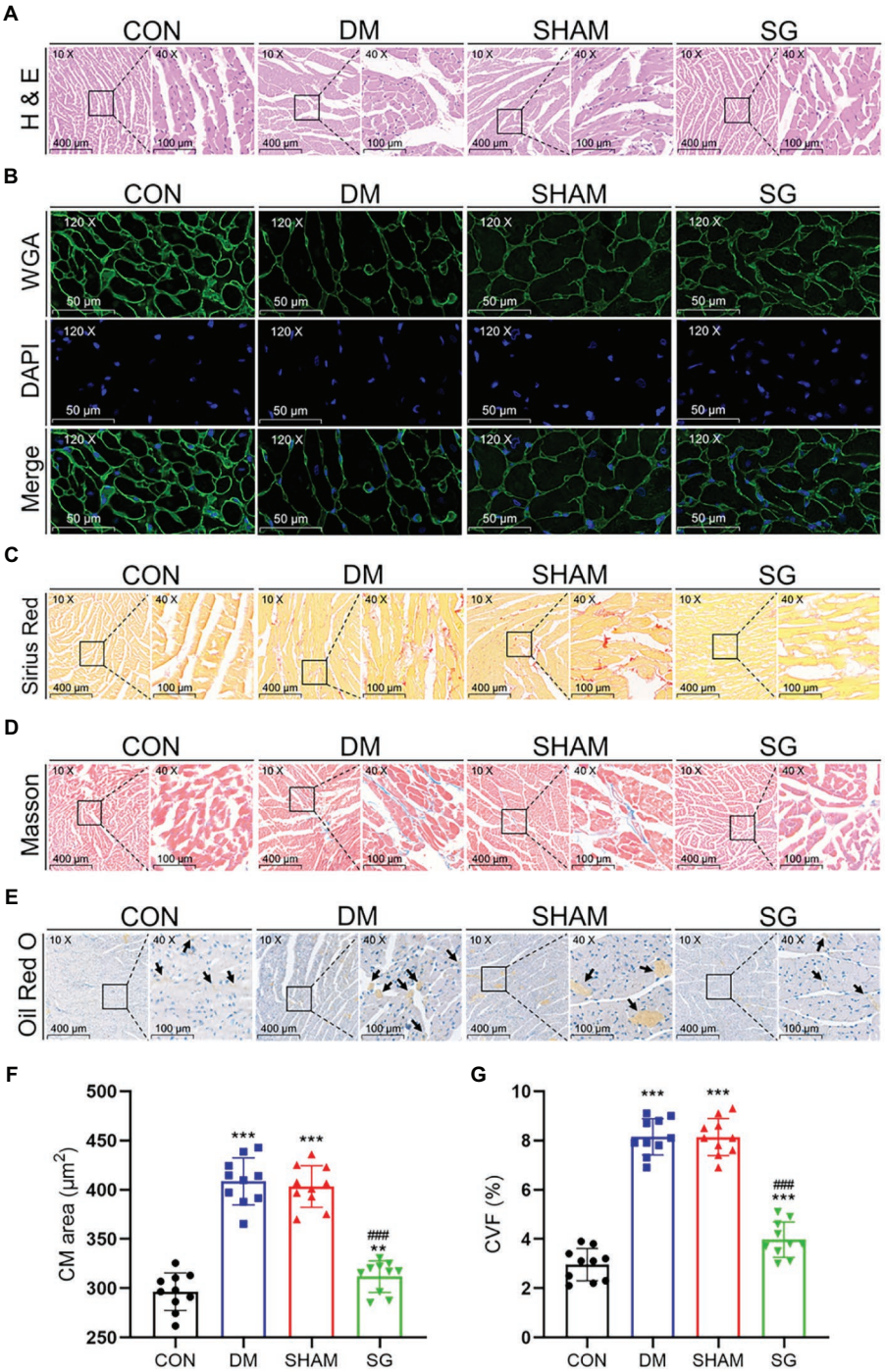

FIGURE 5 | The reversal effect of SG on the heart morphometric and histological. The representative **(A)** H&E, **(B)** WGA, **(C)** Sirius Red, and **(D)** Masson stainings of heart tissue. **(E)** The Oil Red O staining of heart tissue, and arrows show lipid droplets (magnification 10×, scale bars represent 400 μm; magnification 40×, scale bars represent 100 μm; magnification 120×, scale bars represent 50 μm). The **(F)** CM area and **(G)** CVF were calculated and analyzed. Data are expressed as means ± SEM for $n = 10$ per groups. $^{*}p < 0.05$ vs. CON group, $^{**}p < 0.001$ vs. CON group, $^{***}p < 0.0001$ vs. CON group; $^{\#}p < 0.05$ vs. SHAM group, $^{\#\#}p < 0.001$ vs. SHAM group, $^{\#\#\#}p < 0.0001$ vs. SHAM group. H&E, hematoxylin and eosin; WGA, wheat germ agglutinin; CM, cardiac myocyte; CVF, collagen volume fraction; CON, control; DM, diabetes mellitus; SHAM, sham operation; SG, sleeve gastrectomy.

We observed a clear negative correlation between DUSP6 and p-ERK1/2 expression (**Figure 6I**). These results were consistent with our previous results (**Figures 6A–H**). Namely, the results indicated that in the heart tissue, DUSP6 promoted ERK1/2 dephosphorylation, thereby partially ameliorating diabetes-induced cardiac hypertrophy.

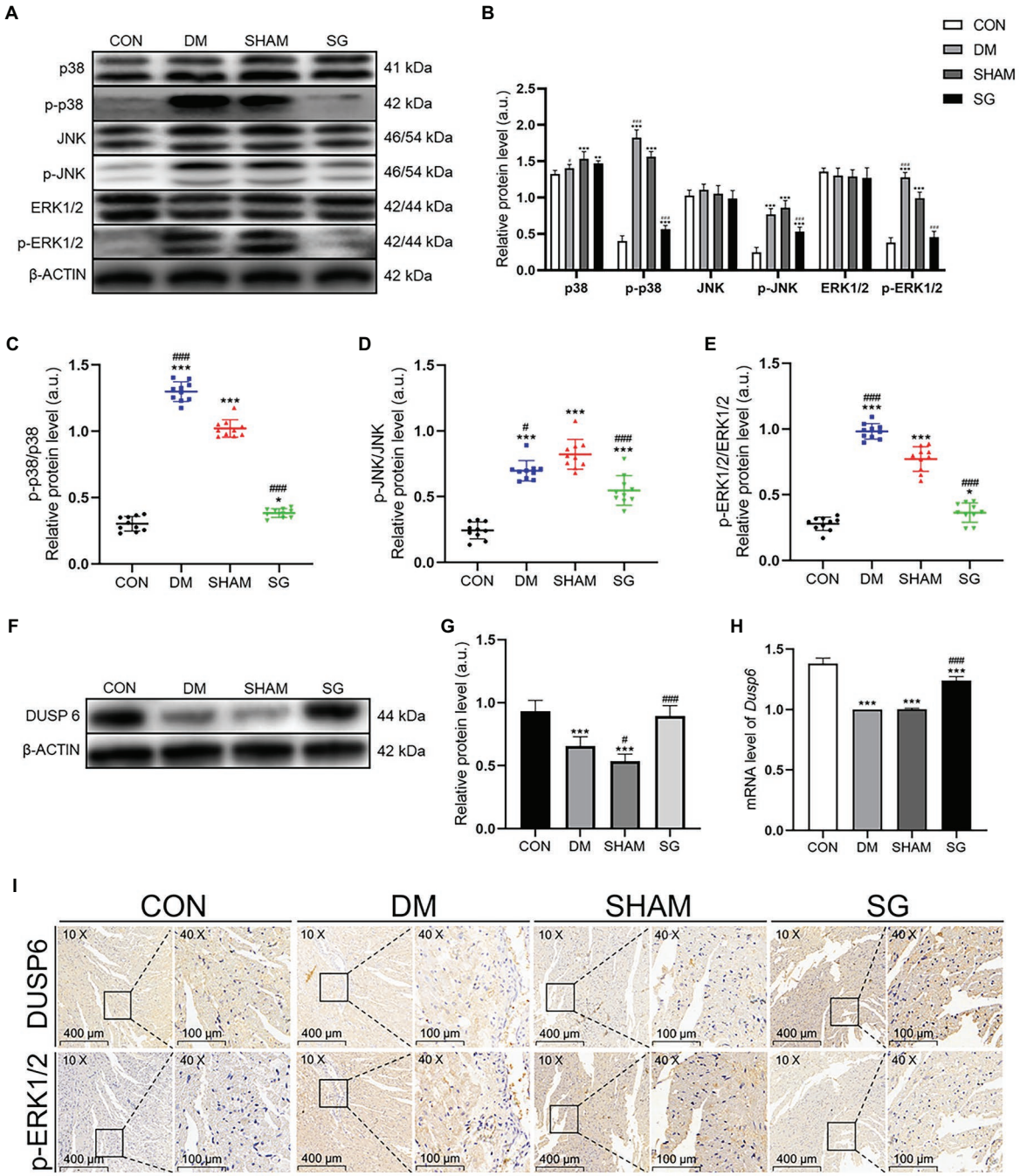

FIGURE 6 | The effect of SG on MAPK signaling pathway and the expression of DUSP6. **(A)** The representative bands of p38, p-p38, JNK, p-JNK, ERK1/2, and p-ERK1/2, and **(B)** relative protein level of p38, p-p38, JNK, p-JNK, ERK1/2, and p-ERK1/2 were quantitatively analyzed. **(C–E)** The expression ratio of p-p38 over total p38, p-JNK over total JNK, and p-ERK1/2 over total ERK1/2, respectively. **(F)** The representative bands of DUSP6 and **(G)** relative protein level of DUSP6 were quantitatively analyzed. **(H)** Cardiac mRNA level of *Dusp6* was measured. **(I)** The representative immunohistochemical staining of DUSP6 and p-ERK1/2 (magnification 10×, scale bars represent 400 μm; magnification 40×, scale bars represent 100 μm). Brown staining is considered positive. Data are expressed as means ± SEM for $n = 10$ per groups. $^{*}p < 0.05$ vs. CON group, $^{**}p < 0.001$ vs. CON group, $^{***}p < 0.0001$ vs. CON group; $^{\#}p < 0.05$ vs. SHAM group, $^{\#\#}p < 0.001$ vs. SHAM group, $^{\#\#\#}p < 0.0001$ vs. SHAM group. CON, control; DM, diabetes mellitus; SHAM, sham operation; SG, sleeve gastrectomy.

DISCUSSION

With the rapid increase in the number of diabetic patients in recent years, increased attention has been paid to the treatment of diabetes and its complications (Zheng et al., 2018). Among these complications, DCM damage has been widely recognized (Kannel et al., 1974; de Simone et al., 2010), which is defined as left ventricular dysfunction in diabetic patients without

coronary heart disease and arterial hypertension (Adeghate and Singh, 2014). One of the main pathological features of DCM is cardiac hypertrophy, which can lead to ventricular dilatation, interstitial fibrosis, and eventually heart failure and death (Kehat and Molkentin, 2010). And the prognosis is mostly poor once the cardiac hypertrophy develops into heart failure (Liu et al., 2019). Unfortunately, the conventional medical therapeutic options for diabetes and obesity, consisting of lowering blood glucose, reversing inflammation, reducing oxidative stress, and gene therapy (Dillmann, 2019; Li and Zhou, 2020), are insufficient (Affinati et al., 2019). Moreover, these above options are not universally effective (Affinati et al., 2019). Thus, more effective therapeutic options are urgently required.

Until 1995, bariatric surgery was only considered as a method for weight loss, but then Pories et al. (1995) proposed that bariatric surgery can treat T2DM and its complications. In recent years, bariatric surgery has gradually become the most effective option for treating diabetes and obesity (Affinati et al., 2019). Among the bariatric surgery procedures, SG has become one of the most used procedures (Pucci and Batterham, 2019). Correspondingly, the HFD-STZ-T2DM rodent model is the most used diabetic model because its characteristics are similar to human T2DM (Gheibi et al., 2017). Thus, in this study, we used this model to investigate the therapeutic effects of SG on diabetes-induced cardiac hypertrophy and the associated mechanisms. It has been reported that 12–16 weeks of diabetes were enough to induce cardiac hypertrophy in this model (Ti et al., 2011; Huang et al., 2019). Herein, we found that after 16 weeks of diabetes, the heart function was significantly damaged. We added healthy controls to determine the real effect of SG on diabetes-induced cardiac hypertrophy, rather than only comparing the SG group with the SHAM group and the DM group. We found that SG significantly reduced body weight, improved hyperglycemia, and reversed insulin resistance, although some rats regained FBG and body weight after SG. Furthermore, damaged heart function, reduced myocardial glucose uptake, larger area of CMs, and severer myocardial fibrosis along with abnormal expression of cardiac hypertrophy markers were found in our DM model rats. Interestingly, these effects were alleviated to various degrees after SG. Taken together, these results showed that SG alleviated diabetes-induced cardiac hypertrophy.

Diabetes-induced cardiac hypertrophy, which is one of the important manifestations of DCM, is an adaptive response of the heart to many kinds of pathological factors (Jia et al., 2018). Its pathological process can be divided into three stages: the progressive stage, the compensatory stage, and the decompensated stage (Goldenberg et al., 2019). Furthermore, it is mainly manifested as CM hypertrophy, myocardial fibrosis, and increased heart weight (Kobayashi and Liang, 2015). Herein, all the above parameters were significantly improved after SG. These results suggest that SG markedly reversed the damage of myocardial morphology. Notably, the heart function improved to a certain extent as assessed by echocardiography. These results are consistent Sassi et al. (2017). The heart function recovered to a certain extent after the improvement in myocardial morphology, providing direct evidence that SG improved myocardial hypertrophy both in terms of morphology and function.

Myocardial glucose uptake has been reported to trigger DCM and diabetes-induced cardiac hypertrophy (Shao and Tian, 2015). Similar to the fetal heart, the hypertrophic heart has more glucose to fuel metabolism (Shao and Tian, 2015). The major changes in glucose metabolism during cardiac hypertrophy are accelerated glycolysis and downregulated fatty acid oxidation, which means that the myocardial glucose uptake may be reduced (Kolwicz and Tian, 2011). Thus, we performed a PET scan on the hearts of the rats, and SUV was used to evaluate the myocardial glucose uptake. The PET scan results showed a markedly elevated SUV in the SG group, but it did not reach the level of the CON group. These results are consistent with a previous study (Huang et al., 2019). And confirming that SG significantly reverse the myocardial glucose uptake in diabetic and obese rats.

The MAPK signaling pathway (also known as the RAS-RAF-MEK-ERK pathway) is widely involved in the regulation of transcription, differentiation, growth, apoptosis, and movement (Miller et al., 2020). MAPKs mainly comprise p38 MAPKs, JNKs, and ERK1/2. These pathways have a cascade of phosphorylation events of at least three levels: a MAPKK kinase (MAPKKK), a MAPK kinase (MAPKK), and a MAPK (Hatzivassiliou et al., 2010). RAS, a small GTP-binding protein, is the first to activate MAPKKK, which in turn phosphorylates and activates MAPKK, which then activates MAPK (Cargnello and Roux, 2011). MAPK activation mainly depends on phosphorylation of both threonine and tyrosine residues (Cargnello and Roux, 2011). The MAPK signaling pathways have been demonstrated to promote the development of pathological cardiac hypertrophy by regulating cell proliferation, differentiation, apoptosis, growth, and metabolism (Liu and Molkentin, 2016; Liao et al., 2019). Particularly, ERK1/2 plays a key role in pathological cardiac hypertrophy (Lu et al., 2019), because it has been shown to significantly regulate individual CM growth, cardiac dilation, and eccentric growth of the heart (Liu and Molkentin, 2016). Cao et al. (2020) have also reported that excessive ERK1/2 activation induced cardiac hypertrophy. A previous study has reported that almost all MAPKs are activated in pathological cardiac hypertrophy (Toischer et al., 2010), and this phenomenon was confirmed in this study. Interestingly, the expression of phosphorylated p38, JNK, and ERK1/2 was significantly reduced after SG. This result suggests that SG ameliorated diabetes-induced cardiac hypertrophy may be associated with the inhibition of MAPK signaling pathways.

DUSPs, which are MAPK phosphatases, can specifically dephosphorylate MAPKs at both the threonine and tyrosine residues (Liu and Molkentin, 2016). So far, multiple studies have demonstrated that DUSPs inhibited MAPK signaling to improve cardiac hypertrophy (Bueno et al., 2001; Auger-Messier et al., 2013; Liu et al., 2016). ERK1/2, the most important factor affecting cardiac hypertrophy, has been shown to be dephosphorylated and inactivated by DUSP6 (Liu and Molkentin, 2016; Ramkissoon et al., 2019). However, loss of DUSP6 has no effect on p38 and JNK. Because no studies have explored the changes in DUSP6 and ERK1/2 after bariatric surgery, we explored whether there is a connection between DUSP6 and ERK1/2. Immunohistochemistry on consecutive paraffin sections showed that DUSP6 and p-ERK1/2 were upregulated and downregulated, respectively, after SG, which is consistent with our Western blot results. Notably, the expression of DUSP6 and p-ERK1/2 exhibit

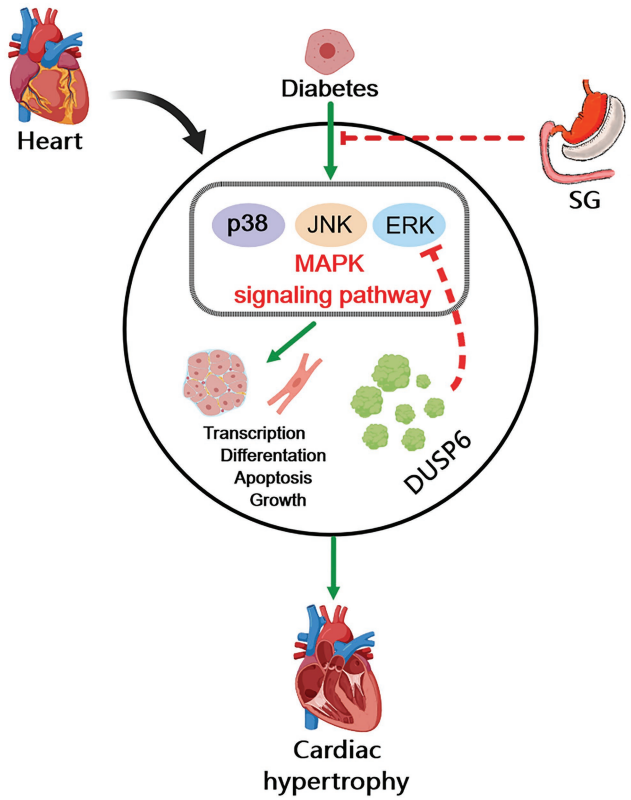

FIGURE 7 | Diagram of possible mechanism of SG improving diabetes-induced cardiac hypertrophy. In diabetes, overactivation of MAPK signaling pathway induces cardiac hypertrophy and heart dysfunction through promoting cell transcription, differentiation, apoptosis, and growth. The inhibition of MAPK signaling pathway is associated with the amelioration of diabetes-induced cardiac hypertrophy by SG. And the dephosphorylation of ERK1/2 by DUSP6 may play a vital role in this possible mechanism.

opposite tendencies. These results suggest that DUSP6 ameliorated diabetes-induced cardiac hypertrophy by dephosphorylating ERK1/2, which is consistent with a previous study (Gallo et al., 2019). These results indicated that SG alleviated diabetes-induced cardiac hypertrophy correlated with the upregulation of DUSP6.

However, there are several limitations to our study. Even though bariatric surgery has an excellent effect on blood glucose and body weight, in the long term, in some patients the blood glucose and body weight return to pre-bariatric surgery levels (Seki et al., 2017). Which leads to the state of the diabetes-induced cardiac hypertrophy after the blood glucose and body weight increase again is still unknown. Therefore, we need to increase the follow-up time in the next study and discuss the long-term ameliorating effect of SG on diabetes-induced cardiac hypertrophy. Additionally, it is unclear whether the SG-induced improvement in diabetes-induced cardiac hypertrophy depends on blood glucose or weight loss. Although we think that the amelioration of the diabetes-induced cardiac hypertrophy depends on improvement in blood glucose and body weight, the exact mechanism remains to be further studied. Finally, to further reveal the SG mechanism in the treatment of diabetes-induced cardiac hypertrophy, we need to investigate the effects of other DUSP isoforms on MAPKs other than ERK1/2 *in vivo* and *in vitro*. We ultimately hope to provide a new strategy for the treatment of diabetes-induced cardiac hypertrophy to reduce the mortality of diabetic patients caused by DCM.

In conclusion, as a common complication of diabetes, DCM significantly increases the incidence of heart failure in patients with diabetes, thereby severely affecting their life. However, the important pathological manifestation of DCM, cardiac hypertrophy, lacks effective treatment. Our study revealed that diabetes-induced cardiac hypertrophy significantly increased myocardial fibrosis, promoted CM hypertrophy, destroyed the normal myocardial structure, reduced myocardial glucose uptake, and ultimately affected the heart function. Furthermore, the MAPK signaling pathway was activated in diabetes-induced cardiac hypertrophy. Interestingly, all these pathological changes were reversed by SG. Namely, SG attenuated diabetes-induced cardiac hypertrophy correlated with the inhibition of MAPK signaling pathway, particularly, the dephosphorylation of ERK1/2 (**Figure 7**). In brief, we believe that our study helps resolve some of the challenges of the therapeutic options for DCM, especially diabetes-induced cardiac hypertrophy. Namely, the activation of the MAPK signaling pathways in patients with diabetes-induced cardiac hypertrophy may be a potential target for therapy.

DATA AVAILABILITY STATEMENT

The raw data supporting the conclusions of this article will be made available by the corresponding author, without undue reservation.

ETHICS STATEMENT

The animal study was reviewed and approved by the Institutional Animal Care and Use Committee of Shandong Provincial Qianfoshan Hospital of Shandong University.

AUTHOR CONTRIBUTIONS

GZ and MZ contributed to the original idea and conceptual design. QX, SL, and SD conceived the experiments and analyzed data. QX and HD contributed to the drafting of the work. BS and LL provided critical review of the article. All authors contributed to the article and approved the submitted version.

FUNDING

This project was supported by the National Natural Science Foundation of China (Grant No. 81873647) and Major basic research project of Natural Science Foundation of Shandong Province (Grant No. ZR2020ZD15).

ACKNOWLEDGMENTS

We thank Michal Bell from Liwen Bianji (Edanz; www.liwenbianji.cn/), for editing the English text of a draft of this manuscript.

REFERENCES

Adeghate, E., and Singh, J. (2014). Structural changes in the myocardium during diabetes-induced cardiomyopathy. *Heart Fail. Rev.* 19, 15–23. doi: 10.1007/s10741-013-9388-5

Affinati, A. H., Esfandiari, N. H., Oral, E. A., and Kraftson, A. T. (2019). Bariatric surgery in the treatment of type 2 diabetes. *Curr. Diab. Rep.* 19:156. doi: 10.1007/s11892-019-1269-4

Angrisani, L., Santonicola, A., Iovino, P., Vitiello, A., Zundel, N., Buchwald, H., et al. (2017). Bariatric surgery and Endoluminal procedures: IFSO worldwide survey 2014. *Obes. Surg.* 27, 2279–2289. doi: 10.1007/s11695-017-2666-x

Arterburn, D. E., Telem, D. A., Kushner, R. F., and Courcoulas, A. P. (2020). Benefits and risks of bariatric surgery in adults: A review. *JAMA* 324, 879–887. doi: 10.1001/jama.2020.12567

Auger-Messier, M., Accornero, F., Goonasekera, S. A., Bueno, O. F., Lorenz, J. N., van Berlo, J. H., et al. (2013). Unrestrained p38 MAPK activation in Dusp1/4 double-null mice induces cardiomyopathy. *Circ. Res.* 112, 48–56. doi: 10.1161/circresaha.112.272963

Ba, L., Gao, J., Chen, Y., Qi, H., Dong, C., Pan, H., et al. (2019). Allicin attenuates pathological cardiac hypertrophy by inhibiting autophagy via activation of PI3K/Akt/mTOR and MAPK/ERK/mTOR signaling pathways. *Phytomedicine* 58:152765. doi: 10.1016/j.phymed.2018.11.025

Bruinsma, B. G., Uygun, K., Yarmush, M. L., and Saeidi, N. (2015). Surgical models of Roux-en-Y gastric bypass surgery and sleeve gastrectomy in rats and mice. *Nat. Protoc.* 10, 495–507. doi: 10.1038/nprot.2015.027

Bueno, O. F., De Windt, L. J., Lim, H. W., Tymitz, K. M., Witt, S. A., Kimball, T. R., et al. (2001). The dual-specificity phosphatase MKP-1 limits the cardiac hypertrophic response in vitro and in vivo. *Circ. Res.* 88, 88–96. doi: 10.1161/01.res.88.1.88

Cao, M., Mao, Z., Peng, M., Zhao, Q., Sun, X., Yan, J., et al. (2020). Extracellular cyclophilin A induces cardiac hypertrophy via the ERK/p47phox pathway. *Mol. Cell. Endocrinol.* 518:110990. doi: 10.1016/j.mce.2020.110990

Cargnello, M., and Roux, P. P. (2011). Activation and function of the MAPKs and their substrates, the MAPK-activated protein kinases. *Microbiol. Mol. Biol. Rev.* 75, 50–83. doi: 10.1128/mmbr.00031-10

Chang, S. H., Liu, C. J., Kuo, C. H., Chen, H., Lin, W. Y., Teng, K. Y., et al. (2011). Garlic oil alleviates MAPKs- and IL-6-mediated diabetes-related cardiac hypertrophy in STZ-induced DM rats. *Evid. Based Complement. Alternat. Med.* 2011:950150. doi: 10.1093/ecam/neq075

de Simone, G., Devereux, R. B., Chinali, M., Lee, E. T., Galloway, J. M., Barac, A., et al. (2010). Diabetes and incident heart failure in hypertensive and normotensive participants of the strong heart study. *J. Hypertens.* 28, 353–360. doi: 10.1097/HJH.0b013e3283331169

Dillmann, W. H. (2019). Diabetic cardiomyopathy. *Circ. Res.* 124, 1160–1162. doi: 10.1161/circresaha.118.314665

Docherty, N. G., and le Roux, C. W. (2020). Bariatric surgery for the treatment of chronic kidney disease in obesity and type 2 diabetes mellitus. *Nat. Rev. Nephrol.* 16, 709–720. doi: 10.1038/s41581-020-0323-4

Echouffo-Tcheugui, J. B., Xu, H., DeVore, A. D., Schulte, P. J., Butler, J., Yancy, C. W., et al. (2016). Temporal trends and factors associated with diabetes mellitus among patients hospitalized with heart failure: findings from get with the guidelines-heart failure registry. *Am. Heart J.* 182, 9–20. doi: 10.1016/j.ahj.2016.07.025

Gallo, S., Vitacolonna, A., Bonzano, A., Comoglio, P., and Crepaldi, T. (2019). ERK: A key player in the pathophysiology of cardiac hypertrophy. *Int. J. Mol. Sci.* 20:2164. doi: 10.3390/ijms20092164

Gheibi, S., Kashfi, K., and Ghasemi, A. (2017). A practical guide for induction of type-2 diabetes in rat: incorporating a high-fat diet and streptozotocin. *Biomed. Pharmacother.* 95, 605–613. doi: 10.1016/j.biopha.2017.08.098

Gibb, A. A., and Hill, B. G. (2018). Metabolic coordination of physiological and pathological cardiac remodeling. *Circ. Res.* 123, 107–128. doi: 10.1161/circresaha.118.312017

Goldenberg, J. R., Carley, A. N., Ji, R., Zhang, X., Fasano, M., Schulze, P. C., et al. (2019). Preservation of acyl coenzyme A attenuates pathological and metabolic cardiac remodeling through selective lipid trafficking. *Circulation* 139, 2765–2777. doi: 10.1161/circulationaha.119.039610

Hatzivassiliou, G., Song, K., Yen, I., Brandhuber, B. J., Anderson, D. J., Alvarado, R., et al. (2010). RAF inhibitors prime wild-type RAF to activate the MAPK pathway and enhance growth. *Nature* 464, 431–435. doi: 10.1038/nature08833

Holman, N., Young, B., and Gadsby, R. (2015). Current prevalence of type 1 and type 2 diabetes in adults and children in the UK. *Diabet. Med.* 32, 1119–1120. doi: 10.1111/dme.12791

Huang, X., Liu, S., Wu, D., Cheng, Y., Han, H., Wang, K., et al. (2018). Facilitated Ca(2+) homeostasis and attenuated myocardial autophagy contribute to alleviation of diabetic cardiomyopathy after bariatric surgery. *Am. J. Physiol. Heart Circ. Physiol.* 315, H1258–h1268. doi: 10.1152/ajpheart.00274.2018

Huang, X., Wu, D., Cheng, Y., Zhang, X., Liu, T., Liu, Q., et al. (2019). Restoration of myocardial glucose uptake with facilitated myocardial glucose transporter 4 translocation contributes to alleviation of diabetic cardiomyopathy in rats after duodenal-jejunal bypass. *J. Diabetes Investig.* 10, 626–638. doi: 10.1111/jdi.12948

Jia, G., Whaley-Connell, A., and Sowers, J. R. (2018). Diabetic cardiomyopathy: a hyperglycaemia- and insulin-resistance-induced heart disease. *Diabetologia* 61, 21–28. doi: 10.1007/s00125-017-4390-4

Kannel, W. B., Hjortland, M., and Castelli, W. P. (1974). Role of diabetes in congestive heart failure: the Framingham study. *Am. J. Cardiol.* 34, 29–34. doi: 10.1016/0002-9149(74)90089-7

Kehat, I., and Molkentin, J. D. (2010). Molecular pathways underlying cardiac remodeling during pathophysiological stimulation. *Circulation* 122, 2727–2735. doi: 10.1161/circulationaha.110.942268

Kobayashi, S., and Liang, Q. (2015). Autophagy and mitophagy in diabetic cardiomyopathy. *Biochim. Biophys. Acta* 1852, 252–261. doi: 10.1016/j.bbadis.2014.05.020

Kolwicz, S. C. Jr., and Tian, R. (2011). Glucose metabolism and cardiac hypertrophy. *Cardiovasc. Res.* 90, 194–201. doi: 10.1093/cvr/cvr071

Li, N., and Zhou, H. (2020). SGLT2 inhibitors: a novel player in the treatment and prevention of diabetic cardiomyopathy. *Drug Des. Devel. Ther.* Volume 14, 4775–4788. doi: 10.2147/dddt.S269514

Liao, H. H., Zhang, N., Meng, Y. Y., Feng, H., Yang, J. J., Li, W. J., et al. (2019). Myricetin alleviates pathological cardiac hypertrophy via TRAF6/TAK1/MAPK and Nrf2 signaling pathway. *Oxidative Med. Cell. Longev.* 2019:6304058. doi: 10.1155/2019/6304058

Liu, J., Liu, X., Hui, X., Cai, L., Li, X., Yang, Y., et al. (2019). Novel role for pleckstrin homology-like domain family A, member 3 in the regulation of pathological cardiac hypertrophy. *J. Am. Heart Assoc.* 8:e011830. doi: 10.1161/jaha.118.011830

Liu, R., and Molkentin, J. D. (2016). Regulation of cardiac hypertrophy and remodeling through the dual-specificity MAPK phosphatases (DUSPs). *J. Mol. Cell. Cardiol.* 101, 44–49. doi: 10.1016/j.yjmcc.2016.08.018

Liu, R., van Berlo, J. H., York, A. J., Vagnozzi, R. J., Maillet, M., and Molkentin, J. D. (2016). DUSP8 regulates cardiac ventricular remodeling by altering ERK1/2 signaling. *Circ. Res.* 119, 249–260. doi: 10.1161/circresaha.115.308238

Lu, C. H., Shen, C. Y., Hsieh, D. J., Lee, C. Y., Chang, R. L., Ju, D. T., et al. (2019). Deep ocean minerals inhibit IL-6 and IGFIIR hypertrophic signaling pathways to attenuate diabetes-induced hypertrophy in rat hearts. *J. Appl. Physiol.* 127, 356–364. doi: 10.1152/japplphysiol.00184.2019

Miller, R.J.H., Cadet, S., Pournazari, P., Pope, A., Kransdorf, E., Hamilton, M.A., Patel, J., Hayes, S., Friedman, J., Thomson, L., Tamarappoo, B., Berman, D.S., and Slomka, P.J. (2020). Quantitative assessment of cardiac hypermetabolism and perfusion for diagnosis of cardiac sarcoidosis. *J. Nucl. Cardiol.* doi: 10.1007/s12350-020-02201-5 [Epub ahead of print].

Mutlak, M., and Kehat, I. (2021). Dual specific phosphatases (DUSPs) in cardiac hypertrophy and failure. *Cell. Signal.* 84:110033. doi: 10.1016/j.cellsig.2021.110033

Nguyen, N. T., and Varela, J. E. (2017). Bariatric surgery for obesity and metabolic disorders: state of the art. *Nat. Rev. Gastroenterol. Hepatol.* 14, 160–169. doi: 10.1038/nrgastro.2016.170

Pabel, S., Wagner, S., Bollenberg, H., Bengel, P., Kovács, Á., Schach, C., et al. (2018). Empagliflozin directly improves diastolic function in human heart failure. *Eur. J. Heart Fail.* 20, 1690–1700. doi: 10.1002/ejhf.1328

Pories, W. J., Swanson, M. S., MacDonald, K. G., Long, S. B., Morris, P. G., Brown, B. M., et al. (1995). Who would have thought it? An operation proves to be the most effective therapy for adult-onset diabetes mellitus. *Ann. Surg.* 222, 339–352; discussion 350-332. doi: 10.1097/00000658-199509000-00011

Pucci, A., and Batterham, R. L. (2019). Mechanisms underlying the weight loss effects of RYGB and SG: similar, yet different. *J. Endocrinol. Investig.* 42, 117–128. doi: 10.1007/s40618-018-0892-2

Ramkissoon, A., Chaney, K. E., Milewski, D., Williams, K. B., Williams, R. L., Choi, K., et al. (2019). Targeted inhibition of the dual specificity phosphatases DUSP1 and DUSP6 suppress MPNST growth via JNK. *Clin. Cancer Res.* 25, 4117–4127. doi: 10.1158/1078-0432.Ccr-18-3224

Ruze, R., Li, J., Xu, Q., Zhong, M., Xiong, Y., Yan, Z., et al. (2020). Sleeve gastrectomy ameliorates alveolar structures and surfactant protein expression in lungs of obese and diabetic rats. *Int. J. Obes.* 44, 2394–2404. doi: 10.1038/s41366-020-0647-y

Sassi, Y., Avramopoulos, P., Ramanujam, D., Grüter, L., Werfel, S., Giosele, S., et al. (2017). Cardiac myocyte miR-29 promotes pathological remodeling of the heart by activating Wnt signaling. *Nat. Commun.* 8:1614. doi: 10.1038/s41467-017-01737-4

Seki, Y., Kasama, K., Haruta, H., Watanabe, A., Yokoyama, R., Porciuncula, J. P., et al. (2017). Five-year-results of laparoscopic sleeve gastrectomy with duodenojejunal bypass for weight loss and type 2 diabetes mellitus. *Obes. Surg.* 27, 795–801. doi: 10.1007/s11695-016-2372-0

Shao, D., and Tian, R. (2015). Glucose transporters in cardiac metabolism and hypertrophy. *Compr. Physiol.* 6, 331–351. doi: 10.1002/cphy.c150016

Shen, E., Diao, X., Wang, X., Chen, R., and Hu, B. (2011). MicroRNAs involved in the mitogen-activated protein kinase cascades pathway during glucose-induced cardiomyocyte hypertrophy. *Am. J. Pathol.* 179, 639–650. doi: 10.1016/j.ajpath.2011.04.034

Singh, G. B., Raut, S. K., Khanna, S., Kumar, A., Sharma, S., Prasad, R., et al. (2017). MicroRNA-200c modulates DUSP-1 expression in diabetes-induced cardiac hypertrophy. *Mol. Cell. Biochem.* 424, 1–11. doi: 10.1007/s11010-016-2838-3

Siti, H. N., Jalil, J., Asmadi, A. Y., and Kamisah, Y. (2021). Rutin modulates MAPK pathway differently from quercetin in angiotensin II-induced H9c2 cardiomyocyte hypertrophy. *Int. J. Mol. Sci.* 22:5063. doi: 10.3390/ijms22105063

Steneberg, P., Lindahl, E., Dahl, U., Lidh, E., Straseviciene, J., Backlund, F., et al. (2018). PAN-AMPK activator O304 improves glucose homeostasis and microvascular perfusion in mice and type 2 diabetes patients. *JCI Insight* 3:e99114. doi: 10.1172/jci.insight.99114

Ti, Y., Xie, G. L., Wang, Z. H., Bi, X. L., Ding, W. Y., Wang, J., et al. (2011). TRB3 gene silencing alleviates diabetic cardiomyopathy in a type 2 diabetic rat model. *Diabetes* 60, 2963–2974. doi: 10.2337/db11-0549

Toischer, K., Rokita, A. G., Unsöld, B., Zhu, W., Kararigas, G., Sossalla, S., et al. (2010). Differential cardiac remodeling in preload versus afterload. *Circulation* 122, 993–1003. doi: 10.1161/circulationaha.110.943431

Zhang, K. Q., Tian, T., Hu, L. L., Wang, H. R., and Fu, Q. (2020). Effect of probucol on autophagy and apoptosis in the penile tissue of streptozotocin-induced diabetic rats. *Asian J. Androl.* 22, 409–413. doi: 10.4103/aja.aja_89_19

Zheng, Y., Ley, S. H., and Hu, F. B. (2018). Global aetiology and epidemiology of type 2 diabetes mellitus and its complications. *Nat. Rev. Endocrinol.* 14, 88–98. doi: 10.1038/nrendo.2017.151

Zimmet, P. Z. (2017). Diabetes and its drivers: the largest epidemic in human history? *Clin. Diabetes Endocrinol.* 3:1. doi: 10.1186/s40842-016-0039-3

Conflict of Interest: The authors declare that the research was conducted in the absence of any commercial or financial relationships that could be construed as a potential conflict of interest.

Publisher's Note: All claims expressed in this article are solely those of the authors and do not necessarily represent those of their affiliated organizations, or those of the publisher, the editors and the reviewers. Any product that may be evaluated in this article, or claim that may be made by its manufacturer, is not guaranteed or endorsed by the publisher.

frontiers in Physiology

ORIGINAL RESEARCH
published: 25 November 2021
doi: 10.3389/fphys.2021.708588

Electroacupuncture Combined With Diet Treatment Has a Therapeutic Effect on Perimenopausal Patients With Abdominal Obesity by Improving the Community Structure of Intestinal Flora

Jili Sheng[1†], Geyao Yang[2†], Xiaoqing Jin[1], Caijuan Si[3], Yuan'an Huang[4], Zhouxiao Luo[5], Tao Liu[1] and Jianfang Zhu[1]*

[1] Acupuncture Department, Zhejiang Hospital, Hangzhou, China, [2] Acupuncture and Massage Department, Hangzhou Geriatric Hospital, Hangzhou, China, [3] Nutritional Department, Zhejiang Hospital, Hangzhou, China, [4] Massage Department, Zhejiang Hospital, Hangzhou, China, [5] Acupuncture Department, Tonglu TCM Hospital, Hangzhou, China

OPEN ACCESS

Edited by:
Yanmin Wang,
California Medical Innovations Institute, United States

Reviewed by:
Sonia Michael Najjar,
Ohio University, United States
Maria Camila Pruper de Freitas,
University of São Paulo, Brazil

****Correspondence:***
Jianfang Zhu
zjyyzjf@163.com

† These authors have contributed equally to this work

Specialty section:
This article was submitted to Metabolic Physiology, a section of the journal Frontiers in Physiology

Received: *12 May 2021*
Accepted: *14 September 2021*
Published: *25 November 2021*

Citation:
Sheng J, Yang G, Jin X, Si C, Huang Y, Luo Z, Liu T and Zhu J (2021) Electroacupuncture Combined With Diet Treatment Has a Therapeutic Effect on Perimenopausal Patients With Abdominal Obesity by Improving the Community Structure of Intestinal Flora. Front. Physiol. 12:708588. doi: 10.3389/fphys.2021.708588

Background: This study explored the influences of electroacupuncture combined with dietary intervention on the intestinal flora in perimenopausal patients with abdominal obesity by using the 16s rRNA sequencing technology.

Methods: Perimenopausal patients with abdominal obesity were divided into the Electroacupuncture group and the Control group. Patients in the Control group received healthy lifestyle education, while those in the Electroacupuncture group received electroacupuncture combined with dietary intervention. Before and after treatment, the weight, height, waist circumference, hip circumference, waist-height ratio (WHtR), waist to hip ratio (WHR), and body mass index (BMI) of the patients were recorded; the levels of serum triglyceride (TG), total cholesterol (TC), low-density lipoprotein (LDL), high-density lipoprotein cholesterol (HDL-C), fasting insulin (FINS), and fasting blood glucose (FGB) were evaluated; and the abundance, diversity, and species differences of intestinal flora were analyzed using 16s rRNA sequencing technology.

Results: The body weight, waist circumference, hip circumference, BMI, WHR, and WHtR of patients in the Electroacupuncture group after treatment were lower than those before treatment. Compared with the Control group, patients in the Electroacupuncture group after treatment displayed lower waist circumference, WHtR, WHR, TG, and LDL levels as well as species abundance, higher species diversity, and lager species difference in the intestinal flora. Besides, the proportions of Klebsiella and Kosakonia in the intestinal flora of patients in the Electroacupuncture group after treatment were larger than those before treatment.

Conclusion: Electroacupuncture combined with diet treatment generated a therapeutic effect on abdominal obesity in perimenopausal patients by improving the community structure of intestinal flora.

Keywords: abdominal obesity, perimenopausal syndrome, 16S rRNA, intestinal flora, electroacupuncture

INTRODUCTION

With the improvement of people's living standards and the changes in dietary structure and environment, the number of obese people has maintained an upward trend (Vandevijvere et al., 2015; González-Muniesa et al., 2017; Mohammadbeigi et al., 2018). Obesity induced by the excessive accumulation of adipose tissue in the abdominal cavity and around the mesentery is defined as abdominal obesity, also termed central obesity (Smith, 2015). Perimenopausal women are prone to suffer from abdominal obesity due to decreased ovarian function, slowed metabolism, reduced exercise, osteoporosis, and overnutrition (Keller et al., 2010; Łokieć et al., 2016). In addition, abdominal obesity may further lead to hypertension, hyperlipidemia, coronary heart disease, type 2 diabetes, cholecystitis, cholelithiasis, and rectal cancer, thereby seriously threatening human health (Smith, 2015; Hu et al., 2017).

The routine treatments for obesity normally are dietary intervention and hypoglycemic drugs, which also provide certain references for perimenopausal women with abdominal obesity (Mastorakos et al., 2010; Bronczyk-Puzon et al., 2015; Ruban et al., 2019). In the treatment of obese patients, pharmacotherapy cannot usually be used alone or as a first-line method (Samat et al., 2008; Tauqeer et al., 2018). In comparison, dietary intervention has proved to be a healthy and effective way to lose weight, but it needs long-term persistence. Accumulating studies have indicated that electroacupuncture can treat abdominal obesity safely and effectively, mainly by stimulating the body's meridians and acupoints, improving body condition as a whole, regulating intake and enhancing body metabolism, so as to achieve the purpose of weight loss and waist thinning (Wang et al., 2008; Lei et al., 2017; Chen et al., 2018; Luo et al., 2018; Huang et al., 2019; Zhang et al., 2019). However, the effect mechanism of electroacupuncture on abdominal obesity in perimenopausal women is still dearth of in-depth exploration.

The prevalence of abdominal obesity has raised people's curiosity of finding the balance factors that affect the occurrence and development of this disease (González-Muniesa et al., 2017). The relationship between intestinal flora and abdominal obesity has gradually become a research hotspot with increasing attention from scholars at home and abroad (Malamut, 2007; Gao X. et al., 2018). The human intestinal flora is a complex ecosystem constituted by bacteria, archaea, yeasts, and fibrous fungi that reside in the intestinal tract (Gao Y. et al., 2018). It is estimated that the adult gastrointestinal tract contains at least 1,000 different microorganisms with a total number of more than 100 trillion, 10 times more than the total number of human cells, and the stability, diversity, and quantity of the intestinal flora vary in different races (Ma and Wu, 2017; Sebastián Domingo and Sánchez Sánchez, 2018). Changes in the diversity and composition of the intestinal flora are closely related to diseases including obesity and behavioral disorders. Studies also proved that drug treatment of obesity can be realized by improving intestinal flora dysfunction (Li et al., 2020); however, whether the effect of electroacupuncture on abdominal obesity is associated with the regulation of flora dysfunction is unknown.

Considering that the 16s rRNA high-throughput sequencing technology is the main and cutting-edge method for microorganism analysis (Gao X. et al., 2018), we, in this study, attempted to explore the effect of electroacupuncture combined with dietary intervention on the intestinal flora in perimenopausal patients with abdominal obesity. Anthropometric measures are simple, non-invasive tools that can be used for the diagnosis and assessment of obesity (Gazarova et al., 2019). Currently, the most widely used indexes are body mass index (BMI), waist circumference (WC), waist-to-hip ratio (WHR), waist-height ratio (WHtR), etc. (Gazarova et al., 2019). In addition, obesity can easily cause metabolic disorders such as glucose and lipids (Jablonowska-Lietz et al., 2017). Therefore, the relevant serum indexes that are also pivotal for assessing obesity are tested, including serum triglyceride (TG), total cholesterol (TC), low-density lipoprotein (LDL), high-density lipoprotein cholesterol (HDL-C), and insulin resistance (HOMA-IR) (Jablonowska-Lietz et al., 2017). In this study, we also tried to explore the effect of electroacupuncture combined with dietary intervention on the intestinal flora in perimenopausal patients with abdominal obesity by studying the changes in the above-mentioned related indicators.

MATERIALS AND METHODS

Ethics Statement

The study has been approved by the Ethics Committee of Zhejiang Hospital [No. 2018 (9K)] and all patients signed the written informed consent.

Patient Population

A total of 73 perimenopausal patients with abdominal obesity who received treatment in the Acupuncture Department of Zhejiang Hospital from December 2017 to January 2019 were recruited in this study. The diagnostic criteria for perimenopausal period were formulated according to the chapter of "Menopausal Syndrome" in the 8th edition of "Obstetrics and Gynecology," combined with "Chinese Obstetrics and Gynecology." The details are as follows: (1) 40–60 years old; (2) Clinical manifestations of menstrual disorders for more than 3 months, or amenorrhea within a year, etc.; (3) One or more of the following possible related symptoms, such as typical symptoms of unstable vasomotor function, psychoneurological symptoms (anxiety, tension, depression, irritability, etc.), physical symptoms (dry skin, muscle, and bone pain, etc.) and symptoms of urogenital atrophy (vaginal dryness, pain during intercourse, leakage of urine, repeated urinary tract infections, etc.); (4) Imaging examination to exclude organic diseases such as uterus and ovaries. The standards for abdominal obesity were formulated with reference to the "Guidelines for the Prevention and Control of Overweight and Obesity in Chinese Adults": waist circumference $\geq$ 80 cm, and (or) WHtR $\geq$ 0.50, and (or) WHR $\geq$ 0.78. The general information of the patients including age and height was recorded (**Table 1**).

The inclusion criteria of patients in this study were as follows: (1) patients were diagnosed with perimenopausal and abdominal

TABLE 1 | Comparison of age and height between the two groups of patients.

Groups	Cases	Age (year)	Height (cm)
Electroacupuncture	37	49.90 ± 4.6	159.02 ± 2.9
Control	36	51.50 ± 4.4	157.35 ± 5.3

obesity; (2) patients had not received weight-loss treatment in the past 3 months. The exclusion criteria of patients in this study were as follows: (1) patients with secondary obesity caused by hypothalamic syndrome, pituitary tumor, Cushing's syndrome, hypothyroidism, insulinoma, or polycystic ovary syndrome; (2) patients who were diagnosed with uterine or ovarian malformations, have undergone uterine or ovarian resection, or in pregnancy or breastfeeding; (3) patients with severe diseases such as hyperthyroidism, diabetes, psychosis, malignant tumors, heart, liver, and kidney diseases, and hematopoietic system diseases.

Study Design

The patients were randomly divided into two groups: the Control group (n = 36) and the Electroacupuncture group (n = 37). The patients in the Control group received healthy lifestyle education, while those in the Electroacupuncture group received electroacupuncture treatment combined with dietary intervention for 8 weeks. Before and after treatment, the stool and blood of the patients were collected for subsequent analyses, and the weight, height, waist circumference and hip circumference of the patients were recorded to calculate waist-height ratio (WHtR), waist to hip ratio (WHR), and body mass index (BMI). Here, the method of measuring waist circumference recommended by the World Health Organization is adopted: the subject takes off his shoes, hat and coat, fasts, and stands upright, with feet being separated by 25–30 cm. The measurement position is at the midpoint of the line between the horizontal anterior superior iliac crest and the inferior edge of the twelfth rib.

Electroacupuncture Treatment

The main acupuncture meridians are Renmai, Stomach, Spleen, and Bladder Meridians. The acupoints are Zhongwan, Qihai, Guanyuan, Tianshu, Daheng, Pishu, Shenshu, and Dachangshu. The acupoint combinations in the study were as follows: Sanyinjiao and Inner Court were combined for the patients who belonged to the gastric-heat stagnation type; Yinlingquan and Fenglong were combined for the patients who pertained to the phlegm dampness Neisheng type; Hegu and Taichong were combined for the patients who appeared liver stagnation; Zusanli and Taibai were combined for the patients with spleen deficiency; and Mingmen and Shenmai were combined for the patients who presented symptoms of spleen and kidney yang.

Regarding the treatment, 0.25 mm × 40 mm (190,030) and 0.30 mm × 50 mm (190,185) disposable acupuncture needles (Huatuo, Suzhou, China) as well as an SDZ-V electronic acupuncture instrument (Huatuo, Suzhou, China) were employed. 1.5 inch acupuncture needles were used at the Backshu acupoints and four-limb acupoints. For the Backshu acupoints, the needle was inserted obliquely at 45° into the spine at 1-inch depth, while for the four-limb acupoints, the needle was inserted straight at 0.8–1.0-inch depth (0.3–0.5-inch depth for Taibai, Taichong, and Neiting). 2.0 inch acupuncture needles were inserted at the acupoints on the abdomen at 2-inch depth. Electroacupuncture was applied to Tianshu, Abdomen Jie, Daheng, and Meridian, and the waveform was a dense wave with a frequency of 2/100Hz. The needle was retained for 30 min. The acupuncture acupoints without electroacupuncture treatment were slightly lifted and twisted3 times every 10 min. Patients in the Electroacupuncture group received electroacupuncture treatment every 2 days (3 times a week) for 8 weeks.

Dietary Intervention

Patients in the Electroacupuncture group were given a strict low-sugar, low-fat, low-salt, and high-fiber diet. The diet contained staple foods, meat, and vegetables (each accounting for one third of the total dietary ingestion), fruits, and vegetables (no less than 250 g), and mineral supplements. Besides, the patients drunk 2,000–2,500 ml of water and no more than 20 g of liqueur, ingested less than 6 g of salt per day, and only ate fish products twice a week. Here, dietary intervention was implemented on the basis of menopausal health management strategies (Zhang, 2015).

Analysis of Physical Indexes

Before and after treatment, the weight (kg), height (cm), waist circumference (cm), and hip circumference (cm) of the patients were recorded. Then WHtR, WHR, and BMI were calculated using the following formulae: WHtR = waist/height; WHR = waist/hip; BMI = weight/height^2.

Analysis of Serum Indexes

Before and after treatment, the serum of all the patients was analyzed using an Automatic biochemical analyzer (BS-280; mindray, Shenzhen, China) to evaluate the levels of serum triglyceride (TG), total cholesterol (TC), low-density lipoprotein (LDL), high-density lipoprotein cholesterol (HDL-C), fasting insulin (FINS), and fasting blood glucose (FBG). Besides, Homeostasis Model Assessment-insulin resistance (HOMA-IR) was calculated according to the formula: HOMA-IR = FBG × FINS/22.5.

Analysis of Intestinal Flora

The intestinal flora in the patients was detected by 16s rRNA sequencing technology according to the previous publication (Di Segni et al., 2018). In brief, after the stool samples were collected, the RNA in the samples was extracted and subsequently subjected to polymerase chain reaction (PCR) (16s rRNA forward primer: 5′-GTGCCAGCMGCCGCGG-3′; 16s rRNA reversed primer: 5′-CCGTCAATTCMTTTRAGTTT-3′). Then the PCR product was harvested and sequenced through Illumina system. Meantime, the Clean Tags of the PCR product were obtained for the Operational Taxonomic Units (OTU) analysis.

In line with the clustering results of OTU, the representative sequence of each OTU was annotated to obtain the

corresponding species annotation information and species abundance distribution. Then, the species abundance in the sample and the species differences between samples were obtained through the visual statistical analysis of OTUs, and the Venn and Partial Least Squares Discrimination Analysis (PLS-DA) diagrams were plotted. Next, the information was subjected to Alpha diversity analysis to acquire the community structure information with differences in the sample. The Linear discriminant analysis (LDA) effect size (LEfSe) statistical analysis was applied to further investigate the differences in community structure among samples, and to identify different species via testing the species composition and community results of the grouped samples.

Statistical Analysis

All data involved in this study except for those from intestinal flora analysis were tested the normality of the variable distribution and analyzed by student's t-test. Statistical data were presented as mean ± standard deviation. The data were recognized as statistically significant when $P < 0.05$. These analyses were performed under SPSS 20.0 software.

RESULTS

Electroacupuncture Combined With Diet Treatment Ameliorated the Physical Indexes of Patients

Given that there was no statistical difference in the general information (cases, age, and height) (**Table 1**) of the two groups of patients, the patients in the two groups received different treatments. The physical indexes (weight, waist circumference, hip circumference, WHtR, WHR, and BMI) (**Table 2**) of patients in the two groups before and after treatment were documented. As shown in **Table 2**, in the Electroacupuncture group, the weight ($P < 0.01$), waist circumference ($P < 0.01$), hip circumference ($P < 0.01$), BMI ($P < 0.01$), WHtR ($P < 0.01$), and WHR ($P < 0.01$) of the patients were decreased after treatment when compared with those before treatment, while the patients in the Control group after treatment showed a larger waist circumference ($P < 0.01$) and a higher WHR ($P < 0.01$) than before treatment. Additionally, the waist circumference ($P < 0.01$), WHtR ($P < 0.01$), and WHR ($P < 0.01$) of patients in the Electroacupuncture group were notably lower than those in the Control group, which indicated that electroacupuncture combined with diet treatment might ameliorate abdominal obesity in perimenopausal patients.

TABLE 2 | Comparison of physical indexes between two groups of patients before and after the treatment.

Physical index	Group	Before	After
Weight (kg)	Electroacupuncture	61.56 ± 7.90	59.64 ± 7.27$^{\Delta\Delta}$
	Control	60.03 ± 6.06	60.03 ± 5.89
Waist circumference (cm)	Electroacupuncture	88.77 ± 6.47	84.81 ± 6.17**$^{\Delta\Delta}$
	Control	88.22 ± 5.07	89.92 ± 5.66$^{\Delta\Delta}$
Hips (cm)	Electroacupuncture	96.70 ± 5.00	93.50 ± 4.42$^{\Delta\Delta}$
	Control	95.00 ± 4.88	95.36 ± 4.65
BMI (kg·m^{-2})	Electroacupuncture	24.33 ± 2.95	23.58 ± 2.76$^{\Delta\Delta}$
	Control	24.45 ± 2.41	24.21 ± 1.91
WHtR	Electroacupuncture	0.558 ± 0.041	0.534 ± 0.040**$^{\Delta\Delta}$
	Control	0.566 ± 0.029	0.567 ± 0.036
WHR	Electroacupuncture	0.918 ± 0.038	0.907 ± 0.041**$^{\Delta\Delta}$
	Control	0.931 ± 0.050	0.943 ± 0.039$^{\Delta\Delta}$

***P < 0.01, vs. Control; $^{\Delta\Delta}$P < 0.01, vs. Before. Hips, hip circumference; BMI, body mass index; WHtR, waist-height ratio; WHR, waist-to-hip ratio.*

Electroacupuncture Combined With Diet Treatment Refined the Serum Indexes of Patients

Then the levels of TG, TC, LDL, HDL-C, FINS, FBG, and HOMA-IR of the patients in the two groups before and after treatment were evaluated. As illustrated in **Table 3**, in the Control group, the LDL level of patients after treatment was elevated ($P < 0.05$) as compared with that before treatment. Moreover, the TG ($P < 0.01$) and LDL levels ($P < 0.01$) of patients in the Electroacupuncture group were markedly lower than those in the Control group, which proved that electroacupuncture combined with diet treatment ameliorated the TG and LDL levels of perimenopausal patients with abdominal obesity.

Electroacupuncture Combined With Diet Treatment Regulated the OTU Number of the Intestinal Flora in Patients

During the analysis of intestinal flora, the information in the Electroacupuncture group before and after treatment was named Z1 team and Z2 team, respectively, and the information in the

TABLE 3 | Comparison of serum indexes between two groups of patients before and after the treatment.

Serum index	Group	Before	After
TG (mmol·L^{-1})	Electroacupuncture	1.62 ± 1.12	1.62 ± 0.85
	Control	1.40 ± 0.49	1.61 ± 0.67
TC (mmol·L^{-1})	Electroacupuncture	4.97 ± 0.91	4.80 ± 0.70**
	Control	5.14 ± 1.25	5.25 ± 0.86
LDL (mmol·L^{-1})	Electroacupuncture	3.05 ± 0.82	2.98 ± 0.65**
	Control	3.16 ± 1.11	3.49 ± 0.69$^{\Delta}$
HDL-C (mmol·L^{-1})	Electroacupuncture	1.27 ± 0.17	1.28 ± 0.25
	Control	1.31 ± 0.21	1.35 ± 0.30
FINS (pmol·L^{-1})	Electroacupuncture	60.48 ± 33.01	56.35 ± 30.22
	Control	56.77 ± 30.85	60.55 ± 18.68
HOMA-IR	Electroacupuncture	14.63 ± 8.65	12.89 ± 6.68
	Control	16.28 ± 16.47	12.83 ± 4.77
FBG (mmol·L^{-1})	Electroacupuncture	5.41 ± 0.81	5.06 ± 0.55
	Control	5.09 ± 0.42	5.02 ± 0.41

***P < 0.01, vs. Control; $^{\Delta}$P < 0.05, vs. Before. TG, serum triglyceride; TC, total cholesterol; LDL, low-density lipoprotein; HDL-C, high-density lipoprotein cholesterol; FINS, fasting insulin; FBG, fasting blood glucose; HOMA-IR, Homeostasis Model Assessment-insulin resistance.*

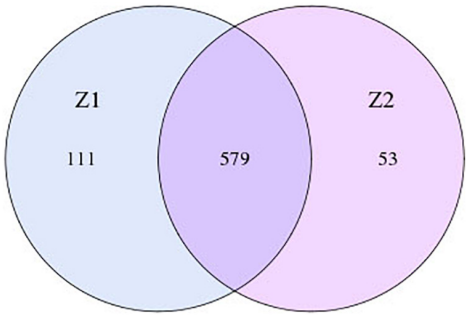

FIGURE 1 | OTU numbers of intestinal flora in the patients in the Electroacupuncture group before and after treatment (Z1, the Electroacupuncture group before treatment; Z2, the Electroacupuncture group after treatment; D1, the Control group before treatment; D2: the Control group after treatment).

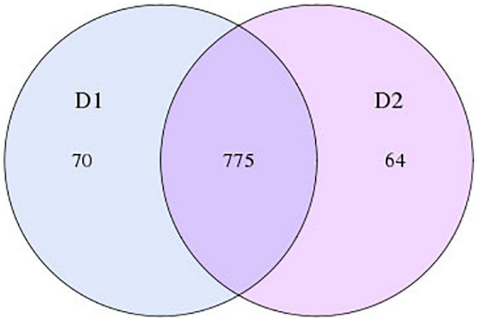

FIGURE 2 | OTU numbers of intestinal flora in the patients in the Control group before and after treatment (Z1, the Electroacupuncture group before treatment; Z2, the Electroacupuncture group after treatment; D1, the Control group before treatment; D2, the Control group after treatment).

Control group before and after treatment was called D1 team and D2 team, respectively. As depicted in **Figure 1**, in the Electroacupuncture group, the number of OTUs that existed both before and after treatment was 579, and that of specific OTUs was reduced from 111 to 53 after treatment. Meanwhile, in the Control group (**Figure 2**), the number of OTUs that existed both before and after treatment was 775, and that of specific OTUs was decreased to 64 after treatment. These discoveries indicated that electroacupuncture combined with diet treatment decreased the abundance of the intestinal flora in the patients.

In addition, according to the PLS-DA analysis based on OTU determination (**Figure 3**), the samples belonging to the same group (the Electroacupuncture group or the Control group) in each team (Z1 and Z2, or D1 and D2) were almost identical to each other; the structure site of the flora sample in each team was relatively low; the distance between the samples of team Z (the Electroacupuncture group) and team D (the Control group) was far; and the difference in bacterial community structure between the two groups was relatively significant. All these results verified that the grouping results were reasonable, accompanied by satisfactory efficiency of the classification model.

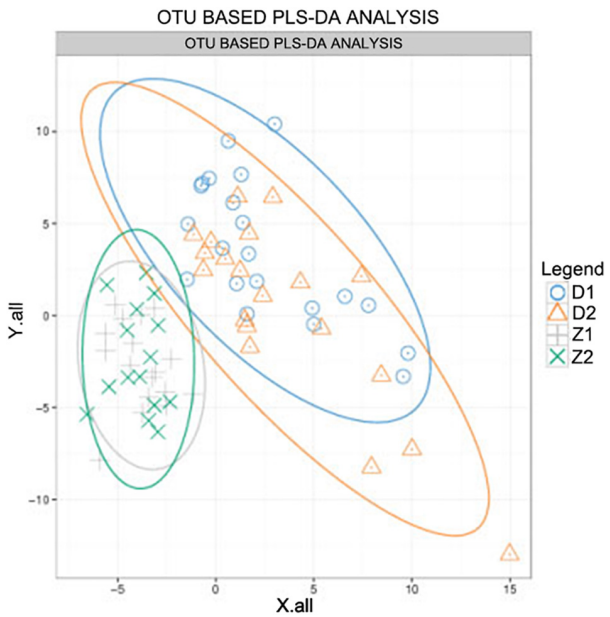

FIGURE 3 | The PLS-DA analysis of OTU determination in the Electroacupuncture group and the Control group (Z1, the Electroacupuncture group before treatment; Z2, the Electroacupuncture group after treatment; D1, the Control group before treatment; D2, the Control group after treatment).

Electroacupuncture Combined With Diet Treatment Modulated the Phylum and Genus Levels of Intestinal Flora in Patients

The phylum-level and genus-level changes of the intestinal flora in patients before and after treatment were exhibited in **Figures 4**, **5**, respectively. As delineated in **Figure 4** and **Table 4**, at the phylum level, the most abundant flora in both groups before (D1 and Z1) and after (D2 and Z2) treatment were Firmicutes, Bacteroidetes, and Proteobacteria. However, difference appeared at the genus-level, as shown in **Figure 5** and **Table 5**. Although the most dominant flora in both groups before (D1 and Z1) and after (D2 and Z2) treatment were Bacteroides, Prevotella, Faecalibacterium, and Roseburia, the Enterococcus level was decreased ($P < 0.05$) and the Enterobacter level was increased in Z2 group, when compared with the Z1 group ($P < 0.05$), while the Blautia level was lessened ($P < 0.05$) and the Enterobacter level was augmented in D2 group, when compared with the D1 group ($P < 0.05$).

Electroacupuncture Combined With Diet Treatment Regulated the Alpha Diversity of Intestinal Flora in Patients

The Alpha diversity of intestinal flora was evaluated. As shown in **Figure 6** and **Table 6**, although there was no statistically difference between Z1 and Z2 groups, the observed species, chao, ace, and shannon indexes in the Electroacupuncture group after treatment (Z2) showed an upward trend, while the simpson

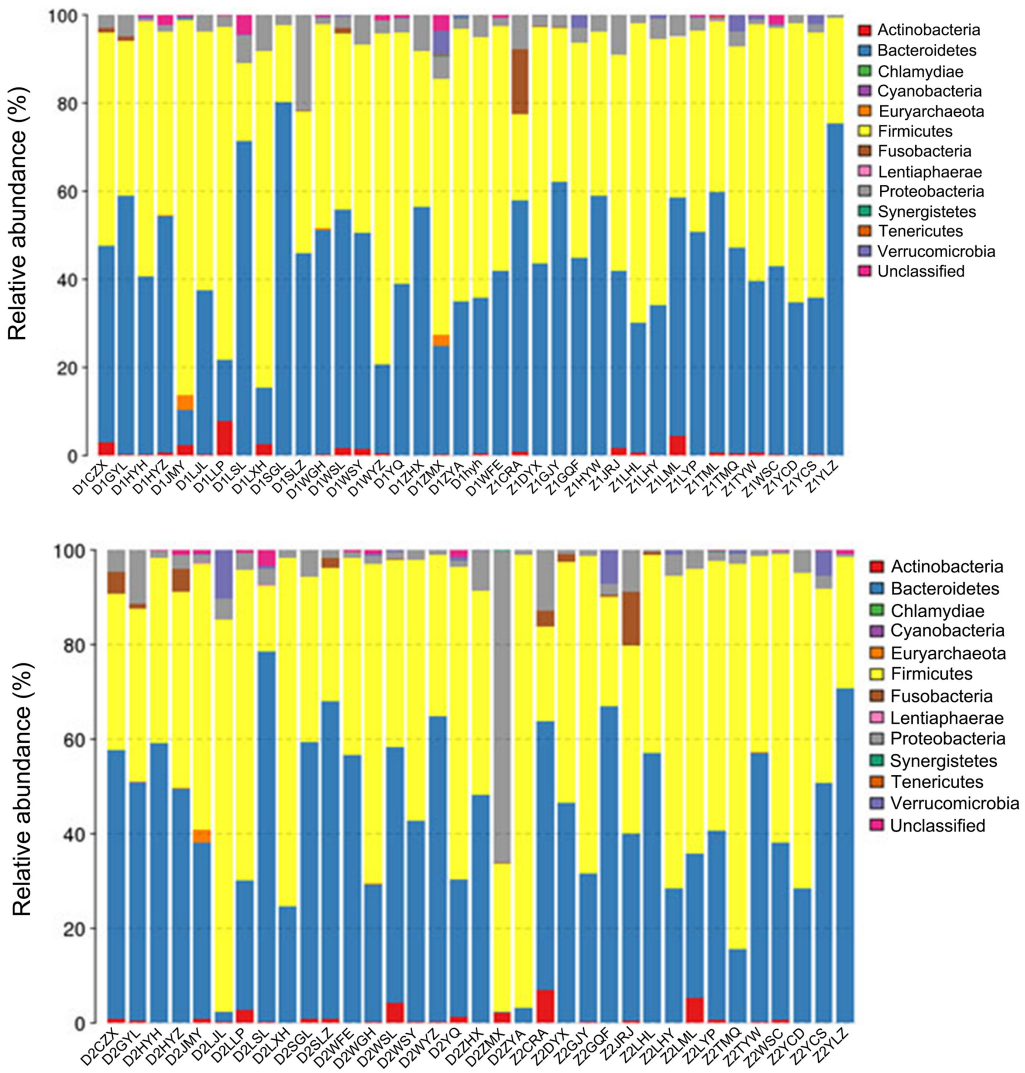

FIGURE 4 | Phylum-level changes of intestinal flora in the patients in the Electroacupuncture group and the Control group (Z1, the Electroacupuncture group before treatment; Z2, the Electroacupuncture group after treatment; D1, the Control group before treatment; D2, the Control group after treatment).

index presented a downward trend, signifying that the species abundance in the Electroacupuncture group after treatment was on the rise. Meanwhile, despite no statistically difference between D1 and D2 groups, the same observed indexes as above in D2 group showed a downward trend, while the simpson index was on the contrary, manifesting that the species abundance in the Control group was inhibited. These results indicated that electroacupuncture combined with diet treatment improved the species diversity of intestinal flora in patients.

Electroacupuncture Combined With Diet Treatment Regulated the Species Differences of Intestinal Flora in Patients

The species difference of intestinal flora in the Electroacupuncture group was analyzed. As profiled in **Figure 7**, the abundance of Enterococcus, Enterococcaceae, Escherichia, Enterobacteriaceae, and Enterobacteriales was reduced yet that of Klebsiella and Kosakonia was enhanced after treatment, which demonstrated that electroacupuncture combined with diet treatment increased the species differences of intestinal flora in patients, and Klebsiella and Kosakonia were instrumental in the treatment of abdominal obesity in perimenopausal patients.

DISCUSSION

More and more researches have proved that acupuncture can safely and effectively treat abdominal obesity, mainly by stimulating the body's meridians and acupoints, improving body condition as a whole, regulating intake, and enhancing body metabolism (Zhang et al., 2019). Acupuncture meridians such as the spleen, stomach, liver, and kidney can warm the kidney and strengthen the spleen, soothe the liver and

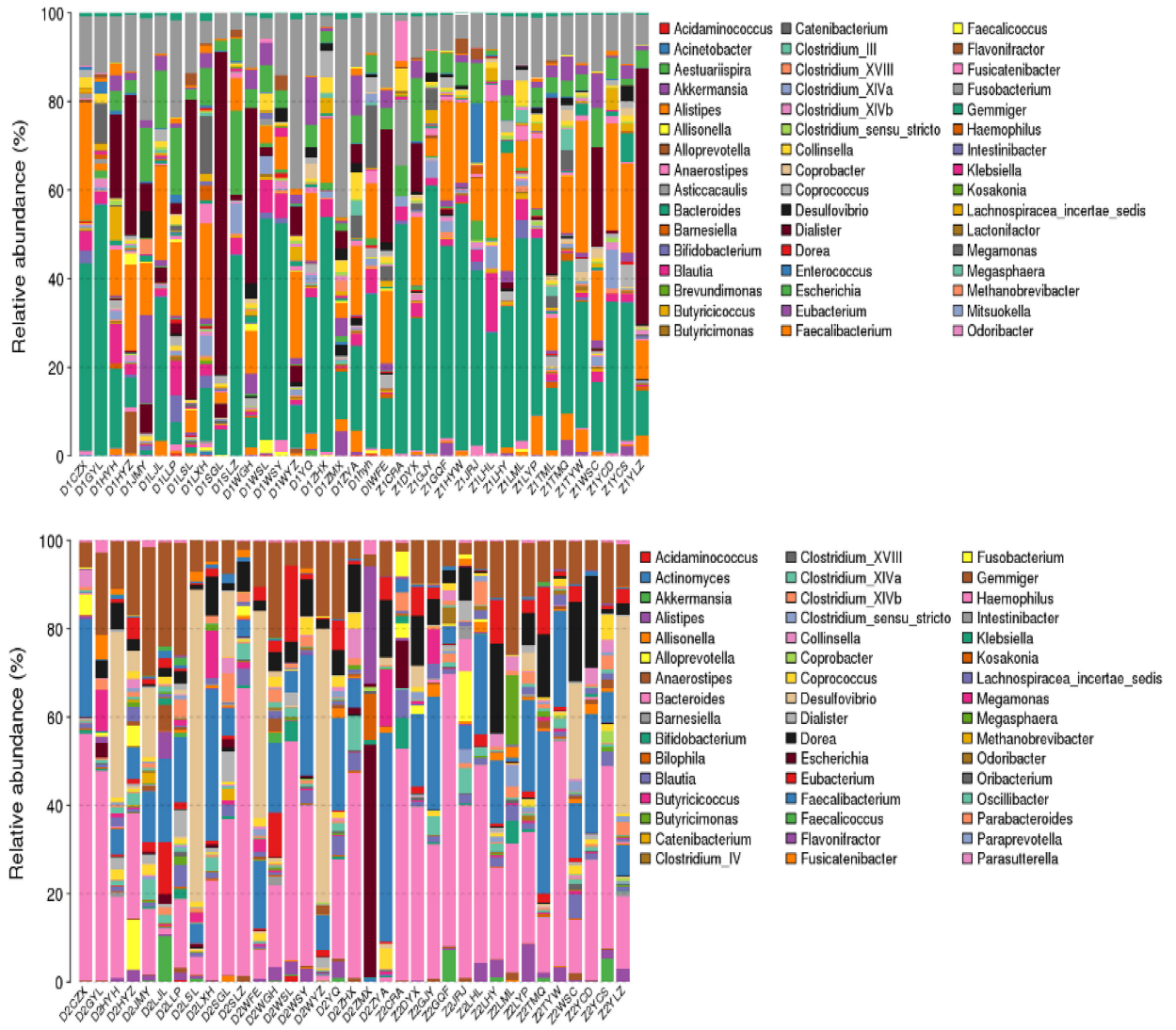

FIGURE 5 | Genus-level changes of intestinal flora in the patients in the Electroacupuncture group and the Control group. (Z1, the Electroacupuncture group before treatment; Z2, the Electroacupuncture group after treatment; D1, the Control group before treatment; D2, the Control group after treatment).

TABLE 4 | Comparison of Phylum level between two groups of patients before and after treatment ($x \pm s$).

Phylum levels	Groups	Before	After
Firmicutes	Electroacupuncture	49.12 ± 11.58	55.76 ± 15.76
	Control	50.16 ± 18.44	47.72 ± 21.38
Bacteroidetes	Electroacupuncture	47.64 ± 12.24	44.29 ± 15.51
	Control	39.85 ± 20.12	42.02 ± 22.34
Proteobacteria	Electroacupuncture	3.12 ± 2.36	3.60 ± 3.53
	Control	5.45 ± 6.42	6.42 ± 14.70

regulate the qi, adjust the function of the internal organs, enhance metabolism, smooth the blood flow, and invigorate the blood of the five internal organs, thereby fulfilling the purpose of weight loss and waist thinning (Wang et al., 2008; Lei et al., 2017; Chen et al., 2018; Luo et al., 2018; Huang et al., 2019; Zhang et al., 2019). In this study, to confirm the effect of electroacupuncture combined with dietary intervention on abdominal obesity, the physical indexes of patients were first detected after treatment. We discovered that electroacupuncture combined with diet treatment reduced the weight, waist circumference, hip circumference, BMI, WHtR, and WHR of the patients when compared with those before treatment, and besides, the combined treatment of electroacupuncture and diet reduced the waist circumference, WHtR, and WHR of patients as compared to patients receiving healthy lifestyle education, which connoted that electroacupuncture combined with diet treatment was feasible in ameliorating abdominal obesity in perimenopausal patients.

In addition to the physical indexes, there are also a series of serum indexes which are closely related to the glycolipid metabolism of obesity patients. TG and TC are two important

TABLE 5 | Comparison of genus level between two groups of patients before and after treatment (x ± s).

Genus levels	Groups	Before	After
Bacteroides	Electroacupuncture	35.06 ± 14.17	34.71 ± 15.15
	Control	22.99 ± 19.18	24.63 ± 20.25
Prevotella	Electroacupuncture	7.74 ± 16.81	4.65 ± 11.86
	Control	13.14 ± 22.24	13.35 ± 22.43
Faecalibacterium	Electroacupuncture	15.66 ± 9.04	14.18 ± 10.63
	Control	11.79 ± 7.38	13.35 ± 12.35
Roseburia	Electroacupuncture	4.57 ± 3.43	7.61 ± 7.23
	Control	4.70 ± 4.14	3.76 ± 3.43
Blautia	Electroacupuncture	2.51 ± 2.98	2.26 ± 1.75
	Control	2.98 ± 2.60	1.41 ± 1.52$^{\Delta}$
Enterobacter	Electroacupuncture	0.16 ± 0.24	0.17 ± 0.50$^{\Delta}$
	Control	0.33 ± 0.55	0.75 ± 2.67$^{\Delta}$
Enterobacter	Electroacupuncture	0.005 ± 0.01	0.0001 ± 0.0005$^{\Delta}$
	Control	0.18 ± 0.70	0.02 ± 0.08

$^{\Delta}P < 0.05$, *vs. Before.*

factors in the glycolipid metabolism, which both display higher levels in obesity patients than in healthy people (Wiesner and Watson, 2017). Furthermore, LDL, a small-diameter lipoprotein, is the main transfer tool in the process of cholesterol transport. Abnormal LDL level is indicative of dyslipidemia, one of the symptoms of obese patients (Howard et al., 2003; Chan et al., 2004; Klop et al., 2013). A study found that electroacupuncture reduced the serum TC, TG, and LDL levels in obese women (Cabioglu and Ergene, 2005), and the same downtrend was discovered in this study when applied electroacupuncture combined with diet treatment to patients, which further verified that electroacupuncture combined with diet treatment had the ability to alleviate abdominal obesity in perimenopausal patients through regulating the serum levels of TG, TC, and LDL.

As one of the complex ecosystems in the gastrointestinal tract, the intestinal flora is related to metabolism-related diseases and multi-system diseases (Di Segni et al., 2018). Acupuncture was proved to alleviate obesity-related lipid metabolism disorders and intestinal microbiota disorders (Gao et al., 2020; Xie et al., 2020). For example, electroacupuncture promoted the diversity of the gut microbiota of obese mice, thus reducing body weight (Dou et al., 2020). Si et al. (2018) found that the structure of the intestinal flora of animals in the acupuncture group was gradually similar to those in the healthy control group. Therefore, we then focused on investigating whether the effect of electroacupuncture on abdominal obesity was realized by regulating the community structure of the intestinal flora in the patients.

The high-throughput sequencing technology has been widely used in microbiome analysis, because it allows scholars to sequence millions of DNA molecules simultaneously and

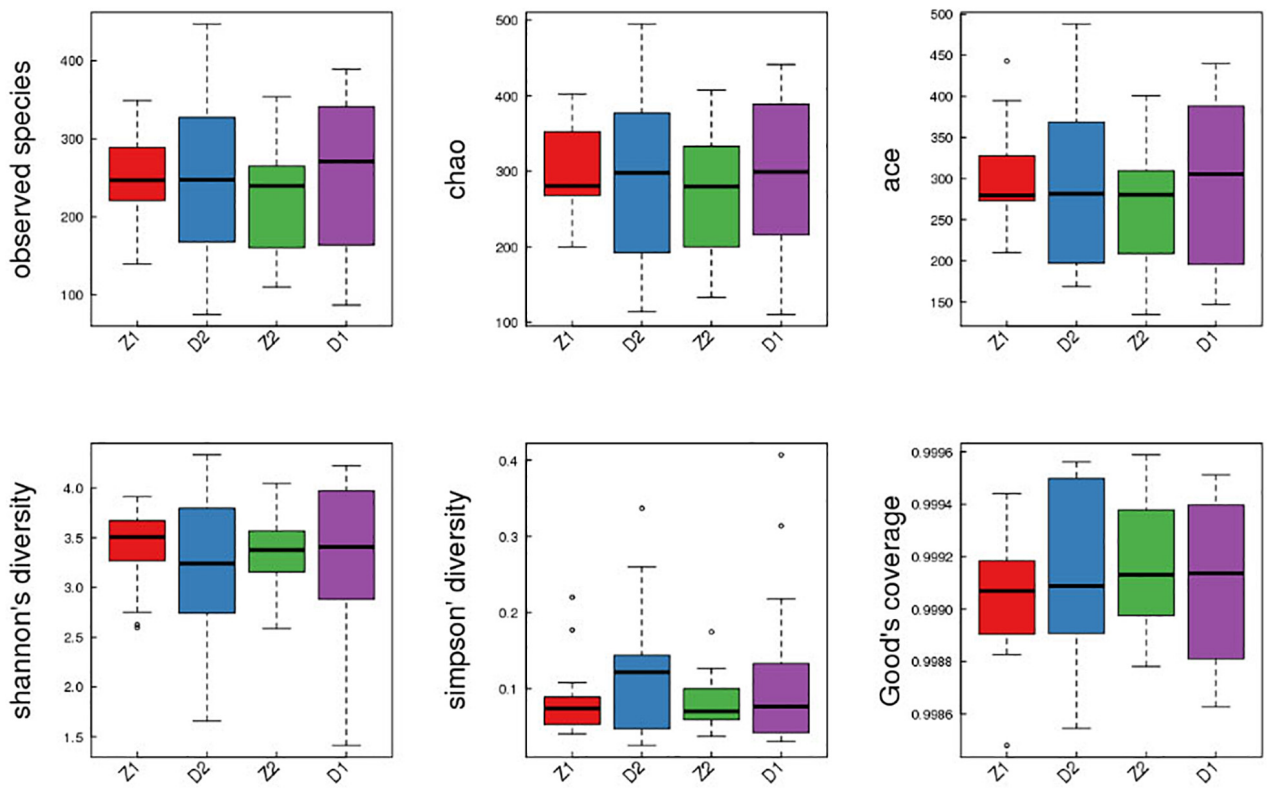

FIGURE 6 | Alpha diversity of intestinal flora in the patients in the Electroacupuncture group and the Control group (Z1, the Electroacupuncture group before treatment; Z2, the Electroacupuncture group after treatment; D1, the Control group before treatment; D2, the Control group after treatment).

TABLE 6 | Comparison of Alpha diversity between two groups of patients before and after treatment (x ± s).

Genus levels	Groups	Before	After
Observed species	Electroacupuncture	221.19 ± 68.04	251.77 ± 92.71
	Control	247.18 ± 55.98	246.85 ± 95.28
Chao	Electroacupuncture	271.37 ± 81.44	295.04 ± 94.56
	Control	301.97 ± 65.14	286.79 ± 102.80
Ace	Electroacupuncture	266.67 ± 70.47	295.53 ± 94.38
	Control	302.49 ± 61.10	290.10 ± 95.63
Shannon	Electroacupuncture	3.33 ± 0.38	3.51 ± 0.74
	Control	3.40 ± 0.42	3.21 ± 0.74
Simpson	Electroacupuncture	0.08 ± 0.03	0.07 ± 0.10
	Control	0.08 ± 0.05	0.17 ± 0.08

provides a data pool to cover the entire microbiome in the gut (Gao X. et al., 2018). On the flip side, the gene encoding 16s rRNA is the most commonly used target for studying bacterial evolution and classification (Gao X. et al., 2018; Li et al., 2020). Hence, in the present study, we used 16s rRNA sequencing technology to analyze the information of the intestinal flora in the patients before and after treatment. The previous study has discovered higher species abundance, lower species diversity, and smaller species differences of the intestinal flora in obese patients (Malamut, 2007; Yazigi et al., 2008; Gao X. et al., 2018; Li et al., 2020). Based on the OTU corresponding species annotation, Alpha diversity, and LEfSe analyses, we for the first time unveiled that electroacupuncture combined with diet treatment lessened the species abundance, and increased the species diversity and differences of intestinal flora in perimenopausal patients with abdominal obesity. Most notably, after electroacupuncture combined with diet treatment, Klebsiella and Kosakonia in patients were increased. Recent research has reported that during the antibiotic treatment of obesity mice, Klebsiella is increased to inhibit the body weight gain (Yao et al., 2020). Therefore, in this research, the role of electroacupuncture combined with diet treatment in perimenopausal patients with abdominal obesity might be realized by improving the community structure of intestinal flora and increasing Klebsiella and Kosakonia.

Taken together, electroacupuncture combined with diet treatment exerted a therapeutic effect on perimenopausal patients with abdominal obesity through improving the community

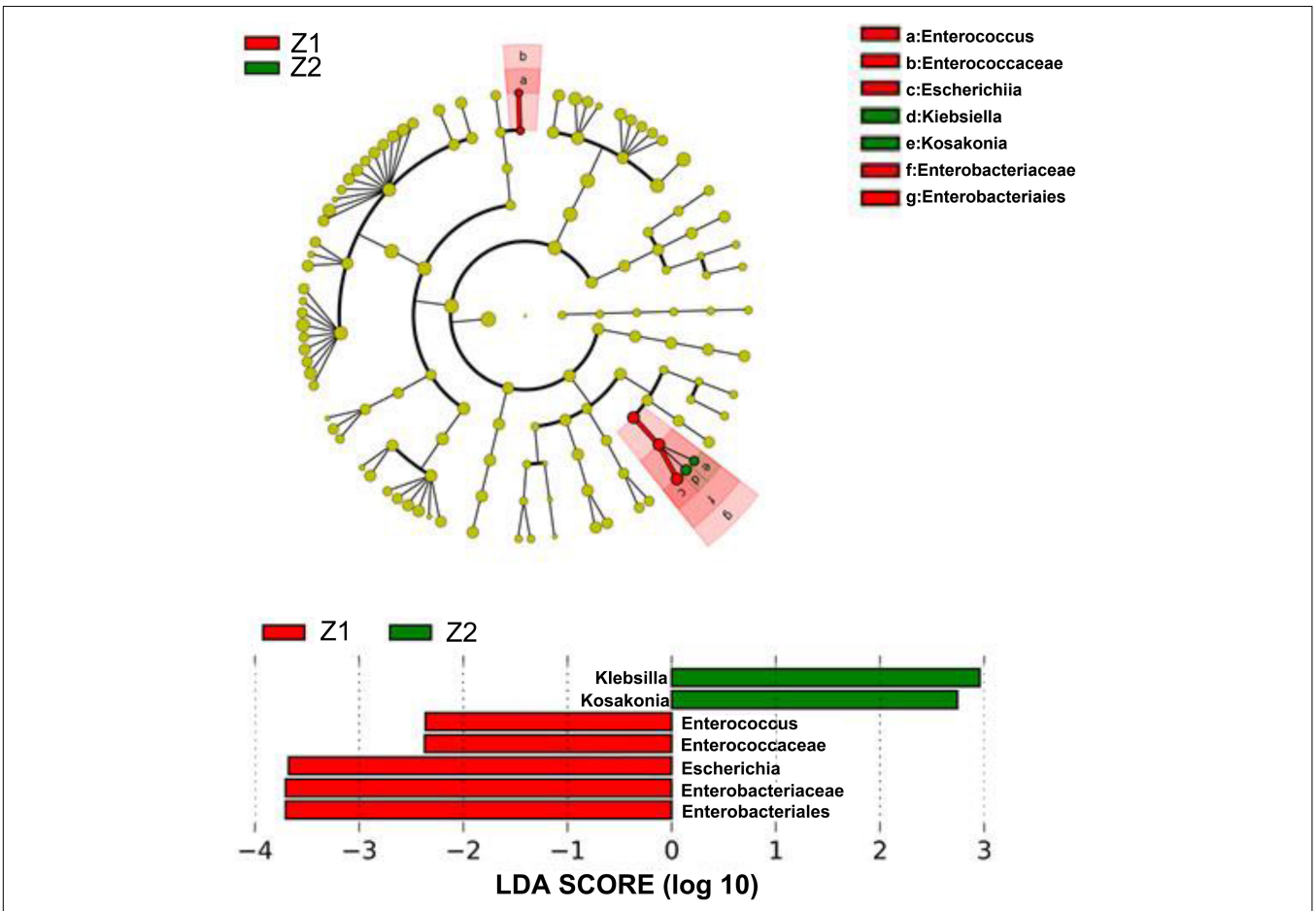

FIGURE 7 | Species differences of intestinal flora in the patients in the Electroacupuncture group and the Control group (Z1, the Electroacupuncture group before treatment; Z2, the Electroacupuncture group after treatment; D1, the Control group before treatment; D2, the Control group after treatment).

structure of intestinal flora. Nevertheless, what failed to be underscored in our study is the design of separate dietary intervention group, that is, the same diet restriction was performed without electroacupuncture, which may be further explored in future studies. Consumption patterns may affect obesity, which may be another aspect that we need to pay attention to in future research.

DATA AVAILABILITY STATEMENT

The raw data supporting the conclusions of this article will be made available by the authors, without undue reservation.

ETHICS STATEMENT

The study has been approved by the Ethics Committee of Zhejiang Hospital [No. 2018 (9K)] and all patients signed the written informed consent.

AUTHOR CONTRIBUTIONS

JS and GY: substantial contributions to conception and design and drafting the article or critically revising it for important intellectual content. JZ, CS, YH, ZL, TL, and XJ: data acquisition, data analysis and interpretation. JS, GY, JZ, CS, Y'aH, ZL, TL, and XJ: final approval of the version to be published and agreement to be accountable for all aspects of the work in ensuring that questions related to the accuracy or integrity of the work are appropriately investigated and resolved. All authors contributed to the article and approved the submitted version.

FUNDING

This work was supported by the Health Science and Technology Plan of Zhejiang Province (2018KY200), the Zhejiang TCM Science and Technology Program (2018ZQ001), the Zhejiang TCM Science and Technology Program (2019ZQ001), and the Construction Plan for the Inheritance Studio of Famous and Old Chinese Medicine Experts in Zhejiang Province (GZS2017011).

SUPPLEMENTARY MATERIAL

The Supplementary Material for this article can be found online at: https://www.frontiersin.org/articles/10.3389/fphys.2021.708588/full#supplementary-material

REFERENCES

Bronczyk-Puzon, A., Piecha, D., Nowak, J., Koszowska, A., Kulik-Kupka, K., Dittfeld, A., et al. (2015). Guidelines for dietary management of menopausal women with simple obesity. *Prz. Menopauzalny* 14, 48–52. doi: 10.5114/pm.2015.48678

Cabioglu, M. T., and Ergene, N. (2005). Electroacupuncture therapy for weight loss reduces serum total cholesterol, triglycerides, and LDL cholesterol levels in obese women. *Am. J. Chin. Med.* 33, 525–533. doi: 10.1142/S0192415X05003132

Chan, D. C., Barrett, H. P., and Watts, G. F. (2004). Dyslipidemia in visceral obesity: mechanisms, implications, and therapy. *Am. J. Cardiovasc. Drugs* 4, 227–246. doi: 10.2165/00129784-200404040-00004

Chen, X., Huang, W., Jin, Y., Hu, F., Cheng, X., Hong, Z., et al. (2018). [Prescription analysis of electroacupuncture for simple obesity based on complex network technique]. *Zhongguo zhen jiu* 38, 331–336. doi: 10.13703/j.0255-2930.2018.03.028

Di Segni, A., Braun, T., BenShoshan, M., Farage Barhom, S., Glick Saar, E., Cesarkas, K., et al. (2018). Guided protocol for fecal microbial characterization by 16S rRNA-amplicon sequencing. *J. Vis. Exp.* 133:56845. doi: 10.3791/56845

Dou, D., Chen, Q. Q., Zhong, Z. Q., Xia, X. W., and Ding, W. J. (2020). Regulating the enteric nervous system against obesity in mice by electroacupuncture. *Neuroimmunomodulation* 27, 48–57. doi: 10.1159/000506483

Gao, X., Jia, R., Xie, L., Kuang, L., Feng, L., and Wan, C. (2018). A study of the correlation between obesity and intestinal flora in school-age children. *Sci. Rep.* 8:14511. doi: 10.1038/s41598-018-32730-6

Gao, Y., Bi, W., Wu, X., Zhu, X., and Luo, Y. (2018). [Bacterial resistance influences intestinal flora and host immune regulation]. *Sheng wu gong cheng xue* 34, 1259–1269. doi: 10.13345/j.cjb.180123

Gao, Y., Wang, Y., Zhou, J., Hu, Z., and Shi, Y. (2020). Effectiveness of electroacupuncture for simple obesity: a systematic review and meta-analysis of randomized controlled trials. *Evid. Based Complement. Alternat. Med.* 2020:2367610. doi: 10.1155/2020/2367610

Gazarova, M., Galsneiderova, M., and Meciarova, L. (2019). Obesity diagnosis and mortality risk based on a body shape index (ABSI) and other indices and anthropometric parameters in university students. *Rocz. Panstw. Zakl. Hig.* 70, 267–275. doi: 10.32394/rpzh.2019.0077

González-Muniesa, P., Mártinez-González, M. A., Hu, F. B., Després, J. P., Matsuzawa, Y., Loos, R. J. F., et al. (2017). Obesity. *Nat. Rev. Dis. Primers* 3:17034. doi: 10.1038/nrdp.2017.34

Howard, B. V., Ruotolo, G., and Robbins, D. C. (2003). Obesity and dyslipidemia. *Endocrinol. Metab. Clin. North Am.* 32, 855–867. doi: 10.1016/s0889-8529(03)00073-2

Hu, L., Huang, X., You, C., Li, J., Hong, K., Li, P., et al. (2017). Prevalence of overweight, obesity, abdominal obesity and obesity-related risk factors in southern China. *PLoS One* 12:e0183934. doi: 10.1371/journal.pone.0183934

Huang, Q., Chen, R., Chen, L., Liang, F. X., He, W. J., Peng, M., et al. (2019). [Electroacupuncture reduces obesity by improving metabolism and up-regulating expression of hypothalamic Sirtuin 1 and proopiomelanocortin in obese rats]. *Zhen ci yan jiu = Acupuncture research* 44, 270–275. doi: 10.13702/j.1000-0607.180190

Jablonowska-Lietz, B., Wrzosek, M., Wlodarczyk, M., and Nowicka, G. (2017). New indexes of body fat distribution, visceral adiposity index, body adiposity index, waist-to-height ratio, and metabolic disturbances in the obese. *Kardiol. Pol.* 75, 1185–1191. doi: 10.5603/KP.a2017.0149

Keller, C., Larkey, L., Distefano, J. K., Boehm-Smith, E., Records, K., Robillard, A., et al. (2010). Perimenopausal obesity. *J. Womens Health (Larchmt)* 19, 987–996. doi: 10.1089/jwh.2009.1547

Klop, B., Elte, J. W., and Cabezas, M. C. (2013). Dyslipidemia in obesity: mechanisms and potential targets. *Nutrients* 5, 1218–1240. doi: 10.3390/nu5041218

Lei, H., Chen, X., Liu, S., and Chen, Z. (2017). Effect of electroacupuncture on visceral and hepatic fat in women with abdominal obesity: a randomized controlled study based on magnetic resonance imaging. *J. Altern. Complement. Med. (New York, NY)* 23, 285–294. doi: 10.1089/acm.2016.0361

Li, X., Shi, W., Xiong, Q., Hu, Y., Qin, X., Wan, G., et al. (2020). Leptin improves intestinal flora dysfunction in mice with high-fat diet-induced obesity. *J. Int. Med. Res.* 48:300060520920062. doi: 10.1177/0300060520920062

Łokieć, K., Błońska, A., Walecka-Kapica, E., and Stec-Michalska, K. (2016). [Effect of treatment with diet on reducing levels of sex hormones in

perimenopausal women with overweight and obesity]. *Pol. Merkur. Lekarski* 40, 362–368.

Luo, D., Liu, L., Liang, F. X., Yu, Z. M., and Chen, R. (2018). Electroacupuncture: a feasible sirt1 promoter which modulates metainflammation in diet-induced obesity rats. *Evid. Based Complement. Alternat. Med.* 2018:5302049. doi: 10.1155/2018/5302049

Ma, M. J., and Wu, J. (2017). [Association between intestinal flora imbalance and nonalcoholic fatty liver disease]. *Zhonghua Gan Zang Bing Za Zhi* 25, 789–793. doi: 10.3760/cma.j.issn.1007-3418.2017.10.017

Malamut, G. (2007). [Obesity and intestinal flora]. *Gastroenterol. Clin. Biol.* 31(8-9 Pt 1), 761–762. doi: 10.1016/s0399-8320(07)91941-7

Mastorakos, G., Valsamakis, G., Paltoglou, G., and Creatsas, G. (2010). Management of obesity in menopause: diet, exercise, pharmacotherapy and bariatric surgery. *Maturitas* 65, 219–224. doi: 10.1016/j.maturitas.2009.12.003

Mohammadbeigi, A., Asgarian, A., Moshir, E., Heidari, H., Afrashteh, S., Khazaei, S., et al. (2018). Fast food consumption and overweight/obesity prevalence in students and its association with general and abdominal obesity. *J. Prev. Med. Hyg.* 59, E236–E240. doi: 10.15167/2421-4248/jpmh2018.59.3.830

Ruban, A., Doshi, A., Lam, E., and Teare, J. P. (2019). Medical devices in obesity treatment. *Curr. Diab. Rep.* 19:90. doi: 10.1007/s11892-019-1217-3

Samat, A., Rahim, A., and Barnett, A. (2008). Pharmacotherapy for obesity in menopausal women. *Menopause Int.* 14, 57–62. doi: 10.1258/mi.2008.008005

Sebastián Domingo, J. J., and Sánchez Sánchez, C. (2018). From the intestinal flora to the microbiome. *Rev. Esp. Enferm. Dig.* 110, 51–56. doi: 10.17235/reed.2017.4947/2017

Si, Y. C., Miao, W. N., He, J. Y., Chen, L., Wang, Y. L., and Ding, W. J. (2018). Regulating gut flora dysbiosis in obese mice by electroacupuncture. *Am. J. Chin. Med.* 46, 1–17. doi: 10.1142/S0192415X18500763

Smith, U. (2015). Abdominal obesity: a marker of ectopic fat accumulation. *J. Clin. Investig.* 125, 1790–1792.

Tauqeer, Z., Gomez, G., and Stanford, F. C. (2018). Obesity in women: insights for the clinician. *J. Womens Health (Larchmt)* 27, 444–457. doi: 10.1089/jwh.2016.6196

Vandevijvere, S., Chow, C. C., Hall, K. D., Umali, E., and Swinburn, B. A. (2015). Increased food energy supply as a major driver of the obesity epidemic: a global analysis. *Bull. World Health Organ.* 93, 446–456. doi: 10.2471/BLT.14.150565

Wang, F., Tian, D. R., and Han, J. S. (2008). Electroacupuncture in the treatment of obesity. *Neurochem. Res.*33, 2023–2027. doi: 10.1007/s11064-008-9822-6

Wiesner, P., and Watson, K. E. (2017). Triglycerides: a reappraisal. *Trends Cardiovasc. Med.* 27, 428–432. doi: 10.1016/j.tcm.2017.03.004

Xie, L. L., Zhao, Y. L., Yang, J., Cheng, H., Zhong, Z. D., Liu, Y. R., et al. (2020). Electroacupuncture prevents osteoarthritis of high-fat diet-induced obese rats. *Biomed. Res. Int.* 2020:9380965. doi: 10.1155/2020/9380965

Yao, H., Fan, C., Lu, Y., Fan, X., Xia, L., Li, P., et al. (2020). Alteration of gut microbiota affects expression of adiponectin and resistin through modifying DNA methylation in high-fat diet-induced obese mice. *Genes Nutr.* 15:12. doi: 10.1186/s12263-020-00671-3

Yazigi, A., Gaborit, B., Nogueira, J. P., Butiler, M. E., and Andreelli, F. (2008). [Role of intestinal flora in insulin resistance and obesity]. *Presse Med. (Paris, France : 1983)* 37, 1427–1430. doi: 10.1016/j.lpm.2007.11.020

Zhang, S. F. B. L. (2015). Menopausal health management strategies. *J. Pract. Obstet. Gynecol.* 31, 333–334.

Zhang, Y. J., Li, J., Huang, W., Mo, G. Y., Wang, L. H., Zhuo, Y., et al. (2019). [Effect of electroacupuncture combined with treadmill exercise on body weight and expression of PGC-1α, Irisin and AMPK in skeletal muscle of diet-induced obesity rats]. *Zhen ci yan jiu* 44, 476–480. doi: 10.13702/j.1000-0607.180460

Conflict of Interest: The authors declare that the research was conducted in the absence of any commercial or financial relationships that could be construed as a potential conflict of interest.

Publisher's Note: All claims expressed in this article are solely those of the authors and do not necessarily represent those of their affiliated organizations, or those of the publisher, the editors and the reviewers. Any product that may be evaluated in this article, or claim that may be made by its manufacturer, is not guaranteed or endorsed by the publisher.

frontiers in Physiology

CORRECTION
published: 08 March 2022
doi: 10.3389/fphys.2022.844424

Corrigendum: Electroacupuncture Combined With Diet Treatment Has a Therapeutic Effect on Perimenopausal Patients With Abdominal Obesity by Improving the Community Structure of Intestinal Flora

Jili Sheng[1†], *Geyao Yang*[2†], *Xiaoqing Jin*[1], *Caijuan Si*[3], *Yuan'an Huang*[4], *Zhouxiao Luo*[5], *Tao Liu*[1] *and Jianfang Zhu*[1*]

[1] Acupuncture Department, Zhejiang Hospital, Hangzhou, China, [2] Acupuncture and Massage Department, Hangzhou Geriatric Hospital, Hangzhou, China, [3] Nutritional Department, Zhejiang Hospital, Hangzhou, China, [4] Massage Department, Zhejiang Hospital, Hangzhou, China, [5] Acupuncture Department, Tonglu TCM Hospital, Hangzhou, China

Keywords: abdominal obesity, perimenopausal syndrome, 16S rRNA, intestinal flora, electroacupuncture

OPEN ACCESS

Approved by:
Frontiers Editorial Office, Frontiers Media SA, Switzerland

***Correspondence:**
Jianfang Zhu
zjyyzjf@163.com

[†] These authors have contributed equally to this work

Specialty section:
This article was submitted to Metabolic Physiology, a section of the journal Frontiers in Physiology

Received: *02 February 2022*
Accepted: *11 February 2022*
Published: *08 March 2022*

Citation:
Sheng J, Yang G, Jin X, Si C, Huang Y, Luo Z, Liu T and Zhu J (2022) Corrigendum: Electroacupuncture Combined With Diet Treatment Has a Therapeutic Effect on Perimenopausal Patients With Abdominal Obesity by Improving the Community Structure of Intestinal Flora. Front. Physiol. 13:844424. doi: 10.3389/fphys.2022.844424

A Corrigendum on

Electroacupuncture Combined With Diet Treatment Has a Therapeutic Effect on Perimenopausal Patients With Abdominal Obesity by Improving the Community Structure of Intestinal Flora

by Sheng, J., Yang, G., Jin, X., Si, C., Huang, Y., Luo, Z., Liu, T., and Zhu, J. (2021). Front. Physiol. 12:708588. doi: 10.3389/fphys.2021.708588

In the original article, there was an error in the **Ethics Statement** as published. A correction has been made to **Materials and Methods** subsection **Ethics Statement** and to the **Ethics Statement**:

"The study has been approved by the Ethics Committee of Zhejiang Hospital [No. 2018 (9K)] and all patients signed the written informed consent."

The authors apologize for this error and state that this does not change the scientific conclusions of the article in any way. The original article has been updated.

frontiers in Physiology

ORIGINAL RESEARCH
published: 10 March 2022
doi: 10.3389/fphys.2022.837798

Sleeve Gastrectomy-Induced AMPK Activation Attenuates Diabetic Cardiomyopathy by Maintaining Mitochondrial Homeostasis *via* NR4A1 Suppression in Rats

*Songhan Li[1], Shuohui Dong[1], Qian Xu[1], Bowen Shi[1], Linchuan Li[2], Wenjie Zhang[1], Jiankang Zhu[2], Yugang Cheng[2], Guangyong Zhang[2] and Mingwei Zhong[1]**

[1] Department of General Surgery, Shandong Qianfoshan Hospital, Cheeloo College of Medicine, Shandong University, Jinan, China, [2] Department of General Surgery, The First Affiliated Hospital of Shandong First Medical University, Jinan, China

OPEN ACCESS

Edited by:
Yanmin Wang,
California Medical Innovations Institute, United States

Reviewed by:
Oscar Lorenzo,
Health Research Institute Foundation Jimenez Diaz (IIS-FJD), Spain
Esma Nur Okatan,
University of Istinye, Turkey

***Correspondence:**
Mingwei Zhong
zmwgz@126.com

Specialty section:
This article was submitted to Metabolic Physiology, a section of the journal Frontiers in Physiology

Received: 17 December 2021
Accepted: 17 February 2022
Published: 10 March 2022

Citation:
Li S, Dong S, Xu Q, Shi B, Li L, Zhang W, Zhu J, Cheng Y, Zhang G and Zhong M (2022) Sleeve Gastrectomy-Induced AMPK Activation Attenuates Diabetic Cardiomyopathy by Maintaining Mitochondrial Homeostasis via NR4A1 Suppression in Rats. Front. Physiol. 13:837798. doi: 10.3389/fphys.2022.837798

Diabetic cardiomyopathy (DCM) is characterized by impaired diastolic and systolic myocardial performance and is a major cause of morbidity and mortality in patients with diabetes. Surgical bariatric procedures, such as sleeve gastrectomy (SG), result in remission of type 2 diabetes (T2DM) and have benefits with myocardial function. Maintaining cardiac mitochondrial homeostasis is a promising therapeutic strategy for DCM. However, whether SG surgery affects mitochondrial function and its underlying mechanism remains unclear. This study aimed to investigate the effect of SG surgery on mitochondrial homeostasis and intracellular oxidative stress in rats with DCM. We also examined cellular phenotypes and molecular mechanisms in high glucose and high fat-stimulated myocytes. The rat model of DCM was established by high-fat diet feeding and low-dose streptozotocin injection. We observed a remarkably metabolic benefit of SG, including a reduced body weight, food intake, blood glucose levels, and restored glucose tolerance and insulin sensitivity post-operatively. Also, SG ameliorated the pathological cardiac hypertrophy, myocardial fibrosis and the dysfunction of myocardial contraction and diastole, consequently delayed the progression of DCM. Also, SG restored the mitochondrial dysfunction and fragmentation through the AMPK signaling activation mediated nuclear receptor subfamily 4 group A member 1 (NR4A1)/DRP1 suppression *in vivo*. H9c2 cardiomyocytes showed that activation of AMPK could reverse the mitochondrial dysfunction somehow. Collectively, our study provided evidence that SG surgery could alleviate mitochondrial dysfunction

in DCM. Moreover, AMPK-activated NR4A1/DRP1 repression might act as a significant reason for maintaining mitochondrial homeostasis in the myocardium, thus contributing to morphological and functional alleviation of DCM.

Keywords: sleeve gastrectomy, diabetic cardiomyopathy, mitochondrial homeostasis, oxidative stress, AMPK, NR4A1

INTRODUCTION

Diabetic cardiomyopathy (DCM) is defined as a distinct disease entity that occurs in patients with diabetes mellitus (DM) independent of coronary artery disease, hypertension, or valvular heart disease (Jia et al., 2018; Tan et al., 2020). During the early phases of diabetes, an absence of insulin or insulin resistance initiates a metabolic alteration in cardiomyocytes, which leads to the activation of fatty acid uptake and β-oxidation to ensure adequate adenosine-triphosphate (ATP) generation. However, as the disease progresses, β-oxidation cannot sufficiently utilize all available fatty acids, resulting in intracellular lipid collection and lipotoxicity. Increased fatty acid concentrations subsequently result in mitochondrial dysfunction and an elevated accumulation of reactive oxygen species (ROS) (Tan et al., 2020). Ultimately, these pathological transformations result in cardiomyocyte death, inflammation, and fibrotic remodeling (Jia et al., 2018). Adenosine monophosphate-activated protein kinase (AMPK) plays an important role in metabolic diseases (Hoffman et al., 2015). Under DCM conditions, the activation of energy deprivation sensors, sirtuin-1 (SIRT1) and phosphorylation of AMPK can promote the removal of dysfunctional mitochondria and peroxisomes to reverse the development of cardiomyopathy (Packer, 2020a). Thus, AMPK signaling shows promising potential as a novel target for DCM treatment.

At present, bariatric surgery, such as sleeve gastrectomy (SG), is one of the most prevalent and valid therapies for obesity and related metabolic disorders (Ulrich-Lai and Ryan, 2014). Ample evidence has shown that SG leads to efficient remission of type 2 diabetes mellitus (T2DM) and its related complications (Mingrone et al., 2015; Rubino et al., 2016). Several studies have revealed that SG has benefits in terms of systolic and diastolic myocardial function in patients with DCM and in rodent models (Leung et al., 2016; Huang et al., 2018). In addition, bariatric surgery can facilitate Ca^{2+} homeostasis and attenuate myocardial autophagy, restore myocardial glucose uptake with myocardial glucose transporter four translocation, and activate MAPK signaling pathway to alleviate DCM (Huang et al., 2018, 2019; Xu et al., 2021). However, it remains unclear whether SG ameliorates DCM by maintaining mitochondrial homeostasis, and further supporting evidence is required.

To clarify these issues, we established a DCM rat model through high-fat-diet (HFD) administration and intraperitoneal injection of low-dose streptozotocin (STZ), with chow diet-fed rats serving as negative controls. SG or sham surgery was performed to investigate the effects of SG on mitochondrial structure and function in rats with DCM. Moreover, we determined that AMPK signaling-mediated nuclear receptor subfamily 4 group A member 1 (NR4A1) suppression might induce mitochondrial homeostasis to protect cardiomyocytes against diabetes-induced mitochondrial dysfunction and oxidative stress. Furthermore, the metabolic phenotypes and protective role of the AMPK pathway were examined in high glucose (HG) and palmitate (PA)-stimulated myocytes.

MATERIALS AND METHODS

Reagents and Antibodies

D-Glucose (50-99-7) and STZ (S0130) were purchased from Sigma, Shanghai, China. We also purchased A-769662 (HY-50662) and 10-*N*-nonyl acridine orange (NAO; HY-D0993) from MedChemExpress, Shanghai, China. A hematoxylin and eosin staining kit (C0105S), an Oil Red O staining kit (C0158S), an ATP detection kit (S0026), a JC-1 staining kit (C2003S), and 2,7-dichlorodihydrofluorescein diacetate (DCFH-DA) probes (S0033S) were purchased from Beyotime, Shanghai, China. A diaminobezidin (DAB) staining kit (ZLI-9017) was purchased from ZSGB-BIO, China. A Mito-Tracker staining kit, Cambridge, United Kingdom (ab112145) was purchased from Abcam (Cambridge, United Kingdom). A total protein extraction kit for muscle (SA-06-MS) and a mitochondria isolation kit for muscle tissues/cultured muscle cells (MM-038) was purchased from Invent Biotechnologies, Beijing, China. A bicinchoninic acid (BCA) protein assay kit (KGP902) was purchased from KeyGEN, Jiangsu, China. TRIzol reagent (15596018) was purchased from Invitrogen, Carlsbad, CA, United States. A ReverTra Ace qPCR RT kit (FSQ-101) and SYBR Green Real-time PCR Master Mix (QPK-201) were purchased from Toyobo, Japan. The following antibodies were used: collagen I (Affinity, AF7001), collagen III (Affinity, AF0136), NR4A1 (Proteintech, 25851-1-AP), DRP1 (Affinity, DF7037), nuclear factor erythroid-2-related factor 2 (NRF2; Proteintech, 16396-1-AP), heme oxygenase 1 (HO-1; Proteintech, 27282-1-AP), CPT-1α (Proteintech, 15184-1-AP), PPARα (Proteintech, 15540-1-AP), superoxide dismutase-2 (SOD2; Abcam, ab68155), ACC1 (Proteintech, 21923-1-AP), phosphate-ACC1 (CST, 11818), AMPKα (CST, 5832), phosphate-AMPK (CST, 50081), SIRT1 (Proteintech, 13161-1-AP), NDUFB8 (Abcam, ab192878), SDHB (Abcam, ab175225), UQCRC2 (Proteintech, 14742-1-AP), MTCO1 (Abcam, ab14705), ATP5A (Proteintech, 14676-1-AP), HSP60 (Proteintech, 15282-1-AP) and β-Tubulin (Proteintech, 10094-1-AP).

Cells Culture

The H9c2 rat embryonic cardiomyocyte line was donated by the Key Laboratory of Cardiovascular Remolding and Function Research of Shandong University (Jinan, China) and was

validated by STR profiling. H9c2 cells were cultured in HG Dulbecco's modified Eagle's medium (DMEM; Gibco, Shanghai, China) supplemented with 10% (v/v) fetal bovine serum (Gibco, Shanghai, China), 100 U/mL penicillin, and 100 mg/mL streptomycin (KeyGEN, Jiangsu, China) at 37°C in a 5% CO_2 humidified incubator. The cells were passaged every 2–3 days using 0.25% trypsin-EDTA for dissociation. To study the effects of high glucose (HG) and high fat conditions on H9c2 cells *in vitro*, cells were starved for 12 h and treated with 33.3 mM D-glucose (Sigma, Shanghai, China) and 500 μM palmitate (PA, Sigma, Shanghai, China) for 48 h. Furthermore, to determine the role of the AMPK pathway in H9c2 cells cultured under HG and high fat conditions, 10 μM A-769662, an AMPK activator (MedChemExpress, Shanghai, China), was added for 48 h.

Animals

Male Wistar rats at the age of about 6 weeks were purchased from Beijing Weitong Lihua Experimental Animal Technology (Beijing, China) and housed in the Animal Center of Shandong Qianfoshan Hospital affiliated to Shandong University. Rats were raised in an environment with access to food and water under 12-h light/dark cycle at a constant temperature of 22°C. After 1 week of acclimatization, rats were randomly separated into three groups; one group was fed with conventional feed (control), whereas the other two groups were fed an HFD (60% of calories as fat; Xietong, Nanjing, China) for 4 weeks to induce obesity and insulin resistance. To further establish the DCM rat model, we intraperitoneally injected rats with STZ (Sigma, Shanghai, China) dissolved in sodium citrate buffer (pH 4.5; Solarbio, Beijing, China) at a dose of 35 mg/kg after 12 h fasting. One week after STZ injection, fasting blood glucose (FBG) level exceeding 11.1 mmol/L was considered to be indicative of successful modeling. All procedures were approved by the Institutional Animal Care and Use Committee of Shandong Qianfoshan Hospital affiliated to Shandong University. All animal studies complied with relevant ethical regulations for animal testing and research.

Surgical Procedures

The established T2DM rat models were subjected to SG or sham surgery randomly. Briefly, rats were fed a liquid diet with 10% Ensure (Abbott Laboratories, Abbott Park, IL, United States) for 48 h, and they underwent fasting for 12 h before surgery. After administration of anesthesia with isoflurane (3% isoflurane for induction and 2% isoflurane for maintenance), SG and sham surgery were performed according to the standard process (Cheng et al., 2019), SG was started with a 4-cm midline abdominal incision at the xiphoid process, after ligation and transection of the vessels of the greater curvature, the greater curvature of the stomach from the cardia to the pylorus was separated. Entire glandular stomach and most of the gastric body was excised, leaving approximately 30% volume of the total stomach. Residual stomach was interruptedly sutured with 7–0 silk and abdominal was closed with 5–0 silk suture after careful examination. As for sham surgery, the abdomen was incised for the exposure of the stomach, esophagus, and small intestine. No other procedure was performed and operative time was prolonged to induce a comparable degree of anesthetic stress to the operated rats. The sham surgery group was used to eliminate the effects of surgical stress and anesthesia. After surgery, the rats were put into separate cages, and the diet was gradually transitioned from a liquid diet to a chow diet. Vital signs were monitored, and surgery-related complications were closely detected. Food intake and body weight were recorded every week. All surgical procedures complied with relevant ethical regulations for animal testing and research.

Oral Glucose Tolerance Test, Insulin Tolerance Test, and Homeostasis Model of Assessment for Insulin Resistance Index

To assess insulin sensitivity, an oral glucose tolerance test (OGTT) and insulin tolerance test (ITT) were performed and homeostasis model of assessment for insulin resistance index (HOMA-IR) was measured before surgery and 8 weeks after surgery. Blood glucose level from the rat tail vein was detected using a glucometer (ACCU-CHEK Performa; Roche, Shanghai, China) at baseline and 10, 30, 60, and 120 min after the administration of intragastric gavage of 20% glucose (1 g/kg) for the OGTT or intraperitoneal injection of human insulin (0.5 IU/kg) for the ITT. HOMA-IR was evaluated using the following formula: HOMA-IR = fasting plasma glucose (mmol/L) × fasting insulin (mIU/L)/22.5.

Assessment of Cardiac Function

To assess the cardiac function of the rats, transthoracic echocardiography imaging was performed on 2% isoflurane-anesthetized rats using a VEVO 3100 ultrasound machine (VisualSonics, Toronto, ON Canada). The main parameters included left ventricular end-diastolic diameter (LVEDd), left ventricular ejection fraction (LVEF), fractional shortening (FS), and early to late mitral diastolic flow ratio (E/A).

Histology and Immunohistochemistry

After the rats were sacrificed, fresh myocardial tissue samples were fixed in formalin to prepare paraffin-embedded blocks, which were cut into 5-μm paraffin sections for histological analysis. The paraffin sections were stained with hematoxylin and eosin (H&E), Masson's trichrome, Sirius red, and wheat germ agglutinin (WGA) to assess the standard histology, distribution of collagen, extent of fibrosis, and morphology of the cardiomyocyte membrane, respectively. For IHC, the paraffin sections were sequentially subjected to dewaxing, dehydration with gradient alcohol, microwave thermal repair in citrate buffer (0.01 M, pH 6.0), endogenous peroxidase blocking, and blocking in 10% goat serum in phosphate-buffered saline. The sections were then incubated with primary antibodies, anti-collagen I (Affinity, 1:1,000) or collagen III (Affinity, 1:500), overnight at 4°C. The next day, sections were incubated with HRP-conjugated anti-rabbit IgG (ZSGB-BIO, Beijing, China), and reactions were detected by DAB staining (ZSGB-BIO, Beijing, China). The nuclei were stained

with hematoxylin and differentiated in 1% acid alcohol, after which the sections were rinsed with running water. Finally, the slides were sealed with a neutral gel. Images were acquired using an Axio Scope A1 microscope (Zeiss, Oberkochen, Germany).

Mitochondrial Visualization by Transmission Electron Microscopy and MitoTracker

One-millimeter cubes of left ventricular myocardial tissue were pre-fixed in 2.5% glutaraldehyde overnight at 4°C and post-fixed in 1% osmium tetroxide for 2 h at 4°C. Fixed samples were subjected to dehydration, embedding, polymerization, and ultrathin section preparation, followed by staining with uranyl acetate and lead citrate. Finally, images were acquired using a Hitachi HT-7800 transmission electron microscope (Hitachi, Tokyo, Japan).

To visualize the mitochondria of the H9c2 cells after the HG and high fat conditions treatment, H9c2 cells were incubated with a solution of MitoTracker (Abcam, Cambridge, United Kingdom) for 1 h at 37°C when the cells reached 80% confluency. After incubation, images were acquired using an Axio Scope A1 microscope (Zeiss, Oberkochen, Germany).

Protein Extraction and Western Blot Analysis

Heart tissue proteins were extracted using a total protein extraction kit for muscles (Invent Biotechnologies, Beijing, China). Isolation of mitochondria was prepared using a mitochondria isolation kit for muscle tissues/cultured muscle cells (Invent Biotechnologies, Beijing, China). Cell proteins were lysed in RIPA lysis buffer (Solarbio, Beijing, China) with a protease inhibitor (KeyGEN, Jiangsu, China) when confluency reached 80%. The lysates of the tissue samples or cells were then centrifuged at 12,000 × *g* for 20 min, and the supernatant was collected. Protein concentrations were determined using a BCA protein assay kit (KeyGEN, Jiangsu, China). Boiled protein solutions were separated by 10% SDS-PAGE (Bio-Rad, Hercules, United States) and transferred to a 0.45-μm PVDF membrane (Millipore, Cork, Ireland). After 1-h blocking in 5% skim milk powder (Beyotime, Shanghai, China), the membrane was incubated with the following primary antibodies at 4°C overnight: NR4A1 (Proteintech, 1:1,000), DRP1 (Affinity, 1:1,000), NRF2 (Proteintech, 1:2,000), HO-1 (Proteintech, 1:1,000), CPT-1α (Proteintech, 1:1,000), PPARα (Proteintech, 1:1,000), SOD2 (Abcam, 1:5,000), ACC1 (Proteintech, 1:1,000), phosphate-ACC1 (CST, 1:1,000), AMPK (CST, 1:1,000), phosphate-AMPK (CST, 1:500), SIRT1 (Proteintech, 1:1,000), NDUFB8 (Abcam, 1:5,000), SDHB (Abcam, 1:100,000), UQCRC2 (Proteintech, 1:1,000), MTCO1 (Abcam, 1:1,000), ATP5A (Proteintech, 1:1,000), HSP60 (Proteintech, 1:10,000) and β-Tubulin (Proteintech, 1:5,000). The secondary antibody was incubated for 1.5 h at room temperature. Proteins were detected by enhanced chemiluminescence (Millipore, Billerica, MA, United States) using an LI-COR Odyssey Imager (LI-COR Biosciences, Lincoln, United States).

RNA Extraction and Reverse Transcription-Quantitative Polymerase Chain Reaction

Total RNA was extracted from heart tissues and H9c2 cells using TRIzol reagent (Invitrogen, Carlsbad, CA, United States), and RNA concentrations were measured using a NanoDrop spectrophotometer (NanoDrop Technologies, Wilmington, United States). cDNA synthesis was performed using a ReverTra Ace qPCR RT kit (Toyobo, Osaka, Japan), and RT-qPCR was performed using SYBR Green Realtime PCR Master Mix (Toyobo, Osaka, Japan) on a Roche LightCycler 480 II instrument (Roche, Basel, Switzerland). Relative mRNA quantification was performed using the ΔΔCt method, and *Tubb3* was used as an internal reference. Detailed primer sequences are listed in **Table 1**.

Mitochondrial DNA Quantification

Total DNA was extracted using a DNeasy kit (Qiagen, Hilden, Germany). RT-qPCR was performed using SYBR Green Real-time PCR Master Mix (Toyobo, Osaka, Japan) on a Roche LightCycler 480 II instrument (Roche, Basel, Switzerland). The mitochondrial gene *Cox1* and nuclear gene *Hbb* were selected as representative genes of mitochondrial and nuclear DNA, respectively.

Adenosine-Triphosphate Measurements

Fresh myocardial tissue samples (20 mg) were homogenized for tissue lysate extraction, and the tissue lysates were centrifuged at 12,000 × *g* for 5 min at 4°C. Myocardial tissue lysates were used to detect the ATP content (Beyotime, Shanghai, China) and protein concentrations. The obtained supernatant was mixed and incubated with the detection solution, and the ATP concentrations were measured using a luminometer. To normalize the results, the ATP levels were normalized to total protein concentrations (BCA assays).

TABLE 1 | Primers used for polymerase chain reaction (PCR).

Experiment	Gene	Primer sequence (5′ → 3′)
Mitochondrial DNA PCR (mtDNA PCR)	*Cox1*	GAGCAGGAATAGTAGGGA GTGTCTGATATTGGGTTAT
	Hbb	GGTGAACCCTGATGATGT TTTAGTGGTACTTGTGAGCC
RTq-PCR	*Nr4a1*	GCGGCTTTGGTGACTGGATAGAC AGTGATGAGGACCAGAGCAGACAG
	Drp1	ACAGCGTCCCAAAGGCAGTAATG CCATGTCCTCGGATTCAGTCAGAAG
	Sirt1	TAGGTTAGGTGGCGAGTA CAGCCTTGAAATCTGGGT
	Sod2	TCCCTGACCTGCCTTACGACTATG TCGTGGTACTTCTCCTCGGTGAC
	Hmox1	ACCTCCTCATTGTTATTGG TACTCGCCACCTAACCTA
	Nrf2	GCCTTCCTCTGCTGCCATTAGTC TGCCTTCAGTGTGCTTCTGGTTG
	Tubb3	CGTCCACCTTCATCGGCAACAG TCGGCCTCGGTGAACTCCATC

Intracellular Reactive Oxygen Species Assay

When H9c2 cells in 6-well plates reached 80% confluency, they were incubated with 2 mL total DMEM containing 10 μM DCFH-DA probes (Beyotime, Shanghai, China) for 1 h at 37°C. The harvested cells were kept on ice and immediately detected by flow cytometry. The FITC-fluorescent signal of 20,000 events was recorded using a BD FACSAria II instrument (BD, Oxford, United Kingdom). Data were analyzed using the FlowJo software.

10-*N*-Nonyl Acridine Orange Staining for Cardiolipin

To detect intracellular cardiolipin content, H9c2 cells were incubated with 100 μM NAO (a highly specific fluorescent probe for cardiolipin) (MedChemExpress, Shanghai, China) for 20 min at 37°C. After incubation, images were acquired using an Axio Scope A1 microscope (Zeiss, Oberkochen, Germany).

Mitochondrial Membrane Potential Detection

To further assess the mitochondria of the H9c2 cells, mitochondrial membrane potential was determined with JC-1 staining. The H9c2 cells were seeded into 6-well plates and grown to 80% confluency, and then the cells were stained with the JC-1 staining kit (Beyotime, Shanghai, China) in accordance with the manufacturer's instructions. The cell images were acquired using an Axio Scope A1 microscope (Zeiss, Oberkochen, Germany).

Statistical Analysis

All data are shown as the mean ± standard deviation. A two-tailed Student's *t*-test was used to compare variables between the two groups, and one-way or two-way analysis of variance was performed for multi-group comparisons. Statistical significance was set at $P < 0.05$. Statistical details are included in the respective figure legends.

RESULTS

General Characteristics and Glucose Homeostasis in Rats With Obesity and Type 2 Diabetes Mellitus Was Significantly Ameliorated After Sleeve Gastrectomy

As illustrated by the body weight curves, body weight in the sham surgery group and the SG group both bottomed out at 1 week after surgery and gradually increased thereafter. The sham and SG groups showed persistent differences (**Figure 1A**). Food intake after surgery was measured to determine changes in feeding behavior. The sham and SG groups consumed fewer calories during the first week after surgery, which may have resulted from the transient surgical stress. However, rats in the sham group were only hypophagic during the first week, while the appetitive deficit of rats in the SG group lasted for a long time, which enabled the maintenance of a reduced body weight (**Figure 1B**). To assess the effects of SG on glucose homeostasis, fasting blood glucose (FBG) concentrations were regularly recorded (**Figure 1C**). The FBG level diminished during the initial 14 days and remained stable thereafter. Rodents in the SG group displayed improvements in the capability to clear the oral gavage of glucose from blood, reflected as a 38% drop in the area under the curve (AUC) compared with sham-operated controls. An insulin tolerance test was performed, and it showed a lower AUC in SG rodents than in the SHAM group, demonstrating that SG further developed insulin sensitivity (**Figures 1D,E**). The HOMA-IR values fundamentally decreased after SG, which is consistent with the results above (**Figure 1F**).

Reversion of Cardiac Dysfunction After Sleeve Gastrectomy

Echocardiographic assessment was done 2 months post-surgical procedure to survey heart function (**Figure 2A**). Rats that underwent sham surgery had a higher LVEDd, more prominent impaired LVEF, FS, and a higher E/A proportion compared to those in the control group. Echocardiographic examination revealed systolic and diastolic dysfunctions in the sham group. Nevertheless, in contrast to the sham group, it can be seen that SG surgery moderated these negative changes, as proven by the fundamentally diminished LVEDd with a reestablished LVEF, FS, and E/A proportion (**Figures 2B–E**).

Myocardial Remodeling Was Reversed After Sleeve Gastrectomy

Diabetic cardiomyopathy is characterized by structural and functional derangement of myocardial tissue, comprising hypertrophy, myocardial fibrosis, and contractile dysfunction in both the diastolic and systolic phases. H&E staining, together with WGA-stained cardiomyocyte outlines, showed hypertrophy of cardiomyocytes in the sham group, which was attenuated after SG (**Figures 3A–C**). Sirius red and Masson's trichrome staining revealed a rising level of cardiac fibrosis in the sham group, although SG surgery eased fibrosis (**Figures 3D–F**). In addition, IHC staining of collagen I and collagen III increased collagen deposition in the sham group, which was reversed after SG operation (**Figures 3G,H**). These results suggested that SG strikingly reversed DCM-induced myocardial remodeling.

Sleeve Gastrectomy Ameliorated Oxidative Stress in the Cardiac Tissue of Diabetic Cardiomyopathy Rats

It is well known that T2DM could increase the burden of oxidative stress (Civitarese et al., 2010). The rising generation of ROS and disabled clearance of ROS appear to contribute to the pathological progression of DCM (Huynh et al., 2014). Western blotting showed that multiple anti-oxidative proteins, including NRF2, SOD2, and HO-1, were suppressed in the sham rats and were upregulated after SG surgery (**Figure 4A**). The real-time PCR analysis yielded consistent results (**Figure 4B**). These data suggest that SG surgery could partially prevent oxidative stress in the myocardial tissues of rats with DCM.

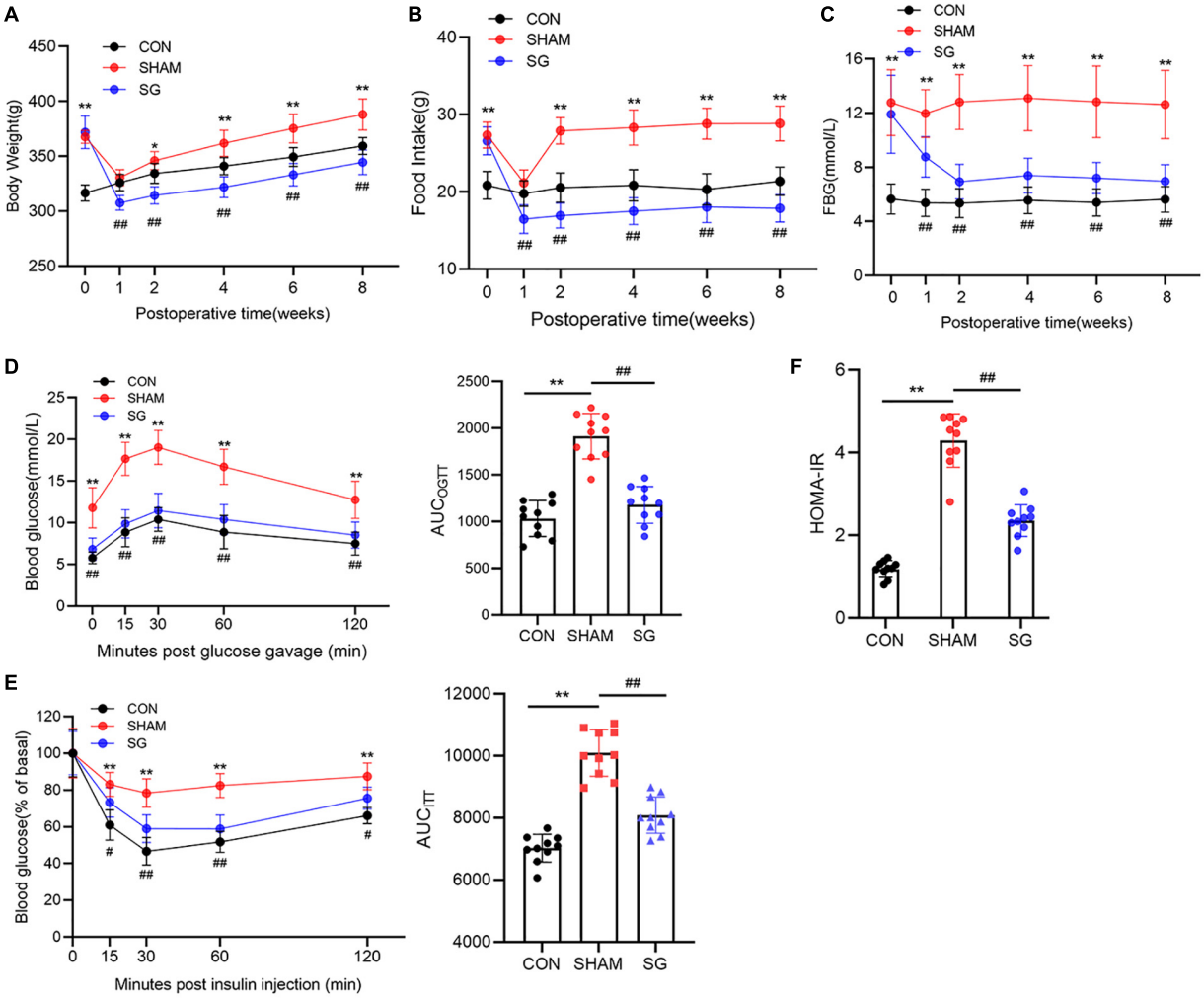

FIGURE 1 | Metabolic alternations of sleeve gastrectomy (SG) on body weight, feeding behavior and glucose homeostasis in STZ-induced diabetic rats. **(A)** Body weight, **(B)** food intake, **(C)** and fasting blood glucose. **(D)** Curves of OGTT and **(E)** ITT were recorded 8 weeks post-operatively. AUC_{OGTT} and AUC_{ITT} was computed, respectively. **(F)** Values of HOMA-IR at 8 weeks after SG surgery. Data are presented as mean ± SD. $^{*}P < 0.05$, $^{**}P < 0.01$ CON vs. SHAM; $^{\#}P < 0.05$, $^{\#\#}P < 0.01$ SG vs. SHAM. $n = 10$ in each group.

The Mitochondrial Function and Structure Were Improved With Sleeve Gastrectomy Performance

Reactive oxygen species are predominantly derived from the mitochondria in diabetes (Wang et al., 2017). We assessed mitochondrial structure and function. Transmission electron microscopy revealed disarranged sarcomeres, swollen mitochondria with disorganized cristae, and loss of intracellular substances in the heart of the sham group. In the SG group, layers of uniformly shaped mitochondria with copious and organized cristae intervened between regularly aligned myofibrils (**Figure 4C**). Heart tissues in the SG group showed higher ATP content than those in the sham-operated rats (**Figure 4D**). In addition, the copies of mtDNA in the myocardium were diminished with SG treatment compared to those in the sham group, indicating of a restoration of excessive mitochondrial fragmentation (**Figure 4E**). Consistently, we found that the proteins of respiratory complexes were upregulated after SG, indicating the restoration of oxidative phosphorylation (OXPHOS) (**Figure 4F**). Taken together, these results suggest that beneficial metabolic alterations may occur *via* the suppression of mitochondrial dysfunction after SG surgery.

Sleeve Gastrectomy Activated Adenosine Monophosphate-Activated Protein Kinase Pathway and Nuclear Receptor Subfamily 4 Group A Member 1 Suppression for the Restoration of Mitochondrial Homeostasis

Adenosine monophosphate-activated protein kinase has been proved to show a beneficial role of metabolic regulation

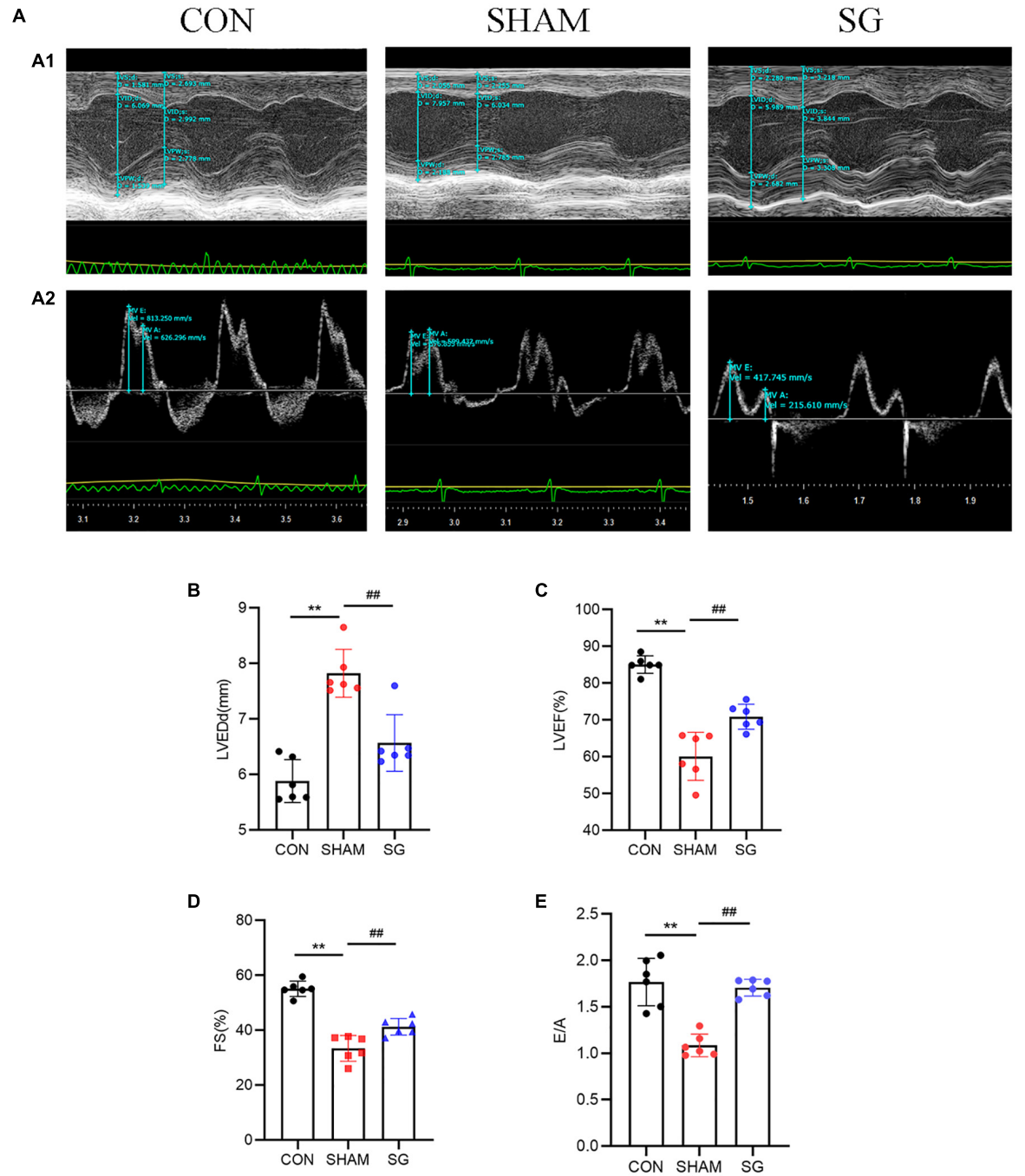

FIGURE 2 | Effects of sleeve gastrectomy (SG) on cardiac function in rat models. **(A)** Echocardiography. **(A1)** Representative images of M-mode echocardiograms, **(A2)** Pulse-wave Doppler echocardiograms showed mitral inflow. Echocardiographic measurements including **(B)** LVEDd, **(C)** LVEF, **(D)** FS and **(E)** ratio of E/A. Data are presented as mean ± SD. $^{**}P < 0.01$ CON vs. SHAM; $^{\#\#}P < 0.01$ SG vs. SHAM. $n = 6$ in each group.

in diabetes (Schaffer et al., 2015). Activation of the AMPK pathway suppresses NR4A1-mediated mitochondrial fission *via* DRP1 (Zhou et al., 2018; Wang et al., 2021). In this study, western blot showed that AMPK pathway was impaired in rats of DCM, as shown by decreased AMPK and ACC phosphorylation. Post-operatively, the AMPK pathway was activated in the heart tissues (**Figure 5A**). It has been reported that SIRT1, which can further downregulate NR4A1, can be activated by AMPK (Fulco et al., 2008; Qiang et al., 2011). Thus, we further determined the expression of SIRT1, NR4A1 and DRP1, and found that SIRT1 was overregulated after SG surgery, whereas the expression of NR4A1 and DRP1

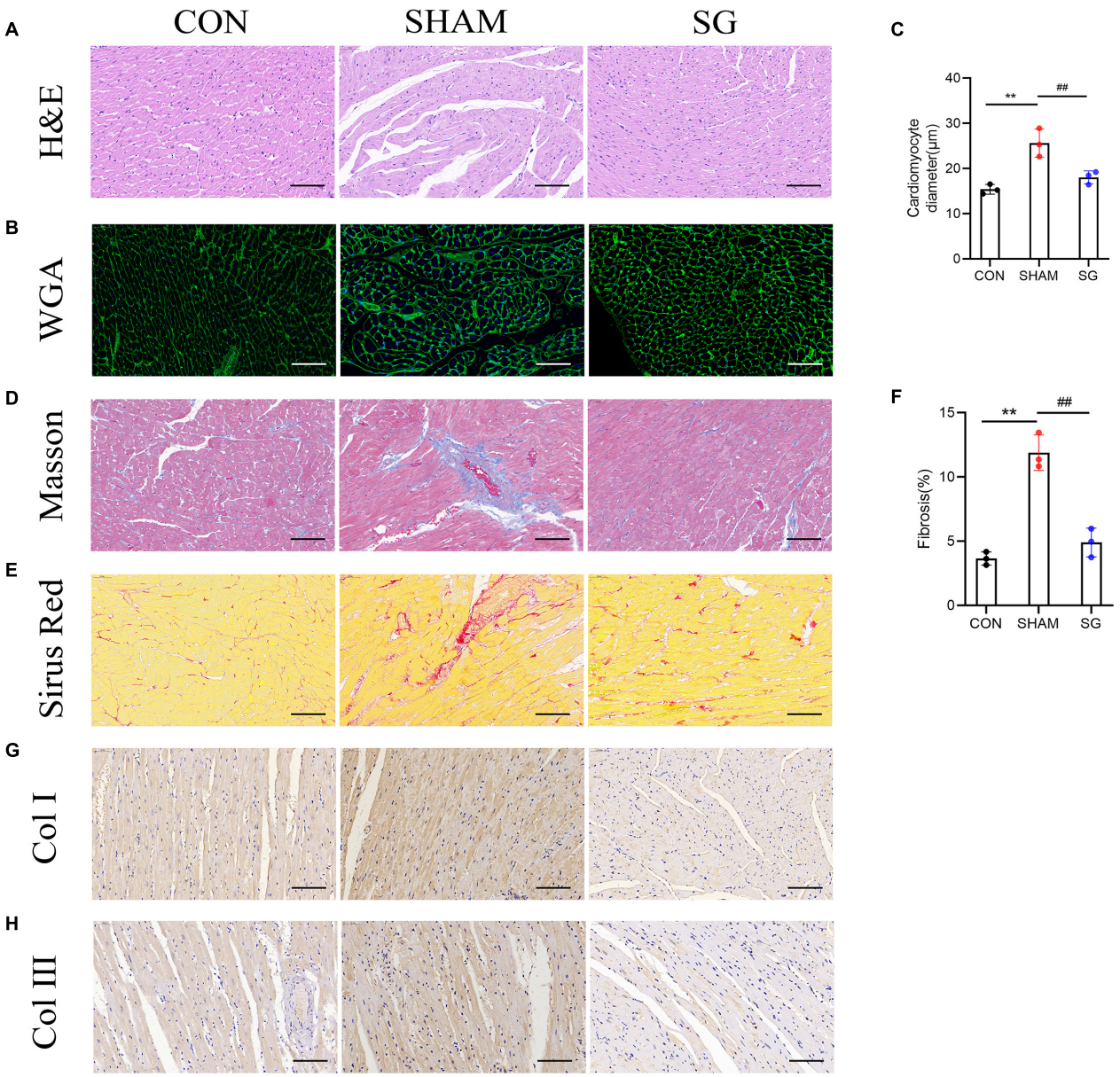

FIGURE 3 | Effects of sleeve gastrectomy (SG) on diabetic-induced cardiac remodeling. **(A)** H&E staining images of left ventricle. **(B)** Plasma membrane stained with WGA. **(C)** Mean diameters of cardiomyocytes in each group **(D)** staining of masson trichrome, of which dark blue indicated collagen fibers. **(E)** Sirus red staining identified the dense collagen staining. **(F)** The percentage of fibrosis was calculated. Immunohistochemical staining of panel **(G)** collagen I, **(H)** collagen III. Scale bar, 50 μm. Data are presented as mean ± SD. $^{**}P < 0.01$ CON vs. SHAM; $^{\#\#}P < 0.01$ SG vs. SHAM. $n = 3$ in each group.

in mitochondrial fractions was reduced post operation (**Figure 5B**). Similarly, real-time RT-PCR showed that the relative transcriptional levels of Sirt1, Nr4a1, and Drp1 were consistent with the protein levels (**Figure 5C**). Fatty acid oxidation in cardiomyocytes was enhanced after SG surgery, indicated by an increased expression of CPT-1α and PPARα (**Figure 5B**). Taken together, these results indicate that AMPK signaling activation and NR4A1 suppression may mediate the effect of SG on maintaining cardiac mitochondrial homeostasis.

Adenosine Monophosphate-Activated Protein Kinase Mediated the Protective Effect of Mitochondrial Function in H9c2 Cells

To further testify the role of AMPK signaling in DCM models, we stimulated H9c2 cells with HG along with PA to mimic the hyperglycemic and hyperlipidemia environment. A-769662, an AMPK activator, was used to evaluate the effects of AMPK on diabetic cardiomyocytes.

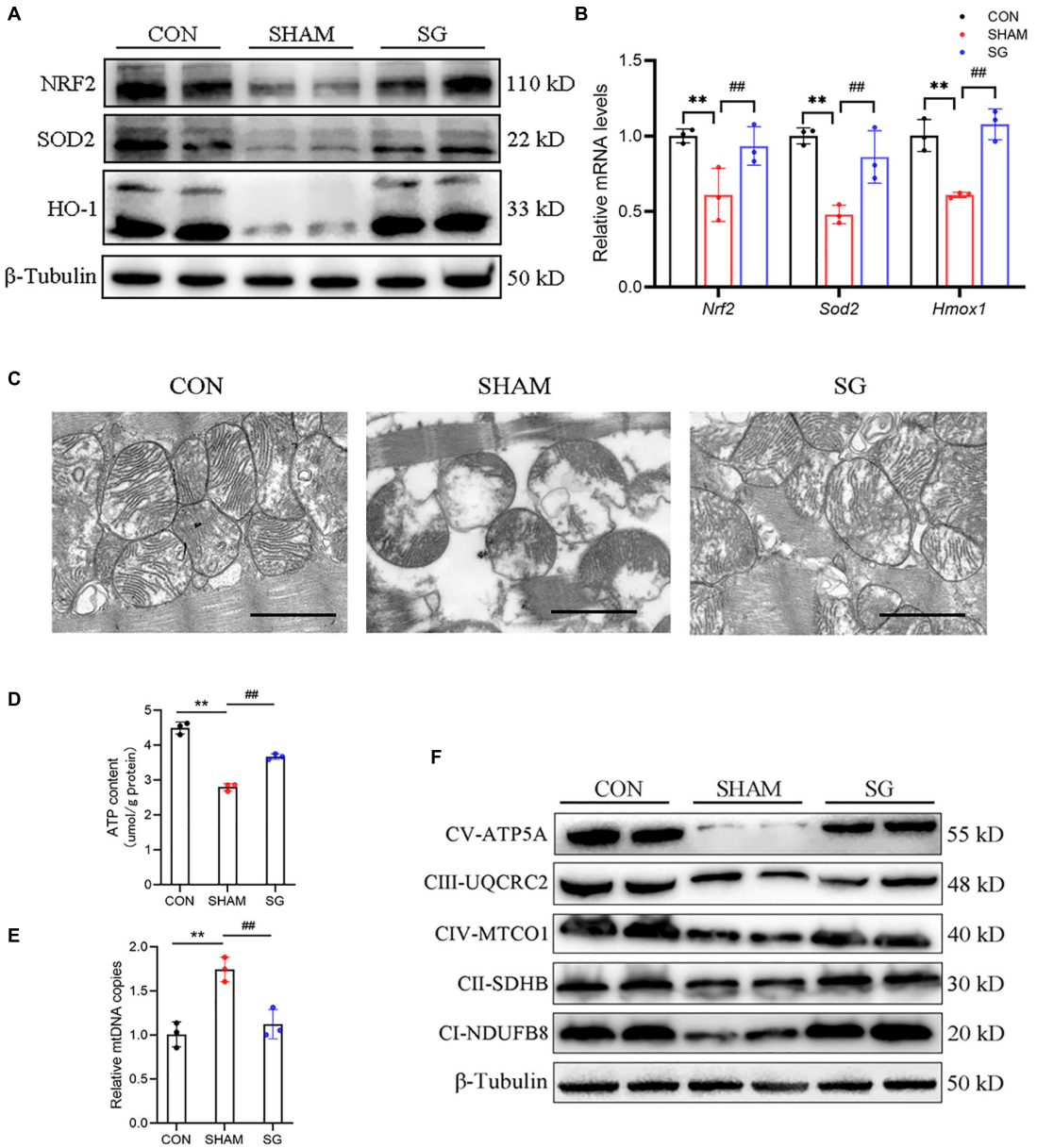

FIGURE 4 | Sleeve gastrectomy (SG) attenuates oxidative stress and improves mitochondrial function in diabetic cardiomyopathy (DCM). **(A)** Protein levels of anti-oxidation molecules shown by western blot. β-Tubulin was an internal reference control. **(B)** Relative mRNA levels of anti-oxidation genes shown by real-time RT-PCR. *Tubb3* served as a reference gene. **(C)** Representative transmission electron micrographs. Scale bar, 1 μm. **(D)** ATP content in heart tissues. **(E)** Relative mtDNA copies per nuclear genome. **(F)** Protein levels of OXHPOS complexes in each group. Data are presented as mean ± SD. $^{**}P < 0.01$ CON vs. SHAM; $^{\#\#}P < 0.01$ SG vs. SHAM. $n = 3$ in each group.

Our data revealed that the protein levels of p-AMPK and SIRT1 were downregulated under HG + PA stimulation and were restored with an AMPK activator. The protein levels of NR4A1 and DRP1 were up-regulated in the HG + PA condition, whereas they were suppressed by AMPK activation (**Figure 6A**). We also determined the intracellular ROS levels with a redox-sensitive fluorescent dye, DCFH-DA, using flow cytometry. HG + PA markedly upregulated the fluorescent staining of ROS, whereas ROS levels were partially cleared following AMPK activation (**Figure 6B**). The Mito-tracker probe was used to stain the morphology of the mitochondria, and our data revealed that mitochondria were impaired with HG + PA stimulus, which could be ameliorated by an AMPK activator (**Figure 6C**). Cardiolipin (CL) is vital for oxidative phosphorylation because its oxidation is related to ROS accumulation and mitochondrial dysfunction (Li et al., 2010). Using NAO fluorescent staining, we found that oxidative damage to the CL was suppressed by AMPK activation (**Figure 6D**). Mitochondrial fission has been reported

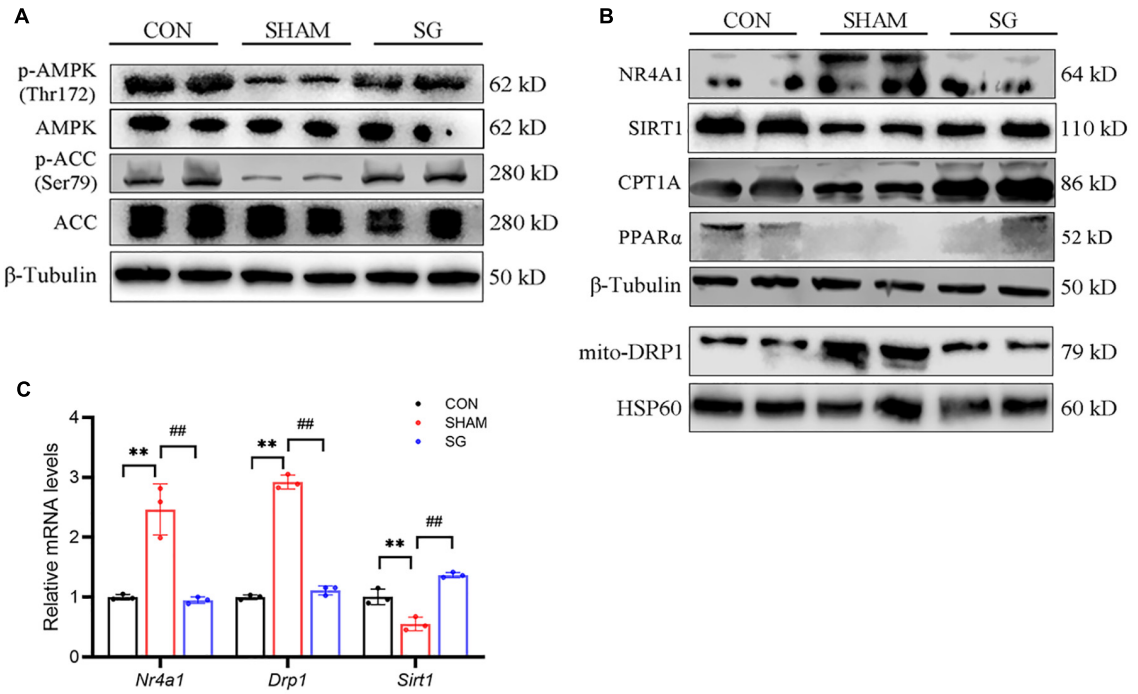

FIGURE 5 | Sleeve gastrectomy (SG) activated adenosine monophosphate-activated protein kinase (AMPK) and depressed NR4A1/DRP1 expression for the restoration of mitochondrial homeostasis. **(A)** Protein levels of AMPK signaling shown by western blot. β-Tubulin was an internal reference control. **(B)** Western blot analysis of NR4A1/DRP1 signaling and CPT1α and PPARα. β-Tubulin was an internal reference control. **(C)** Relative mRNA levels of Nr4a1/Drp1 shown by real-time RT-PCR. *Tubb3* served as a reference gene. $^{**}P < 0.01$ CON vs. SHAM; $^{\#\#}P < 0.01$ SG vs. SHAM. $n = 3$ in each group.

to induce depolarization of the mitochondrial membrane (Baixauli et al., 2011). Thus, we surveyed membrane potential using JC-1 fluorescent dye and found that AMPK protected cardiomyocytes from membrane potential disruption induced by HG + PA treatment (**Figures 6E,F**). These data suggest that AMPK preserves mitochondrial function in cardiomyocytes *in vitro*.

DISCUSSION

Diabetic cardiomyopathy is a pivotal cause of morbidity and mortality in patients with T2DM, and is defined by morphological, functional, and metabolic transformations in the heart as a significant cardiovascular complication in diabetic patients (Adeghate and Singh, 2014; Bugger and Abel, 2014). Ample evidence has showed that bariatric surgery had significant metabolic advantages in obesity, T2DM, and following complications (Ikramuddin et al., 2018; McGlone et al., 2020). In the present study, we induced DCM rat models by HFD feeding followed with low-dose intraperitoneal injection of STZ. We performed SG surgery or sham surgery in rats with DCM and compared the general metabolic characteristics to ensure that SG surgery had beneficial effects in the remission of T2DM and obesity. Additionally, as shown by echocardiography, SG partially restored cardiac function in rats with DCM. Histological assessment indicated reversion of myocardial remodeling and cardiac hypertrophy after SG surgery. We detected several indicators of oxidative stress in the myocardium, suggesting that SG surgery remarkably relieved the ROS burden in cardiac tissues. When emphasizing mitochondria, SG surgery imposed favorable effects on both the structure and function of the mitochondria. Further mechanistic *in vivo* and *in vitro* studies revealed that AMPK-mediated NR4A1 repression and subsequent mitochondrial improvement might be the underlying mechanism of the therapeutic effect of SG surgery on DCM.

In the present study, we have adopted the routine HFD feeding combined with low-dose STZ injection intraperitoneally to establish the DCM model. Because it mimics the regular pathological progression of T2DM, this technique has been widely utilized by numerous specialists (Reed et al., 2000; Sahin et al., 2007; Skovsø, 2014). In addition, this method is ordinarily adopted in the induction of DCM models (Ménard et al., 2010; Ti et al., 2011). In accordance with the findings of previous research (Chambers et al., 2011), metabolic improvement of SG procedure was observed in our study, shown by a decreased body weight, food intake, and FBG level and improved glucose tolerance and insulin sensitivity post-operatively. These data confirmed the impact of the SG operation (**Figure 1**).

Diabetic cardiomyopathy is initially characterized by diastolic dysfunction, which may precede systolic dysfunction (Brooks et al., 2008). Using cardiac echocardiography, cardiac function was identified in this study, and we found that diastolic and systolic function, which was impaired in DCM rats,

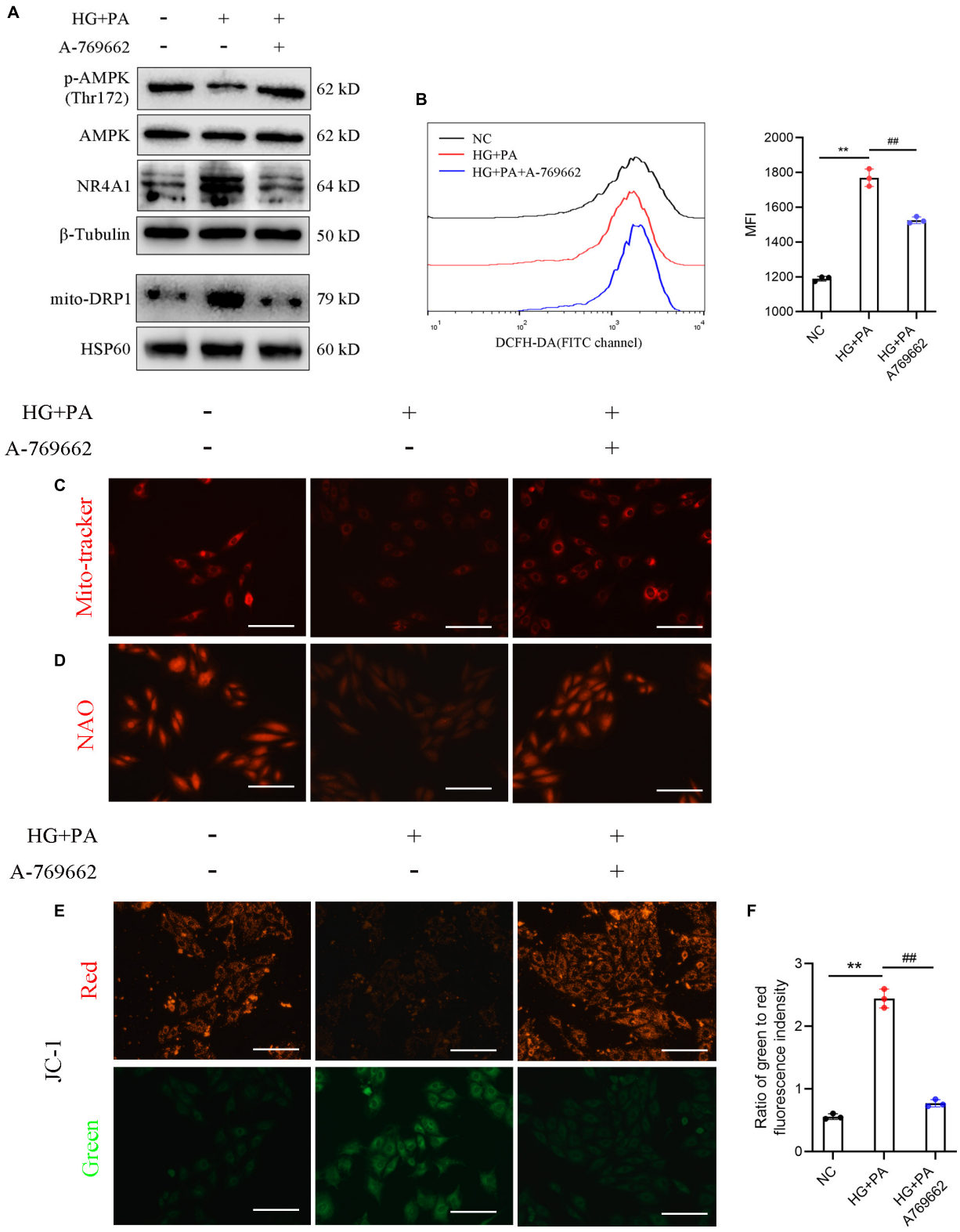

FIGURE 6 | Adenosine monophosphate-activated protein kinase (AMPK) mediated the protective effect of mitochondrial function in H9c2 cells. **(A)** Protein levels of AMPK signaling. β-Tubulin was an internal reference control. **(B)** Reactive oxygen species (ROS) levels detected by flow cytometry with DCFH-DA probe. **(C)** Mito-tracker staining and **(D)** 10-*N*-nonyl acridine orange (NAO) staining **(E)** membrane potential shown by the ratio of intensity with JC-1 dye at 529 nm (green) to 590 nm (red). $^{**}P < 0.01$ NC vs. HG + PA; $^{\#\#}P < 0.01$ HG + PA vs. HG + PA + A-769662. $n = 3$ in each group.

improved after SG surgery. The pathogenesis of DCM remains disputable, and several mechanisms have been proposed, including myocardial hypertrophy, fibrotic remodeling, oxidative stress, and superfluous lipid deposition. Myocardial hypertrophy contributes to impaired contractility and reduced myocardial compliance (Aneja et al., 2008). In this study, SG surgery significantly alleviated cardiac hypertrophy, as shown by the reduced diameters of the cardiomyocytes. Interstitial and perivascular fibrosis in heart biopsies contribute to the impairment of contractility (Regan et al., 1977). Excessive collagen deposition in both the interstitial and perivascular regions was strikingly reduced post-operatively. These data reveal that owing to morphological improvements, functional benefits were obtained with SG (**Figures 2**, **3**).

Mitochondrial dysfunction, abnormal mitochondrial ultrastructure, and the accumulation of oxidative stress have been reported to participate in the progression of DCM, characterized by impaired mitochondrial respiratory capacity and increased mitochondrial oxidative stress (Bugger and Abel, 2014). Under physiological conditions, mitochondrial fragmentation can increase ATP production to fulfill the energetic needs of the heart (Coronado et al., 2018). Nevertheless, superfluous mitochondrial fission causes disruption of the membrane potential, subsequently leading to mitochondrial dysfunction, cytochrome c leakage, and increased mitochondrial ROS accumulation (Veeranki et al., 2016; Ding et al., 2018). Our data confirmed that SG surgery could alleviate the abnormal mitochondrial ultrastructure, and could upregulate the impaired expression of anti-oxidative signaling proteins, which implied a clearance of overburdened ROS. In addition, our results showed that SG could decrease number of mtDNA copies, which might reveal the amelioration of excessive mitochondrial fragmentation or mitochondrial biogenesis and might be the key contributor to cardiac recovery. Also, ATP content was increased after SG performance, along with the fact that SG restored the expression of respiratory complexes in OXPHOS. That is, we determined that SG surgery suppressed pathologically excessive fragmentation in mitochondria and restored respiratory capability in DCM (**Figure 4**).

Previous studies have reported that SG can activate AMPK signaling in adipose and pancreatic beta cells to gain metabolic benefits (Liu et al., 2020; Li et al., 2021). SIRT1/AMPK activation ameliorated the development and progression of DCM (Packer, 2020b). In this study, we confirmed that SG promotes the activation of SIRT1/AMPK signaling. As has been shown in previous studies, AMPK can inhibit the expression of NR4A1, which seems as a culprit factor in the heart, as it promotes mitochondrial fragmentation and decreases the mitochondrial membrane potential to result in the disruption of mitochondrial homeostasis (Zhou et al., 2018; Wang et al., 2021). *In vivo* experiments showed that SG could decrease the expression of NR4A1 and DRP1, accompanied with enhanced fatty acid oxidation in cardiomyocytes. AMPK agonists suppress NR4A1 and DRP1 in *in vitro* models, along with a decrease in ROS levels and restoration of mitochondrial structure and homeostasis. Taken together, these data imply that the therapeutic effects of SG surgery on DCM may be mediated by restraining mitochondrial homeostasis. Moreover, *in vitro* findings suggested that AMPK/NR4A1 suppression-mediated mitochondrial homeostasis might be the underlying mechanism in the SG treatment of DCM (**Figures 5**, **6**).

Although the pathological progression of DCM is initiated and exacerbated by hyperglycemia and insulin resistance, blood glucose control has only limited effects on the alleviation of cardiovascular diseases (Brown et al., 2010). Additionally, a clinical trial showed that hypoglycemic agents, such as GLP-1R agonists and DPP-4 inhibitors, could not reduce the risk of heart failure (Murtaza et al., 2019). Therefore, we have speculated that despite the hypoglycemic effects of SG surgery, the favorable metabolic effects of SG on DCM have some deep mechanisms. Activation of AMPK signaling and restoration of mitochondrial homeostasis might be vital mechanisms.

This study has several limitations. Firstly, these results were based on an obese diabetic rat model; the relevance of this animal model with obese patients with DCM undergoing bariatric surgery needs to be further investigated. Secondly, the two general effects of SG are the weight loss and improvements in glucose metabolism, which both contribute to the amelioration of DCM development. So, it is tough to define which factor plays the most direct role. Experiments will be required in the future to directly associate SG with cardiac performance *via* AMPK activation.

Taken together, ROS overburden and mitochondrial dysfunction ascribing to NR4A1/DRP1 induced mitochondrial fission and fragmentation play significant roles in the progression of DCM. SG surgery could activate AMPK and decrease NR4A1 levels, correct mitochondrial dysfunction, and enhance myocardial energy production to protect against myocardial remodeling and dysfunction. Whether this restoration of mitochondrial homeostasis and its upstream mechanisms in SG operation could be used as a new therapeutic target for DCM remains to be elucidated.

DATA AVAILABILITY STATEMENT

The original contributions presented in the study are included in the article/supplementary material, further inquiries can be directed to the corresponding author.

ETHICS STATEMENT

The animal study was reviewed and approved by the Institutional Animal Care and Use Committee of Shandong Qianfoshan Hospital Affiliated to Shandong University.

AUTHOR CONTRIBUTIONS

SL, MZ, and GZ contributed to the conception of the study. SL, SD, QX, and BS performed the experiments. SL, LL, and WZ analyzed the data. SL and SD contributed to the drafting of the

work. JZ and YC helped to perform the analysis with constructive discussions. All authors contributed to the article and approved the submitted version.

FUNDING

This project was supported by the National Natural Science Foundation of China (Grant Nos. 82070869 and 81900705) and Major basic research project of Natural Science Foundation of Shandong Province (Grant No. ZR2020ZD15).

ACKNOWLEDGMENTS

We would like to thank Editage (www.editage.cn) for English language editing.

REFERENCES

Adeghate, E., and Singh, J. (2014). Structural changes in the myocardium during diabetes-induced cardiomyopathy. *Heart Fail Rev.* 19, 15–23. doi: 10.1007/s10741-013-9388-5

Aneja, W. H., Bansilal, S., Garcia, M. J., and Farkouh, M. E. (2008). Diabetic cardiomyopathy: insights into pathogenesis, diagnostic challenges, and therapeutic options. *Am. J. Med.* 121, 748–757. doi: 10.1016/j.amjmed.2008.03.046

Baixauli, F., Martín-Cófreces, N. B., Morlino, G., Carrasco, Y. R., Calabia-Linares, C., Veiga, E., et al. (2011). The mitochondrial fission factor dynamin-related protein 1 modulates T-cell receptor signalling at the immune synapse. *EMBO J.* 30, 1238–1250. doi: 10.1038/emboj.2011.25

Brooks, B., Ban, C. R., Swaraj, K., Yue, D. K., Celermajer, D. S., and Twigg, S. M. (2008). Diastolic dysfunction and abnormalities of the microcirculation in type 2 diabetes. *Diabetes Obes. Metab.* 10, 739–746. doi: 10.1111/j.1463-1326.2007.00803.x

Brown, L., Reynolds, R., and Bruemmer, D. (2010). Intensive glycemic control and cardiovascular disease: an update. *Nat. Rev. Cardiol.* 7, 369–375. doi: 10.1038/nrcardio.2010.35

Bugger, H., and Abel, E. D. (2014). Molecular mechanisms of diabetic cardiomyopathy. *Diabetologia* 57, 660–671. doi: 10.1007/s00125-014-3171-6

Chambers, P., Jessen, L., Ryan, K. K., Sisley, S., Wilson-Pérez, H. E., Stefater, M. A., et al. (2011). Weight-independent changes in blood glucose homeostasis after gastric bypass or vertical sleeve gastrectomy in rats. *Gastroenterology* 141, 950–958. doi: 10.1053/j.gastro.2011.05.050

Cheng, Y., Huang, X., Wu, D., Liu, Q., Zhong, M., Liu, T., et al. (2019). Sleeve Gastrectomy with Bypass of Proximal Small Intestine Provides Better Diabetes Control than Sleeve Gastrectomy Alone Under Postoperative High-Fat Diet. *Obes. Surg.* 29, 84–92. doi: 10.1007/s11695-018-3520-5

Civitarese, E., MacLean, P. S., Carling, S., Kerr-Bayles, L., McMillan, R. P., and Pierce, A. (2010). Regulation of skeletal muscle oxidative capacity and insulin signaling by the mitochondrial rhomboid protease PARL. *Cell Metab.* 11, 412–426. doi: 10.1016/j.cmet.2010.04.004

Coronado, M., Fajardo, G., Nguyen, K., Zhao, M., Kooiker, K., Jung, G., et al. (2018). Physiological Mitochondrial Fragmentation Is a Normal Cardiac Adaptation to Increased Energy Demand. *Circ. Res.* 122, 282–295. doi: 10.1161/circresaha.117.310725

Ding, M., Feng, N., Tang, D., Feng, J., Li, Z., Jia, M., et al. (2018). Melatonin prevents Drp1-mediated mitochondrial fission in diabetic hearts through SIRT1-PGC1α pathway. *J. Pineal. Res.* 65:e12491. doi: 10.1111/jpi.12491

Fulco, M., Cen, Y., Zhao, P., Hoffman, E. P., McBurney, M. W., Sauve, A. A., et al. (2008). Glucose restriction inhibits skeletal myoblast differentiation by activating SIRT1 through AMPK-mediated regulation of Nampt. *Dev. Cell.* 14, 661–673. doi: 10.1016/j.devcel.2008.02.004

Hoffman, N. J., Parker, B. L., Chaudhuri, R., Fisher-Wellman, K. H., and Kleinert, M. (2015). Global Phosphoproteomic Analysis of Human Skeletal Muscle Reveals a Network of Exercise-Regulated Kinases and AMPK Substrates. *Cell Metab.* 22, 922–935. doi: 10.1016/j.cmet.2015.09.001

Huang, X., Liu, S., Wu, D., Cheng, Y., Han, H., Wang, K., et al. (2018). Facilitated Ca(2+) homeostasis and attenuated myocardial autophagy contribute to alleviation of diabetic cardiomyopathy after bariatric surgery. *Am. J. Physiol. Heart Circ. Physiol.* 315, H1258–H1268. doi: 10.1152/ajpheart.00274.2018

Huang, X., Wu, D., Cheng, Y., Zhang, X., Liu, T., Liu, Q., et al. (2019). Restoration of myocardial glucose uptake with facilitated myocardial glucose transporter 4 translocation contributes to alleviation of diabetic cardiomyopathy in rats after duodenal-jejunal bypass. *J. Diab. Investig.* 10, 626–638. doi: 10.1111/jdi.12948

Huynh, K., Bernardo, B. C., McMullen, J. R., and Ritchie, R. H. (2014). Diabetic cardiomyopathy: mechanisms and new treatment strategies targeting antioxidant signaling pathways. *Pharmacol. Ther.* 142, 375–415. doi: 10.1016/j.pharmthera.2014.01.003

Ikramuddin, S., Korner, J., Lee, W. J., Thomas, A. J., Connett, J. E., Bantle, J. P., et al. (2018). Lifestyle Intervention and Medical Management With vs Without Roux-en-Y Gastric Bypass and Control of Hemoglobin A1c, LDL Cholesterol, and Systolic Blood Pressure at 5 Years in the Diabetes Surgery Study. *JAMA* 319, 266–278. doi: 10.1001/jama.2017.20813

Jia, G., Hill, M. A., and Sowers, J. R. (2018). Diabetic Cardiomyopathy: An Update of Mechanisms Contributing to This Clinical Entity. *Circ. Res.* 122, 624–638. doi: 10.1161/CIRCRESAHA.117.311586

Leung, M., Xie, M., Durmush, E., Leung, D. Y., and Wong, V. W. (2016). Weight Loss with Sleeve Gastrectomy in Obese Type 2 Diabetes Mellitus: Impact on Cardiac Function. *Obes. Surg.* 26, 321–326. doi: 10.1007/s11695-015-1748-x

Li, J., Romestaing, C., Han, X., Li, Y., Hao, X., Wu, Y., et al. (2010). Cardiolipin remodeling by ALCAT1 links oxidative stress and mitochondrial dysfunction to obesity. *Cell Metab.* 12, 154–165. doi: 10.1016/j.cmet.2010.07.003

Li, R., Sun, X., Li, P., Li, W., Zhao, L., Zhu, L., et al. (2021). GLP-1-Induced AMPK Activation Inhibits PARP-1 and Promotes LXR-Mediated ABCA1 Expression to Protect Pancreatic β-Cells Against Cholesterol-Induced Toxicity Through Cholesterol Efflux. *Front. Cell Dev. Biol.* 9:646113. doi: 10.3389/fcell.2021.646113

Liu, L., Zhang, T., Hu, J., Ma, R., He, B., Wang, M., et al. (2020). Adiponectin/SIRT1 Axis Induces White Adipose Browning After Vertical Sleeve Gastrectomy of Obese Rats with Type 2 Diabetes. *Obes. Surg.* 30, 1392–1403. doi: 10.1007/s11695-019-04295-4

McGlone, E. R., Carey, I., Veličković, V., Chana, P., Mahawar, K., Batterham, R. L., et al. (2020). Bariatric surgery for patients with type 2 diabetes mellitus requiring insulin: Clinical outcome and cost-effectiveness analyses. *PLoS Med.* 17:e1003228. doi: 10.1371/journal.pmed.1003228

Ménard, S. L., Croteau, E., Sarrhini, O., Gélinas, R., Brassard, P., Ouellet, R., et al. (2010). Abnormal in vivo myocardial energy substrate uptake in diet-induced type 2 diabetic cardiomyopathy in rats. *Am. J. Physiol. Endocrinol. Metab.* 298, E1049–E1057. doi: 10.1152/ajpendo.00560.2009

Mingrone, G., Panunzi, S., De Gaetano, A., Guidone, C., Iaconelli, A., Nanni, G., et al. (2015). Bariatric-metabolic surgery versus conventional medical treatment in obese patients with type 2 diabetes: 5 year follow-up of an open-label, single-centre, randomised controlled trial. *Lancet* 386, 964–973. doi: 10.1016/s0140-6736(15)00075-6

Murtaza, G., Virk, H. U. H., Khalid, M., Lavie, C. J., Ventura, H., Mukherjee, D., et al. (2019). Diabetic cardiomyopathy - A comprehensive updated review. *Prog. Cardiovasc. Dis.* 62, 315–326. doi: 10.1016/j.pcad.2019.03.003

Packer, M. (2020a). Autophagy-dependent and -independent modulation of oxidative and organellar stress in the diabetic heart by glucose-lowering drugs. *Cardiovasc. Diabetol.* 19:62. doi: 10.1186/s12933-020-01041-4

Packer, M. (2020b). Longevity genes, cardiac ageing, and the pathogenesis of cardiomyopathy: implications for understanding the effects of current and future treatments for heart failure. *Eur. Heart J.* 41, 3856–3861. doi: 10.1093/eurheartj/ehaa360

Qiang, L., Lin, H. V., Kim-Muller, J. Y., Welch, C. L., Gu, W., and Accili, D. (2011). Proatherogenic abnormalities of lipid metabolism in SirT1 transgenic

mice are mediated through Creb deacetylation. *Cell Metab.* 14, 758–767. doi: 10.1016/j.cmet.2011.10.007

Reed, M. J., Meszaros, K., Entes, L. J., Claypool, M. D., Pinkett, J. G., Gadbois, T. M., et al. (2000). A new rat model of type 2 diabetes: the fat-fed, streptozotocin-treated rat. *Metabolism* 49, 1390–1394. doi: 10.1053/meta.2000.17721

Regan, T. J., Lyons, M. M., Ahmed, S. S., Levinson, G. E., Oldewurtel, H. A., Ahmad, M. R., et al. (1977). Evidence for cardiomyopathy in familial diabetes mellitus. *J. Clin. Invest.* 60, 884–899. doi: 10.1172/jci108843

Rubino, F., Nathan, D. M., Eckel, R. H., Schauer, P. R., Alberti, K. G., Zimmet, P. Z., et al. (2016). Metabolic Surgery in the Treatment Algorithm for Type 2 Diabetes: A Joint Statement by International Diabetes Organizations. *Surg. Obes. Relat. Dis.* 12, 1144–1162. doi: 10.1016/j.soard.2016.05.018

Sahin, K., Onderci, M., Tuzcu, M., Ustundag, B., Cikim, G. I, Ozercan, H., et al. (2007). Effect of chromium on carbohydrate and lipid metabolism in a rat model of type 2 diabetes mellitus: the fat-fed, streptozotocin-treated rat. *Metabolism* 56, 1233–1240. doi: 10.1016/j.metabol.2007.04.021

Schaffer, B. E., Levin, R. S., Hertz, N. T., Maures, T. J., Schoof, M. L., Hollstein, P. E., et al. (2015). Identification of AMPK Phosphorylation Sites Reveals a Network of Proteins Involved in Cell Invasion and Facilitates Large-Scale Substrate Prediction. *Cell Metab.* 22, 907–921. doi: 10.1016/j.cmet.2015.09.009

Skovsø, S. (2014). Modeling type 2 diabetes in rats using high fat diet and streptozotocin. *J. Diab. Investig.* 5, 349–358. doi: 10.1111/jdi.12235

Tan, Y., Zhang, Z., Zheng, C., Wintergerst, K. A., Keller, B. B., and Cai, L. (2020). Mechanisms of diabetic cardiomyopathy and potential therapeutic strategies: preclinical and clinical evidence. *Nat. Rev. Cardiol.* 17, 585–607. doi: 10.1038/s41569-020-0339-2

Ti, Y., Xie, G. L., Wang, Z. H., Bi, X. L., Ding, W. Y., Wang, J., et al. (2011). TRB3 gene silencing alleviates diabetic cardiomyopathy in a type 2 diabetic rat model. *Diabetes* 60, 2963–2974. doi: 10.2337/db11-0549

Ulrich-Lai, Y. M., and Ryan, K. K. (2014). Neuroendocrine circuits governing energy balance and stress regulation: functional overlap and therapeutic implications. *Cell Metab.* 19, 910–925. doi: 10.1016/j.cmet.2014.01.020

Veeranki, S., Givvimani, S., Kundu, S., Metreveli, N., Pushpakumar, S., and Tyagi, S. C. (2016). Moderate intensity exercise prevents diabetic cardiomyopathy associated contractile dysfunction through restoration of mitochondrial function and connexin 43 levels in db/db mice. *J. Mol. Cell Cardiol.* 92, 163–173. doi: 10.1016/j.yjmcc.2016.01.023

Wang, D., Yin, Y., Wang, S., Zhao, T., Gong, F., Zhao, Y., et al. (2021). FGF1(ΔHBS) prevents diabetic cardiomyopathy by maintaining mitochondrial homeostasis and reducing oxidative stress *via* AMPK/Nur77 suppression. *Signal. Transduct. Target Ther.* 6:133. doi: 10.1038/s41392-021-00542-2

Wang, Q., Zhang, M., Torres, G., Wu, S., Ouyang, C., Xie, Z., et al. (2017). Metformin Suppresses Diabetes-Accelerated Atherosclerosis *via* the Inhibition of Drp1-Mediated Mitochondrial Fission. *Diabetes* 66, 193–205. doi: 10.2337/db16-0915

Xu, Q., Ding, H., Li, S., Dong, S., Li, L., Shi, B., et al. (2021). Sleeve Gastrectomy Ameliorates Diabetes-Induced Cardiac Hypertrophy Correlates With the MAPK Signaling Pathway. *Front. Physiol.* 12:785799. doi: 10.3389/fphys.2021.785799

Zhou, H., Wang, J., Zhu, P., Zhu, H., Toan, S., Hu, S., et al. (2018). NR4A1 aggravates the cardiac microvascular ischemia reperfusion injury through suppressing FUNDC1-mediated mitophagy and promoting Mff-required mitochondrial fission by CK2α. *Basic Res. Cardiol.* 23:113. doi: 10.1007/s00395-018-0682-1

Conflict of Interest: The authors declare that the research was conducted in the absence of any commercial or financial relationships that could be construed as a potential conflict of interest.

Publisher's Note: All claims expressed in this article are solely those of the authors and do not necessarily represent those of their affiliated organizations, or those of the publisher, the editors and the reviewers. Any product that may be evaluated in this article, or claim that may be made by its manufacturer, is not guaranteed or endorsed by the publisher.

frontiers in Physiology

REVIEW
published: 16 March 2022
doi: 10.3389/fphys.2022.826740

Bile Acid Detection Techniques and Bile Acid-Related Diseases

*Xiang Zhao[1], Zitian Liu[1], Fuyun Sun[1], Lunjin Yao[1], Guangwei Yang[1] and Kexin Wang[2]**

[1] Cheeloo College of Medicine, Shandong University, Jinan, China, [2] Department of General Surgery, Qilu Hospital of Shandong University, Jinan, China

Bile acid is a derivative of cholinergic acid (steroidal parent nucleus) that plays an important role in digestion, absorption, and metabolism. In recent years, bile acids have been identified as signaling molecules that regulate self-metabolism, lipid metabolism, energy balance, and glucose metabolism. The detection of fine changes in bile acids caused by metabolism, disease, or individual differences has become a research hotspot. At present, there are many related techniques, such as enzyme analysis, immunoassays, and chromatography, that are used for bile acid detection. These methods have been applied in clinical practice and laboratory research to varying degrees. However, mainstream detection technology is constantly updated and replaced with the passage of time, proffering new detection technologies. Previously, gas chromatography (GS) and gas chromatography-mass spectrometry (GC-MS) were the most commonly used for bile acid detection. In recent years, high-performance liquid chromatography-tandem mass spectrometry (HPLC-MS/MS) has developed rapidly and has gradually become the mainstream bile acid sample separation and detection technology. In this review, the basic principles, development and progress of technology, applicability, advantages, and disadvantages of various detection techniques are discussed and the changes in bile acids caused by related diseases are summarized.

Keywords: bile acid, detection techniques, related diseases, enzyme analysis, chromatography

OPEN ACCESS

Edited by:
Chun Yang,
Nanjing Medical University, China

Reviewed by:
Mengqiu Wu,
Children's Hospital of Nanjing Medical University, China
Mainak Dutta,
Birla Institute of Technology and Science, United Arab Emirates

****Correspondence:***
Kexin Wang
wkx3726@163.com

Specialty section:
This article was submitted to Metabolic Physiology, a section of the journal Frontiers in Physiology

Received: *01 December 2021*
Accepted: *22 February 2022*
Published: *16 March 2022*

Citation:
Zhao X, Liu Z, Sun F, Yao L, Yang G and Wang K (2022) Bile Acid Detection Techniques and Bile Acid-Related Diseases. Front. Physiol. 13:826740. doi: 10.3389/fphys.2022.826740

INTRODUCTION

Bile acids are a component of bile. They play a role in human metabolism by facilitating the digestion and absorption of lipids, maintaining the dissolved state of cholesterol in bile, and inhibiting its precipitation. In addition, bile acids can also act as signaling molecules to regulate self-metabolism, lipid metabolism, energy balance, and glucose metabolism by binding to the "membrane bile acid receptor"—Takeda G protein-coupled receptor 5 (TGR5) and nuclear hormone receptors, such as farnesoid X receptor (FXR) (Thomas et al., 2008).

Although there is little difference in the structure as well as physical and chemical properties of various bile acids, their functions are different. In experimental studies, the separation and detection of bile acids have been widely used, but they have not been popularized in clinical diagnosis. However, with the increasingly clear relationship between the occurrence of diseases and changes in bile acids, separation and detection of bile acids will play an increasingly important diagnostic value and guiding role in the future. Recently, detecting and separating bile acids accurately and quickly has become an important aspect of experimental studies. This review lists the methods used for bile acid detection according to the technical classification. The aim is to explore the basic

principles, applicable conditions, advantages, and disadvantages of the various technologies, as well as the clinical application of bile acid detection in the diagnosis of diseases.

BILE ACIDS OVERVIEW

Structure and Classification of Bile Acids

Bile acids comprise a mixture of several compounds that are similar in shape, structure, and function. They can be divided into free and conjugated bile acids. The free bile acids mainly include cholic acid (CA), chenodeoxycholic acid (CDCA), deoxycholic acid (DCA), and a small amount of lithocholic acid (LCA). The 24 carboxyl groups of the above free bile acids can combine with glycine or taurine to form various conjugated bile acids, including glycocholic acid, taurocholic acid, glycochenodeoxycholic acid, and taurochenodeoxycholic acid (**Table 1**). In addition to aminoacyl amidation with glycine or taurine and sulfation, three glycosidic conjugation pathways have been established both *in vivo* and *in vitro* at the end of the last century: glucuronidation, glucosidation, and *N*-acetylglucosaminidation (Marschall et al., 1992), and that let us recognize more bile acid types in the body.

The different structures of bile acids are mainly reflected in the occurrence of hydroxyl or carbonyl groups on the carbon atoms at specific positions. The basic structure of most bile acids is shown in **Figure 1**. The molecular structures of some common bile acids, based on replacing the functional groups shown in **Figure 1** are listed in **Table 1** (Tagliacozzi et al., 2003; Mano et al., 2006; Gowda, 2011; Jantti et al., 2014; Liu et al., 2018; Dutta et al., 2019).

Bile acids can be divided into primary and secondary bile acids based on their sources. Primary bile acids are synthesized by the liver and stored in the gallbladder as an important component of bile. They mainly include CA, CDCA, and their combined products with glycine and taurine.

Bile Acid Synthesis and Enterohepatic Circulation

In the classical pathway, primary bile acids are synthesized in four steps: (a) initiation of synthesis by 7-hydroxylation of sterol precursors, (b) further modification of the ring structures, (c) oxidation and shortening of the side chain, and (d) conjugation of the bile acids with an amino acid (Russell, 2003). Secondary bile acids are synthesized by deconjugation, dehydrogenation, and dehydroxylation reactions of the gut microbiota (**Figure 1**; Chiang, 2013; Winston and Theriot, 2020). The gut microbial community, owing to its ability to produce bile acid metabolites different from those produced by the liver, may be considered an "endocrine organ" with the potential to alter host physiology, perhaps to benefit the parasitic gut microbiome (Ridlon and Bajaj, 2015).

Bile acids circulate in the digestive tract and internal circulation through enterohepatic circulation. Approximately 95% of bile acids that enter the digestive tract can be reabsorbed, and the remainder is excreted in the stool. Bile acids can be reabsorbed in two ways: Conjugated bile acids are actively reabsorbed in the ileum by bile acid transporters, while free bile acids are passively reabsorbed in all parts of the small intestine and large intestine. Reabsorbed bile acids re-enter the liver via the portal vein. In hepatocytes, free bile acids are reconverted into conjugated bile acids, which are secreted into the intestine with bile along with reabsorbed and newly synthesized conjugated bile acids. This cycle is called the enterohepatic circulation of bile acids. Small amounts of bile acids that are not acquired by liver cells enter the blood circulation through the hepatic vein. Thus, in addition to the liver and bile, bile acids are also present in the blood, urine, stool, amniotic fluid (Ushijima et al., 2001), sputum (Higashi et al., 2010; Durc et al., 2020), pleural effusion (Che et al., 2018), and bronchoalveolar lavage fluid (Bessonneau et al., 2014). The first three are often used as typical samples for bile acid detection.

Relationship Between Bile Acids and Diseases

Because of the close relationship between bile acids and metabolism, the concentration of bile acids in each component also changes during diseases, such as hepatobiliary disease (Li et al., 2017; Jia et al., 2018), gastrointestinal disease (Duboc et al., 2013; Lee et al., 2020), metabolic disease (Wu et al., 2015; Lackey and Olefsky, 2016), and nervous system disease (Grant and DeMorrow, 2020). 3α-Hydroxysteroid dehydrogenase (HSD) enzyme assays have been used to detect total bile acid (TBA) concentration in clinical practice to diagnose the occurrence of diseases. However, most diseases only lead to an increase or decrease in the concentration of one or several bile acids, but not TBA. For example, Zheng et al. (2021) found an association between hyocholic acid (HCA) and metabolic disorders, such as obesity and diabetes. The feasibility of using HCA to assess the risk of metabolic abnormalities in the future is further clarified. Thus, the separation of various bile acids and detection of their concentration changes in samples are conducive to scientific research, disease diagnosis, and even disease prediction, which is very important in the development of human medical and health undertakings. Therefore, the significance of bile acid detection needs to be evaluated.

BILE ACID DETECTION TECHNIQUES REPORTED IN LITERATURE

Since the 1950s and the 1960s, there has been an increased interest in bile acid metabolism, and the related separation and detection technologies have emerged in an endless stream. Some of these methods have already been widely used in other detection fields and later applied to the detection of bile acids, such as spectrophotometry and early chromatography. In addition, after decades of research on bile acid metabolism, new separation and detection techniques have been established and quickly applied to the detection of bile acids.

The separation and detection methods of bile acids can be broadly divided into two categories: non-chromatographic and chromatographic. Non-chromatographic methods include

TABLE 1 | Chemical structure of some common bile acids, including free bile acids, glycine/taurine-conjugated bile acids, and sulfated bile acids.

Abbreviation	Compound	R1	R2	R3	R4	R5
CA	Cholic acid	α-OH	H	α-OH	OH	OH
CDCA	Chenodeoxycholic acid	α-OH	H	α-OH	H	OH
DCA	Deoxycholic acid	α-OH	H	H	OH	OH
7-oxo-DCA	7-oxo-deoxycholic acid	α-OH	H	=O	OH	OH
LCA	Lithocholic acid	α-OH	H	H	H	OH
12-oxo-LCA	12-oxo-lithocholic acid	α-OH	H	H	=O	OH
UDCA	Ursodeoxycholic acid	α-OH	H	β-OH	H	OH
α-MCA	α-muricholic acid	α-OH	β-OH	α-OH	H	OH
β-MCA	β-muricholic acid	α-OH	β-OH	β-OH	H	OH
ω-MCA	ω-muricholic acid	α-OH	α-OH	β-OH	H	OH
HCA	Hyocholic acid	α-OH	α-OH	α-OH	H	OH
HDCA	Hyodeoxycholic acid	α-OH	α-OH	H	H	OH
7-oxo-HDCA	7-oxo-hyodeoxycholic acid	α-OH	α-OH	=O	H	OH
DHCA	Dehydrocholic acid	=O	H	=O	=O	OH
MDCA	Murideoxycholic acid	α-OH	β-OH	H	H	OH
Unconjugated						OH
Glycine conjugates						NHCH2CO2H
Taurine conjugates						NHCH2CH2SO3H
Sulfated BAs	HSO4					

α-MCA, β-MCA and ω-MCA do not have corresponding glycine conjugated bile acids, while bile acids with carboxyl groups (7-oxo-DCA, 12-oxo-LCA, 7-oxo-HDCA) do not have corresponding taurine and glycine conjugates.

enzyme analysis, radioimmunoassay (RIA), enzyme-linked immunosorbent assay (ELISA), nuclear magnetic resonance (NMR), and capillary electrophoresis (CE) (**Table 2**); among these, 3α-HSD enzyme analysis has been used in clinical diagnosis, and other methods are widely used in scientific research to varying degrees. Chromatography originated in the early twentieth century and developed rapidly after the 1950s. The basic principles underlying all kinds of chromatography are the same. Earlier, gas chromatography (GC) or gas chromatography-mass spectrometry (GC-MS) was the most commonly used bile acid detection method; in recent years, high-performance liquid chromatography-tandem mass spectrometry (HPLC-MS/MS) has developed rapidly and has gradually become the mainstream method for bile acid sample separation and detection. These methods have high sensitivity, good specificity, and low detection limit; however, they also have a few shortcomings.

To understand the practical application of bile acid detection technology in scientific research in recent years, we reviewed 105 articles reporting bile acid detection technology (the search was conducted on PubMed using the keyword "bile acid," and the filter condition was "5 years." Five hundred articles were selected, with an emphasis on those with an impact factor above 3). These studies are expected to aid the selection of appropriate bile acid detection technology.

First criteria was the geographical distribution of the detection technology (**Figure 2A**). Bile acid detection technology has been used in the United States, China, Germany, Japan, Canada, Sweden, and many other countries. Among them, the United States and China published the most relevant reports, with 24 and 22 articles, respectively.

Second criteria was the use of detection technology (**Figure 2B**). Many of the techniques mentioned in this review, such as RIA and CE, have not been used in scientific research. Most of these studies (79 in total) used LC-MS (LC includes HPLC and UPLC; MS includes MS and MS/MS), and GC-MS. Most MS detectors mentioned in specific experimental steps are tandem mass spectrometry. Kit/enzymatic tests were also frequently reported, but they only detect TBA as needed. It is a simple and convenient detection technique for experiments that do not require individual bile acid separation and detection. Among the statistical studies, 11 used two detection techniques, most of which are enzymatic methods combined with LC-MS, to separate and detect the concentration of individual bile acid components while measuring the TBA.

The third criteria was the specimens tested (**Figure 2C**). The sample sources were abundant. In addition to human specimens, there were various other types, such as experimental animals, *in vitro* simulations, cell culture, and even environmental bile acids can be detected. The most important specimens were mice, humans, and rats, accounting for 38, 30, and 15 articles, respectively. Five studies used two types of specimens according to experimental requirements. Because the experimental animals, such as rats and mice, can be subjected to anatomy experiments and extraction of the organs according to the rules and regulations, a wide range of specimens may be expected with an extensive sample detection range. Human specimens more accurately represent the metabolic changes in the body, not only in research experiments, but also in the clinic. Compared to experimental animals, human sample extraction is more likely to be less invasive or non-invasive, considering that the specimens do not usually include the liver, gut, or gallbladder.

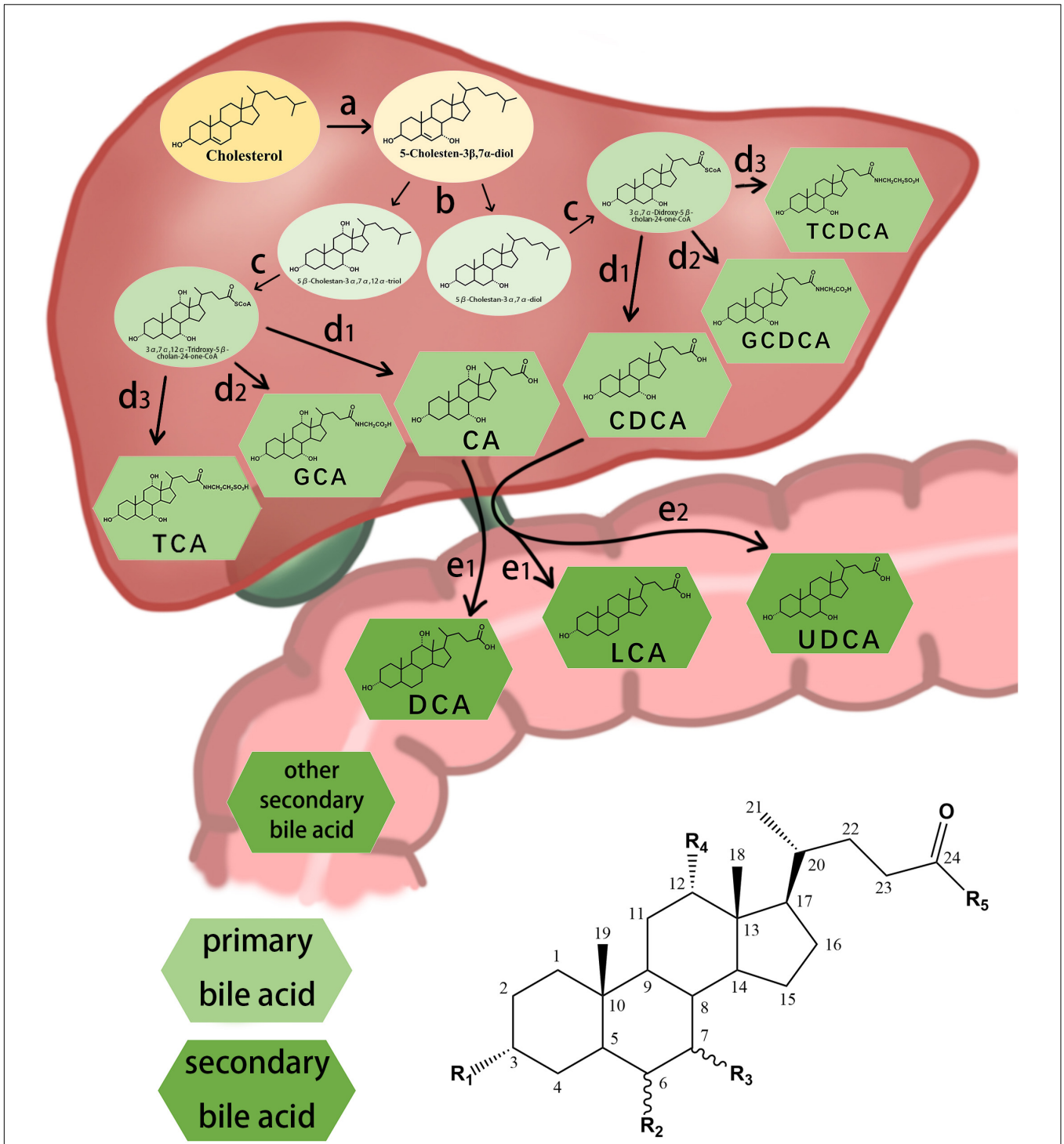

FIGURE 1 | Chemical structure of some common bile acids and the synthesis primary bile acid and generation of secondary bile acid. (a) initiation of synthesis by 7-hydroxylation of sterol precursors, (b) further modification of the ring structures, (c) oxidation and shortening of the side chain, (d1) hydrolyzation of the bile acids, (d2) conjugation of the bile acids with glycine, (d3) conjugation of the bile acids with taurine, (e1) dehydroxylation of the bile acids, (e2) conversion of chenodesoxycholic acid acid 7α-hydroxyl to 7β-hydroxyl.

Finally, the species and time required for bile acid detection were the two important aspects of our evaluation (**Figures 2D,E**). Among the four main detection techniques (UPLC-MS/MS, HPLC-MS/MS, LC-MS/MS, and HPLC), UPLC-MS/MS has the advantages of detecting more bile acid types and a shorter detection time, making

TABLE 2 | Advantages and disadvantages of the bile acid detection techniques.

Method		Advantages	Disadvantages
Enzyme analysis		Simple operation; low cost; applicable for clinical and scientific research to detect TBA, especially for clinical diagnosis	Only applicable for bile acids containing 3α-OH; high detection limit; failure to distinguish between the specific types of bile acids
RIA		Applicable for detection of trace bioactive substances at that time	Need of special equipment; radioactivity; cross-reactivity
ELISA		Small number of instruments; short analysis time; simple operation	Cross reaction; difficult to recover from serum; low accuracy
Spectrophotometry		Small number of instruments; short analysis time; low cost; simple operation process	Failure for the separation and detection of bile acids; low detection accuracy
NMR		Small sample size; simple sample pretreatment; capable of non-invasive	Relative low sensitivity compared to MS-based approaches
Chromatography	TLC	Simple operation process; low cost; good repeatability	Lack of direct quantification and low accuracy
	HPLC	High sensitive; simple to perform	Time-consuming; complex sample pretreatment
	SFC	Short detection time; not limited by the volatility and thermal instability of the compounds	Low reproducibility
	LC-MS	Short detection time; narrow peak width; low detection limit; high retention capacity; high signal-to-noise ratio	High cost
	GC-MS	Low detection limit; high retention capacity; high degree of separation	Complex sample preparation
CE		Good separation capacity and detection speed	Technically demanding; usually unreliable

it the preferred technology for the precise detection of bile acids.

BILE ACID DETECTION METHODS

Enzyme Analysis

One of the chemical characteristics of bile acids is that they contain an α-hydroxyl group on the third carbon. 3α-HSD extracted from *Pseudomonas testosteroni* catalyzes the redox reaction of hydroxyl groups, and NAD^+ is converted into NADH. The concentration of NADH is determined by spectrophotometry at 340 nm; thus, the concentration of bile acids in the sample is obtained indirectly. Based on this principle, Iwata and Yamasaki (1964) developed a method for measuring TBA (including free bile acids and bound bile acids) in samples. The method is relatively simple and fast, with a minimum detection limit of 5 μ g.

In order to avoid the use of special instruments and relatively cumbersome pretreatments in the detection of TBA in plasma while ensuring satisfactory sensitivity, Mashige and his team improved the enzyme analysis method to measure bile acid concentrations in 1981 (Yamanaka et al., 1981). This method enabled the H of NADH generated in the first reaction to convert nitrotetrazolium blue into diformazan through diaphorase, and then detected the diformazan formed at 540 nm using a spectrophotometer. The minimum detection limit was 0.1 nmol. This method greatly improves the practicability of enzyme analysis in the detection of bile acid concentrations, is more suitable for general conventional laboratories, and has the characteristics for mechanization.

In addition to 3α-HSD, 7α-HSD can be used for bile acid detection. Roda and coworkers used a highly specific continuous flow method to detect the concentration of 7-α-hydroxyl bile acid by bioluminescence using nylon-immobilized bacterial enzymes (Bovara et al., 1984).

Enzyme analysis has been used in clinical and scientific research, especially for clinical diagnosis. Compared with this method, the other methods mentioned later have not been widely used in clinical practice. The total bile acid assay kit (total bile acid enzyme circulation method) has commercialized detection technology, facilitating the detection of TBA. The kit uses NADH, thio-NAD^+, and bile acids to perform a redox cycle catalyzed by 3α-HSD, amplifying the signal and finally measuring the concentration of TBA by determining the absorption value of thio-NAD^+ at 405/660 nm at 37°C using a spectrophotometer.

The disadvantages of enzyme analysis method are also particularly apparent. The method can only detect bile acids containing 3α hydroxyl groups and cannot be used if the hydroxyl groups are replaced by sulfuric or glucuronic groups. Moreover, the detection limit of this method is high, and it cannot accurately detect the bile acid content in some samples, such as saliva. In addition, enzyme analysis can only detect TBA and cannot distinguish between the specific types of bile acids. Therefore, the experimental data provided by this method only includes the total concentration, which is relatively limited. To obtain the respective concentrations of various bile acids, other methods that can separate and detect them should be selected.

Immunoassay

Radioimmunoassay

Radioimmunoassay was established in 1959 by American scientists Professor Yalow and Berson as an *in vitro* method for ultrafine analysis. It resolved the issue of detection of trace bioactive substances, which was difficult to determine at that time, thus playing a significant role in promoting the development of modern medicine. RIA for bile acids in samples was first proposed by Simmonds et al. (1973). RIA utilizes the principle of specific binding between antigen and antibody and measures the concentration of the bound product by radioisotope

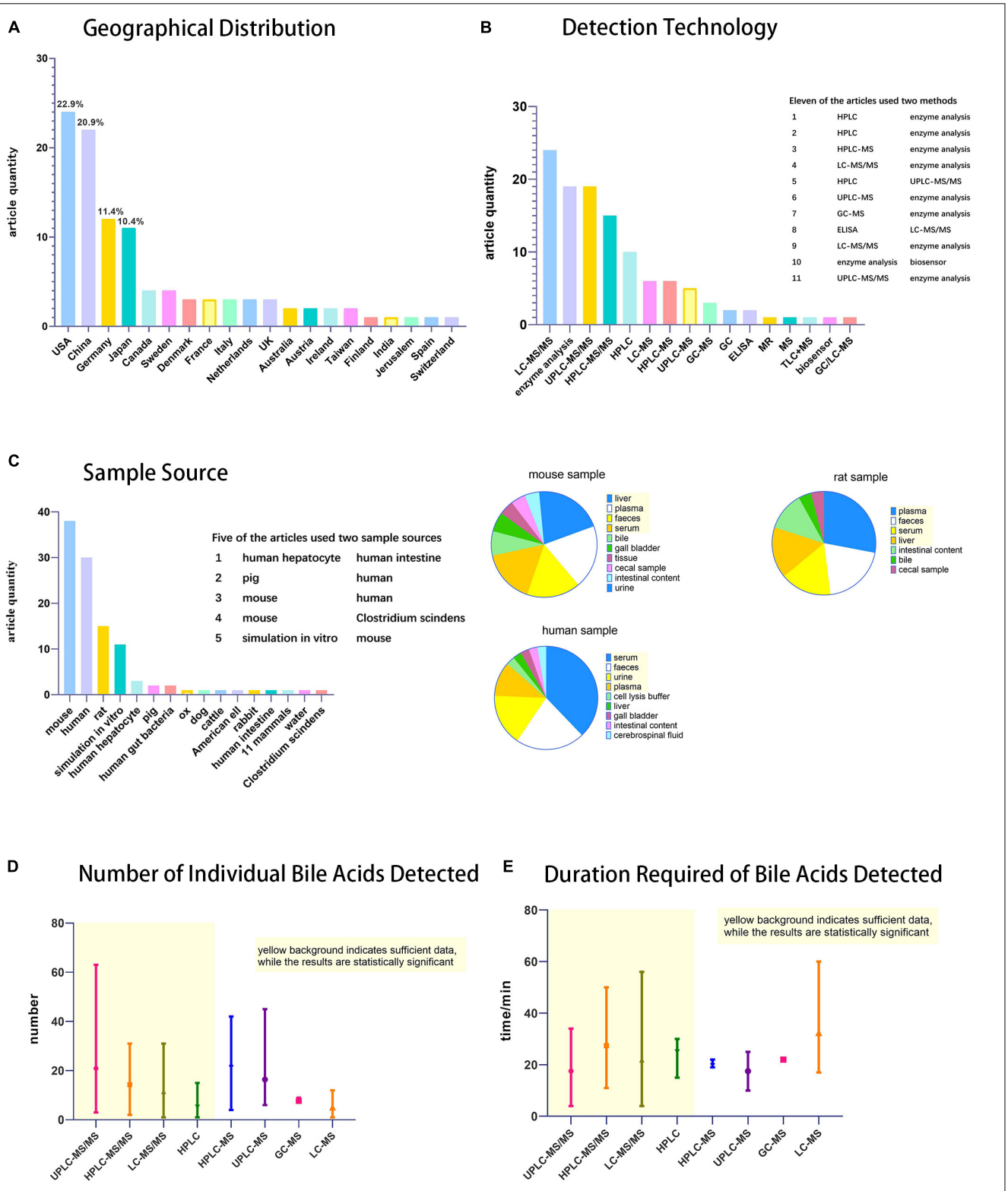

FIGURE 2 | Statistical chart of bile acids detection techniques. **(A)** Histogram of geographical distribution of articles (n = 105) on bile acid detection technology, **(B)** Histogram of techniques used for bile acid detection. **(C)** Histogram of specimen sources and pie charts of specimen taken from mouse, human and rat. **(D)** Statistical chart of the number of individual bile acids detected and **(E)** duration required. Among **Figures 2D,E**, the part with yellow background indicates that the data is sufficient and therefore has statistical significance, while the rest has little statistical significance because of the small number of statistics.

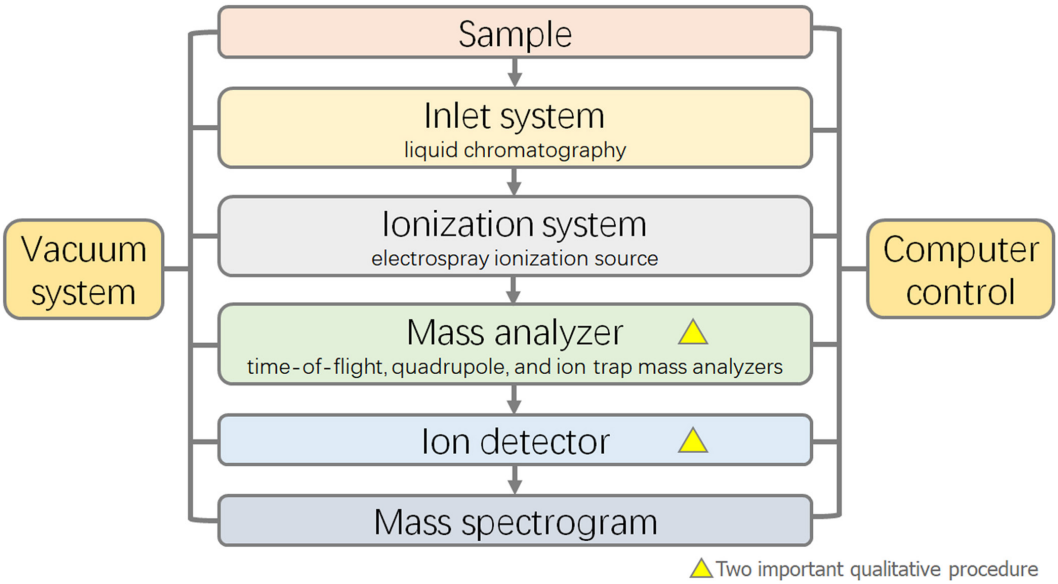

FIGURE 3 | Flow diagram of Liquid Chromatograph-Mass Spectrometer (LC-MS).

labeling. However, because of the need for special equipment, radioactivity, and cross-reactivity, RIA has not been widely used, and few people have used this method to detect bile acid concentrations in recent years (Mäentausta and Jänne, 1979; Samuelson, 1980).

Enzyme-Linked Immunosorbent Assay

Since Engvall and Perlmann (1971) invented the ELISA technique in 1971, it has become an extremely important clinical and scientific assay. ELISA detects soluble antibodies or antigens in a sample. ELISA combines two basic principles: antigen–antibody specificity combined with enzymes and substrates for efficient catalysis. The results are based on the color changes of the enzyme substrate, using standard apparatus for quantitative analysis, with the sensitivity reaching the ng level. ELISA can be used to detect bile acid concentration in saliva samples that enzyme analysis cannot. Enzymes commonly used for marking include horseradish peroxidase and alkaline phosphatase. These enzymes are stable and can be preserved for a long time.

In 2017, Liu et al. (2017) used four different monoclonal antibodies to detect five bile acids [CA, DCA, CDCA, UDCA, and hyodeoxycholic acid (HDCA)] in plasma. Cui et al. (2017) established a biotinylated single-chain variable fragment-based ELISA method for the determination of glycocholic acid, and used a chicken single-chain variable fragment (scFv) antibody to detect glycocholic acid.

The method has the same sensitivity and accuracy as the RIA method, but does not require expensive equipment and is not radioactive. The experiment does not require the use of a large number of instruments and can effectively avoid the result error caused by cross contamination. The detection speed is faster than that of RIA or chromatography, and the operation is simple and easy to use; thus, it can be promoted in basic clinical detection. Its disadvantage is that the cross reaction between antigen and antibody occurs easily, which affects the accuracy of detection, false positives, and other false results (Dutta et al., 2019). Moreover, bile acids are difficult to recover from serum, and the recovery rate is always higher than the theoretical value measured by the standard curve without human serum.

Spectrophotometry

Spectrophotometry is one of the most commonly used techniques in biochemical experiments. Its principle involves qualitative and quantitative analysis of the test substance by measuring the absorption of light at a specific wavelength or wavelength range. Most of the chemical bonds in bile acids are carbon–carbon single bonds without conjugated structures and luminescent groups; therefore, they cannot be measured directly by spectrophotometry. However, certain chemical reactions can cause the bile acids to exhibit an absorption peak at a certain wavelength or produce substances with an absorption peak at a certain wavelength. The principle is the same as that of the 3α-HSD enzyme analysis mentioned above. With regard to spectrophotometry, this review introduces other detection methods that use spectrophotometry.

Spectrophotometry eliminates the complex sample processing process and requires only a spectrometer, which is a common instrument in general QC laboratories. This method can be applied to a large number of samples because of its speed, low cost, and simple operation process. However, this method can only detect TBA or a certain type of bile acid at one time, and cannot be used for the separation and detection of bile acids, making it difficult to achieve accurate quantitative analysis of complex bile acid samples. Therefore, it is generally used for preliminary qualitative or simple quantitative analysis.

Nuclear Magnetic Resonance

Nuclear magnetic resonance is a less commonly used method for the detection of bile acids. It is a spectroscopic technique that applies NMR phenomenon to the determination of the molecular structure. It can be used to detect and simultaneously quantify bile acid concentrations in the samples. In addition, NMR can provide detailed molecular structures and quantitative information. Duarte et al. (2009) first applied high-field NMR spectroscopy (800 MHz for 1 H observation) for the detection of human liver bile components (Duarte et al., 2009). NMR spectra of the entire extract showed the main bile acids (CA, DCA, and chenodesoxycholic acid), but failed to distinguish the conjugated bile acids of glycine and taurine. However, this method can be used to detect isomers of glycodeoxycholic acid and glycochenodeoxycholic acid, which cannot be detected by conventional liquid mass chromatography.

Owing to the high signal overlap of the NMR peaks of bile acids and the signal widening due to the low water solubility and aggregation of the main components of bile, NMR analysis is limited. This limitation was improved with the advent of two-dimensional (2D) NMR. 2D NMR overcomes the problem of overlapping resonances in the proton 1D NMR spectrum and is thus able to detect and align more metabolites than the 1D method.

Various other bile acid detection methods involve sample extraction, which is an invasive procedure. In recent years, NMR detection of bile acids has been of great significance in non-invasive *in vivo* examinations. Prescot et al. (2003) demonstrated the potential of monomeric magnetic resonance for non-invasive detection of the metabolic composition of bile in the human gallbladder. Unfortunately, the mass spectrum cannot detect molecules other than phospholipids, such as bile acids. More recently, Kunnecke et al. (2007) developed a non-invasive method for detecting bile composition in cynomolgus monkeys. Compared to the 1.5 T magnetic field strength used by Prescot et al. (2003) and Kunnecke et al. (2007) used a relatively high magnetic field (4.7 T) to detect and quantify different bile acid molecules, their taurine and glycine derivatives, and phospholipids for the first time.

The NMR method is relatively simple, requires a small sample size, has simple sample pretreatment steps, and avoids the detection errors caused by extraction, derivatization, hydrolysis, and purification. For example, the distribution of bile lipids in micromicelles and vesicles can be measured by NMR, which can provide information about the etiology of gallstone occurrence that is not possible with ordinary analytical methods, because other methods usually involve purification of the test substance.

Chromatography

Chromatography is a common separation and analysis method that has a wide range of applications in analytical chemistry, organic chemistry, biochemistry, and other fields. This method is based on the slight difference in the distribution coefficient of the separated material between the two phases (stationary and mobile phases). This is a multistage separation technique. The principle is that when the two phases are in relative motion, the measured substance is repeatedly allocated between the two phases, further expanding the original small difference between the two and separating the components. According to the different stationary and mobile phases, chromatography can be divided into thin layer chromatography (TLC), HPLC, supercritical fluid chromatography (SFC), liquid chromatography-mass spectrometry (LC-MS), and GC-MS. The application of these five methods for bile acid sample detection is described below.

Thin Layer Chromatography

Thin layer chromatography is a chromatography separation technique that uses a support coated on the support plate as the stationary phase (in bile acid detection, it is commonly coated with silica) and an appropriate solvent as the mobile phase for the separation, identification, and quantification of mixed samples. It first appeared in the 1950s and was quickly widely used in the separation and detection of fatty acids, amino acids, nucleotides, and other substances (Stahl, 1956).

Thin layer chromatography can distinguish between free bile acids and glycine- and taurine-conjugated bile acids, but it cannot effectively detect and separate isomers of dihydroxyl-bound bile acids, such as DCA and CDCA. TLC has low specificity and cannot detect samples below 10 nmol per point; therefore, it is often used to detect bile or mixed standard solutions. Based on the basic TLC technique, two new techniques—2D TLC and reversed-phase TLC—have been developed (Momose et al., 1998; Onisor et al., 2010).

Since its conception and development, TLC technology has been characterized by its simplicity, low cost, and good repeatability. Owing to its lack of direct quantification and low accuracy, it widely used in routine clinical analysis and bile acid detection with low data requirements. When more accurate detection is required, the following chromatographic methods are selected (Poole, 2003).

High Performance Liquid Chromatography

High performance liquid chromatography is a widely used bile acid detection technique. For bile acid detection in samples, HPLC is performed with acetonitrile, ammonium formate, and formic acid solution as the mobile phase. Using a high-pressure infusion system, the pretreated samples and a mobile phase containing bile acids is pumped into a stationary phase chromatographic column (often as C18 reverse phase silica gel column), where each component is separated in the column and enters the detector for testing. An ultraviolet (UV) detector is commonly used for sample analysis. In HPLC, the modification of the chromatography method and the choice of detector and column depend on the sample type and purpose of the analysis. As the absorption of UV light by bile acids is very weak, derivations are often required prior to detection. However, detection of taurine and glycine combined with bile acid derivations are relatively simple compared with GC, and bile acids can be detected in the form of bile or other biological fluids.

In 1976, Shaw and Elliott (1976) first used HPLC to isolate and detect conjugated bile acids in human bile samples. Owing to the wide application of HPLC, many optimization

techniques have been developed. Shi et al. (2015) reacted with 2-bromo-4′-nitroacetophenone with a carboxyl group on free bile acids under the catalysis of crown ether, resulting in a reaction product with a conjugated structure that could be detected sensitively by a UV detector at 263 nm. Onishi et al. (1982) used the post-column reaction technique of immobilized 3α-hydroxysteroid dehydrogenase to analyze bile acids using HPLC.

High performance liquid chromatography is highly sensitive and simple to perform; however, it is time-consuming and requires complex sample pretreatment, making it unsuitable for large-scale sample detection. Moreover, this method is limited by the matrix effect and the specificity of the detector coupled with the low absorption efficiency of bile acids for UV requires the selection of a lower wavelength UV light, which would aggravate the impact of this effect; thus, it is not suitable for the detection of complex samples, such as a variety of complex conjugated bile acids (Liu et al., 2018).

Supercritical Fluid Chromatography

Supercritical fluid refers to a fluid whose temperature and pressure are both higher than the critical point. Supercritical fluids have the dual characteristics of liquids and gases. SFC is similar to a separation and detection technology combined with HPLC and GC.

The mobile phase of SFC is carbon dioxide in the supercritical state. This is because the material has a relatively low critical temperature (31.1°C) and pressure (73.8 bar), is non-flammable, chemically inert, low cost, and has no waste problems (Scalia, 1995). In the supercritical state, carbon dioxide exhibits a solvation intensity close to that of a liquid, and can provide a lower viscosity and higher analyte diffusion coefficient, which is more efficient per unit time. The most interesting advantage is the flexibility of polarity. Polarity can be easily increased by adding a polar solvent, such as methanol. Therefore, the polarity of substances detected by SCF can be very wide (log Pow = −4.6–7.05) (Ishibashi et al., 2012). In 1991, Scalia and Games (1992) first used packed column SFC to detect free bile acids in preparations later applied this technique to detect conjugated bile acids in 1992 (Scalia and Games, 1993).

Owing to the small volume of gas generated by the mobile phase, SCF may be more easily linked to mass spectrometry than HPLC. In 2013, Taguchi et al. (2013), for the first time, used supercritical fluid chromatography-mass spectrometry to simultaneously detect 25 bile acids, including glycine- and taurine-conjugated bile acids, in rat serum samples within 13 min. Compared with HPLC, the detection time of SFC is shorter, the eluent has higher transparency at low UV wavelengths, and can use a sensitive and universal flame ionization detector. In contrast to GC, SFC is not limited by the volatility and thermal instability of the compounds. However, the SFC method has several disadvantages. The conjugated dihydroxyl isomers cannot be completely separated, and the reproducibility of the technique is lower than that of HPLC because the temperature and pressure of the critical fluid under the experimental conditions are not easily controlled. In addition, as the detection of bile acids by GC and HPLC has been relatively complete, SFC plays a less important role in the detection of bile acids.

Liquid Chromatography-Mass Spectrometry

Liquid chromatography-mass spectrometry is the most widely used technique for the detection of mixed bile acids because it can separate isomers of bile acids (Gómez et al., 2020). The separation ability was improved by using HPLC as a separation technique and mass spectrometry as a detection technique instead of a UV detector. The bile acids in the samples were separated by HPLC, and qualitative analysis was carried out by mass spectrometry using the ion mass-to-charge ratio. The principle and characteristics of HPLC are essentially the same as those mentioned above. In recent years, tandem mass spectrometry (MS/MS) has been commonly used for mass spectrometry analysis. Compared with first-order mass spectrometry, tandem mass spectrometry can selectively analyze partial fragments of the target, improving the sensitivity, accuracy, and signal-to-noise ratio. The core components of the mass spectrometer mainly include the ion source, mass analyzer, and ion detector (Yang et al., 1997). In the detection of bile acid samples, the majority of ion sources are electrospray ionization sources. Mass analyzers are commonly used in time-of-flight mass analyzers, quadrupole mass analyzers, and ion trap mass analyzers (**Figure 3**). While the full scan mode can be used for the identification and qualitative analysis of bile acids, selective ion monitoring (SIM) (Wegner et al., 2017), selective reaction monitoring (SRM) (Fu et al., 2020), and multiple reaction monitoring (MRM) (Tu et al., 2020) modes in tandem mass spectrometry are more helpful for the optimal selectivity and accurate quantification of bile acids (Dutta et al., 2019).

Liquid chromatography-mass spectrometry usually has high accuracy, with a detection limit usually of up to 0.1 ng/mL. The method is usually linear in the detection range of 0.01–1 μM. Biological samples used for bile acid detection mainly include serum, plasma, bile, tissue homogenate, saliva, adipose tissue, intestinal contents, urine, and feces. Before detection, simple sample pretreatment and the addition of an appropriate internal standard are needed for the quantitative detection of bile acids. The main purpose of pretreatment is to remove proteins, lipids, and inorganic salts. At present, protein precipitation, solid-phase extraction, and liquid–liquid extraction are used for sample treatment (Liu et al., 2018). The most commonly used method for plasma or serum is the protein precipitation method, which is simple in operation, requires less time, and is cost-effective. Acetonitrile or methanol is used as the precipitant, and the supernatant after high-speed centrifugation is used for detection. The internal standard method involves adding a pure bile acids of certain weight to the analysis sample as the internal standard. There are a variety of internal standards, such as deuterated bile acids (Alnouti et al., 2008; Bobeldijk et al., 2008; Higashi et al., 2010; Jantti et al., 2014), norDCA (Kakiyama et al., 2014), and dehydrocholic acid (Yang et al., 2017), among them, deuterated bile acids are the most common used. Then, chromatographic analysis of the sample containing the internal standard is carried out to determine the peak area and relative correction factor of the internal standard and the component

to be measured, followed by quantitative detection of bile acids. To obtaining quantitative data on bile acids in samples, it is necessary to establish a standard curve. Bile acid calibration standard is dissolved in methanol. Normal samples identical to the samples to be tested are incubated with activated carbon to remove the original bile acids, and the blank sample solution is used as the biological matrix. The calibration standard curve can be obtained by adding a certain amount of dissolved calibration standard and testing it in the same way as the sample. The content of bile acids in samples can be quantitatively detected by combining the internal standard method with a standard curve (Krautbauer et al., 2016).

In addition to the conventional detection of free bile acids and glycine- and taurine-conjugated bile acids, this method has been widely applied to the detection of other bile acid derivatives. Ikegawa et al. (1999) developed a method for the simultaneous determination of 24-glucuronide bile acid in human urine by liquid chromatography-electrospray ionization-mass spectrometry. Bathena et al. (2013) developed a method for the simultaneous determination of bile acids and their sulfuric acid metabolites in human serum and urine by liquid chromatography-tandem mass spectrometry. Most LC-MS methods take longer than 20 min and exhibit moderate coverage of bile acid species (from 11 to 32 monitored species) as mentioned below.

Compared with GC, the pretreatment process of LC-MS is simple and less time-consuming. Compared with ordinary HPLC, the mass spectrometry detector of LC-MS is more expensive and complex. Although optimization of the mass spectrometry parameters requires certain experience, it has higher specificity, shorter detection time, and lower sample size, making it suitable for large-scale clinical or pharmacological toxicological detection (Kakiyama et al., 2014).

With accumulating new evidence on the involvement of bile acids in a growing number of human physiological and pathological conditions, there is renewed interest in improving the measuring techniques for various bile acids in different biological samples. Ultra-performance liquid chromatography-tandem mass spectrometry (UPLC-MS/MS) is a new method developed in the last 20 years (Sun et al., 2019; Hu et al., 2020; Lawler et al., 2020). Using the theory and principle of HPLC, UPLC has improved and innovated a number of chromatographic technologies, including small particle fillers, very low system volumes, and rapid detection methods, which increase the flux, sensitivity, and chromatographic peak capacity of analysis (Wang et al., 2015). In 2004, Waters launched the world's first newly developed UPLC instrument (Plumb et al., 2004).

Han et al. (2015) developed an ultra-fast liquid chromatography/multireaction monitoring-mass spectrometry method for the separation and detection of 50 known bile acids. High-throughput-compatible 96-well phospholipid-depletion solid-phase extraction was adopted as a new sample preparation method. A single analysis of human serum bile acid species in the sub-nanometer concentration range has been achieved, which is far more sensitive than the previous HPLC-MS/MS. Sarafian et al. (2015) developed a 15-min UPLC method for the separation of bile acids from human biological liquid samples, requiring minimal sample preparation, for sensitive, quantitative, and targeted analysis of 145 bile acids, including primary, secondary, and tertiary bile acids. Among these, 57 bile acids were quantitatively measured using 16 marketable stability markers.

Compared with HPLC, this method has a shorter detection time, narrower peak width, lower detection limit, higher retention capacity, and higher signal-to-noise ratio. The application of UPLC technology has made a breakthrough in liquid chromatography at a higher level. Through the efforts of the majority of experimental workers in recent years, the UPLC technology has seen wide application in all walks of life, proving it to be feasible with broad application prospects.

Gas Chromatography-Mass Spectrometry

Gas chromatography refers to the gas mobile phase chromatographic separation method. In the early years of research, when GC/GC-MS had higher detection capabilities than liquid chromatography and HPLC, GC and GC-MS were the most commonly used bile acid detection techniques and were regarded as a reference method (Scalia, 1995). GC was first used in bile acid series analysis in 1960, and only four methyl bile acid derivatives were detected (VandenHeuvel et al., 1960).

Bile acids contain functional groups, such as carboxyl, hydroxyl, and oxo groups, and hydrogen bonds are formed between the molecules (Dutta et al., 2019). Therefore, bile acids have thermal instability and insufficient volatility for GC, and the samples need to be derived in advance. The sample needs to be fractionated in advance according to the different binders, followed by the concentration and derivation steps, which are time-consuming. The first step in the pretreatment of samples is the dissociation of conjugates, wherein alkaline hydrolysis (4 M sodium hydroxide, 115°C, pressure 15 psi) is commonly used to hydrolyze bile (Batta and Salen, 1999). Other enzymes may also be used to hydrolyze the conjugates; for example, glycine or taurine conjugates are usually hydrolyzed with a choloylglycine hydrolase, and β-glucuronidase is used to hydrolyze bile acid glucosides. The second step is transformation. The carboxyl groups in bile acids are usually converted to methyl esters, commonly using fresh diazomethane (Campbell et al., 1975). In addition, anhydrous methanol hydrochloric acid, methanol-5% sulfuric acid, or methyl alcohol in the presence of p-toluenesulfonic acid may be used. The hydroxyl groups in bile acids are often converted to trimethylsilyl ether derivatives, usually using trimethylsilanylation agents, such as *N*,*O*-bis(trimethylsilyl)acetamide and bis (trimethylsilyl)trifluoroacetamide. Oxo functional groups are susceptible to strict alkaline hydrolysis; therefore, in the presence of bile acids containing Oxo functional groups, enzymes are usually used to hydrolyze conjugated bile acids, which can be detected without oxo functional group conversion or by *o*-methyloxime or dimethylhydrazone conversion.

In order to prevent errors caused by sample pretreatment, it is necessary to select an appropriate quantitative internal standard for GC. Commonly used internal standards are coprostanol (Setchell and Matsui, 1983), nor-deoxycholic acid

(Child et al., 1987), 7α,12α-dihydroxy-5β-cholan-24-oic acid (Bailey et al., 1987), Notably, bile acids labeled with stable isotopes give the most accurate results (Sjövall et al., 1985).

One of the drawbacks of GC and GC-MS is that they are very time-consuming in sample preparation, which involves extraction, purification, hydrolysis, and derivatization, as well as the inaccurate identification of stereoisomerization forms of bile acids with a single gas column, which limits the wide application of GC/GC-MS. The development of improved separation procedures and their automation will increase the analytical potential of capillary gas chromatography separation capabilities. Compared with the latest electrospray HPLC-MS, traditional GC and GC-MS have a lower sensitivity, and as a result, they have been replaced.

Capillary Electrophoresis (Capillary Micellar Electrokinetic Chromatography)

Capillary electrophoresis for the determination of bile acid concentration is a new technique that appeared at the end of the last century, but it is not commonly used in bile acid detection. CE is a new type of liquid phase separation technology with a capillary as the separation channel and a high-voltage DC electric field as the driving force. CE consists of electrophoresis, chromatography, and their cross content. The traditional pressure driving force of chromatography is changed to a voltage driving force. Capillary isokinetic electrophoresis and micellar electrokinetic capillary chromatography are commonly used for bile acid detection. Conductance detectors and indirect UV absorption detectors are commonly used. Dimethylcyclodextrin (D-β-CD) and trimethylcyclodextrin (T-β-CD) are often added to the buffer solution to improve the selectivity of the analysis.

When the technology was first developed, it could only detect pure bile acid samples or impurities in pure bile acid drugs. For example, UDCA plays an important role in the treatment of cholesterol calculi. Quaglia et al. (1997) detected UDCA and its common impurities using high-performance capillary zone electrophoresis (UPCE) combined with indirect UV absorption detection. Yang et al. (2011) used capillary electrophoresis frontal analysis (CEFA) to study the effects of four different bile salts, cholate, deoxycholate, taurocholate, and monoketone cholate, on membrane binding of the cationic model drug, proderol.

In recent years, this technique has been applied for the detection of biological samples. Reijenga et al. (1983) used isokinetic electrophoresis combined with a conductivity detector and indirect UV absorption detector in a non-aqueous solvent (95% methanol) to detect the amounts of various conjugated bile acids in human bile. Yarabe et al. (1998) optimized the indirect photometric method of capillary zone electrophoresis (CZE) to detect the concentrations of 15 common bile acids in human plasma samples for the first time. The addition of γ-cyclodextrin to the running electrolyte significantly improved the peak resolution; however, the sensitivity of bile acid detection required further improvement.

Capillary electrophoresis has good separation capacity and detection speed, but it is not as sophisticated as HPLC. Moreover, these procedures are technically demanding and unreliable and therefore not suitable for routine analysis of biological samples (Scalia, 1995). In the future, with the improvement in detection technology, CE may be comparable to traditional HPLC.

BILE ACID-RELATED DISEASES

Bile acid synthesis has extensive inter-individual variation; for example, it is lower in women than in men, and is positively correlated with serum triglyceride levels (Galman et al., 2011). In addition to the individual differences in bile acids, various diseases, such as hepatobiliary, gastrointestinal, metabolic, and nervous system diseases, can also cause changes in the amount or type of bile acid in the human body. Bile acids are produced by the liver and are involved in the metabolism of intestinal microorganisms in the gut. New evidence suggests that the intestinal microflora are closely related to the risk, development, and progression of gastrointestinal cancer and hepatocellular carcinoma (Jia et al., 2018; Lee et al., 2020). Therefore, it is of great significance to understand the interconnection between the liver, bile acids, and digestive microflora. Using the relevant techniques mentioned in the previous sections, we can monitor changes in metabolism and diagnose or predict the occurrence of related diseases.

Gastrointestinal Diseases

The intestinal tract is the main site where bile acids promote the digestion and absorption of lipids. Secondary bile acids are synthesized by intestinal flora via deconjugation, dehydrogenation, and dehydroxylation. Therefore, gastrointestinal diseases, such as inflammatory bowel disease (IBD) and gastric cancer, are closely related to bile acid metabolism in the body.

Inflammatory bowel disease is an idiopathic inflammatory bowel disease involving the ileum, rectum, and colon. Clinical manifestations include diarrhea, abdominal pain, and even bloody stools. The disease includes ulcerative colitis (UC) and Crohn's disease (CD). Gut microbes metabolize bile acids, and because of the ecological dysregulation that occurs in IBD, bile acid metabolism is disrupted. Duboc et al. (2013) found that fecal conjugated bile acid levels were significantly elevated and secondary bile acid levels were significantly reduced in active IBD. Interestingly, patients with active IBD had higher levels of 3-OH-sulphated bile acids in their feces. Microbial deconjugation, transformation, and desulfurization activities in patients with IBD are impaired.

Gastric cancer is a malignant tumor originating from the gastric mucosal epithelium, and the vast majority of gastric cancers are adenocarcinomas. Gastric cancer has no noticeable symptoms in the early stage or has non-specific symptoms, such as upper abdominal discomfort and belching, which are often similar to the symptoms of chronic gastric diseases, such as gastritis and gastric ulcer, and are easily ignored. Therefore, the rate of early diagnosis of gastric cancer is still low (Tan, 2019). In the western world, it is most often diagnosed at an advanced stage, after distant metastasis (Digklia and Wagner, 2016). Lee et al. (2020) successfully analyzed 70 human gastric juice samples from

patients with chronic superficial gastritis, intestinal metaplasia, and gastric cancer, and studied the correlation between bile acid metabolism and gastric cancer. According to the progression of chronic superficial gastritis to intestinal metaplasia and gastric cancer, there were statistical differences in the metabolism of CA and DCA. Therefore, the progression of gastric cancer may be related to changes in the composition of the intestinal microbiome. This study provides insights into the etiological mechanisms of gastric cancer progression and biomarkers for the diagnosis and treatment of gastric cancer.

Hepatobiliary Diseases

Bile acids are produced in the liver, stored in the gallbladder, and serve a function in the gut; only a small fraction enters the blood circulation. In hepatobiliary disease, the bile acid levels in the serum vary greatly. The membrane bile acid receptor TGR5 and the FXR of the nuclear hormone receptor FXR-α are not only regulatory factors for the synthesis and transport of bile acids, but also the transcription factors and the protection sensors that are regulated by the bile acids, which induce protective cell reactions of the liver and gastrointestinal tissues, regulating inflammation, immune response, and liver regeneration (Jia et al., 2018). Thus, the metabolic changes in the liver can be reflected in the changes in bile acid contents and types, and the detection of bile acid changes can be used for the diagnosis of hepatobiliary diseases.

Bile deposition is a pathological physiological process caused by the secretion of bile and excretion disorder. It is characterized by an excessive accumulation of bile (in the liver and body circulation), cholesterol, and bilirubin, which can cause damage to liver cells and the body; moreover, long-term persistent bile silting is caused by liver fibrosis and even cirrhosis (Li et al., 2017). Bile flow damage causes bile deposition, which is characterized by elevated bile acid levels in the liver and serum, followed by liver cells, and biliary damage. The amide proton region of ^{1}H MR in human bile plays an important role in distinguishing cholestasis patterns from normal ones. Ijare et al. (2009) used this method to obtain bile from normal bile ducts containing bile acids with taurine and glycine conjugates, CA, CDCA, and DCA. A lack of glycine-bound CDCA was observed in bile samples from patients with primary sclerosing cholangitis.

Intrahepatic cholestasis of pregnancy (ICP) is a special complication that occurs in the second and third trimesters of pregnancy. It is characterized by itchy skin and elevated levels of bile acid. It mainly harms the fetus and increases the morbidity and mortality of perinatal children. ICP diagnosis involves a liver anomaly examination. Its etiology is unknown and it will get better during childbirth. Liver examination includes measurement of liver transaminase, bilirubin, or bile acid levels. Tribe et al. (2010) identified changes in bile acid spectra during normal pregnancy and pregnancy with intrahepatic cholestasis and pruritus and found that ICP was associated with a significant increase in taurine- and glycine-conjugated cholic acid levels after 24 weeks of gestation; ursodeoxycholic acid (UDCA) therapy significantly reduced serum taurocholic acid and taurodeoxycholic acid concentrations. In addition to the serum bile acid test, urobile acids can also be used to detect or exclude ICP. Huang et al. (2007) tested this assay and found that urine bile acid sulfate (UBAS) ratio from UBASTEC-AUTO could distinguish patients with ICP from healthy pregnancies. At the same level of sensitivity, urine bile acid sulfate has a higher specificity than non-sulfuric urine bile acids. Nevertheless, Manzotti et al. (2019) believe that serum TBA, serum bile acid spectrum, or both, for the diagnosis of ICP is overestimated as the overall risk of bias is high; additionally, there are concerns about the applicability of the results in clinical practice, making it difficult to make recommendations and draw final conclusions based on available literature.

Urine and serum metabolomic analyses revealed bile acids as potential biomarkers for primary biliary cirrhosis (Kakiyama et al., 2013). Tang et al. (2015), using the ultra-high performance liquid chromatography-quadrupole time-of-flight mass spectrometry (UPLC/Q-TOF MS) method, showed that bile acid levels increased with the progression of primary biliary cirrhosis, and carnitine levels, such as that of propionate carnitine and butyl carnitine, decreased with the progression of primary biliary cirrhosis. Thus, they could be used to diagnose the onset and progression of primary biliary cirrhosis.

Metabolic Disease

Low-grade tissue inflammation induced by obesity can lead to insulin resistance, which is a key cause of type 2 diabetes. Cells of the innate immune system produce cytokines and other factors that impair insulin signaling, which contributes to the link between obesity and the development of type 2 diabetes (Lackey and Olefsky, 2016). As signaling molecules, bile acids are involved in the regulation of energy metabolism and immune response *in vivo*. Therefore, when obesity or type 2 diabetes occurs, the bile acid pool in the body undergoes corresponding changes. TBA concentrations were elevated in obese patients and correlated with body mass index, but not with type 2 diabetes. In patients with type 2 diabetes, both fasting and post-prandial systemic TBA concentrations were found to be increased. However, different qualitative components of bile acids have been reported in different studies. Wu et al. (2015) found elevated levels of nine metabolites in the serum of patients with type 2 diabetes, three of which were bile acids—taurochenodeoxycholic acid, 12α-hydroxy-3-oxocholadienic acid, and glycocholic acid. Wewalka et al. (2014) found that fasting serum taurine-conjugated bile acid concentrations were higher in patients with type 2 diabetes than in those with normal glucose tolerance and were not associated with the intensification of insulin levels, but with fasting and post-load glucose. Interestingly, patients with insulin resistance, but not type 2 diabetes, showed an increased 12α-hydroxylated:non-12α-hydroxylated bile acid ratio (Chavez-Talavera et al., 2017).

Zheng et al. (2021) studied the association of HCA with obesity and diabetes. They found a strong association between metabolic disorders and HCA. The serum concentration of HCA in obese or diabetic patients was lower than that in healthy adults, and the serum HCA level was increased in post-Sleeve Gastrectomy (SG) patients. They further demonstrated

that low levels of HCA were found in the feces of prediabetic patients and that increased concentrations of HCA after SG predicted remission 2 years after diabetes, thus demonstrating the feasibility of using HCA to assess the risk of future metabolic diseases.

Bile acid levels also change after metabolic surgery. Roux-en-Y gastric bypass (RYGB) surgery can alleviate type 2 diabetes; however, the mechanism of action is not fully understood. Gerhard et al. (2013) found that after Roux-en-Y Gastric Bypass (RYGB) surgery, FGF19 and bile acid levels (especially that of cholic and deoxycholic acids) were highly increased in diabetes-RYGB patients than in non-diabetic or diabetes-non-RYGB patients, suggesting that the FGF19-CYP7A1-BA pathway plays a role in the remission of type 2 diabetes after RYGB surgery. Moreover, changes in serum bile acid content can also be used to monitor the therapeutic effect of type 2 diabetes drugs. For example, after colesevelam treatment, CA synthesis was enhanced, but CDCA and DCA levels decreased in patients with type 2 diabetes. Interestingly, the total content of hydrophobic bile acids decreased, and the total bile acid pool remained stable (Brufau et al., 2010).

Gestational diabetes is defined as diabetes with normal glucose metabolism before pregnancy or diabetes with underlying glucose tolerance that does not appear until or is diagnosed during pregnancy. Gao et al. (2016) found that the levels of eight bile acids, including two dihydroxy conjugated, one trihydroxy unconjugated, and five sulfated bile acids, were significantly increased in the serum of patients with gestational diabetes compared with the control group. β-Muricholic acid (β-MCA) and dihydroxy conjugated bile acids were identified as the most suitable metabolic markers for the diagnosis and differential diagnosis, respectively, of gestational diabetes.

Cardiovascular Disease

Metabolic syndrome is an increasingly worldwide public health problem. It refers to the pathological state of metabolic disorder of proteins, fats, carbohydrates and other substances in human body. It is a group of complex metabolic disorder syndrome. Metabolic syndrome is a constellation of five clinical symptoms, hypertension, hyperglycemia, hypertriglyceridemia, insulin resistance, and obesity (Porez et al., 2012; Spinelli et al., 2016). In addition to metabolic diseases such as diabetes mentioned above, cardiovascular diseases are also an important component. Pushpass et al. (2021) suggest that bile acids may be the link between gut microbiome and cardiovascular health. Although results from human studies have been inconsistent, there is growing evidence that these dietary components are associated with improvements in lipid cardiovascular disease risk markers, which may be related to the regulatory role of gut microbiota and bile acid metabolism. These include an increase in newly synthesized bile acids due to bile chelation, the metabolic activity of bile salts, and short-chain fatty acids produced by bacterial fermentation of fibers. Desai et al. (2017) propose that the decreased expression of Pgc1α is associated with metabolic dysfunction in cholecystitis, and that lowering serum bile acid concentration helps to inhibit cardiac metabolic and pathological changes.

Nervous System Disease

Recent studies have shown that bile acid signaling plays a broad role in the central nervous system. Some bile acids, such as taurine DCA and UDCA, have shown neuroprotective potential in a number of experimental animal models and clinical studies on neurological diseases (Grant and DeMorrow, 2020). Recent epidemiological and molecular studies have shown that disruption of cholesterol homeostasis is associated with an increased risk of Alzheimer's disease. In addition, brain cholesterol accumulation contributes to the progression of hepatic encephalopathy through the role of bile acid-mediated FXR. Targeting the gut microbiome–bile acid–brain axis may be a novel strategy against Alzheimer's disease and hepatic encephalopathy. However, further research on this axis is still needed to fully understand and treat Alzheimer's disease and hepatic encephalopathy (Jia et al., 2020).

CONCLUSION AND PERSPECTIVES

In summary, there are a number of bile acid detection methods; LC-MS and its derivatives are used as the mainstream techniques in laboratory research, while enzyme analysis for the detection of TBA is also being used in clinical diagnosis. Each of these methods has its own advantages and disadvantages, and the applicable conditions are different. The relationship between disease and bile acid metabolism has also becoming clearer with progress in research; however, there is still much to be learned. In terms of scientific research and technology, whether there are some properties of bile acids that have not been used in the existing detection method or whether emerging technologies can be used in the detection of bile acids needs to be addressed, in clinical diagnosis, studies are required to improve the sensitivity and specificity of these techniques, making them suitable for application in the diagnosis, identification, and even prediction of diseases. Such techniques when applied to the clinic will benefit humanity, with far-reaching significance, and further studies are needed to explore their potential.

AUTHOR CONTRIBUTIONS

XZ was involved in data collection and writing of the manuscript. ZL and FS were involved in conception, design, and coordination of the study. LY and GY were involved in picture and table formatting. KW supervised the project and revised the manuscript. All authors have critically reviewed the manuscript and have approved the publication of this final version of the manuscript.

FUNDING

This research was supported by National Natural Science Foundation of China (No. 82070852/H0713).

REFERENCES

Alnouti, Y., Csanaky, I. L., and Klaassen, C. D. (2008). Quantitative-profiling of bile acids and their conjugates in mouse liver, bile, plasma, and urine using LC-MS/MS. *J. Chromatogr. B. Analyt. Technol. Biomed. Life Sci.* 873, 209–217. doi: 10.1016/j.jchromb.2008.08.018

Bailey, E., Brooks, A. G. F., Purchase, R., Meakings, M., Davies, M., and Walters, D. G. (1987). Improved method for the determination of the major neutral steroids and unconjugated bile acids in human faeces using capillary gas chromatography. *J. Chromatogr. B* 421, 21–31. doi: 10.1016/0378-4347(87)80375-4

Bathena, S. P., Mukherjee, S., Olivera, M., and Alnouti, Y. (2013). The profile of bile acids and their sulfate metabolites in human urine and serum. *J. Chromatogr. B Analyt. Technol. Biomed. Life Sci.* 942-943, 53–62. doi: 10.1016/j.jchromb.2013.10.019

Batta, A. K., and Salen, G. (1999). Gas chromatography of bile acids. *J. Chromatogr. B Biomed. Sci. Appl.* 723, 1–16. doi: 10.1016/s0378-4347(98)00528-3

Bessonneau, V., Bojko, B., Azad, A., Keshavjee, S., Azad, S., and Pawliszyn, J. (2014). Determination of bronchoalveolar lavage bile acids by solid phase microextraction liquid chromatography-tandem mass spectrometry in combination with metabolite profiling: comparison with enzymatic assay. *J. Chromatogr. A* 1367, 33–38. doi: 10.1016/j.chroma.2014.09.061

Bobeldijk, I., Hekman, M., de Vries-van der Weij, J., Coulier, L., Ramaker, R., Kleemann, R., et al. (2008). Quantitative profiling of bile acids in biofluids and tissues based on accurate mass high resolution LC-FT-MS: compound class targeting in a metabolomics workflow. *J. Chromatogr. B. Analyt. Technol. Biomed. Life Sci.* 871, 306–313. doi: 10.1016/j.jchromb.2008.05.008

Bovara, R., Carrea, G., Grigolo, B., Ghini, S., Girotti, S., and Roda, A. (1984). Continuous-flow determination of primary bile acids, by bioluminescence, with use of nylon-immobilized bacterial enzymes. *Clin. Chem.* 30, 206–210. doi: 10.1093/clinchem/30.2.206

Brufau, G., Stellaard, F., Prado, K., Bloks, V. W., Jonkers, E., Boverhof, R., et al. (2010). Improved glycemic control with colesevelam treatment in patients with type 2 diabetes is not directly associated with changes in bile acid metabolism. *Hepatology* 52, 1455–1464. doi: 10.1002/hep.23831

Campbell, C. B., McGuffie, C., and Powell, L. W. (1975). The measurement of sulphated and non-sulphated bile acids in serum using gas-liquid chromatography. *Clin. Chim. Acta* 63, 249–262. doi: 10.1016/0009-8981(75)90045-5

Chavez-Talavera, O., Tailleux, A., Lefebvre, P., and Staels, B. (2017). Bile Acid Control of Metabolism and Inflammation in Obesity, Type 2 Diabetes, Dyslipidemia, and Nonalcoholic Fatty Liver Disease. *Gastroenterology* 152, 679–1694e1673. doi: 10.1053/j.gastro.2017.01.055

Che, N., Ma, Y., Ruan, H., Xu, L., Wang, X., Yang, X., et al. (2018). Integrated semi-targeted metabolomics analysis reveals distinct metabolic dysregulation in pleural effusion caused by tuberculosis and malignancy. *Clin. Chim. Acta* 477, 81–88. doi: 10.1016/j.cca.2017.12.003

Chiang, J. Y. (2013). Bile acid metabolism and signaling. *Compr. Physiol.* 3, 1191–1212. doi: 10.1002/cphy.c120023

Child, P., Aloe, M., and Mee, D. (1987). Separation and quantitation of fatty acids, sterols and bile acids in feces by gas chromatography as the butyl ester—acetate derivatives. *J. Chromatogr. B* 415, 13–26. doi: 10.1016/s0378-4347(00)83187-4

Cui, X., Vasylieva, N., Wu, P., Barnych, B., Yang, J., Shen, D., et al. (2017). Development of an Indirect Competitive Enzyme-Linked Immunosorbent Assay for Glycocholic Acid Based on Chicken Single-Chain Variable Fragment Antibodies. *Anal. Chem.* 89, 11091–11097. doi: 10.1021/acs.analchem.7b03190

Desai, M. S., Mathur, B., Eblimit, Z., Vasquez, H., Taegtmeyer, H., Karpen, S. J., et al. (2017). Bile acid excess induces cardiomyopathy and metabolic dysfunctions in the heart. *Hepatology* 65, 189–201. doi: 10.1002/hep.28890

Digklia, A., and Wagner, A. D. (2016). Advanced gastric cancer: Current treatment landscape and future perspectives. *World J. Gastroenterol.* 22, 2403–2414. doi: 10.3748/wjg.v22.i8.2403

Duarte, I. F., Legido-Quigley, C., Parker, D. A., Swann, J. R., Spraul, M., Braumann, U., et al. (2009). Identification of metabolites in human hepatic bile using 800 MHz 1H NMR spectroscopy, HPLC-NMR/MS and UPLC-MS. *Mol. Biosyst.* 5, 180–190. doi: 10.1039/b814426e

Duboc, H., Rajca, S., Rainteau, D., Benarous, D., Maubert, M. A., Quervain, E., et al. (2013). Connecting dysbiosis, bile-acid dysmetabolism and gut inflammation in inflammatory bowel diseases. *Gut* 62, 531–539. doi: 10.1136/gutjnl-2012-302578

Durc, P., Dosedelova, V., Foret, F., Dolina, J., Konecny, S., Himmelsbach, M., et al. (2020). Analysis of major bile acids in saliva samples of patients with Barrett's esophagus using high-performance liquid chromatography-electrospray ionization-mass spectrometry. *J. Chromatogr. A* 1625:461278. doi: 10.1016/j.chroma.2020.461278

Dutta, M., Cai, J., Gui, W., and Patterson, A. D. (2019). A review of analytical platforms for accurate bile acid measurement. *Anal. Bioanal. Chem.* 411, 4541–4549. doi: 10.1007/s00216-019-01890-3

Engvall, E., and Perlmann, P. (1971). Enzyme-linked immunosorbent assay (ELISA) quantitative assay of immunoglobulin G. *Immunochemistry* 8, 871–874. doi: 10.1016/0019-2791(71)90454-x

Fu, X., Xiao, Y., Golden, J., Niu, S., and Gayer, C. P. (2020). Serum bile acids profiling by liquid chromatography-tandem mass spectrometry (LC-MS/MS) and its application on pediatric liver and intestinal diseases. *Clin. Chem. Lab. Med.* 58, 787–797. doi: 10.1515/cclm-2019-0354

Galman, C., Angelin, B., and Rudling, M. (2011). Pronounced variation in bile acid synthesis in humans is related to gender, hypertriglyceridaemia and circulating levels of fibroblast growth factor 19. *J. Intern. Med.* 270, 580–588. doi: 10.1111/j.1365-2796.2011.02466.x

Gao, J., Xu, B., Zhang, X., Cui, Y., Deng, L., Shi, Z., et al. (2016). Association between serum bile acid profiles and gestational diabetes mellitus: a targeted metabolomics study. *Clin. Chim. Acta* 459, 63–72. doi: 10.1016/j.cca.2016.05.026

Gerhard, G. S., Styer, A. M., Wood, G. C., Roesch, S. L., Petrick, A. T., Gabrielsen, J., et al. (2013). A role for fibroblast growth factor 19 and bile acids in diabetes remission after Roux-en-Y gastric bypass. *Diabetes Care* 36, 1859–1864. doi: 10.2337/dc12-2255

Gómez, C., Stücheli, S., Kratschmar, D. V., Bouitbir, J., and Odermatt, A. (2020). Development and Validation of a Highly Sensitive LC-MS/MS Method for the Analysis of Bile Acids in Serum, Plasma, and Liver Tissue Samples. *Metabolites* 10:7. doi: 10.3390/metabo10070282

Gowda, G. A. (2011). NMR spectroscopy for discovery and quantitation of biomarkers of disease in human bile. *Bioanalysis* 3, 1877–1890. doi: 10.4155/bio.11.152

Grant, S. M., and DeMorrow, S. (2020). Bile Acid Signaling in Neurodegenerative and Neurological Disorders. *Int. J. Mol. Sci.* 21:17. doi: 10.3390/ijms21175982

Han, J., Liu, Y., Wang, R., Yang, J., Ling, V., and Borchers, C. H. (2015). Metabolic profiling of bile acids in human and mouse blood by LC-MS/MS in combination with phospholipid-depletion solid-phase extraction. *Anal. Chem.* 87, 1127–1136. doi: 10.1021/ac503816u

Higashi, T., Shibayama, Y., Ichikawa, T., Ito, K., Toyo'oka, T., Shimada, K., et al. (2010). Salivary chenodeoxycholic acid and its glycine-conjugate: their determination method using LC-MS/MS and variation of their concentrations with increased saliva flow rate. *Steroids* 75, 338–345. doi: 10.1016/j.steroids.2010.01.015

Hu, T., An, Z., Shi, C., Li, P., and Liu, L. (2020). A sensitive and efficient method for simultaneous profiling of bile acids and fatty acids by UPLC-MS/MS. *J. Pharm. Biomed. Anal.* 178:112815. doi: 10.1016/j.jpba.2019.112815

Huang, W. M., Seubert, D. E., Donnelly, J. G., Liu, M., and Javitt, N. B. (2007). Intrahepatic cholestasis of pregnancy: detection with urinary bile acid assays. *J. Perinat. Med.* 35, 486–491. doi: 10.1515/JPM.2007.128

Ijare, O. B., Bezabeh, T., Albiin, N., Arnelo, U., Bergquist, A., Lindberg, B., et al. (2009). Absence of glycochenodeoxycholic acid (GCDCA) in human bile is an indication of cholestasis: a 1H MRS study. *NMR Biomed.* 22, 471–479. doi: 10.1002/nbm.1355

Ikegawa, S., Okuyama, H., Oohashi, J., Murao, N., and Goto, J. (1999). Separation and Detection of Bile Acid 24-Glucuronides in Human Urine by Liquid Chromatography Combined with Electrospray Ionization Mass Spectrometry. *Analy. Sci.* 15, 625–631. doi: 10.2116/analsci.15.625

Ishibashi, M., Ando, T., Sakai, M., Matsubara, A., Uchikata, T., Fukusaki, E., et al. (2012). High-throughput simultaneous analysis of pesticides by supercritical fluid chromatography/tandem mass spectrometry. *J. Chromatogr. A* 1266, 143–148. doi: 10.1016/j.chroma.2012.09.067

Iwata, T., and Yamasaki, K. (1964). Enzymatic Determination and Thin-Layer Chromatography of Bile Acids in Blood. *J. Biochem.* 56, 424–431. doi: 10.1093/oxfordjournals.jbchem.a128013

Jantti, S. E., Kivilompolo, M., Ohrnberg, L., Pietilainen, K. H., Nygren, H., Oresic, M., et al. (2014). Quantitative profiling of bile acids in blood, adipose tissue, intestine, and gall bladder samples using ultra high performance liquid chromatography-tandem mass spectrometry. *Anal. Bioanal. Chem.* 406, 7799–7815. doi: 10.1007/s00216-014-8230-9

Jia, W., Rajani, C., Kaddurah-Daouk, R., and Li, H. (2020). Expert insights: The potential role of the gut microbiome-bile acid-brain axis in the development and progression of Alzheimer's disease and hepatic encephalopathy. *Med. Res. Rev.* 40, 1496–1507. doi: 10.1002/med.21653

Jia, W., Xie, G., and Jia, W. (2018). Bile acid-microbiota crosstalk in gastrointestinal inflammation and carcinogenesis. *Nat. Rev. Gastroenterol. Hepatol.* 15, 111–128. doi: 10.1038/nrgastro.2017.119

Kakiyama, G., Muto, A., Takei, H., Nittono, H., Murai, T., Kurosawa, T., et al. (2014). A simple and accurate HPLC method for fecal bile acid profile in healthy and cirrhotic subjects: validation by GC-MS and LC-MS. *J. Lipid. Res.* 55, 978–990. doi: 10.1194/jlr.D047506

Kakiyama, G., Pandak, W. M., Gillevet, P. M., Hylemon, P. B., Heuman, D. M., Daita, K., et al. (2013). Modulation of the fecal bile acid profile by gut microbiota in cirrhosis. *J. Hepatol.* 58, 949–955. doi: 10.1016/j.jhep.2013.01.003

Krautbauer, S., Büchler, C., and Liebisch, G. (2016). Relevance in the Use of Appropriate Internal Standards for Accurate Quantification Using LC-MS/MS: Tauro-Conjugated Bile Acids as an Example. *Anal. Chem.* 88, 10957–10961. doi: 10.1021/acs.analchem.6b02596

Kunnecke, B., Bruns, A., and von Kienlin, M. (2007). Non-invasive analysis of gallbladder bile composition in cynomolgus monkeys using in vivo 1H magnetic resonance spectroscopy. *Biochim. Biophys. Acta* 1771, 544–549. doi: 10.1016/j.bbalip.2007.01.006

Lackey, D. E., and Olefsky, J. M. (2016). Regulation of metabolism by the innate immune system. *Nat. Rev. Endocrinol.* 12, 15–28. doi: 10.1038/nrendo.2015.189

Lawler, K., Huang-Doran, I., Sonoyama, T., Collet, T. H., Keogh, J. M., Henning, E., et al. (2020). Leptin-Mediated Changes in the Human Metabolome. *J. Clin. Endocrinol. Metab.* 105, 2541–2552. doi: 10.1210/clinem/dgaa251

Lee, W., Um, J., Hwang, B., Lee, Y. C., Chung, B. C., and Hong, J. (2020). Assessing the progression of gastric cancer via profiling of histamine, histidine, and bile acids in gastric juice using LC-MS/MS. *J. Steroid. Biochem. Mol. Biol.* 197:105539. doi: 10.1016/j.jsbmb.2019.105539

Li, M., Cai, S. Y., and Boyer, J. L. (2017). Mechanisms of bile acid mediated inflammation in the liver. *Mol. Aspects Med.* 56, 45–53. doi: 10.1016/j.mam.2017.06.001

Liu, S., Zhang, Y., Qu, B., Qin, G., Cheng, J., Lu, F., et al. (2017). Detection of total bile acids in biological samples using an indirect competitive ELISA based on four monoclonal antibodies. *Analy. Methods* 9, 625–633. doi: 10.1039/c6ay03243e

Liu, Y., Rong, Z., Xiang, D., Zhang, C., and Liu, D. (2018). Detection technologies and metabolic profiling of bile acids: a comprehensive review. *Lipids Health Dis.* 17:121. doi: 10.1186/s12944-018-0774-9

Mäentausta, O., and Jänne, O. (1979). Radioimmunoassay of conjugated cholic acid, chenodeoxycholic acid, and deoxycholic acid from human serum, with use of 125I-labeled ligands. *Clin. Chem.* 25, 264–268.

Mano, N., Mori, M., Ando, M., Goto, T., and Goto, J. (2006). Ionization of unconjugated, glycine- and taurine-conjugated bile acids by electrospray ionization mass spectrometry. *J. Pharm. Biomed. Anal.* 40, 1231–1234. doi: 10.1016/j.jpba.2005.09.012

Manzotti, C., Casazza, G., Stimac, T., Nikolova, D., and Gluud, C. (2019). Total serum bile acids or serum bile acid profile, or both, for the diagnosis of intrahepatic cholestasis of pregnancy. *Cochrane Database Syst. Rev.* 7:CD012546. doi: 10.1002/14651858.CD012546.pub2

Marschall, H. U., Matern, H., Wietholtz, H., Egestad, B., Matern, S., and Sjovall, J. (1992). Bile acid N-acetylglucosaminidation. In vivo and in vitro evidence for a selective conjugation reaction of 7 beta-hydroxylated bile acids in humans. *J. Clin. Invest.* 89, 1981–1987. doi: 10.1172/JCI115806

Momose, T., Mure, M., Iida, T., Goto, J., and Nambara, T. (1998). Method for the separation of the unconjugates and conjugates of chenodeoxycholic acid and deoxycholic acid by two-dimensional reversed-phase thin-layer chromatography with methyl β-cyclodextrin. *J Chromatogr. A* 811, 171–180. doi: 10.1016/s0021-9673(98)00213-1

Onishi, S., Itoh, S., and Ishida, Y. (1982). Assay of free and glycine- and taurine-conjugated bile acids in serum by high-pressure liquid chromatography by using post-column reaction after group separation. *Biochem. J.* 204, 135–139. doi: 10.1042/bj2040135

Onisor, C., Posa, M., Kevresan, S., Kuhajda, K., and Sarbu, C. (2010). Estimation of chromatographic lipophilicity of bile acids and their derivatives by reversed-phase thin layer chromatography. *J. Sep. Sci.* 33, 3110–3118. doi: 10.1002/jssc.200900879

Plumb, R., Castro-Perez, J., Granger, J., Beattie, I., Joncour, K., and Wright, A. (2004). Ultra-performance liquid chromatography coupled to quadrupole-orthogonal time-of-flight mass spectrometry. *Rapid. Commun. Mass Spectr.* 18, 2331–2337. doi: 10.1002/rcm.1627

Poole, C. F. (2003). Thin-layer chromatography: challenges and opportunities. *J. Chromatogr. A* 1000, 963–984. doi: 10.1016/s0021-9673(03)00435-7

Porez, G., Prawitt, J., Gross, B., and Staels, B. (2012). Bile acid receptors as targets for the treatment of dyslipidemia and cardiovascular disease. *J. Lipid Res.* 53, 1723–1737. doi: 10.1194/jlr.R024794

Prescot, A. P., Collins, D. J., Leach, M. O., and Dzik-Jurasz, A. S. (2003). Human gallbladder bile: noninvasive investigation in vivo with single-voxel 1H MR spectroscopy. *Radiology* 229, 587–592. doi: 10.1148/radiol.2292021156

Pushpass, R. G., Alzoufairi, S., Jackson, K. G., and Lovegrove, J. A. (2021). Circulating bile acids as a link between the gut microbiota and cardiovascular health: impact of prebiotics, probiotics and polyphenol-rich foods. *Nutr. Res. Rev.* 2021, 1–20. doi: 10.1017/S0954422421000081

Quaglia, M. G., Farina, A., Bossù, E., Dell'Aquila, C., and Doldo, A. (1997). The indirect UV detection in the analysis of ursodeoxycholic acid and related compounds by HPCE. *J. Pharm. Biomed. Anal.* 16, 281–285. doi: 10.1016/s0731-7085(97)00034-4

Reijenga, J. C., Slaats, H. J. L. A., and Everaerts, F. M. (1983). Determination of conjugated bile acids in human bile by isotachophoresis in a non-aqueous solvent using a.c. conductivity and UV detection. *J. Chromatogr. A* 267, 85–89. doi: 10.1016/s0021-9673(01)90821-0

Ridlon, J. M., and Bajaj, J. S. (2015). The human gut sterolbiome: bile acid-microbiome endocrine aspects and therapeutics. *Acta Pharm. Sin. B* 5, 99–105. doi: 10.1016/j.apsb.2015.01.006

Russell, D. W. (2003). The enzymes, regulation, and genetics of bile acid synthesis. *Annu. Rev. Biochem.* 72, 137–174. doi: 10.1146/annurev.biochem.72.121801.161712

Samuelson, K. (1980). Radioimmunoassay compared to an enzymatic method for serum bile acid determination. *Scand. J. Clin. Lab. Invest.* 40, 289–291. doi: 10.3109/00365518009095581

Sarafian, M. H., Lewis, M. R., Pechlivanis, A., Ralphs, S., McPhail, M. J., Patel, V. C., et al. (2015). Bile acid profiling and quantification in biofluids using ultra-performance liquid chromatography tandem mass spectrometry. *Anal. Chem.* 87, 9662–9670. doi: 10.1021/acs.analchem.5b01556

Scalia, S. (1995). Bile acid separation. *J. Chromatogr. B* 671, 299–317. doi: 10.1016/0378-4347(95)00215-5

Scalia, S., and Games, D. E. (1992). Analysis of conjugated bile acids by packed-column supercritical fluid chromatography. *J. Chromatogr. B* 574, 197–203. doi: 10.1016/0378-4347(92)80030-t

Scalia, S., and Games, D. E. (1993). Determination of free bile acids in pharmaceutical preparations by packed column supercritical fluid chromatography. *J. Pharm. Sci.* 82, 44–47. doi: 10.1002/jps.2600820110

Setchell, K. D. R., and Matsui, A. (1983). Serum bile acid analysis. *Clin. Chim. Acta* 127, 1–17. doi: 10.1016/0009-8981(83)90070-0

Shaw, R., and Elliott, W. H. (1976). Bile acids. *Anal. Biochem.* 74, 273–281. doi: 10.1016/0003-2697(76)90208-6

Shi, Y., Xiong, J., Sun, D., Liu, W., Wei, F., Ma, S., et al. (2015). Simultaneous quantification of the major bile acids in artificial Calculus bovis by high-performance liquid chromatography with precolumn derivatization and its application in quality control. *J. Sep. Sci.* 38, 2753–2762. doi: 10.1002/jssc.201500139

Simmonds, W. J., Korman, M. G., Go, V. L. W., and Hofmann, A. F. (1973). Radioimmunoassay of Conjugated Cholyl Bile Acids in Serum. *Gastroenterology* 65, 705–711. doi: 10.1016/s0016-5085(19)33005-7

Sjövall, J., Lawson, A. M., and Setchell, K. D. (1985). Mass spectrometry of bile acids. *Methods Enzymol.* 111, 63–113. doi: 10.1016/s0076-6879(85)11006-2

Spinelli, V., Chavez-Talavera, O., Tailleux, A., and Staels, B. (2016). Metabolic effects of bile acid sequestration: impact on cardiovascular risk factors.

Curr. Opin. Endocrinol. Diabetes Obes. 23, 138–144. doi: 10.1097/MED.0000000000000235

Stahl, E. (1956). [Thin-layer chromatography; methods, influencing factors and an example of its use]. *Pharmazie* 11, 633–637.

Sun, L., Pang, Y., Wang, X., Wu, Q., Liu, H., Liu, B., et al. (2019). Ablation of gut microbiota alleviates obesity-induced hepatic steatosis and glucose intolerance by modulating bile acid metabolism in hamsters. *Acta Pharm. Sin. B* 9, 702–710. doi: 10.1016/j.apsb.2019.02.004

Tagliacozzi, D., Mozzi, A. F., Casetta, B., Bertucci, P., Bernardini, S., Di Ilio, C., et al. (2003). Quantitative analysis of bile acids in human plasma by liquid chromatography-electrospray tandem mass spectrometry: a simple and rapid one-step method. *Clin. Chem. Lab. Med.* 41, 1633–1641. doi: 10.1515/cclm.2003.247

Taguchi, K., Fukusaki, E., and Bamba, T. (2013). Simultaneous and rapid analysis of bile acids including conjugates by supercritical fluid chromatography coupled to tandem mass spectrometry. *J. Chromatogr. A* 1299, 103–109. doi: 10.1016/j.chroma.2013.05.043

Tan, Z. (2019). Recent Advances in the Surgical Treatment of Advanced Gastric Cancer: a Review. *Med. Sci. Monit.* 25, 3537–3541. doi: 10.12659/msm.916475

Tang, Y. M., Wang, J. P., Bao, W. M., Yang, J. H., Ma, L. K., Yang, J., et al. (2015). Urine and serum metabolomic profiling reveals that bile acids and carnitine may be potential biomarkers of primary biliary cirrhosis. *Int. J. Mol. Med.* 36, 377–385. doi: 10.3892/ijmm.2015.2233

Thomas, C., Pellicciari, R., Pruzanski, M., Auwerx, J., and Schoonjans, K. (2008). Targeting bile-acid signalling for metabolic diseases. *Nat. Rev. Drug Discov.* 7, 678–693. doi: 10.1038/nrd2619

Tribe, R. M., Dann, A. T., Kenyon, A. P., Seed, P., Shennan, A. H., and Mallet, A. (2010). Longitudinal profiles of 15 serum bile acids in patients with intrahepatic cholestasis of pregnancy. *Am. J. Gastroenterol.* 105, 585–595. doi: 10.1038/ajg.2009.633

Tu, Y., Zhou, L., Li, L., Wang, L., Gao, S., and Hu, M. (2020). Development and validation of an LC-MS/MS method for the quantification of flavonoid glucuronides (wogonoside, baicalin, and apigenin-glucuronide) in the bile and blood samples: application to a portal vein infusion study. *Anal. Biochem.* 601:113723. doi: 10.1016/j.ab.2020.113723

Ushijima, K., Kimura, A., Inokuchi, T., Yamato, Y., Maeda, K., Yamashita, Y., et al. (2001). Placental transport of bile acids: analysis of bile acids in maternal serum and urine, umbilical cord blood, and amniotic fluid. *Kurume Med. J.* 48, 87–91. doi: 10.2739/kurumemedj.48.87

VandenHeuvel, W. J. A., Sweeley, C. C., and Horning, E. C. (1960). Microanalytical separations by gas chromatography in the sex hormone and bile acid series. *Biochem. Biophys. Res. Comm.* 3, 33–36. doi: 10.1016/0006-291x(60)90098-x

Wang, H., Yeh, C. Y., Li, K., Chung-Davidson, Y. W., and Li, W. (2015). An UPLC-MS/MS method for quantitative profiling of bile acids in sea lamprey plasma and tissues. *J. Chromatogr. B Analyt. Technol. Biomed. Life Sci.* 980, 72–78. doi: 10.1016/j.jchromb.2014.12.018

Wegner, K., Just, S., Gau, L., Mueller, H., Gérard, P., Lepage, P., et al. (2017). Rapid analysis of bile acids in different biological matrices using LC-ESI-MS/MS for the investigation of bile acid transformation by mammalian gut bacteria. *Anal. Bioanal. Chem.* 409, 1231–1245. doi: 10.1007/s00216-016-0048-1

Wewalka, M., Patti, M. E., Barbato, C., Houten, S. M., and Goldfine, A. B. (2014). Fasting serum taurine-conjugated bile acids are elevated in type 2 diabetes and do not change with intensification of insulin. *J. Clin. Endocrinol. Metab.* 99, 1442–1451. doi: 10.1210/jc.2013-3367

Winston, J. A., and Theriot, C. M. (2020). Diversification of host bile acids by members of the gut microbiota. *Gut. Microbes* 11, 158–171. doi: 10.1080/19490976.2019.1674124

Wu, T., Xie, G., Ni, Y., Liu, T., Yang, M., Wei, H., et al. (2015). Serum metabolite signatures of type 2 diabetes mellitus complications. *J. Proteome Res.* 14, 447–456. doi: 10.1021/pr500825y

Yamanaka, M., Kamei, S., Maki, A., Tanaka, N., and Mashige, F. (1981). Direct spectrophotometry of total bile acids in serum. *Clin. Chem.* 27, 1352–1356. doi: 10.1093/clinchem/27.8.1352

Yang, L., Tucker, I. G., and Ostergaard, J. (2011). Effects of bile salts on propranolol distribution into liposomes studied by capillary electrophoresis. *J. Pharm. Biomed. Anal.* 56, 553–559. doi: 10.1016/j.jpba.2011.06.020

Yang, T., Shu, T., Liu, G., Mei, H., Zhu, X., Huang, X., et al. (2017). Quantitative profiling of 19 bile acids in rat plasma, liver, bile and different intestinal section contents to investigate bile acid homeostasis and the application of temporal variation of endogenous bile acids. *J. Steroid. Biochem. Mol. Biol.* 172, 69–78. doi: 10.1016/j.jsbmb.2017.05.015

Yang, Y., Griffiths, W. J., Nazer, H., and Sjövall, J. (1997). Analysis of bile acids and bile alcohols in urine by capillary column liquid chromatography-mass spectrometry using fast atom bombardment or electrospray ionization and collision-induced dissociation. *Biomed. Chromatogr.* 11, 240–255. doi: 10.1002/(sici)1099-0801(199707)11:4<240::Aid-bmc686<3.0.Co;2-6

Yarabe, H. H., Shamsi, S. A., and Warner, I. M. (1998). Capillary zone electrophoresis of bile acids with indirect photometric detection. *Anal. Chem.* 70, 1412–1418. doi: 10.1021/ac970922t

Zheng, X., Chen, T., Zhao, A., Ning, Z., Kuang, J., Wang, S., et al. (2021). Hyocholic acid species as novel biomarkers for metabolic disorders. *Nat. Commun.* 12:1487. doi: 10.1038/s41467-021-21744-w

Conflict of Interest: The authors declare that the research was conducted in the absence of any commercial or financial relationships that could be construed as a potential conflict of interest.

Publisher's Note: All claims expressed in this article are solely those of the authors and do not necessarily represent those of their affiliated organizations, or those of the publisher, the editors and the reviewers. Any product that may be evaluated in this article, or claim that may be made by its manufacturer, is not guaranteed or endorsed by the publisher.

frontiers | Frontiers in Physiology

ORIGINAL RESEARCH
published: 01 April 2022
doi: 10.3389/fphys.2022.854017

The Gut Microbiota in Liver Transplantation Recipients During the Perioperative Period

Zhiyong Lai[1]†, Zongkun Chen[2]†, Anhong Zhang[1], Zhiqiang Niu[1], Meng Cheng[2], Chenda Huo[2] and Jun Xu[1]**

[1]Department of Hepatobiliary and Pancreatic Surgery and Liver Transplant Center, the First Hospital of Shanxi Medical University, Taiyuan, China, [2]Shanxi Medical University, Taiyuan, China

Background: Chronic liver disease is a global problem, and an increasing number of patients receive a liver transplant yearly. The characteristics of intestinal microbial communities may be affected by changes in the pathophysiology of patients during the perioperative.

Methods: We studied gut fecal microbial community signatures in 37 Chinese adults using 16S rRNA sequencing targeting V3-V4 hypervariable regions, with a total of 69 fecal samples. We analyzed the Alpha and Beta diversities of various groups. Then we compared the abundance of bacteria in groups at the phylum, family, and genus levels.

Results: The healthy gut microbiota predominantly consisted of the phyla Firmicutes and Bacteroidestes, followed by Proteobacteria and Actinobacteria. Compared with healthy people, due to the dominant bacteria in patients with chronic liver disease losing their advantages in the gut, the antagonistic effect on the inferior bacteria was reduced. The inferior bacteria multiplied in large numbers during this process. Some of these significant changes were observed in bacterial species belonging to *Enterococcus*, *Klebsiella*, and *Enterobacter*, which increased in patients' intestines. There were low abundances of signature genes such as *Bacteroides*, *Prevotella*, and *Ruminococcus*. *Blautia* and *Bifidobacterium* (considered probiotics) almost disappeared after liver transplantation.

Conclusion: There is an altered microbial composition in liver transplantation patients and a distinct signature of microbiota associated with the perioperative period.

Keywords: chronic liver disease, liver transplantation, gut, microbial composition, alpha diversities, beta diversities

OPEN ACCESS

Edited by:
Sanyuan Hu,
Shandong University, China

Reviewed by:
Dong Sun,
Shandong University, China
Oscar Medina-Contreras,
Federico Gómez Children's Hospital, Mexico

***Correspondence:**
Zhiyong Lai
609774722@qq.com
Jun Xu
junxutytg@163.com

†*These authors have contributed equally to this work*

Specialty section:
This article was submitted to Metabolic Physiology, a section of the journal Frontiers in Physiology

Received: *13 January 2022*
Accepted: *01 March 2022*
Published: *01 April 2022*

Citation:
Lai Z, Chen Z, Zhang A, Niu Z, Cheng M, Huo C and Xu J (2022) The Gut Microbiota in Liver Transplantation Recipients During the Perioperative Period. Front. Physiol. 13:854017. doi: 10.3389/fphys.2022.854017

INTRODUCTION

Around 2 million deaths annually are attributable to liver disease worldwide: 1 million dues to cirrhosis and 1 million due to viral hepatitis and hepatocellular carcinoma (GBD 2017 Cirrhosis Collaborators, 2020). Cirrhosis is the 11th most common cause of death and the third leading cause of death among people aged 45–64 years. With liver cancer, cirrhosis accounts for 3.5% of global deaths (Asrani et al., 2019). Liver disease affects 1.3 billion people worldwide. Chronic liver disease and cirrhosis cause 44,000 deaths in the United States and 2 million deaths worldwide every year (Mokdad et al., 2014; Tapper et al., 2018). Asia is one of the regions with the highest prevalence of liver diseases. In China alone, 300 million people are affected, making the country a global leader in

the prevalence of liver diseases. The incidence of cirrhosis is the leading cause of associated mortality and morbidity. The annual mortality rate is more than 1 million, which has increased in some countries (Rowe, 2017; Wang et al., 2014).

Cirrhosis is the terminal phase of liver disease. In the absence of liver transplantation, patients face dire outcomes. Innovations in surgical equipment and the development of new immunosuppressants have increased the success rate of liver transplantation and prolonged postoperative survival. Nevertheless, in all patients with liver disease, the proportion of malnutrition is as high as 25%–56% and 65%–90% in patients with advanced liver cirrhosis (Yao et al., 2018). There are many factors leading to malnutrition, including nausea, anorexia, alterations in taste receptors, loss of appetite, reduced oral intake of energy and protein, increased basal metabolic rate, unnecessary fasting, and restricted diet.

Under the influence of many factors, the intestinal microbiota of patients with liver disease is significantly different from that of ordinary people. The most dominant bacterial phyla in the human gut are Firmicutes, Bacteroidetes, Actinobacteria, and Proteobacteria, and the most recorded bacterial genera are *Bacteroides*, *Clostridium*, *Peptococcus*, *Bifidobacterium*, *Eubacterium*, *Ruminococcus*, *Faecalibacterium*, and *Peptostreptococcus* (Shapira, 2016). It is well known that human intestinal microbiota is a substantial bacterial library, and there are trillions of microorganisms in 1 G of feces (Turnbaugh et al., 2009). Throughout evolutionary history, humans have developed a symbiotic relationship with bacteria, which protect the gut by providing the host with essential vitamins and nutrients (Schnabl et al., 2014). The gut microbiota performs several essential functions, including protection from pathogens by colonizing mucosal surfaces and creation of various antimicrobial substances, enhancing the immune system, playing a vital role in digestion and metabolism, controlling epithelial cell proliferation and differentiation, modifying insulin resistance, and affecting its secretion, influencing brain-gut communication, and thus affecting the mental and neurological functions of the host. In brief, the gut microbiota plays a significant role in maintaining normal gut physiology and health (Zheng et al., 2019; Kelly et al., 2015; Mills et al., 2019; Rothschild et al., 2018; Wiley et al., 2017).

The balance between microorganisms parasitic in the human intestinal tract may be destroyed, resulting in adrenoleukodystrophy, inflammatory bowel disease, infections, autism, Parkinson's disease, and cancer. However, 20%–60% of bacteria in the human body cannot be cultured with current methods (Kwong et al., 2021). Sequence analysis of 16S rRNA identified several hundred bacterial species in the intestinal ecosystem, most of which cannot be cultured.

Therefore, in this study, 16S rRNA amplicon sequencing was used to analyze the diversity of intestinal microbiota in patients undergoing liver transplantation, to compare the differences of intestinal microbiota between patients undergoing liver transplantation and healthy people. Systematic bacterial profile analysis was carried out at the highest taxonomic level (L2) and the lowest possible in this research method (L6) to obtain a general picture and a detailed analysis of differences in the gut microbiota composition. We explored the impact of intestinal microbiota on patients undergoing liver transplantation and its possible mechanisms to provide a theoretical basis for fecal bacterial transplantation in the future.

MATERIALS AND METHODS

Study Population and Sample Collection

The gut fecal microbial community signatures of 37 Chinese adults were studied for 69 fecal samples. Stool samples were collected from the First Hospital of Shanxi Medical University in 2020–2021. The entire study design and procedures involved were established following the Declaration of Helsinki. Written informed consent forms were signed before the time of sample collection. The Ethics Committee of the First Hospital of Shanxi Medical University approved the protocols. We excluded participants suffering from any symptoms of constipation, bloody stool, diarrhea, or other gastrointestinal disease and those who were administered antibiotics (oral or injectable) in the previous 3 months. In addition, all liver transplant patients in the study were used the same Immunosuppressant treatment regimen, including Tacrolimus, Sirolimus, Mycophenol ethyl ester, and Methylprednisolone, and all patients were used Cefoperazone sodium sulbactam sodium to prevent infection during the perioperative period. Furthermore, abdominal drainage fluid were cultured daily after liver transplantation, and the Antibiotic treatment strategy was adjusted according to the results of bacterial culture of drainage fluid. All stool samples were collected within 4 h. Stool samples were collected in sterile containers provided to the volunteers and were stored at −80°C. Sampling was performed using all standard protocols and regulations. Our analysis was conducted on a total of 69 fecal samples subdivided as follows: before liver transplantation (BLT, 16 samples); liver transplantation 1 week (LT1W, 16 samples); liver transplantation 2 weeks (LT2W, 16 samples); and control group (CG, 21 samples).

Sampling and DNA Extraction

Upon collection, fecal samples were frozen at −80°C immediately upon collection and stored for later use. At the beginning of the experiment, 180–200 mg of each sample was weighed out and transferred to a 2-ml centrifuge tube, which was then placed on ice. According to the manufacturer's instructions, DNA was extracted from the samples using the FastDNA® Spin Kit for Soil (MP Biomedical, LLC, catalog 116560-200). We used Nanodrop to measure the extracted nucleic acid concentrations and stored samples at −80°C.

16S rRNA Gene Amplicon Sequencing

For sequencing, isolated fecal DNA was used as a template for amplification, and the V4 region of 16S rRNA was amplified by performing PCR assays using the universal bacterial primer set 342F (5′-CCTACGGGAGGCAGCAG-3′) and 806R (5′-GGACTACHVGGGTWTCTAAT-3′). The PCR reaction triplicate 50 μL mixture contained 5 μL of 10X Taq DNA polymerase PCR buffer, 1 μL of dNTP mix, 0.5 μL of Taq

DNA polymerase, 2 μL of each primer (10 μM), and 10 ng/μL DNA. The reaction steps were as follows: initialized at 94°C for 5 min, 32 cycles at 94°C for 30 s, 53°C for 30 s and 72°C for 1 min and final extension at 72°C for 5 min. According to the manufacturer's instructions, the resulting PCR products were purified *via* separation on a 2% agarose gel, followed by DNA isolation using the GeneJETTM Gel Extraction Kit (Thermo Scientific). According to the manufacturer's instructions, the purified DNA was quantified using Ion Plus Fragment Library Kit (Life Technologies) and generated sequencing libraries. The partial 16S rRNA genes were sequenced on an Ion S5 Sequencing platform (Sun et al., 2017).

Bioinformatics Analysis and Statistical Processing

16S rRNA sequencing data were processed using QIIME 2 software. After the original data were sequenced off the machine, FastQC software preprocessed the data, deleted incorrect sequences, and had quality control. Then, the DADA2 and Deblur method was used to perform denoising, remove low-quality sequences, short sequences, and chimera sequences in the data. This process retained 40–60% sequences (the length of 300–600 bp) and generated a feature table and representative sequences for downstream analysis. In the case of non-normal distribution, the Kruskal-Wallis analysis of variance was used to calculate variability between the four study groups. The Wilcoxon rank-sum test was used to analyze variability between the two study groups. Alpha and Beta diversities were evaluated using QIIME software, and differences were significant at $p < 0.05$.

Usearch was used to bin reads into operational taxonomic units (OTUs) with a 0.97 identity cut-off. Samples with more sequenced reads had more observed OTUs (Spearman's rank correlation analysis) when all reads were binned into OTUs. Thus, we randomly chose reads with the same number (10,000) and then identified representative OTU reads. Finally, we mapped all randomly chosen reads against representative OTU reads to obtain the OTU composition of all samples. Diversity and richness calculation. Shannon, Simpson, and invsimpson indices were calculated using the "vegan" package in R with a normalized OTU matrix. The observed species, Chao1, and ICE indices were calculated using the "fossil" package in R with a non-normalized OTU matrix. The Hellinger distance was calculated using the "topicmodels" package in R. The JSD distance was calculated using a custom R script provided by the European Molecular Biology Laboratory enterotyping tutorial (http://enterotype.embl.de/enterotypes.html) (Sun et al., 2017).

Alpha diversity index (Shannon Diversity Index, Observed Species, Chao 1) was calculated and displayed using QIIME2 (2020.6.0) and R software (v 4.0.2). To evaluate the sequencing depth and status of sampling, the coverage of GOOD was calculated, and rarefaction curves were constructed. Based on OTU abundance and system development branch length, unweighted UniFrac distances were used in QIIME to calculate Beta diversity between samples. Principal coordinates analysis (PCoA) was performed using vegan (v 2.4–4), ggplot2 (v 3.2), and stats (v 3.6.2) packages. Alpha diversity analysis was performed using R (v 4.0.2, 2020.6), with Wilcoxon Rank-Sum test, Kruskal-Wallis Rank-Sum test, and Spearman correlation analysis. Permutation multivariate analysis of variance (PERMANOVA) and the Wilcoxon Rank-Sum test were used to test the significance of the community composition and structural differences among the groups.

Clusters of Orthologous Genes and Pathway Profiles

COG profiles were constructed using PICRUSt (v 2.3.0-Beta) genome prediction software. First, our custom representative OTU reads were aligned against the Greengenes v.13.5 database 16S rRNA Fasta reference database, and the abundances of representative OTU reads from the same 16S rRNA reference were summed. The reference profile normalized by the 16S rRNA copy number was used to predict the COG profile, and PICRUSt2 software was used to determine the abundance of COG pathways and modules. Finally, R software calculated the top 20 taxonomic phyla and family abundances.

RESULTS

Quality Control

The gut microbiota signatures of 37 Chinese adults were studied using 16S rRNA sequencing targeting V3-V4 hypervariable regions. FastQC was used to control the length and quality of sequencing data. If the sequencing data were V3 and V4 regions, the data with a length between 300 and 600 nt were retained, and if the sequencing data were V3 regions, the data with a length between 100 and 300 nt were retained. The sequences with similarities above 97% were divided into an operational taxonomic unit (OTU).

According to the results of OTUs analysis, we obtained a total of 3713 OTUs, including 1553 OTUs unique to CG group, 792 OTUs unique to BLT group, 502 OTUs unique to LT1W group and 375 OTUs unique to LT2W group (**Figure 1**). The top 10 OTUs unique to CG: OTU89 (d__Bacteria; p__Bacteroidota; c__Bacteroidia; o__Bacteroidales; f__*Bacteroidaceae*; g__*Bacteroides*), OTU101 (d__Bacteria; p__Firmicutes; c__Bacilli; o__Erysipelotrichales; f__Erysipelotrichaceae; g__Dubosiella; s__Uncultured_bacterium), OTU119 (d__Bacteria; Alloprevotella), OTU187 (d__Bacteria; p__Bacteroidota; c__Bacteroidia; o__Bacteroidales; f__*Prevotellaceae*; g__Prevotella), OTU213 (d__Bacteria; p__Bacteroidota; c__Bacteroidia; o__Bacteroidales; f__*Bacteroidaceae*; g__*Bacteroides*; s__*Bacteroides*_stercoris); The top 10 OTUs unique to BLT group:OTU41 (d__Bacteria; p__Bacteroidota; c__Bacteroidia; o__Bacteroidales; f__*Bacteroidaceae*; g__*Bacteroides*; s__*Bacteroides*_plebeius), OTU63 (d__Bacteria; p__Fusobacteriota; c__Fusobacteriia; o__Fusobacteriales; f__Fusobacteriaceae; g__*Fusobacterium*; s__*Fusobacterium*_mortiferum), OTU118 (d__Bacteria; p__Bacteroidota; c__Bacteroidia; o__Bacteroidales; f__*Prevotellaceae*; g__Prevotella), OTU147 (d__Bacteria; p__Firmicutes; c__Clostridia; o__Oscillospirales; f__Ruminococcaceae; g__Faecalibacterium), OTU162

(d__Bacteria; p__Verrucomicrobiota; c__Verrucomicrobiae; o__Verrucomicrobiales; f__Akkermap__Firmicutes; c__Clostridia; o__Oscillospirales; f__Ruminococcaceae; g__CAG-352; s__uncultured_bacterium), OTU120 (d__Bacteria; p__Bacteroidota; c__Bacteroidia; o__Bacteroidales; f__*Bacteroidaceae*; g__*Bacteroides*; s__*Bacteroides*_coprophilus), OTU146 (d__Bacteria; p__Firmicutes; c__Negativicutes; o__Veillonellales-Selenomonadales; f__Selenomonadaceae; g__Megamonas), OTU151 (d__Bacteria; p__Bacteroidota; c__Bacteroidia; o__Bacteroidales; f__*Bacteroidaceae*; g__*Bacteroides*), OTU158 (d__Bacteria; p__Proteobacteria; c__Gammaproteobacteria; o__Enterobacterales; f__Enterobacteriaceae; g__Escherichia-Shigella), OTU173 (d__Bacteria; p__Bacteroidota; c__Bacteroidia; o__Bacteroidales; f__*Prevotellaceae*; g__ nsiaceae; g__Akkermansia), OTU167 (d__Bacteria; p__Firmicutes; c__Clostridia; o__Oscillospirales; f__Ruminococcaceae; g__Faecalibacterium), OTU169 (d__Bacteria; p__Bacteroidota; c__Bacteroidia; o__Bacteroidales; f__*Bacteroidaceae*; g__*Bacteroides*; s__*Bacteroides*_stercoris), OTU183 (d__Bacteria; p__Bacteroidota; c__Bacteroidia; o__Bacteroidales; f__*Prevotellaceae*; g__Prevotella), OTU199 (d__Bacteria; p__Bacteroidota; c__Bacteroidia; o__Bacteroidales; f__*Prevotellaceae*; g__Prevotella), OTU218 (d__Bacteria; p__Firmicutes; c__Clostridia; o__Oscillospirales; f__Ruminococcaceae; g__Faecalibacterium); The top 10 OTUs unique to LT1W group: OTU73 (d__Bacteria; p__Proteobacteria; c__Gammaproteobacteria; o__Enterobacterales; f__Enterobacteriaceae; g__Escherichia-Shigella), OTU108 (d__Bacteria; p__Firmicutes; c__Bacilli; o__Lactobacillales; f__*Enterococcaceae*; g__*Enterococcus*), OTU154 (d__Bacteria; p__Proteobacteria; c__Gammaproteobacteria; o__Pseudomonadales; f__Moraxellaceae; g__*Acinetobacter*; s__*Acinetobacter*_baumannii), OTU170 (d__Bacteria; p__Firmicutes; c__Bacilli; o__Lactobacillales; f__*Lactobacillaceae*; g__*Lactobacillus*), OTU174 (d__Bacteria; p__Actinobacteriota; c__Actinobacteria; o__Bifidobacteriales; f__*Bifidobacteriaceae*; g__Bifidobacterium; s__Bifidobacterium_breve), OTU200 (d__Bacteria; p__Firmicutes; c__Negativicutes; o__Veillonellales-Selenomonadales; f__Veillonellaceae; g__Veillonella), OTU245 (d__Bacteria; p__Actinobacteriota; c__Coriobacteriia; o__Coriobacteriales; f__Atopobiaceae; g__Olsenella), OTU265 (d__Bacteria; p__Actinobacteriota; c__Actinobacteria; o__Bifidobacteriales; f__*Bifidobacteriaceae*; g__Bifidobacterium; s__Bifidobacterium_breve), OTU270 (d__Bacteria; p__Firmicutes; c__Negativicutes; o__Veillonellales-Selenomonadales; f__Veillonellaceae; g__Veillonella), OTU280 (d__Bacteria; p__Firmicutes; c__Clostridia; o__Peptostreptococcales-Tissierellales; f__Peptostreptococcales-Tissierellales; g__Parvimonas); The top 10 OTUs unique to LT2W group: OTU29 (d__Bacteria; p__Proteobacteria; c__Gammaproteobacteria; o__Enterobacterales; f__Enterobacteriaceae), OTU62 (d__Bacteria; p__Proteobacteria; c__Gammaproteobacteria; o__Enterobacterales; f__Yersiniaceae; g__*Serratia*),OTU74 (d__Bacteria; p__Proteobacteria; c__Gammaproteobacteria; o__Enterobacterales; f__Yersiniaceae; g__*Serratia*), OTU79 (d__Bacteria; p__Proteobacteria; c__Gammaproteobacteria; o__Enterobacterales; f__Yersiniaceae; g__*Serratia*), OTU178 (d__Bacteria; p__Proteobacteria; c__Gammaproteobacteria; o__Enterobacterales; f__Enterobacteriaceae), OTU196 (d__Bacteria; p__Proteobacteria; c__Gammaproteobacteria; o__Enterobacterales; f__Enterobacteriaceae; g__*Klebsiella*), OTU197 (d__Bacteria; p__Proteobacteria; c__Gammaproteobacteria; o__Enterobacterales; f__Enterobacteriaceae; g__*Enterobacter*), OTU228 (d__Bacteria; p__Proteobacteria; c__Gammaproteobacteria; o__Enterobacterales; f__Enterobacteriaceae), OTU231 (d__Bacteria; p__Proteobacteria; c__Gammaproteobacteria; o__Enterobacterales; f__Enterobacteriaceae; g__*Enterobacter*), OTU250 (d__Bacteria; p__Proteobacteria; c__Gammaproteobacteria; o__Enterobacterales; f__Enterobacteriaceae).

We counted the number of sequences contained in all OTUs in each sample, sorted OTUs from high to low according to abundance, and generated rank abundance curves (**Figure 1**). In terms of horizontal axis distribution, CG was relatively wider than the other three groups, suggesting that the species distribution of CG is more abundant; From the vertical axis distribution, the curves distribution of CG were gentle downward compared with the other three groups, suggesting that the uniformity of species composition in the healthy control group is relatively high. LT1W and LT2W groups were considerably narrow on the horizontal axis, suggesting that the species abundance of the two groups is low, and the vertical axis was steep, suggesting that the species distribution uniformity is poor.

Diversity Analysis

Alpha Diversity Analysis

Alpha diversity was quantified using the Chao1 index, observed features, and Shannon diversity indexes, which relate OTU richness and evenness and the total number of observed species. Evaluation of taxonomic pattern of gut microbiota in liver transplantation patients showed that the alpha-diversity calculated using chao1 index was higher in the control group, reflecting a reduction of gut microbiota diversity following liver transplantation (**Figure 2**). The Chao1 of CG and BLT groups were significantly higher than those of other groups, while the Chao1 of LT1W and LT2W groups was relatively low (**Table 1**). The species richness of CG was significantly higher than the BLT group ($p < 0.05$). The species richness in the LT1W and LT2W groups was significantly lower than that of the other two groups ($p < 0.05$). Interestingly, there was no significant difference between LT1W and LT2W groups ($p > 0.05$). As indicated in the Shannon index, there were significant differences in microbial community abundances between transplant patients and healthy controls (**Table 2**). As we expected, observed features showed similar results (**Table 3**). An evident difference in the gut microbiota was observed at all taxonomic levels between these four groups. These findings suggest that a decrease in taxonomic diversity characterizes gut microbiota in liver transplant patients. The difference between the BLT and CG groups may be related to liver disease. Chronic liver disease severely affects appetite and digestive function, and it is

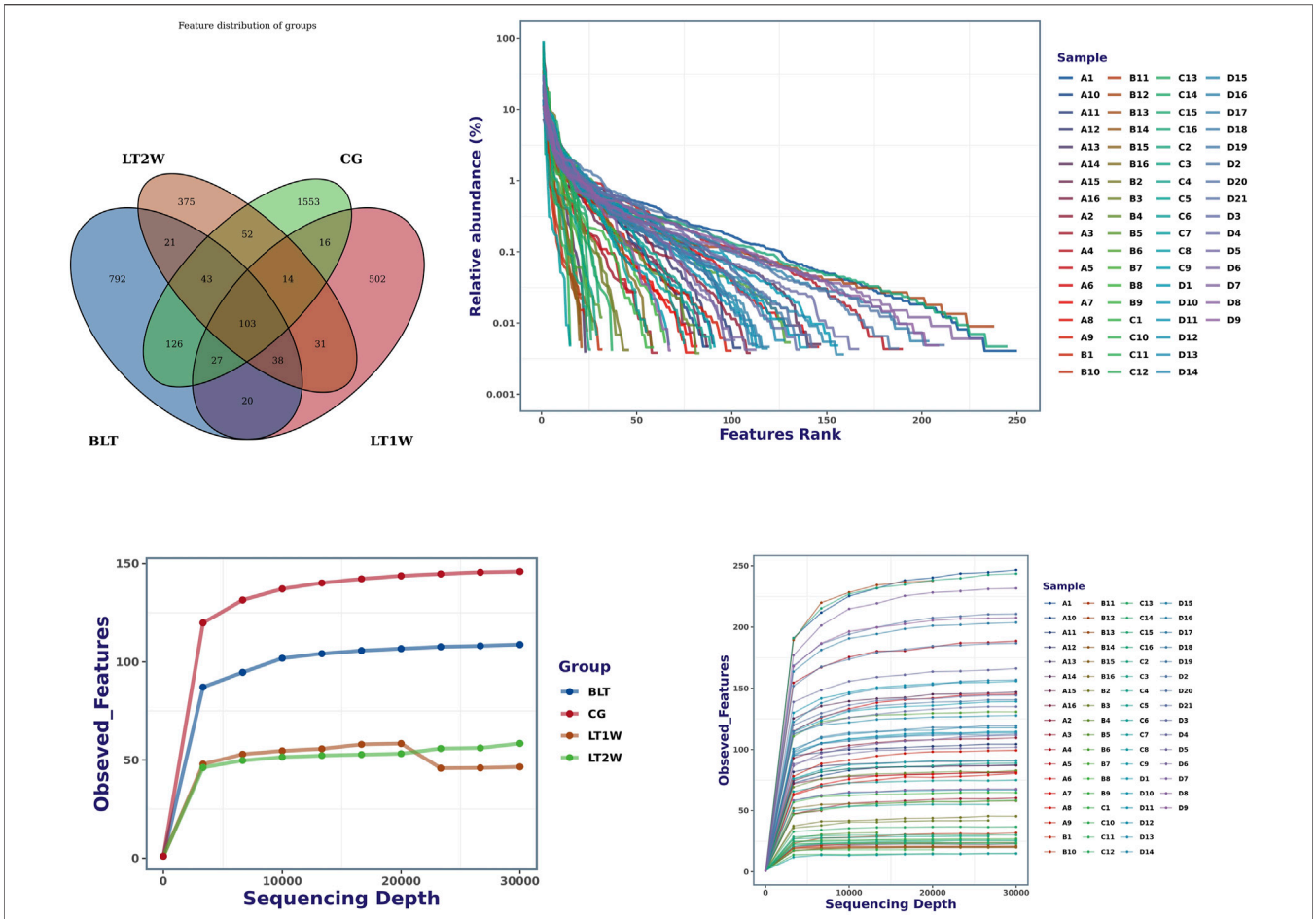

FIGURE 1 | Venn diagram and rank abundance curves for all groups at the OTU level. A = BLT, B = LT1W, C = LT2W, and D = CG. Species accumulation curves were used to determine the sampling depth. The sample diversity and degree of uniformity were measured using the rank abundance curve method.

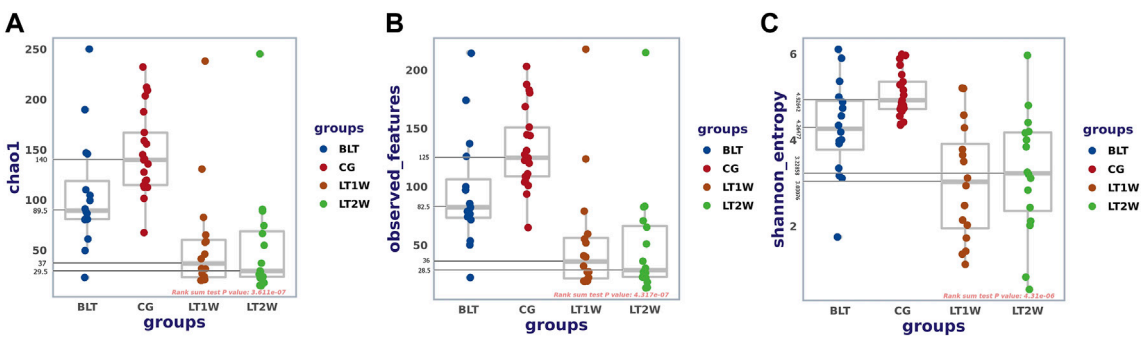

FIGURE 2 | Alpha diversity between liver transplantation patients. Comparison of Boxplots depicting chao1 **(A)**, observed-features **(B)**, and Shannon index **(C)**. Diversity among CG (*n* = 21), BLT (*n* = 16), LT1W (*n* = 16), and LT2W (*n* = 16) groups.

challenging to avoid severe ascites, the end stage of liver disease, which further affects intestinal peristalsis and causes bacterial translocation. The intestinal diversity of postoperative patients has been substantially destroyed, which may be related to antibiotics and immunosuppressants. About a week after surgery, the patients began eating by mouth, and the dosage of antibiotics began to decrease. It can be seen from the figure that the microbial richness of the LT2W group began to rise compared with the LT1W group. We believe that this is the signal that intestinal function and microecology begin to recover.

TABLE 1 | Chao 1 index analysed with Kruskal-Wallis rank sum.

Group 1	Group 2	H	*p*-value	q-value
BLT (n = 16)	CG (n = 21)	8.130687	0.004352	0.005223
BLT (n = 16)	LT1W (n = 16)	9.558144	0.001991	0.002986
BLT (n = 16)	LT2W (n = 16)	9.559897	0.001989	0.002986
CG (n = 21)	LT1W (n = 16)	17.64841	2.66E-05	7.97E-05
CG (n = 21)	LT2W (n = 16)	19.49565	1.01E-05	6.05E-05
LT1W (n = 16)	LT2W (n = 16)	0.128337	0.720162	0.720162

TABLE 2 | Shannon entropy analysed with Kruskal-Wallis rank sum.

Group 1	Group 2	H	*p*-value	q-value
BLT (n = 16)	CG (n = 21)	6.015038	0.014184	0.021277
BLT (n = 16)	LT1W (n = 16)	6.1875	0.012866	0.021277
BLT (n = 16)	LT2W (n = 16)	4.454545	0.034808	0.04177
CG (n = 21)	LT1W (n = 16)	17.8985	2.33E-05	6.99E-05
CG (n = 21)	LT2W (n = 16)	17.8985	2.33E-05	6.99E-05
LT1W (n = 16)	LT2W (n = 16)	0.171875	0.678451	0.678451

TABLE 3 | Observed features analysed with Kruskal-Wallis rank sum.

Group 1	Group 2	H	*p*-value	q-value
BLT (n = 16)	CG (n = 21)	8.483148	0.003585	0.004301
BLT (n = 16)	LT1W (n = 16)	9.102588	0.002552	0.003829
BLT (n = 16)	LT2W (n = 16)	9.329862	0.002254	0.003829
CG (n = 21)	LT1W (n = 16)	17.39583	3.03E-05	9.10E-05
CG (n = 21)	LT2W (n = 16)	19.3605	1.08E-05	6.49E-05
LT1W (n = 16)	LT2W (n = 16)	0.102816	0.748476	0.748476

Beta Diversity Analysis

Beta diversity (the degree of pair-wise similarity in the species composition among populations) was assessed using PCoA on the unweighted UniFrac metric. The calculation was based on unweighted UniFrac distance matrices constructed to demonstrate the overall dissimilarity of bacterial communities in the four groups of individuals from the Chinese population (**Figure 3**). According to PCoA, CG and BLT groups are highly coincident, the BLT group only partially overlaps with LT1W and LT2W groups, and the LT1W and LT2W groups almost wholly coincide. PERMANOVA demonstrates that CG and BLT groups show significant differences in Beta diversity, and the BLT group has significant in Beta diversity with the LT1W and LT2W group; by contrast, the difference of Beta diversity between LT1W and LT2W groups is not substantial (**Figure 3**).

Species Composition

Phylum Level (L2)

At the phylum level, the Firmicutes and Bacteroidetes prevailed in all groups (**Figure 4A**), with relative abundances of 57.502% and 37.379% (CG), 48.834% and 40.617% (BLT group), 48.018%, and 25.594% (LT1W group), 37.168% and 26.072% (LT2W group) (**Table 4**). Moreover, the relative abundances of Chloroflexi, Nitrospirota, and Crenarchaeota were lower or even completely absent after liver transplantation, decreasing significantly 2 weeks after surgery. After liver transplantation, the relative abundance of Proteobacteria was significantly higher ($p < 0.05$). Microbiota of healthy volunteers was characterized by higher levels of Deferribacterota and Parabasalia, while gut microbiota from the BLT, LT1W, and LT2W groups contained none. The

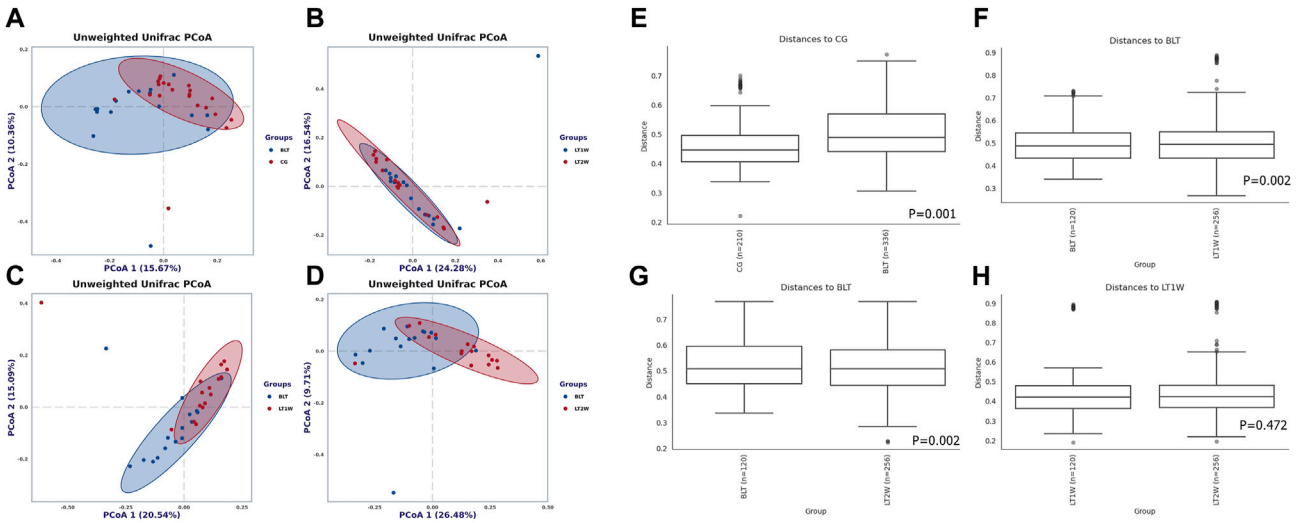

FIGURE 3 | Beta diversity of gut microbial communities in liver transplantation patients and healthy participants. Principal coordinates analysis plot based on unweighted UniFrac distance. Each dot represents one sample from each group. The unweighted UniFrac patterns indicate that the liver transplantation and healthy individuals cluster separately, representing 15.67% and 10.36% **(A)**, 24.38% and 16.54% **(B)**, 20.54% and 15.09% **(C)**, and 26.48% and 9.71% **(D)** of the total variance on the *x*-axis and *y*-axis, respectively. The distance between dots on the plot indicates the degree of similarity of taxonomic composition of the samples. Charts **(E–H)** show the distance between groups and within groups, $p < 0.05$ indicating that the beta diversity between groups was significant.

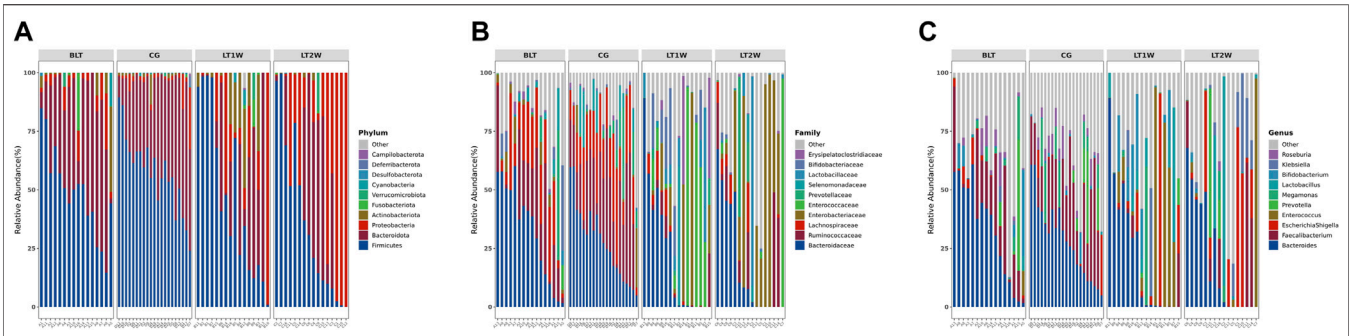

FIGURE 4 | The relative abundance of gut bacteria in liver transplantation patients and healthy participants. **(A)** Relative percentage of most abundant phyla in each sample between liver transplantation patients (n = 16) and healthy individuals (n = 21). **(B)** Relative abundance of bacteria at family level in CG, BLT, LT1W, and LT2W groups. **(C)** Relative abundance of bacteria at the genus level in all groups.

TABLE 4 | The significantly different relative abundance of gut microbiota at phylum, family, and genus level. (a) The relative abundance of gut bacteria in all groups using Kruskal-Wallis rank-sum tests. (b c, d) The relative abundance of gut bacteria in double groups using Wilcoxon's rank sum tests (b: BLT vs CG, c: BLT vs LT1W, d: BLT vs LT2W).

	CG (%)	BLT (%)	LT1W (%)	LT2W (%)	*p* Value
Phylum (L2)					
p__Firmicutes	57.502	48.834	48.018	37.168	$p < 0.05$ac $p > 0.05$bd
p__Bacteroidota	37.379	40.617	25.594	26.072	$p < 0.05$c $p > 0.05$abd
p__Proteobacteria	3.244	6.081	15.833	35.095	$p < 0.05$ad $p > 0.05$bc
Family (L5)					
f__*Lachnospiraceae*	20.249	18.010	2.679	3.667	$p < 0.05$acd $p > 0.05$d
f__Monoglobaceae	0.328	0.253	0.000	0.006	$p < 0.05$abcd
f__Burkholderiaceae	0.000	0.000	0.092	0.058	$p < 0.05$acd Na b
f__Oscillospiraceae	1.007	0.921	0.058	0.260	$p < 0.05$acd $p > 0.05$b
f__*Enterococcaceae*	0.010	0.161	17.716	7.085	$p < 0.05$ac $p > 0.05$bd
f__Butyricicoccaceae	0.262	0.125	0.000	0.043	$p < 0.05$acd $p > 0.05$b
f__Clostridiaceae	0.109	1.078	0.431	1.741	$p < 0.05$abcd
f__uncultured	0.046	0.000	0.026	0.006	$p > 0.05$ac Na bd
Genus (L6)					
g__Roseburia	4.055	3.516	0.024	0.256	$p < 0.05$acd $p > 0.05$b
g__Erysipelotrichaceae_UCG.003	0.344	0.811	0.000	0.027	$p < 0.05$acd $p > 0.05$b
g__Blautia	2.342	2.817	0.433	0.323	$p < 0.05$acd $p > 0.05$b
g__Lachnospira	1.091	0.639	0.003	0.033	$p < 0.05$acd $p > 0.05$b
g__Monoglobus	0.328	0.253	0.000	0.006	$p < 0.05$acd $p > 0.05$b
g__*Enterococcus*	0.010	0.161	17.716	7.050	$p < 0.05$ac $p > 0.05$bd
g__Dorea	0.313	0.262	0.000	0.041	$p < 0.05$acd $p > 0.05$b
g__[Eubacterium]_hallii_group	0.656	0.236	0.000	0.044	$p < 0.05$abcd
g__Intestinibacter	0.049	0.110	0.000	0.017	$p < 0.05$acd $p > 0.05$b
g__Romboutsia	0.344	0.240	0.000	0.002	$p < 0.05$acd $p > 0.05$b
g__Lautropia	0.000	0.000	0.029	0.058	$p < 0.05$acd NAb
g__[Eubacterium]_eligens_group	0.767	3.062	0.004	0.031	$p < 0.05$acd $p > 0.05$b
g__*Bacteroides*	27.476	34.593	22.576	18.264	$p < 0.05$acd $p > 0.05$b
g__Faecalibacterium	21.454	16.635	2.891	8.984	$p < 0.05$acd $p > 0.05$b
g__Escherichia-Shigella	1.778	2.082	9.630	10.842	$p > 0.05$abcd
g__Bifidobacterium	1.176	2.241	7.376	0.415	$p > 0.05$abc $p < 0.05$d
g__*Lactobacillus*	0.057	0.262	6.419	7.607	$p < 0.05$abc $p > 0.05$d
g__Erysipelatoclostridium	0.125	0.184	6.207	0.817	$p > 0.05$abcd

Actinobacteriota began to appear in the BLT group, and then its proportion increased dramatically in the LT1W group. Interestingly, Actinobacteriota almost disappeared in the LT2W group.

Family Level (L5)

At the family level, the gut microbiota of liver transplantation patients contained high levels of the following: *Bacteroidaceae*, Ruminococcaceae, *Lachnospiraceae*, *Prevotellaceae*, and

Enterobacteriaceae (BLT group); *Bacteroidaceae*, *Enterococcaceae*, Enterobacteriaceae, *Bifidobacteriaceae* and *Lactobacillaceae* (LT1W group); and Enterobacteriaceae, *Bacteroidaceae*, Ruminococcaceae, *Lactobacillaceae* and *Enterococcaceae* (LT2W group). The CG was characterized by a higher content of *Bacteroidaceae*, Ruminococcaceae, *Lachnospiraceae*, *Prevotellaceae*, and Selenomonadaceae (**Figure 4B**). *Burkholderiaceae*, Anaerolineaceae, *Aerococcaceae*, P5D1-392, *Mycoplasmataceae*, Steroidobacteraceae, Hydrogenophilaceae, Uncultured, and Bathyarchaeia, appeared alone 1 week after liver transplantation and decreased significantly 2 weeks after surgery. *Deferribacteraceae*, Helicobacteraceae, *Tritrichomonadea*, and Hafniaceae were only present in the CG group, which may be related to liver disease. *Lachnospiraceae*, Monoglobaceae, Oscillospiraceae, and Butyricicoccaceae decreased significantly 1 week after liver transplantation ($p < 0.05$). They began to recover after 2 weeks. *Enterococcaceae* were significantly different between BLT and CG groups, increased sharply 1 week after surgery, and declined 2 weeks later (**Table 4**).

Genus Level (L6)

At the genus level, the gut microbiota of the CG and BLT groups contained high levels of *Bacteroides* and *Faecalibacterium*. By contrast, the LT1W and LT2W groups were characterized by a higher content of *Bacteroides*, *Enterococcus*, *Escherichia-Shigella*, *Bifidobacterium*, *Lactobacillus*, and *Erysipelatoclostridium* (**Figure 4C**). Among the four groups, the bacteria with the greatest differences were *Roseburia*, Erysipelotrichaceae_UCG.003, *Blautia*, *Lachnospira*, *Monoglobus*, *Enterococcus*, *Dorea*, [Eubacterium]_hallii_group, *Intestinibacter*, *Romboutsia*, and [Eubacterium]_eligens_group. Compared with the CG group, the richness of these microorganisms decreased in the BLT group, seemingly due to liver diseases. Following surgery, these microorganisms decreased significantly 1 week later and began to recover after 2 weeks. *Enterococcus* and *Lautropia* appeared immediately after surgery (**Table 4**).

Species Diversity Analysis

Numerous bacteria, including the phyla Nitrospirota, Chloroflexi, and Crenarchaeota, the families Anaerolineaceae, Aerococcaceae, P5D1-392, *Mycoplasmataceae*, Steroidobacteraceae, Hydrogenophilaceae, and Bathyarchaeia, and the genera *Olsenella*, *Serratia*, and *Enterobacter* were present in the group of patients after liver transplantation only; the phyla Deferribacterota, and Parabasalia, the families *Deferribacteraceae*, Helicobacteraceae, *Tritrichomonadea*, and Hafniaceae, and the genera *Dubosiella*, *Coprobacter*, *Psychrobacter*, and *Mucispirillum* were absent in the diseased individuals and was observed only in healthy individuals (**Table 5**). Comparison of data of analysis of the taxonomic composition of gut microbiota from patients and CG showed statistically significant differences in the content of some microbial phylum, family, and genus in these groups. These findings suggest that gut microbiota post-transplant are characterized by a decrease in taxonomic diversity and significant differences in the representation of two phyla (Bacteroidetes and Desulfobacterota), 11 families (Barnesiellaceae, Rmuinococcaceae, Burkholderiacrar, *Enterococcaceae*, Desulfovibrionaceae, Marinifilaceae, Rikenellaceae, *Lachnospiraceae*, Oscillosopiraceae, and Monoglobaceae) and five genera (*Enterobacter*, *Enterococcus*, *Blautia*, [Eubacterium]_hallii_group, and *Roseburia*) (**Figure 5**).

Differences in Metabolic Pathways Between Groups

We transformed the composition of the OTUs sequences into COG to analyze the differences in the metabolic pathways represented in the gut microbiota among BLT, LT1W, and LT2W group samples. We generated COG profiles and then compared the components of functional genomics in COG pathways. In general, 11 COG functional modules were significantly enriched in the BLT group, nine COG functional modules were significantly less. 19 COG functional modules significantly less, and only one COG functional module was enriched in the LT1W group. On the other hand, compared with the BLT group, 20 functional modules were less represented in the LT1W group. Five COG functional modules were enriched, and 15 COG modules were less represented in the LT2W group than the LT1W group (**Figure 6** and **Tables 6–9**).

DISCUSSION

Overall, the healthy gut microbiota is dominated by the phyla Firmicutes and Bacteroidetes, followed by Proteobacteria and Actinobacteria. Core microbial diversity and the ratio of Firmicutes and Bacteroidetes are general health indicators. Traditionally, the Firmicutes to Bacteroidetes (F/B) ratio is implicated in predisposition to disease states (Ley et al., 2006). The F/B ratio in the LT1W and LT2W groups were higher than the BLT group. The F/B of the LT1W group was the largest of the four groups, suggesting patients were most susceptible to infection during the first week after liver transplantation. At this point, the structure of intestinal bacteria of the patients had undergone significant changes.

Obligate anaerobic bacteria (such as the phyla Firmicutes and Bacteroidetes) encode various enzymes for hydrolyzing complex carbohydrates not digestible by the host, such as resistant starch and fiber. Genera such as *Lactobacillus* and *Bifidobacterium* specialize in oligosaccharide fermentation, utilizing galactooligosaccharides, fructooligosaccharides, and the polysaccharide inulin (Sims et al., 2014). Carbohydrate fermentation by anaerobes provides the host with essential short-chain fatty acids (SCFAs) such as acetate, propionate, and butyrate (Andoh, 2016). It is known that antibiotics deplete microbes that ferment essential SCFAs such as butyrate, which are typically responsible for maintaining microbial homeostasis. The lack of butyrate silences metabolic signaling in the gut. Mitochondrial Beta-oxidation in colonocytes becomes disabled, resulting in oxygen transfer, which freely

TABLE 5 | The gut microbiota that occur only before or after liver transplantation.

	CG (%)	BLT (%)	LT1W (%)	LT2W (%)	*p*-value
Phylum (L2)					
p__Nitrospirota	0.000	0.000	0.028	0.000	0.345907
p__Chloroflexi	0.000	0.000	0.091	0.000	0.225497
p__Crenarchaeota	0.000	0.000	0.016	0.000	0.345907
p__Deferribacterota	0.152	0.000	0.000	0.000	0.200251
p__Parabasalia	0.015	0.000	0.000	0.000	0.515263
Family (L5)					
f__Anaerolineaceae	0.000	0.000	0.073	0.000	0.225497
f__Aerococcaceae	0.000	0.000	0.057	0.000	0.003122
f__P5D1-392	0.000	0.000	0.038	0.000	0.345907
f__*Mycoplasmataceae*	0.000	0.000	0.031	0.000	0.345907
f__Steroidobacteraceae	0.000	0.000	0.027	0.000	0.345907
f__Hydrogenophilaceae	0.000	0.000	0.026	0.000	0.345907
f__Bathyarchaeia	0.000	0.000	0.016	0.000	0.345907
f__*Deferribacteraceae*	0.152	0.000	0.000	0.000	0.200251
f__uncultured	0.046	0.000	0.000	0.000	0.345907
f__Helicobacteraceae	0.042	0.000	0.000	0.000	0.515263
f__*Tritrichomonadea*	0.015	0.000	0.000	0.000	0.515263
f__Hafniaceae	0.012	0.000	0.000	0.000	0.515263
Genus (L6)					
g__Dubosiella	0.616	0.000	0.000	0.000	0.515263
g__Coprobacter	0.226	0.000	0.000	0.000	0.002209
g__Psychrobacter	0.221	0.000	0.000	0.000	0.515263
g__[Eubacterium]_ventriosum_group	0.168	0.187	0.000	0.000	2.22E-07
g__Mucispirillum	0.152	0.000	0.000	0.000	0.200251
g__Olsenella	0.000	0.000	0.387	0.000	0.345907
g__Rothia	0.000	0.013	0.336	0.056	0.027494
g__Chloroplast	0.000	0.147	0.303	0.000	0.003862
g__*Serratia*	0.000	0.000	0.000	3.989	0.345907
g__*Enterobacter*	0.000	0.000	0.014	1.270	0.081291

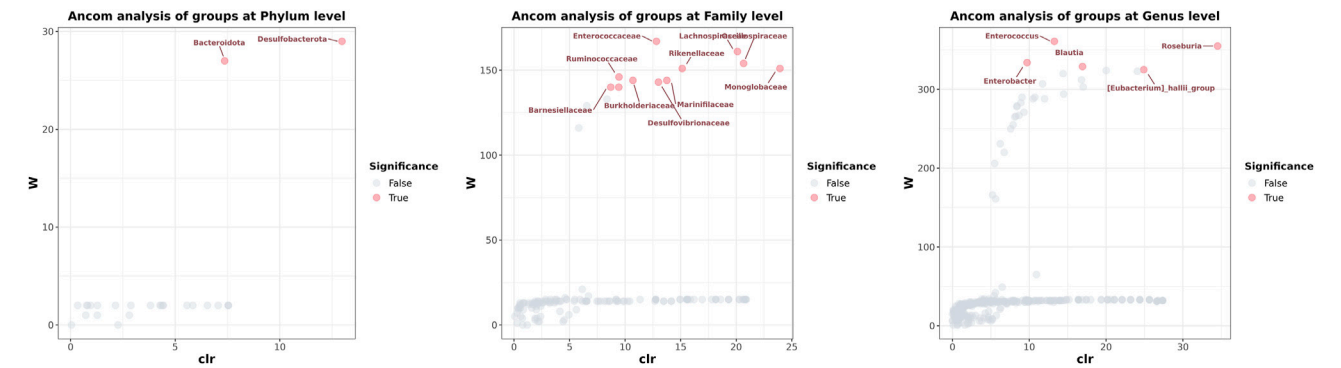

FIGURE 5 | The analysis of composition of microbiomes determined which microorganisms in the samples were significant. Each dot represents a species taxonomic composition. The gray (False) dots indicate that the diversity between groups was not significant, and the red (True) dots indicated that the diversity between groups was significant. The *x*-axis clr represents the relative abundance between groups. The higher the *y*-axis W value, the higher the significance of the species among the groups.

diffuses across cell membranes from the blood to the gut lumen. Oxygen in the colon then allows for pathogenic facultative anaerobes such as *E. coli* to outcompete the benign obligate anaerobes that characterize a healthy gut (Winter et al., 2013; Byndloss et al., 2017; Wassenaar, 2016).

Facultative anaerobes, including Proteobacteria, further affect nutrition by catabolizing SCFAs present in the lumen (Litvak et al., 2018). Microbial homeostasis is typically maintained by peroxisome proliferator-activated receptor gamma (PPAR-γ). PPAR-γ is a nuclear receptor activated by butyrate and other

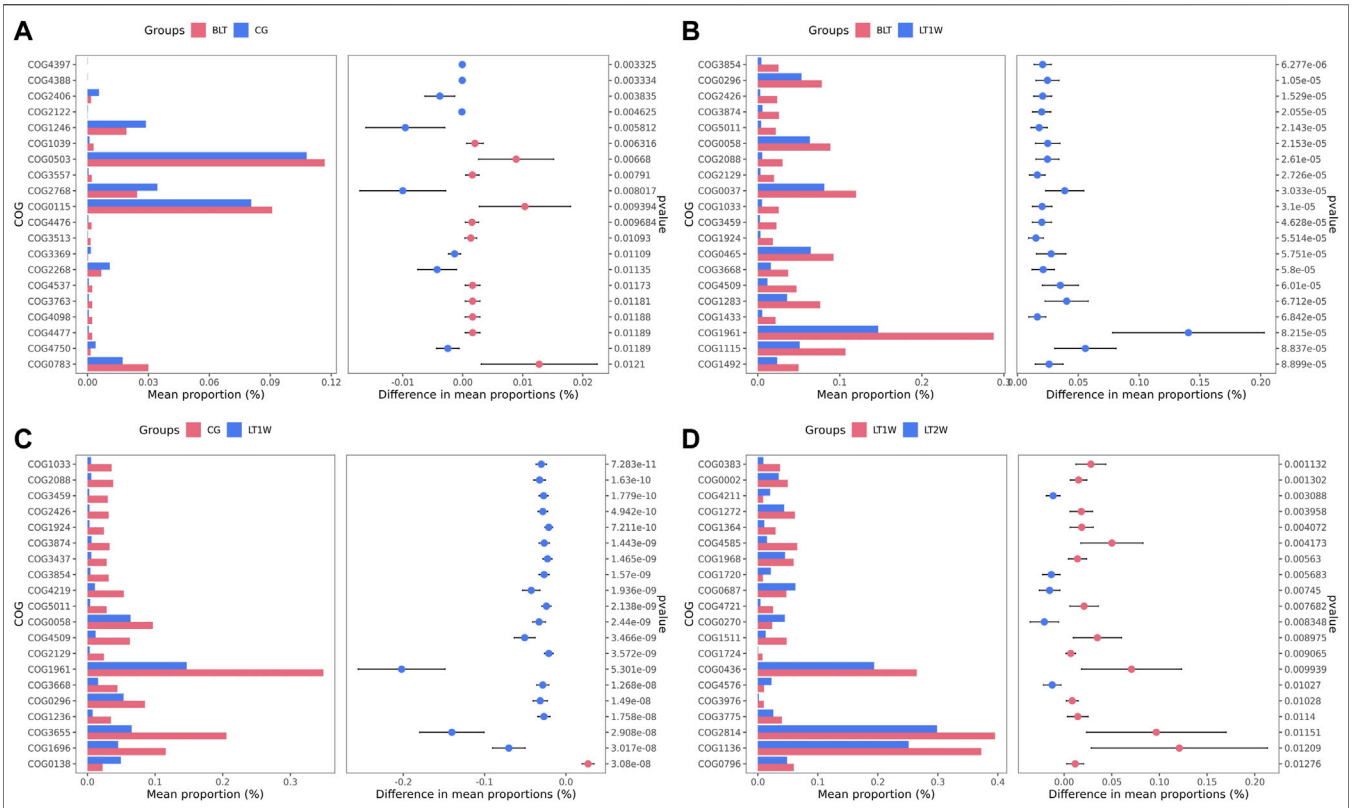

FIGURE 6 | The COG profiles and the components of functional genomics in COG pathways. **(A)**: BLT vs. CG; **(B)**: BLT vs. LT1W; **(C)**: CG vs. LT1W; **(D)**: LT1W vs. LT2W.

TABLE 6 | The COG of BLT vs. CG.

ID	p-value	Functional description
COG4397	0.003324577	Mu-like prophage major head subunit gpT
COG4388	0.003333848	Mu-like prophage I protein
COG2406	0.003835026	Protein distantly related to bacterial ferritins
COG2122	0.00462527	Uncharacterized conserved protein
COG1246	0.005812124	N-acetylglutamate synthase and related acetyltransferases
COG1039	0.006316055	Ribonuclease HIII
COG0503	0.006680033	Adenine/guanine phosphoribosyltransferases and related PRPP-binding proteins
COG3557	0.007910423	Uncharacterized domain/protein associated with RNAses G and E
COG2768	0.00801657	Uncharacterized Fe-S center protein
COG0115	0.009394288	Branched-chain amino acid aminotransferase/4-amino-4-deoxychorismate lyase
COG4476	0.009683741	Uncharacterized protein conserved in bacteria
COG3513	0.010933294	Uncharacterized protein conserved in bacteria
COG3369	0.011092671	Uncharacterized conserved protein
COG2268	0.0113543	Uncharacterized protein conserved in bacteria
COG4537	0.011729973	Competence protein ComGC
COG3763	0.011809479	Uncharacterized protein conserved in bacteria
COG4098	0.011884764	Superfamily II DNA/RNA helicase required for DNA uptake (late competence protein)
COG4477	0.011889677	Negative regulator of septation ring formation
COG4750	0.011893088	CTP:phosphocholine cytidylyltransferase involved in choline phosphorylation for cell surface LPS epitopes
COG0783	0.01209744	DNA-binding ferritin-like protein (oxidative damage protectant)

ligands, is found in adipocytes and colonocytes, and is responsible for activating genes involved in glucose and lipid metabolism (Winter et al., 2014). Dysbiosis of the gut microbiota occurred in the patients after surgery. Blooms of facultative anaerobes, particularly Enterobacteriaceae, are associated with inflammatory conditions in the gut. However, the healthy

TABLE 7 | The COG of BLT vs. LT1W.

ID	*p*-value	Functional description
COG3854	6.27678E-06	Stage III sporulation protein SpoIIIAA
COG0296	1.04985E-05	1,4-alpha-glucan branching enzyme
COG2426	1.52853E-05	Predicted membrane protein
COG3874	2.0547E-05	Uncharacterized conserved protein
COG5011	2.14315E-05	Uncharacterized protein conserved in bacteria
COG0058	2.15279E-05	Glucan phosphorylase
COG2088	2.61E-05	Uncharacterized protein, involved in the regulation of septum location
COG2129	2.72612E-05	Predicted phosphoesterases, related to the Icc protein
COG0037	3.03301E-05	Predicted ATPase of the PP-loop superfamily implicated in cell cycle control
COG1033	3.09983E-05	Predicted exporters of the RND superfamily
COG3459	4.62774E-05	Cellobiose phosphorylase
COG1924	5.51436E-05	Activator of 2-hydroxyglutaryl-CoA dehydratase (HSP70-class ATPase domain)
COG0465	5.75095E-05	ATP-dependent Zn proteases
COG3668	5.80032E-05	Plasmid stabilization system protein
COG4509	6.00954E-05	Uncharacterized protein conserved in bacteria
COG1283	6.71153E-05	Na+/phosphate symporter
COG1433	6.84207E-05	Uncharacterized conserved protein
COG1961	8.21533E-05	Site-specific recombinases, DNA invertase Pin homologs
COG1115	8.83694E-05	Na+/alanine symporter
COG1492	8.89871E-05	Cobyric acid synthase

TABLE 8 | The COG of LT1W vs. CG.

ID	*p*-value	Functional description
COG1033	7.28286E-11	Predicted exporters of the RND superfamily
COG2088	1.62982E-10	Uncharacterized protein, involved in the regulation of septum location
COG3459	1.77916E-10	Cellobiose phosphorylase
COG2426	4.94246E-10	Predicted membrane protein
COG1924	7.21105E-10	Activator of 2-hydroxyglutaryl-CoA dehydratase (HSP70-class ATPase domain)
COG3874	1.44265E-09	Uncharacterized conserved protein
COG3437	1.46492E-09	Response regulator containing a CheY-like receiver domain and an HD-GYP domain
COG3854	1.56993E-09	Stage III sporulation protein SpoIIIAA
COG4219	1.93588E-09	Antirepressor regulating drug resistance, predicted signal transduction N-terminal membrane component
COG5011	2.13803E-09	Uncharacterized protein conserved in bacteria
COG0058	2.43995E-09	Glucan phosphorylase
COG4509	3.4655E-09	Uncharacterized protein conserved in bacteria
COG2129	3.57172E-09	Predicted phosphoesterases, related to the Icc protein
COG1961	5.30064E-09	Site-specific recombinases, DNA invertase Pin homologs
COG3668	1.26795E-08	Plasmid stabilization system protein
COG0296	1.49041E-08	1,4-alpha-glucan branching enzyme
COG1236	1.75778E-08	Predicted exonuclease of the beta-lactamase fold involved in RNA processing
COG3655	2.90768E-08	Predicted transcriptional regulator
COG1696	3.01671E-08	Predicted membrane protein involved in D-alanine export
COG0138	3.08025E-08	AICAR transformylase/IMP cyclohydrolase PurH (only IMP cyclohydrolase domain in Aful)

colon is almost entirely anaerobic, and there, obligate anaerobes rely on the fermentation of carbohydrates and amino acids to generate energy. By-products of this process include the SCFAs, which are thought to play essential roles in maintaining epithelial integrity and supporting an anti-inflammatory state (Goverse et al., 2017; Desai et al., 2016; Wu et al., 2017). Enterobacteriaceae multiply in large numbers in patients, suggesting that the intestinal permeability had been broken. There is evidence that inflammation is associated with increased Enterobacteriaceae abundance (Lopez et al., 2012). Some of these significant changes were observed in bacterial species belonging to *Enterococcus*, *Klebsiella*, and *Enterobacter*, seen in patients' intestines (**Figure 5**; **Supplementary Figure S2**). These are members of the ESKAPE group (*Enterococcus faecium*, *Staphylococcus aureus*, *Klebisiella pneumoniae*, *Acinetobacter baumannii*, *Pseudomonas aeruginosa* and *Enterobacter* spp. are collectively knowen as ESKAPE group pathogen), described as the leading cause of resistant nosocomial infections (Davin-Regli et al., 2019).

Indeed, loss of balance in microbial population and function, or dysbiosis, provokes the disruption of the intestinal barrier tight junctions. This morphological alteration leads to increased intestinal permeability (also known as leaky gut) and an increment in the portal influx of bacteria or their products to

TABLE 9 | The COG of LT1W vs. LT2W.

ID	*p*-value	Functional description
COG0383	0.001132206	Alpha-mannosidase
COG0002	0.001302019	Acetylglutamate semialdehyde dehydrogenase
COG4211	0.003087535	ABC-type glucose/galactose transport system, permease component
COG1272	0.003958178	Predicted membrane protein, hemolysin III homolog
COG1364	0.004072359	N-acetylglutamate synthase (N-acetylornithine aminotransferase)
COG4585	0.004172932	Signal transduction histidine kinase
COG1968	0.005630082	Uncharacterized bacitracin resistance protein
COG1720	0.005683167	Uncharacterized conserved protein
COG0687	0.007449622	Spermidine/putrescine-binding periplasmic protein
COG4721	0.007681902	Predicted membrane protein
COG0270	0.008347795	Site-specific DNA methylase
COG1511	0.008975009	Predicted membrane protein
COG1724	0.009064968	Predicted periplasmic or secreted lipoprotein
COG0436	0.009938515	Aspartate/tyrosine/aromatic aminotransferase
COG4576	0.010274524	Carbon dioxide concentrating mechanism/carboxysome shell protein
COG3976	0.010283793	Uncharacterized protein conserved in bacteria
COG3775	0.011395885	Phosphotransferase system, galactitol-specific IIC component
COG2814	0.011505916	Arabinose efflux permease
COG1136	0.012085984	ABC-type antimicrobial peptide transport system, ATPase component
COG0796	0.01276487	Glutamate racemase

the liver (Albillos et al., 2020). An increment in permeability in the gut and the translocation of bacteria facilitate microbial metabolites entering the liver, leading to impairment of bile acid metabolism and promoting systemic inflammation and gut dysmotility. Bile acids in the gut can maintain the balance of intestinal microbiota by controlling the pH of the intestinal environment and inhibiting the growth of pathogens.

Our findings suggest that the operation of liver transplantation and the use of antibiotics substantially alter the balance of microecology in patients' intestines. The number and proportion of probiotics decreased significantly, and the number and proportion of pathogenic bacteria showed a considerable upward trend. The ratio of Bifidobacterium to Enterobacteriaceae (B/E rate) includes the primary obligate anaerobic beneficial bacteria and the facultative anaerobic conditional pathogens, which constitute the colonization resistance of the gut. The B/E rate can be used to represent intestinal microbiota imbalance. B/E <1 indicates dysbiosis of the gut microbiota, and the lower B/E, the greater the degree of dysbiosis of the gut microbiota. Compared with healthy people (CG, B/E = 0.991), due to the dominant bacteria in patients with chronic liver disease (BLT, B/E = 0.921) lose their advantages in the gut, the antagonistic effect on the inferior bacteria is reduced, and the inferior bacteria produce a large amount of endotoxin during the process (Islam et al., 2011). The decline of liver function affects the production of bile acids. The B/E of LT1W and LT2W groups were 0.921 and 0.481, respectively. By contrast, gastrointestinal dysfunction and intestinal peristalsis often occur after liver transplantation, creating an intestinal environment conducive to the reproduction of conditionally pathogenic bacteria.

It is noteworthy that, at the genus level, *Blautia* almost disappeared after liver transplantation (**Figure 5**). As a genus of the *Lachnospiraceae* family, *Blautia* has been of particular interest because of its contribution to alleviating inflammatory diseases and metabolic diseases and its antibacterial activity against specific microorganisms (Kalyana et al., 2018). *Blautia* is a dominant genus in the intestinal microbiota, and there are significant correlations with host physiological dysfunctions such as obesity, diabetes, cancer, and various inflammatory diseases. Liu et al. speculated that the ability to produce bacteriocins provides *Blautia* with the potential to inhibit the colonization of pathogenic bacteria in the gut, and it can also affect the composition of intestinal microbiota. *Blautia* inhibits the proliferation of *C.perfringens* and vancomycin-resistant *Enterococci*, which makes it possible to become potential probiotics and exert probiotic functions (Liu et al., 2021).

The abundance of the phylum Proteobacteria was markedly high, and its absence and low abundance of signature genera such as *Bacteroides*, *Prevotella*, and *Ruminococcus* suggest an unhealthy gut microbiota in patients in the first week after liver transplantation (Hollister et al., 2014). Even if an organ preservation solution can effectively ensure the survival of the liver, it is still difficult to avoid hypoxia and mechanical damage to the liver. The degree of transaminase and disturbance of bile acid secretion after surgery also aggravates the reproduction of pathogenic bacteria in the gut.

We generated COG profiles and compared the representations of COG functional pathways. Compared with healthy samples, the functional modules related to protein distantly related to bacterial ferritins, N-acetylglutamate synthase and related acetyltransferases, protein synthesis, and phosphocholine cytidylyltransferase involved in choline phosphorylation for cell surface lipopolysaccharide epitopes in patients before surgery were significantly reduced. Notably, 19 of the top 20 functional modules decreased significantly in patients 1 week after liver transplantation, including cellulose hydrolysis, glucose metabolism, DNA synthesis, and RNA transcription. In the LT1W group, the top 20 functional modules were less

represented than the BLT group: COG1492 is a member of a metabolic pathway for the synthesis of vitamin 12; COG1961 is related to DNA synthesis; COG1115 is related to alanine; and COG0296/COG0058/COG2129 is related to glucose metabolism. Five COG functional modules were enriched, 15 COG modules were less represented in the LT2W group than the LT1W group: COG2814/COG1136 is related to biological transport processes; COG0436 is related to amino acid metabolism; COG0270 is related to cell proliferation; and COG0383 plays a decisive role in the synthesis of protein and folding in correct conformations (**Figure 6**; **Tables 6**–**9**).

Live *Bifidobacterium* capsules are commercially available; these probiotics colonize the gut, antagonize the growth of pathogenic bacteria in the gut, form a biofilm barrier, inhibit the growth of pathogenic bacteria, reduce intestinal endotoxin and bacterial translocation, reduce the damage of intestinal mucosal epithelium, reduce its permeability, and reduce or delay its atrophy (Holma et al., 2014; Baek et al., 2014; Gianotti et al., 2010; Horvat et al., 2010; Rafter et al., 2007; Zhu et al., 2012). *Bifidobacterium* also accelerates the decomposition and absorption of nutrients in the gastrointestinal tract, producing many acidic substances, acidifying the intestinal cavity, accelerating the excretion of endotoxin, and reducing the damage of intestinal mucosa (Li et al., 2010; Gorska et al., 2009; Ohland et al., 2010).

The active use of liver bacteria preparations or fecal bacteria transplantation in the perioperative period of liver transplantation patients is expected to improve patients' intestinal microecology, reduce postoperative complications, and accelerate postoperative recovery.

CONCLUSION

We characterized the gut microbiome in patients during the perioperative liver transplantation period and compared the diversity, richness, and compositional variation of the gut microbiome between the healthy control and patient groups. We observed an altered microbial composition post-liver transplantation, suggesting a distinct signature of microbiota associated with the procedure in liver transplant patients. Although numerous bacterial species were particularly present or absent in patient samples, we could not effectively compare the species-level composition due to low sequencing depth and small numbers of samples. Although this is a preliminary study to explore the liver transplantation gut microbiome compared to the healthy gut microbiome of the population, it is subject to limitations resulting from low sample numbers and sequencing depth. Most participants were sampled only once; a time-series monitoring of multiple samples at various time points and a more significant number of participants would provide more insights that might have been missed due to low sequencing depth. Nevertheless, the present study is significant because it provides the scientific community with a glimpse of the signature microbiota associated with liver transplantation individuals in Shanxi province. Furthermore, it provides a road map for future studies. We believe that this signature of liver transplantation individuals in the Chinese population will aid future studies.

DATA AVAILABILITY STATEMENT

The datasets presented in this study can be found in online repositories. The names of the repository/repositories and accession number(s) can be found below: NCBI with BioProject ID PRJNA811387.

ETHICS STATEMENT

The studies involving human participants were reviewed and approved by the Ethics Committee of the First Hospital of Shanxi Medical University. The patients/participants provided their written informed consent to participate in this study.

AUTHOR CONTRIBUTIONS

JX, ZL, and ZC conceived and designed the study. ZL and ZC wrote the manuscript. ZL and JX reviewed and edited the manuscript. AZ, ZN, MC, and CH collected Biological samples and sequencing analysis data. All authors reviewed the manuscript.

FUNDING

The project was supported by the "Four Batch Innovation Team Scientific Research Projects" of Shanxi Provincial Health Commission and Natural Science Foundation of Shanxi Province (20210302124408).

ACKNOWLEDGMENTS

We thank members of our laboratory for helpful discussion and Novel Bio-informatics Ltd., Co. for the support of bioinformatics analysis with their NovelBio Cloud Analysis Platform.

SUPPLEMENTARY MATERIAL

The Supplementary Material for this article can be found online at: https://www.frontiersin.org/articles/10.3389/fphys.2022.854017/full#supplementary-material

REFERENCES

Albillos, A., de Gottardi, A., and Rescigno, M. (2020). The Gut-Liver axis in Liver Disease: Pathophysiological Basis for Therapy. *J. Hepatol.* 72 (3), 558–577. doi:10.1016/j.jhep.2019.10.003

Andoh, A. (2016). Physiological Role of Gut Microbiota for Maintaining Human Health. *Digestion* 93 (3), 176–181. doi:10.1159/000444066

Asrani, S. K., Devarbhavi, H., Eaton, J., and Kamath, P. S. (2019). Burden of Liver Diseases in the World. *J. Hepatol.* 70 (1), 151–171. doi:10.1016/j.jhep.2018.09.014

Baek, S.-J., Kim, S.-H., Lee, C.-K., Roh, K.-H., Keum, B., Kim, C.-H., et al. (2014). Relationship between the Severity of Diversion Colitis and the Composition of Colonic Bacteria: A Prospective Study. *Gut Liver* 8 (2), 170–176. doi:10.5009/gnl.2014.8.2.170

Byndloss, M. X., Olsan, E. E., Rivera-Chávez, F., Tiffany, C. R., Cevallos, S. A., Lokken, K. L., et al. (2017). Microbiota-activated PPAR-γ Signaling Inhibits Dysbiotic Enterobacteriaceae Expansion. *Science* 357 (6351), 570–575. doi:10.1126/science.aam9949

Davin-Regli, A., Lavigne, J.-P., and Pagès, J.-M. (2019). Enterobacter spp.: Update on Taxonomy, Clinical Aspects, and Emerging Antimicrobial Resistance. *Clin. Microbiol. Rev.* 32 (4), e00002. doi:10.1128/CMR.00002-19

Desai, M. S., Seekatz, A. M., Koropatkin, N. M., Kamada, N., Hickey, C. A., Wolter, M., et al. (2016). A Dietary Fiber-Deprived Gut Microbiota Degrades the Colonic Mucus Barrier and Enhances Pathogen Susceptibility. *Cell* 167 (5), 1339–1353. doi:10.1016/j.cell.2016.10.043

GBD 2017 Cirrhosis Collaborators (2020). The Global, Regional, and National burden of Cirrhosis by Cause in 195 Countries and Territories, 1990-2017: A Systematic Analysis for the Global Burden of Disease Study 2017. *Lancet Gastroenterol. Hepatol.* 5 (3), 245–266. doi:10.1016/S2468-1253(19)30349-8

Gianotti, L., Morelli, L., Galbiati, F., Rocchetti, S., Coppola, S., Beneduce, A., et al. (2010). A Randomized Double-Blind Trial on Perioperative Administration of Probiotics in Colorectal Cancer Patients. *World J. Gastroenterol.* 16 (2), 167–175. doi:10.3748/wjg.v16.i2.167

Górska, S., Jarzab, A., and Gamian, A. (2009). Probiotic Bacteria in the Human Gastrointestinal Tract as a Factor Stimulating the Immune System. *Postepy Hig Med. Dosw (Online)* 63, 653–667.

Goverse, G., Molenaar, R., Macia, L., Tan, J., Erkelens, M. N., Konijn, T., et al. (2017). Diet-Derived Short Chain Fatty Acids Stimulate Intestinal Epithelial Cells to Induce Mucosal Tolerogenic Dendritic Cells. *J.I.* 198 (5), 2172–2181. doi:10.4049/jimmunol.1600165

Hollister, E. B., Gao, C., and Versalovic, J. (2014). Compositional and Functional Features of the Gastrointestinal Microbiome and Their Effects on Human Health. *Gastroenterology* 146 (6), 1449–1458. doi:10.1053/j.gastro.2014.01.052

Holma, R., Kekkonen, R. A., Hatakka, K., Poussa, T., Vapaatalo, H., Adlercreutz, H., et al. (2014). Low Serum Enterolactone Concentration Is Associated with Low colonicLactobacillus-Enterococcuscounts in Men but Is Not Affected by a Synbiotic Mixture in a Randomised, Placebo-Controlled, Double-Blind, Cross-Over Intervention Study. *Br. J. Nutr.* 111 (2), 301–309. doi:10.1017/S0007114513002420

Horvat, M., Krebs, B., Potrč, S., Ivanecz, A., and Kompan, L. (2010). Preoperative Synbiotic Bowel Conditioning for Elective Colorectal Surgery. *Wien. Klin. Wochenschr.* 122 (Suppl. 2), 26–30. doi:10.1007/s00508-010-1347-8

Islam, K. B. M. S., Fukiya, S., Hagio, M., Fujii, N., Ishizuka, S., Ooka, T., et al. (2011). Bile Acid Is a Host Factor that Regulates the Composition of the Cecal Microbiota in Rats. *Gastroenterology* 141 (5), 1773–1781. doi:10.1053/j.gastro.2011.07.046

Kalyana Chakravarthy, S., Jayasudha, R., Sai Prashanthi, G., Ali, M. H., Sharma, S., Tyagi, M., et al. (2018). Dysbiosis in the Gut Bacterial Microbiome of Patients with Uveitis, an Inflammatory Disease of the Eye. *Indian J. Microbiol.* 58 (4), 457–469. doi:10.1007/s12088-018-0746-9

Kelly, C. J., Zheng, L., Campbell, E. L., Saeedi, B., Scholz, C. C., Bayless, A. J., et al. (2015). Crosstalk between Microbiota-Derived Short-Chain Fatty Acids and Intestinal Epithelial HIF Augments Tissue Barrier Function. *Cell Host & Microbe* 17 (5), 662–671. doi:10.1016/j.chom.2015.03.005

Kwong, E. K., and Puri, P. (2021). Gut Microbiome Changes in Nonalcoholic Fatty Liver Disease & Alcoholic Liver Disease. *Transl Gastroenterol. Hepatol.* 6, 3. doi:10.21037/tgh.2020.02.18

Ley, R. E., Turnbaugh, P. J., Klein, S., and Gordon, J. I. (2006). Human Gut Microbes Associated with Obesity. *Nature* 444 (7122), 1022–1023. doi:10.1038/4441022a

Li, Y., Chen, Y., Zhang, J., Zhu, J.-F., Liu, Z.-J., Liang, S.-Y., et al. (2010). Protective Effect of Glutamine-Enriched Early Enteral Nutrition on Intestinal Mucosal Barrier Injury after Liver Transplantation in Rats. *Am. J. Surg.* 199 (1), 35–42. doi:10.1016/j.amjsurg.2008.11.039

Litvak, Y., Byndloss, M. X., and Bäumler, A. J. (2018). Colonocyte Metabolism Shapes the Gut Microbiota. *Science* 362 (6418), eaat9076. doi:10.1126/science.aat9076

Liu, X., Mao, B., Gu, J., Wu, J., Cui, S., Wang, G., et al. (2021). Blautia-a New Functional Genus with Potential Probiotic Properties? *Gut Microbes* 13 (1), 1–21. doi:10.1080/19490976.2021.1875796

Lopez, C. A., Winter, S. E., Rivera-Chávez, F., Xavier, M. N., Poon, V., Nuccio, S.-P., et al. (2012). Phage-mediated Acquisition of a Type III Secreted Effector Protein Boosts Growth of salmonella by Nitrate Respiration. *mBio* 3 (3), e00143. doi:10.1128/mBio.00143-12

Mills, S., Stanton, C., Lane, J., Smith, G., and Ross, R. (2019). Precision Nutrition and the Microbiome, Part I: Current State of the Science. *Nutrients* 11 (4), 923. doi:10.3390/nu11040923

Mokdad, A. A., Lopez, A. D., Shahraz, S., Lozano, R., Mokdad, A. H., Stanaway, J., et al. (2014). Liver Cirrhosis Mortality in 187 Countries between 1980 and 2010: A Systematic Analysis. *BMC Med.* 12, 145. doi:10.1186/s12916-014-0145-y

Ohland, C. L., and Macnaughton, W. K. (2010). Probiotic Bacteria and Intestinal Epithelial Barrier Function. *Am. J. Physiology-Gastrointestinal Liver Physiol.* 298 (6), G807–G819. doi:10.1152/ajpgi.00243.2009

Rafter, J., Bennett, M., Caderni, G., Clune, Y., Hughes, R., Karlsson, P. C., et al. (2007). Dietary Synbiotics Reduce Cancer Risk Factors in Polypectomized and colon Cancer Patients. *Am. J. Clin. Nutr.* 85 (2), 488–496. doi:10.1093/ajcn/85.2.488

Rothschild, D., Weissbrod, O., Barkan, E., Kurilshikov, A., Korem, T., Zeevi, D., et al. (2018). Environment Dominates over Host Genetics in Shaping Human Gut Microbiota. *Nature* 555 (7695), 210–215. doi:10.1038/nature25973

Rowe, I. A. (2017). Lessons from Epidemiology: The Burden of Liver Disease. *Dig. Dis.* 35 (4), 304–309. doi:10.1159/000456580

Schnabl, B., and Brenner, D. A. (2014). Interactions between the Intestinal Microbiome and Liver Diseases. *Gastroenterology* 146 (6), 1513–1524. doi:10.1053/j.gastro.2014.01.020

Shapira, M. (2016). Gut Microbiotas and Host Evolution: Scaling up Symbiosis. *Trends Ecol. Evol.* 31 (7), 539–549. doi:10.1016/j.tree.2016.03.006

Sims, I. M., Ryan, J. L. J., and Kim, S. H. (2014). *In Vitro* fermentation of Prebiotic Oligosaccharides by Bifidobacterium Lactis HN019 and Lactobacillus Spp. *Anaerobe* 25, 11–17. doi:10.1016/j.anaerobe.2013.11.001

Sun, L.-Y., Yang, Y.-S., Qu, W., Zhu, Z.-J., Wei, L., Ye, Z.-S., et al. (2017). Gut Microbiota of Liver Transplantation Recipients. *Sci. Rep.* 7 (1), 3762. doi:10.1038/s41598-017-03476-4

Tapper, E. B., and Parikh, N. D. (2018). Mortality Due to Cirrhosis and Liver Cancer in the United States, 1999-2016: Observational Study. *BMJ* 362, k2817. doi:10.1136/bmj.k2817

Turnbaugh, P. J., and Gordon, J. I. (2009). The Core Gut Microbiome, Energy Balance and Obesity. *J. Physiol.* 587 (Pt 17), 4153–4158. doi:10.1113/jphysiol.2009.174136

Wang, F. S., Fan, J. G., Zhang, Z., Gao, B., and Wang, H. Y. (2014). The Global burden of Liver Disease: The Major Impact of China. *Hepatology* 60 (6), 2099–2108. doi:10.1002/hep.27406

Wassenaar, T. M. (2016). Insights from 100 Years of Research with probioticE. Coli. *Eur. J. Microbiol. Immunol.* 6 (3), 147–161. doi:10.1556/1886.2016.00029

Wiley, N. C., Dinan, T. G., Ross, R. P., Stanton, C., Clarke, G., and Cryan, J. F. (2017). The Microbiota-Gut-Brain axis as a Key Regulator of Neural Function and the Stress Response: Implications for Human and Animal Health. *J. Anim. Sci.* 95 (7), 3225–3246. doi:10.2527/jas2016.1256

Winter, S. E., and Bäumler, A. J. (2014). Dysbiosis in the Inflamed Intestine. *Gut Microbes* 5 (1), 71–73. doi:10.4161/gmic.27129

Winter, S. E., Winter, M. G., Xavier, M. N., Thiennimitr, P., Poon, V., Keestra, A. M., et al. (2013). Host-derived Nitrate Boosts Growth of E. Coli in the Inflamed Gut. *Science* 339 (6120), 708–711. doi:10.1126/science.1232467

Wu, W., Sun, M., Chen, F., Cao, A. T., Liu, H., Zhao, Y., et al. (2017). Microbiota Metabolite Short-Chain Fatty Acid Acetate Promotes Intestinal IgA Response to Microbiota Which Is Mediated by GPR43. *Mucosal Immunol.* 10 (4), 946–956. doi:10.1038/mi.2016.114

Yao, C. K., Fung, J., Chu, N. H. S., and Tan, V. P. Y. (2018). Dietary Interventions in Liver Cirrhosis. *J. Clin. Gastroenterol.* 52 (8), 663–673. doi:10.1097/MCG.0000000000001071

Zheng, P., Zeng, B., Liu, M., Chen, J., Pan, J., Han, Y., et al. (2019). The Gut Microbiome from Patients with Schizophrenia Modulates the Glutamate-Glutamine-GABA Cycle and Schizophrenia-Relevant Behaviors in Mice. *Sci. Adv.* 5 (2), u8317. doi:10.1126/sciadv.aau8317

Zhu, D., Chen, X., Wu, J., Ju, Y., Feng, J., Lu, G., et al. (2012). Effect of Perioperative Intestinal Probiotics on Intestinal flora and Immune Function in Patients with Colorectal Cancer. *Nan Fang Yi Ke Da Xue Xue Bao* 32 (8), 1190–1193.

Conflict of Interest: The authors declare that the research was conducted in the absence of any commercial or financial relationships that could be construed as a potential conflict of interest.

frontiers | Frontiers in Physiology

ORIGINAL RESEARCH
published: 07 April 2022
doi: 10.3389/fphys.2022.836918

Alteration of Ileal lncRNAs After Duodenal–Jejunal Bypass Is Associated With Regulation of Lipid and Amino Acid Metabolism

Yongjun Liang[1,2], Minghua Yu[1,2], Yueqian Wang[1], Mengyi Li[3], Zhongtao Zhang[3], Zhengdong Qiao[1]* and Peng Zhang[3]**

[1]Center for Medical Research and Innovation, Shanghai Pudong Hospital, Fudan University Pudong Medical Center, Shanghai, China, [2]Shanghai Key Laboratory of Vascular Lesions Regulation and Remodeling, Shanghai Pudong Hospital, Fudan University Pudong Medical Center, Shanghai, China, [3]Department of Surgery, Capital Medical University Beijing Friendship Hospital, Beijing, China

OPEN ACCESS

Edited by:
Sanyuan Hu,
Shandong University, China

Reviewed by:
Zhi-Qiang Cheng,
Shandong University, China
Ling Yang,
Temple University, United States
Guangyong Zhang,
The First Affiliated Hospital of Shandong First Medical University, China

***Correspondence:**
Zhongtao Zhang
zhangzht@ccmu.edu.cn
Zhengdong Qiao
zhengdong_qiao@hotmail.com
Peng Zhang
zhangpg@yahoo.com

Specialty section:
This article was submitted to Lipid and Fatty Acid Research, a section of the journal Frontiers in Physiology

Received: *12 January 2022*
Accepted: *07 March 2022*
Published: *07 April 2022*

Citation:
Liang Y, Yu M, Wang Y, Li M, Zhang Z, Qiao Z and Zhang P (2022) Alteration of Ileal lncRNAs After Duodenal–Jejunal Bypass Is Associated With Regulation of Lipid and Amino Acid Metabolism. Front. Physiol. 13:836918. doi: 10.3389/fphys.2022.836918

Metabolic and bariatric surgery (MBS) can generate a drastic shift of coding and noncoding RNA expression patterns in the gastrointestinal system, which triggers organ function remodeling and may induce type 2 diabetes (T2D) remission. Our previous studies have demonstrated that the altered expression profiles of duodenal and jejunal long noncoding RNAs (lncRNAs) after the duodenal–jejunal bypass (DJB), an investigational procedure and research tool of MBS, can improve glycemic control by modulating the entero-pancreatic axis and gut–brain axis, respectively. As an indiscerptible part of the intestine, the ileal lncRNA expression signatures after DJB and the critical pathways associated with postoperative correction of the impaired metabolism need to be investigated too. High-fat diet-induced diabetic mice were randomly assigned into two groups receiving either DJB or sham surgery. Compared to the sham group, 1,425 dysregulated ileal lncRNAs and 552 co-expressed mRNAs were identified in the DJB group. Bioinformatics analysis of the differently expressed mRNAs and predicted target genes or transcriptional factors indicated that the dysregulated ileal lncRNAs were associated with lipid and amino acid metabolism-related pathways. Moreover, a series of lncRNAs and their potential target mRNAs, especially NONMMUT040618, *Pxmp4*, *Pnpla3*, and *Car5a*, were identified on the pathway. In conclusion**,** DJB can induce remarkable alteration of ileal lncRNA and mRNA expression. The role of the ileum in DJB tends to re-establish the energy homeostasis by regulating the lipid and amino acid metabolism.

Keywords: duodenal–jejunal bypass, lncRNAs, ileum, lipid metabolism, amino acid metabolism

INTRODUCTION

The prevalence of type 2 diabetes mellitus (T2DM) has been soaring globally. According to the International Diabetes Federation's Diabetes Atlas 7th edition, about 415 million people in the world are suffering from diabetes, and the projected total number of T2DM patients will reach 642 million by 2035 eventually (Ogurtsova et al., 2017). T2DM is a complex metabolic homeostasis disorder and mainly manifested as hyperglycemia, which, if uncontrolled, can potentially lead to an increased risk of microvascular- and macrovascular-related complications (Lai et al., 2014).

Metabolic and bariatric surgery (MBS), such as Roux-en-Y gastric bypass (RYGB) and sleeve gastrectomy (SG) procedures, emerged as a weight-reduction therapy originally and has been clinically shown to be able to induce long-term remission of T2DM (Carlsson et al., 2012; Mingrone et al., 2012; Chang et al., 2014), to reduce cardiovascular risk factors (Sjostrom et al., 2012), and to decrease overall mortality (Sjostrom et al., 2007; Chang et al., 2014) in addition to drastic weight loss. During the past decades, a great deal of research efforts has been invested in the investigation of the mechanisms of MBS. Some related factors, such as weight reduction, caloric restriction, change in bile acid secretion, fibroblast growth factor 19 (*FGF19*), gut microbiome, and gastrointestinal (GI) hormonal changes, were proposed. However, none of the factors can explain all biological and physiological changes after MBS. So far, the exact underlying mechanism remains unknown.

All MBS procedures are involved with the anatomical alteration of the GI tract, which seems to be the origin of all the biological and physiological benefits induced by MBS. Therefore, in order to better understand the mechanisms of MBS, it is crucial to illustrate the functional role of the GI tract in metabolic modulation, although the GI tract was traditionally considered the digestive system. During the past few years, our team carried out a series of studies to investigate the role of each GI segment in metabolic regulation using diabetic animal models and gene microarray analysis. Whole transcriptome analysis of long noncoding RNAs (lncRNAs) and co-expressed mRNAs is a fundamental and powerful tool to understand the functional alteration of organs caused by surgical intervention. Once considered to be "transcriptional noise", lncRNAs are currently defined as transcripts longer than 200 nucleotides that lack protein-coding capability but regulate almost all biological processes (Mercer and Mattick, 2013). Under normal circumstances, serving as signals, decoys, guides, and scaffolds, lncRNAs maintain physiological homeostasis. While under the pathological conditions, abnormal expression of lncRNAs participates in the human disease development (Kwok and Tay, 2017). For instance, peripheral insulin resistance (Zhu et al., 2016) and inflammatory diabetes complications (Reddy et al., 2014) are precisely governed by lncRNAs.

From our previous studies, we have revealed that 1) gastric volume reduction is essential for T2DM remission after RYGB (Zhang et al., 2016); 2) drastic changes in lncRNA and mRNA expression profiles of the duodenum induced by duodenal exclusion attenuate inflammation and initiate insulin secretion via the entero-pancreatic axis (Liang et al., 2017); and 3) alteration of the jejunal Roux limb lncRNA and mRNA expression pattern triggers both neuromodulation and endocrine-related pathways and participates in T2DM remission after duodenal–jejunal bypass (DJB) via the gut–brain axis (Liang et al., 2018). Apparently, beyond the traditional cognition, the duodenum and jejunum are more like metabolic regulators cross-talking with peripheral organs and executing surgical information, rather than solely digestive and absorptive organs. Reasonably, considering the altered anatomical structure and the faster passage of meal chyme after surgery, the ileum should also be involved in metabolic reconstruction, although its role has not been characterized yet. As an investigational procedure and research tool of MBS, DJB only causes anatomical changes in the intestine, which can rule out interference from other factors. Therefore, in the present study, we utilized a rodent T2DM model to elucidate the molecular mechanism on how the ileum modulates metabolic regulation after DJB.

MATERIALS AND METHODS

Animal Model and Phenotyping

All procedures of this study were approved (NO. 2021-DS-M-09) by the Institutional Animal Care and Utilization Committee of the Fudan University Pudong Medical Center. A cohort of male C57BL/6 mice was received from Shanghai Slyke Laboratory Animal Corporation (Shanghai, China). After 1-week acclimatization, the mice started to undergo high-fat diet (HFD, 5.24 kcal/g with kcal percentages 60% fat, 20% protein, and 20% carbohydrate, Cat. #D12492, Research Diets Inc., New Brunswick, NJ, United States) at an age of 6 weeks for 12 weeks. At the end of the 12-week HFD, according to the weight (≈50 g), fasting blood glucose (FBG≥11 mmol/L), and impaired oral glucose tolerance test (OGTT), eight animals with typical diabetic phenotypes were selected and randomized into DJB or sham groups based upon the procedure received. The DJB procedure was performed with the 5-cm biliopancreatic limb and 4-cm Roux limb under general anesthesia, and the sham group only underwent the same general anesthesia and laparotomy but without intestinal transection and rerouting. Please refer to our previously published studies for the details of DJB and sham procedures (Liang et al., 2017; Liang et al., 2018). Another five age-matched mice served as the chow diet control without undergoing any surgical procedures. The mice were sacrificed two weeks after surgery, and the ileum was collected for RNA analysis. The body weight and FBG were measured after 6 h of fasting at 0 week (before initiation of HFD), 12 weeks (12 weeks after HFD), and 14 weeks (2 weeks after DJB/sham procedure). According to the manual, the plasma insulin levels were measured using enzyme-linked immunosorbent assay kits (Cat. #10-1247-01, Mercodia, Uppsala, Sweden). The OGTT was conducted after a 12-h overnight fast. After a 20% (w/v) glucose solution challenge at a dose of 2 g/kg weight, blood glucose levels were measured at different time points. The area under curve of the glucose excursions during OGTT was calculated.

Ileal RNA Preparation and Microarray Analysis

Ileal RNA isolation, quality control, labeling, and hybridization methods have been described in detail previously (Liang et al., 2017; Liang et al., 2018). In brief, after hybridization, the "flag" value of each gene is calculated and classified into three levels of A, M, and P according to the signal strength. The genes with low hybridization signals (A or M) in both groups have been filtered out. Then, lncRNAs and mRNAs showing statistically significant differences in expression between the two groups were identified

through p value/false-discovery (FDR) rate filtering. Hierarchical clustering was performed to demonstrate the expression patterns of critical lncRNAs and mRNAs. Significant differentially expressed lncRNA and mRNA were identified through fold change ≥2 and $p < 0.05$ and displayed by the scatter plot and volcano plot.

Bioinformatic Analysis

The Gene Ontology (GO) and Kyoto Encyclopedia of Genes and Genomes (KEGG) pathway analysis were performed based on the function of lncRNA-co-expressed mRNAs. The target genes of lncRNAs were predicted via cis- or trans-regulatory patterns. Cis-regulated target gene prediction used the University of California Santa Cruz genome Browser to identify the potential targets located within a 10-kb window upstream or downstream of lncRNAs. Trans-regulated target gene prediction used Basic Local Alignment Search Tool software to screen the mRNAs that had sequences complementary to the lncRNAs, followed by identification of trans-acting target genes with RNAplex software (University of Vienna, Vienna, Austria). The potential transcription factors (TFs) targeting lncRNAs were predicted using TFSearch (National Institute of Advanced Industrial Science and Technology, Tsukuba, Japan). Co-expression and interaction networks were constructed to identify the core lncRNAs or mRNAs. The Pearson's correlation coefficient (PCC) was used to calculate the expression correlation of lncRNAs and mRNAs. The pairs with PCC values >0.99 were selected as linkages in the network using Cytoscape 3.8.2 software (Agilent and IBS).

Microarray Validation

Real-time PCR was used to confirm microarray results with a randomly selected subset of differentially expressed lncRNAs and mRNAs. The primers used in this study are shown in the **Supplementary Material**. Total RNAs were extracted using TRIzol reagent (Cat. #15596018, Invitrogen, Grand Island, NY, United States) and were reverse transcribed to cDNA with the PrimeScript RT Reagent Kit (Cat. #RR047A, Takara, Dalian, China). Real-time PCR was carried out in triplicate for each sample, with GAPDH as an internal reference, using PowerUp™ SYBR™ Green PCR Master Mix (Cat. #A25742, Life Technologies, Grand Island, NY, United States). Probe specificity was confirmed by melting curve analysis, and the relative expression of the genes was calculated using the $2^{-\triangle\triangle Ct}$ method.

Statistical Analysis

Data were expressed as means ± SEM. Statistical analysis was performed using Student's t-test to compare the differences between DJB and sham groups with SPSS software (Version 22.0; SPSS Inc., Chicago, IL, United States). Statistical significance was set at $p < 0.05$.

RESULTS

DJB Improved Diabetic Phenotypes

DJB surgery performed in our study is shown in **Figure 1A**. Before HFD induction (week 0), the baseline values of weight, FBG, plasma insulin, and oral glucose tolerance test (OGTT) of mice in different groups were almost identical (**Figures 1B–E,H**). After 12-week HFD, the mice in both DJB and sham groups successfully established diabetic phenotypes with elevated body weight, hyperglycemia, and hyperinsulinemia (**Figures 1B–D,F,H**). Compared to the sham group, two weeks after surgery (week 14), all metabolic parameters in the DJB group were rapidly improved and approached to the level of the chow diet control group (**Figures 1B–D,G,H**). Overall, the success of diabetic mouse model establishment and surgical procedure ensured the reliability of the following ileal microarray analysis.

DJB Altered Ileal Transcriptome

The transcriptomes of eight ileal samples randomly selected from the DJB or sham group were investigated and found that their intensity values were nearly identical (**Figure 2A**). Compared to the sham group, 366 up- and 186 downregulated mRNAs were identified in the DJB group (**Figure 2B**). The number of mRNAs with different multiples was calculated (**Supplementary Table S1**), and the top 10 dysregulated mRNAs are listed in **Supplementary Table S2**. As a member of the phospholipase A2 enzyme family, *Pla2g4c* usually contributes to lipid metabolism by hydrolyzing glycerophospholipids to produce free fatty acids and lysophospholipids. While another gene *Cpvl*, a novel serine carboxypeptidase, participates in amino acid homeostasis via cleaving amino acids from the C-terminus of a protein substrate. Except the two mentioned previously, some of the other mRNAs listed in **Supplementary Table S2** were demonstrated to be associated with lipid and amino acid metabolism. Hierarchical clustering analysis of the 552 differently expressed mRNAs was performed and shown in **Figure 2C**.

Altered Ileal Transcriptome Contributed to the Lipid and Amino Acid Metabolism

Normally, lncRNAs exert their functions by interacting with mRNAs under different patterns. To reveal the potential functions of the ileal lncRNAs after DJB, the pathway and Gene Ontology (GO) analysis of aberrantly co-expressed mRNAs were performed. The top 30 significantly enriched pathways were featured and ranked with enrichment scores (**Figure 2D**). Further analysis indicated that 26 pathways were upregulated and three pathways were downregulated. Apparently, metabolic pathways, including lipid metabolism (12/30), amino acid metabolism (5/30), carbohydrate metabolism (2/30), and energy metabolism (1/30), occupied a respectable majority. Most importantly, robust enrichment was observed in lipid metabolism-related pathways, such as fatty acid degradation, fatty acid elongation, fatty acid biosynthesis, PPAR signaling pathway, biosynthesis of unsaturated fatty acids, and peroxisome as well as in amino acid metabolism-related pathways, such as beta-alanine metabolism, tryptophan metabolism, and valine, leucine, and isoleucine degradation. Overall, the lncRNA-co-expressed mRNA-enriched pathways, which are triggered by the surgery, contribute to the metabolic improvement, especially to lipid and amino acid homeostasis.

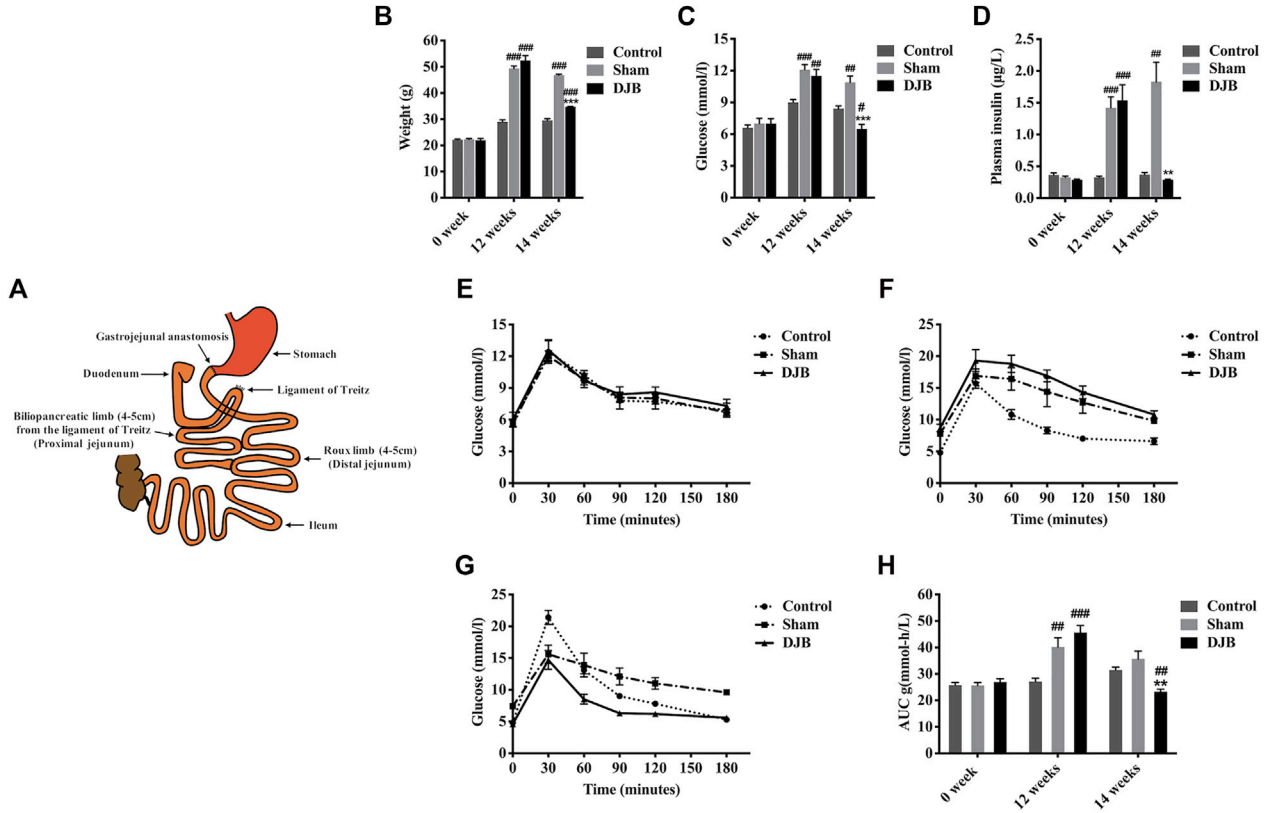

FIGURE 1 | Characterization of the HFD-induced T2DM mouse model and surgical outcomes. Schematic diagram of DJB surgery **(A)**. Weight **(B)**, FBG **(C)**, plasma insulin **(D)**, OGTT before HFD induction **(E)**, OGTT at 12 weeks after HFD induction and before DJB **(F)**, 14 weeks on HFD and 2 weeks after DJB surgery **(G)**, and area under the curve (AUC) of OGTT glucose excursion **(H)**. All values are shown as mean ± SEM. Statistical differences were analyzed by the Student's *t*-test. * For DJB group versus sham group, # for DJB or sham group versus control group (*p <0 .05, **p <0 .01, ***p <0 .001, #p <0 .05, ##p <0 .01, ###p <0 .001).

Consistent with pathway analysis, the items of "biological processes," including very long-chain fatty acid catabolic process, negative regulation of fatty acid oxidation, long-chain fatty acid import, and negative regulation of lipoprotein particle clearance, were enriched and involved in the lipid metabolism by manipulating cellular or circulating lipids clearance (**Figure 2E**). Furthermore, the GO terms for molecular function were correlated with long-chain fatty acid transporter activity, fatty acid transporter activity, and acylglycerol lipase activity, which were essential for lipid metabolism (**Figure 2E**). Collectively, DJB triggered a shift in the ileal transcriptome somehow, and the altered lncRNAs and co-expressed mRNAs reprogrammed the metabolic systems of the ileum, particularly in the lipid and amino acid metabolism, which finally contributed to the remission of metabolic disorders possibly through increased resting energy expenditure.

DJB Induced Ileal lncRNA Expression Profiling Shifting

DJB surgery triggered distinctive alteration of ileal lncRNAs' expression signature with 226 up- and 1,199 downregulated lncRNAs (**Figures 3A,B**). The 1,425 lncRNAs were further sorted based on the fold change (**Supplementary Table S1**), and the top 10 up- and downregulated lncRNA are displayed in **Supplementary Table S3**. The lncRNA *Gas5* with functional annotation, which was reported to play an important role in pancreatic β-cell function and peripheral insulin resistance, was identified in the microarray. Although another lncRNA *Tmem132cos*, named as transmembrane protein 132C (*Tmem132c*) opposite strand, has not been investigated yet, the *Tmem132c* was found correlated negatively with insulin secretion, suggesting that the downregulation of *Tmem132c*os may play a therapeutical role in T2DM remission. Hierarchical clustering indicated that the lncRNA expression patterns between the DJB and sham groups were distinguishable (**Figure 3C**). In addition, systematic analysis and statistics of differentially expressed ileal lncRNA from different dimensions were carried out and displayed in **Figures 3D–F**.

Predicted Target Genes Are Associated With Ileal lncRNAs' Positive Effect on Metabolic Homeostasis Reconstruction

Since lncRNAs exert functions indirectly, prediction of target genes and construction of the interaction network are crucial

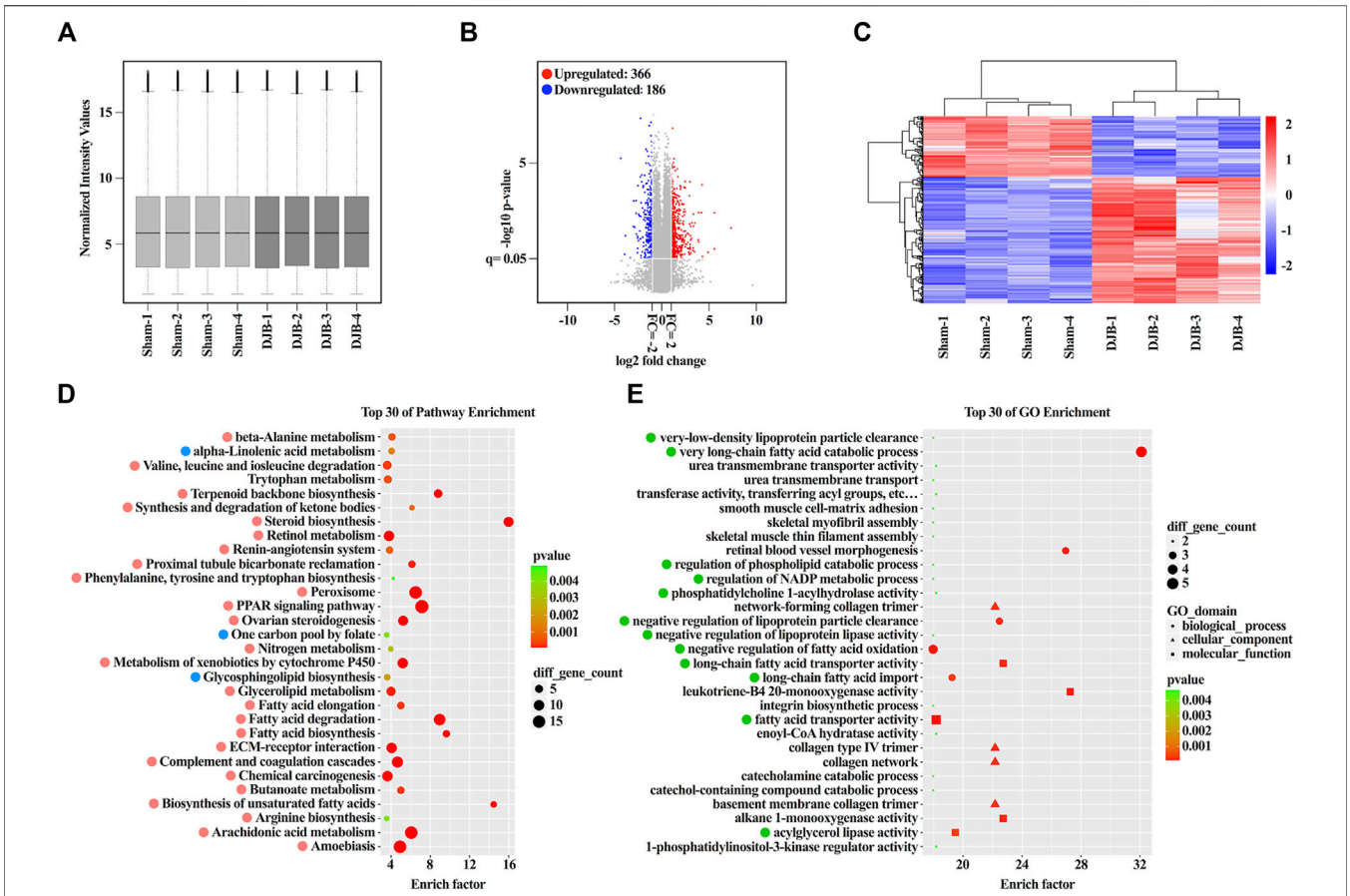

FIGURE 2 | Overview and bioinformatic analysis of lncRNA-co-expressed mRNA profiles. **(A)** Box-plot showing the normalization of all samples. **(B)** Volcano plot of differentially expressed mRNAs between DJB and sham groups. **(C)** Heat map of mRNAs showed hierarchical clustering of differentially expressed mRNAs in DJB and sham mice (fold change ≥2, $p < 0.05$). Red and blue, respectively, represent high and low relative expression. **(D)** Top 30 significantly enriched pathways ranked with an enrichment score ($p < 0.05$). Up- and downregulated pathways are marked with soft red and soft blue, respectively. **(E)** Top 30 significantly enriched GO items ($p < 0.05$). The important items are marked with green.

to identify the most influential ileal lncRNAs after DJB. Utilizing the Cytoscape program, the network was generated with 998 ileal lncRNAs, 2,261 target genes, and 20,876 lncRNA-target gene pairs (**Figure 4A**). Pathway annotations of predicted target genes indicated that altered ileal lncRNAs may maintain lipid homeostasis by regulating lipid metabolism-related pathways, mainly including biosynthesis of unsaturated fatty acids, fatty acid elongation, AMPK signaling pathway, glycerophospholipid metabolism, and steroid biosynthesis and sphingolipid metabolism (**Figure 4B**). Furthermore, pathways of taurine and hypotaurine metabolism, sulfur relay system, and nitrogen metabolism, which were associated with the amino acid metabolism, were annotated and beneficial for T2DM amelioration after surgery (**Figure 4B**, **Supplementary Figures S1A–C**). Generally, the metabolic benefits from DJB, including the changes in lipid and amino acid metabolism caused by ileal lncRNAs, were comparable between DJB and sham groups.

Ileal lncRNA–mRNA Pairs Remodeled the Lipid and Amino Acid Metabolism

In order to screen out the most functional ileal lncRNA–mRNA pairs with potential targeting relationship, the co-expression network was constructed, and bioinformatic analysis was performed. By overlapping the ileal lncRNA-co-expressed mRNAs and predicted target genes, a subgroup containing 82 mRNAs was created. Combining 203 corresponding lncRNAs targeting the 82 mRNAs, 1,459 transcript pairs were generated and finally constituted the network (**Figure 5A**). The pathways enriched by the subset of lncRNA-co-expressed mRNAs were mostly involved in lipid metabolism, such as fatty acid elongation, fatty acid degradation, fatty acid biosynthesis, biosynthesis of

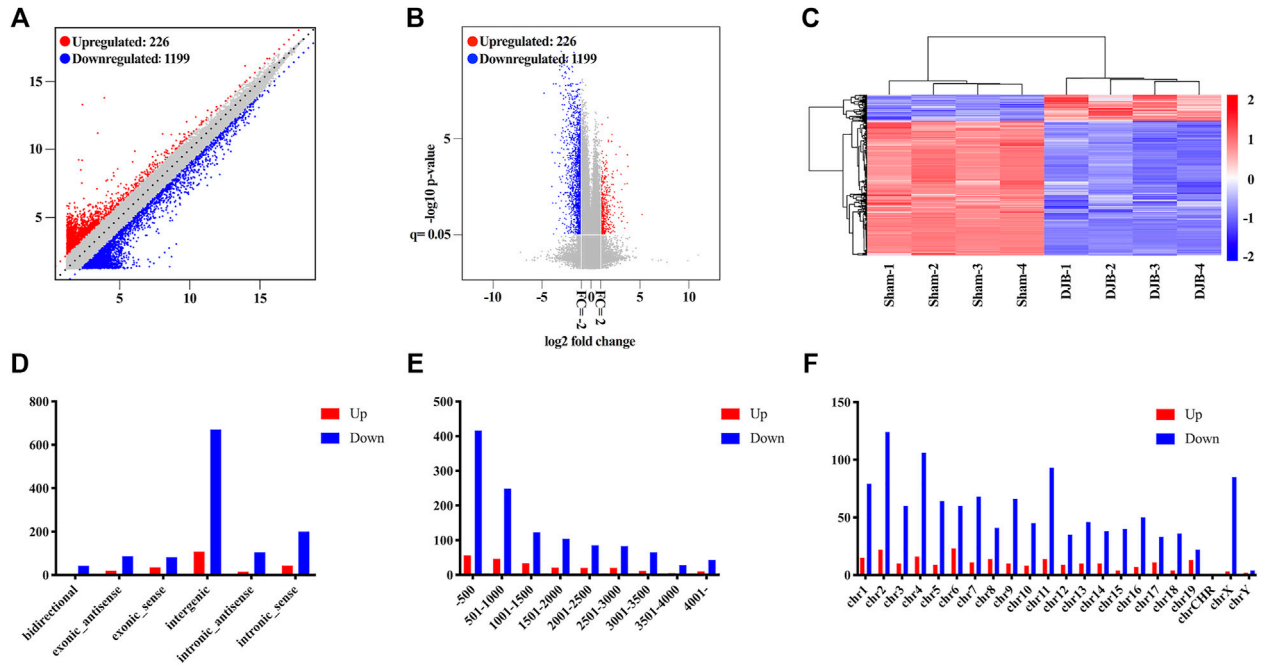

FIGURE 3 | Identification and analysis of distinctively expressed lncRNAs. Scatter plot **(A)** and volcano plot **(B)** of differentially expressed lncRNAs between the DJB and sham groups. **(C)** Heat map of lncRNAs showed hierarchical clustering of differentially expressed lncRNAs in DJB and sham mice (fold change ≥2, $p < 0.05$). Analysis of up- and downregulated lncRNAs based on classification **(D)**, length distribution **(E)**, and chromosome locus **(F)**.

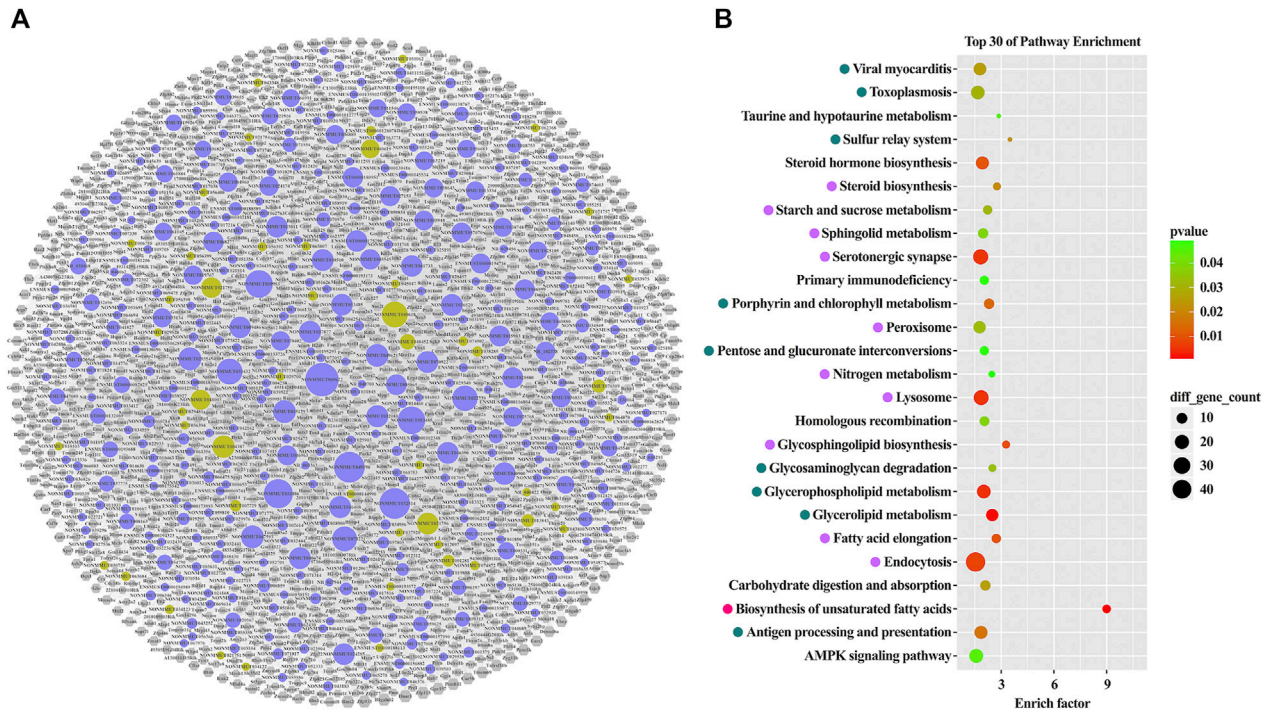

FIGURE 4 | Construction of the lncRNA-target genes interaction network and pathway analysis of the target genes. **(A)** lncRNA-target genes interaction network. Circle nodes with strong yellow and orchid represent up- and downregulated lncRNAs, respectively. Hexagon nodes with gray represent target genes. **(B)** Top 30 significantly enriched pathways ranked with an enrichment score ($p < 0.05$). Trans-, CIS-, and trans and CIS-regulatory pathways are marked with light violet, dark cyan, and pure pink, respectively.

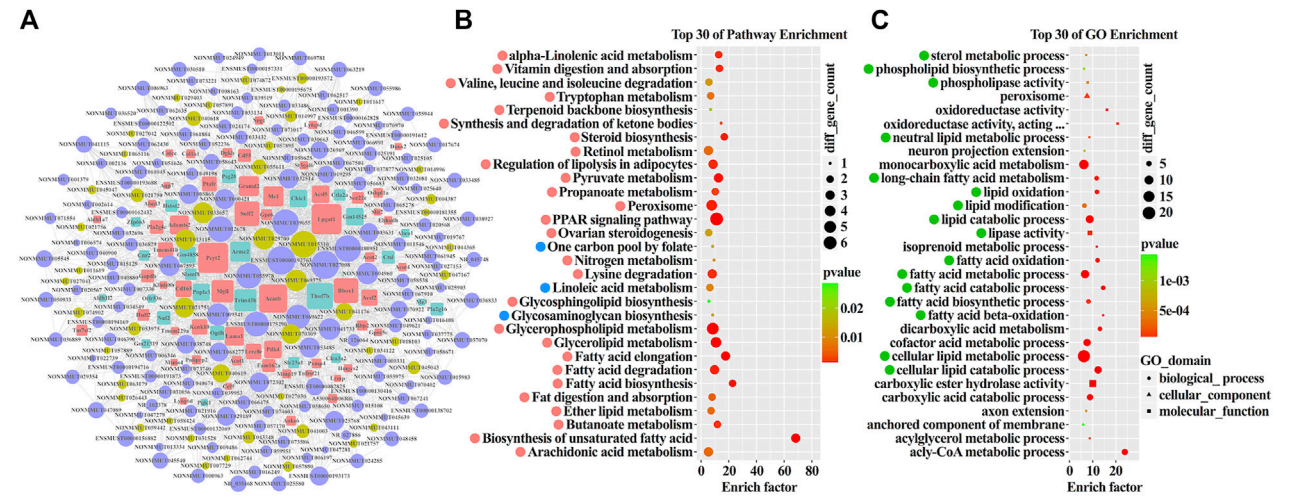

FIGURE 5 | Construction of the lncRNA–mRNA co-expression network and bioinformatic analysis. **(A)** lncRNA–mRNA co-expression network. Circle nodes with strong yellow and orchid represent up- and downregulated lncRNAs, respectively. Square nodes with soft red and slightly desaturated cyan represent up- and downregulated mRNAs, respectively. **(B)** Top 30 significantly enriched pathways ranked with an enrichment score ($p < 0.05$). Up- and downregulated pathways are marked with soft red and soft blue, respectively. **(C)** Top 30 significantly enriched GO items (p <0 .05). The important items are marked with green.

unsaturated fatty acids, PPAR signaling pathway, peroxisome, glycerophospholipid metabolism, and glycerolipid metabolism (**Figure 5B**, **Supplementary Figure S2A**). In addition, pathways of valine, leucine, and isoleucine degradation, tryptophan metabolism, lysine degradation, and nitrogen metabolism, which probably acted on postoperative reconstruction of amino acid metabolic homeostasis, were enriched as well (**Figure 5B**, **Supplementary Figures S2A, B**). Moreover, the most important GO items, marked with green, referred to lipid biosynthesis, oxidation, and modification (**Figure 5C**). In short, the subset of ileal mRNAs and their upstream lncRNAs played critical roles in metabolic remission via remodeling the ileal lipid and amino acid metabolism after DJB.

Identification of Lipid and Amino Acid Metabolism-Related lncRNA–mRNA Pairs

All the aforementioned systematic analyses demonstrated that DJB caused great change of ileal lncRNAs' expression signature, which further re-established lipid and amino acid metabolic homeostasis of the ileum and participated in the T2DM remission after DJB. Therefore, identification of specific ileal lncRNA–mRNA pairs involved in lipid and amino acid metabolism-related pathways was extremely important. The up- or downregulated mRNAs and CIS- or trans-target genes were input into the Venn program, and 49 CIS-mRNAs, 38 trans-mRNAs, and 8 CIS- and trans-mRNAs were screened out (**Figure 6A**; **Supplementary Table S4**). By overlapping the CIS-mRNAs with genes involved in lipid metabolism pathways, 6 CIS-mRNAs, and 13 upstream lncRNAs were verified (**Figures 6B,C**). In the same way, six trans-mRNAs and 13 lncRNAs were acquired and depicted in **Figures 6D,E**. Furthermore, amino acid metabolism-related CIS- or trans-mRNAs and relevant lncRNAs are presented in **Figures 6F–I**, respectively. Notably, the ileal lncRNA NONMMUT040618 and its target mRNAs (*Pxmp4*, *Pnpla3*, and *Car5a*), which were involved in lipid and amino acid metabolism-related pathways, might play vital roles in the remission of metabolic disorders after DJB.

Ileal Transcription Factors Analysis

To elucidate the upstream regulation network, a group of 63 TFs, targeting 203 ileal lncRNAs involved in the co-expression network, was predicted. All these transcripts and 6,993 lncRNA–TF-targeting pairs constituted the interaction network (**Figure 7A**). Among the TF group, seven up- and six downregulated TFs were found in the microarray (**Figures 7B,D**). Moreover, intersecting the distinct subsets of lncRNAs generated by each upregulated TF, eight dysregulated ileal lncRNAs were screened out (**Figure 7C**, **Supplementary Figure S3A**). The six downregulated TFs were analyzed with the identical procedure (**Figure 7E**, **Supplementary Figure S3B**). Pathway annotation of predicted TFs indicated that the lipid and amino acid metabolism-related pathways were enriched (**Supplementary Figure S3C**).

Verification of the Ileal Microarray Data

In order to validate the accuracy as well as reliability, 10 dysregulated transcripts in the ileal microarray were randomly selected (**Supplementary Table S5**), and their expression levels both in samples for microarray and tissues obtained from another cohort of mice undergoing the identical process (**Figures 8A–G**) were detected using qRT-PCR. The qRT-PCR results from the ileal samples employed in the microarray or newly gained ileal tissues were highly consistent with original microarray data (**Figures 8H,I**).

DISCUSSION

DJB induced significant alterations in intestinal lncRNA and mRNA expression patterns. All the dysregulated lncRNAs in

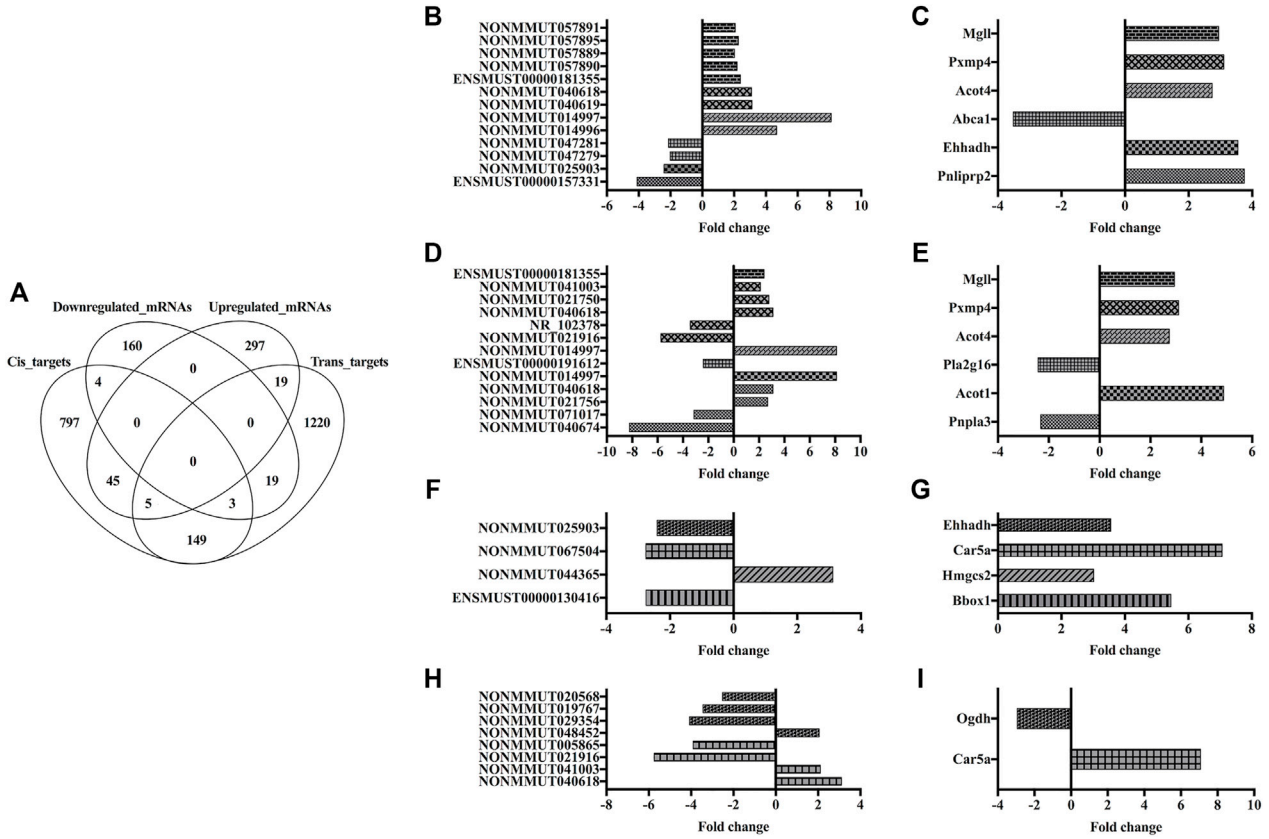

FIGURE 6 | Identification of lipid and amino acid metabolism-related lncRNAs and downstream mRNAs. **(A)** Venn diagram showing the overlapping of up- and downregulated mRNAs with trans- and CIS-targets. Histograms of lipid metabolism pathway-related lncRNA–mRNA pairs via CIS- **(B,C)** or trans- **(D,E)** regulatory patterns. Histograms of amino acid metabolism pathway-related lncRNA–mRNA pairs via CIS- **(F,G)** or trans- **(H,I)** regulatory patterns. The columns with the same fill pattern represent lncRNA–mRNA pairs.

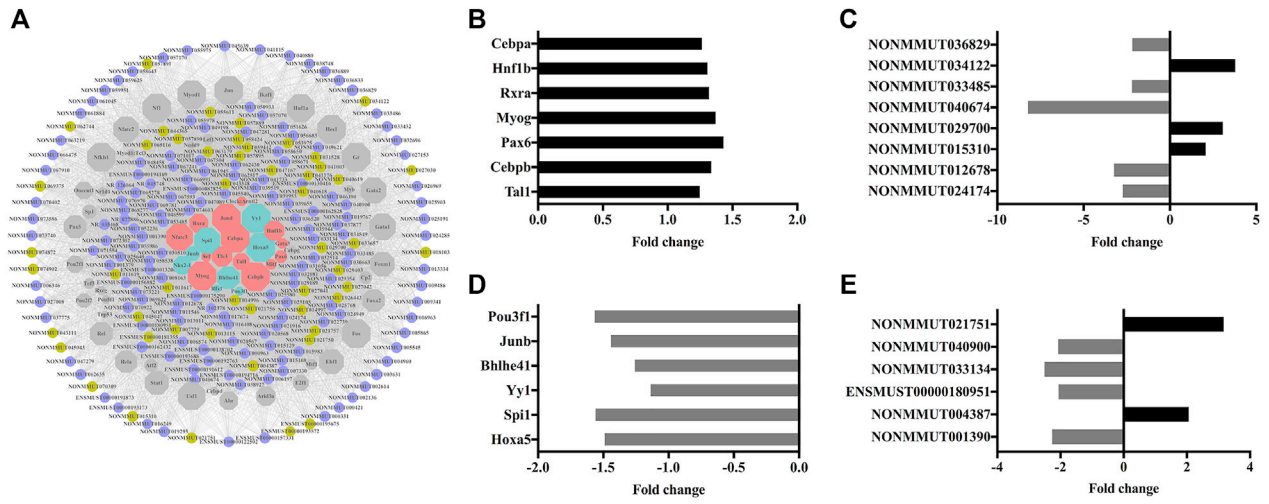

FIGURE 7 | Construction of the lncRNA–TF interaction network and identification of distinctly expressed TFs. **(A)** lncRNA–TF interaction network. Circle nodes with strong yellow and orchid represent up- and downregulated lncRNAs, respectively. Hexagon nodes with soft red, slightly desaturated cyan, and gray represent up-, down-, and unregulated TFs, respectively. Histogram of upregulated TFs **(B)** and their downstream lncRNAs **(C)**. Histogram of downregulated TFs **(D)** and their downstream lncRNAs **(E)**.

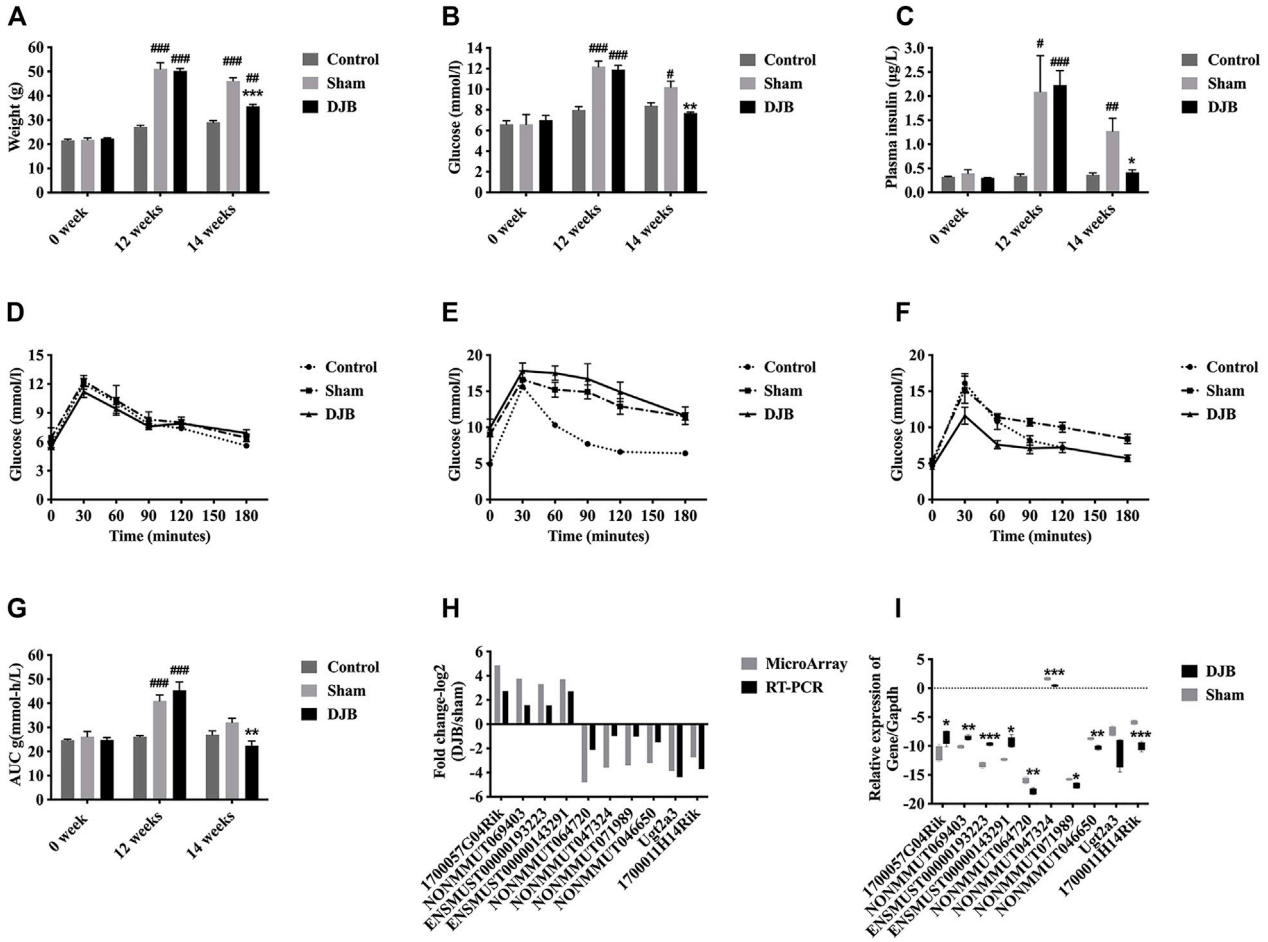

FIGURE 8 | Microarray validation. Weight **(A)**, FBG **(B)**, plasma insulin **(C)**, OGTT **(D)**, week 0 **(E)**, week 12 **(F)**, and week 14 and AUC **(G)** of another cohort of diabetic mice. **(H)** Histograms showing the comparison between microarray data and qRT-PCR results of 10 transcripts. **(I)** Box plot showing the qRT-PCR results of the 10 transcripts with another cohort of mice. All values are shown as mean ± SEM. Statistical differences were analyzed by the Student's *t*-test. * For DJB group versus sham group, # for DJB or sham group versus control group (**p* <0 .05, ***p* <0 .01, ****p* <0 .001, #*p* <0 .05, ##*p* <0 .01, ###*p* <0 .001).

the ileum recomposed energy metabolism homeostasis, especially lipid and amino acid metabolism-related pathways. The target genes also indicated that lipid and amino acid metabolism-related pathways were modified by surgical intervention. In addition, the altered TFs, which were responsible for converting surgical information into transcriptome alteration, also served in lipid metabolism- or diabetes-related pathways as expected. These findings imply that the major role of the ileum in MBS is associated with re-establishment of energy homeostasis by alteration of the lipid and amino acid metabolism. Moreover, functional lncRNAs NONMMUT040618 and downstream mRNAs including *Pxmp4*, *Pnpla3*, and *Car5a* were altered by DJB the most, and therefore, are worthy of further investigations.

MBS leads to effective and long-term remission of T2DM as well as other metabolic disorders such as dyslipidemia, hypertension, hypothyroidism, and polycystic ovary syndrome (PCOS) (Pareek et al., 2018; Mintziori et al., 2020). So far, its underlying mechanism is not fully understood. Altered enterohepatic circulation of bile acids (Wahlstrom et al., 2016), gut microbiota, GI hormones, nutritional deficiency, and weight loss (Aron–Wisnewsky and Clement, 2014; Liu et al., 2017), etc., are thought to contribute to the mechanism of MBS. However, none of the aforementioned factors can explain all the consequences of MBS. Rather than studying on a single mechanism, our series of studies focus on the intestinal transcriptome analysis in order to illuminate the functional roles of different small intestinal segments in metabolic regulation after MBS represented by DJB. MBS involves anatomical alteration of the GI tract including size reduction and/or segment bypass. Also as a result, food intake restriction and/or malabsorption as well as increased resting energy expenditure (Das et al., 2003) are induced to cause weight loss. Moreover, it is also the anatomical change that induces beneficial effects in metabolic regulation. We have previously reported that lncRNAs in the duodenum are associated with pancreatic islet secretion and inflammation process, implying that bypass of the duodenum may initiate insulin secretion and attenuate inflammation (Liang et al., 2017), and those in the

jejunal Roux limb are associated with gut–brain cross talk and endocrine regulation (Liang et al., 2018). Both are related to the beneficial consequence of MBS including T2DM remission, improvement in lipid metabolism, and endocrine hormonal effects. The present study is the part 3 of this series of studies, which is focused on the role of the ileum.

Ileum, the final segment of the small intestine following the duodenum and jejunum, is primarily responsible for absorption of vitamin B_{12}, bile salts, and any nutrients that passed the jejunum under normal circumstances (Matsumoto et al., 2017). In addition to absorption function, cells located in the lining of the ileum secrete protease and carbohydrase enzymes to facilitate protein and carbohydrate digestion (Williams et al., 2011). In addition, we also observed that the whole lipid metabolism networks, especially PPAR signaling pathway, fatty acid elongation, fatty acid degradation, fatty acid biosynthesis, and biosynthesis of unsaturated fatty acids as well as other related pathways, were reprogrammed by the dysregulated ileal lncRNAs after DJB. Thus, MBS may ameliorate the disturbed energy homeostasis via altering lipid metabolism function of the ileum, accelerating energy expenditure.

Ileal amino acid metabolism was another significant function generated by DJB and exerted positive regulation in glycemic control. Under normal physiological conditions, increased plasma amino acid levels after food intake provoke insulin release and mTOR-dependent protein synthesis in muscle (Kimball, 2007). On the cellular level, amino acid homeostasis is maintained by conversion of essential and nonessential amino acids and transfer of amidogen from oxidized amino acids to synthesized amino acids. Once the balance is disrupted, a phenomenon usually preceding or accompanied by dysregulation of glycemia, T2DM could be triggered. For instance, an inappropriate amino acid metabolism results in pancreatic β-cell function disorder and insulin secretion deficiency by disturbing mitochondrial metabolism acutely or altering the insulin granules exocytosis-related genes chronically (Newsholme et al., 2005). Meanwhile, insulin resistance is induced by abnormal plasma levels of essential amino acids and their derivatives (Adams, 2011; Lynch and Adams, 2014). Conversely, improved β-cell function and insulin sensitivity after MBS partially attribute to corrected branched-chain amino acid metabolism and circulation concentrations (Gerszten and Wang, 2011; Magkos et al., 2013). Although the liver is the major site of nitrogen metabolism, surgery-induced amino acid metabolism function in the ileum should be vital for re-establishment of amino acids homeostasis and remission of T2DM.

The limitation of this study is that the screened lncRNAs or mRNAs with potential functions have not been verified yet at the molecular, cellular, and animal levels, which will be carried out in our future studies.

CONCLUSION

The present study serves as a fundamental tool for gene analysis after MBS. From this study, we have demonstrated that DJB is able to regulate transcriptional activities of transcriptional factors, which alter lncRNA expression profiles. The target genes of dysregulated lncRNAs in the ileum involve in lipid and amino acid metabolism-related pathways. These findings imply that the role of the ileum in DJB tends to re-establish the energy homeostasis by regulating the lipid and amino acid metabolism. Concluding the present study on the ileum and our previous gene microarray studies on the duodenum and jejunum, different segments of the intestine play different roles in metabolic regulation after MBS.

DATA AVAILABILITY STATEMENT

The datasets presented in this study can be found in online repositories. The names of the repository/repositories and accession number(s) can be found below: https://www.ncbi.nlm.nih.gov/geo/, GSE190949.

ETHICS STATEMENT

The animal study was reviewed and approved by the Institutional Animal Care and Utilization Committee of the Fudan University Pudong Medical Center.

AUTHOR CONTRIBUTIONS

PZ, ZZ and MY contributed to the conception and design of the work. YL, YW, ZQ and ML contributed to the acquisition, analysis, and interpretation of data for the work. YL drafted the manuscript. PZ and ZQ revised the manuscript critically.

FUNDING

This study was funded by the Pudong New Area Clinical Plateau Discipline Project (PWYgy2021-03), National Natural Science Foundation of China (Grant No. 82070580), Natural Science Foundation of Shanghai (Grant No. 18ZR1434000), Shanghai Pudong Key Medical Discipline Construction Project (Grant No. PWZxk2017-16), and Science and Technology Development Fund of Shanghai Pudong New Area (Grant No. PKJ2018-Y33).

ACKNOWLEDGMENTS

The authors thank Wen Wu and Xiong Zhang from the Fudan University Pudong Medical Center and Michelle Hsueer Zhang from the University of California at Los Angeles for assistance with experiment execution.

SUPPLEMENTARY MATERIAL

The Supplementary Material for this article can be found online at: https://www.frontiersin.org/articles/10.3389/fphys.2022.836918/full#supplementary-material

REFERENCES

Adams, S. H. (2011). Emerging Perspectives on Essential Amino Acid Metabolism in Obesity and the Insulin-Resistant State. *Adv. Nutr.* 2, 445–456. doi:10.3945/an.111.000737

Aron-Wisnewsky, J., and Clement, K. (2014). The Effects of Gastrointestinal Surgery on Gut Microbiota: Potential Contribution to Improved Insulin Sensitivity. *Curr. Atheroscler. Rep.* 16, 454. doi:10.1007/s11883-014-0454-9

Carlsson, L. M. S., Peltonen, M., Ahlin, S., Anveden, Å., Bouchard, C., Carlsson, B., et al. (2012). Bariatric Surgery and Prevention of Type 2 Diabetes in Swedish Obese Subjects. *N. Engl. J. Med.* 367, 695–704. doi:10.1056/NEJMoa1112082

Chang, S.-H., Stoll, C. R. T., Song, J., Varela, J. E., Eagon, C. J., and Colditz, G. A. (2014). The Effectiveness and Risks of Bariatric Surgery: an Updated Systematic Review and Meta-Analysis, 2003-2012. *JAMA Surg.* 149, 275–287. doi:10.1001/jamasurg.2013.3654

Das, S. K., Roberts, S. B., McCrory, M. A., Hsu, L. G., Shikora, S. A., Kehayias, J. J., et al. (2003). Long-Term Changes in Energy Expenditure and Body Composition after Massive Weight Loss Induced by Gastric Bypass Surgery. *Am. J. Clin. Nutr.* 78, 22–30. doi:10.1093/ajcn/78.1.22

Gerszten, R. E., and Wang, T. J. (2011). Two Roads Diverge: Weight Loss Interventions and Circulating Amino Acids. *Sci. Transl. Med.* 3, 80ps15. doi:10.1126/scitranslmed.3002377

Kimball, S. R. (2007). The Role of Nutrition in Stimulating Muscle Protein Accretion at the Molecular Level. *Biochem. Soc. Trans.* 35, 1298–1301. doi:10.1042/bst0351298

Kwok, Z. H., and Tay, Y. (2017). Long Noncoding RNAs: Lincs between Human Health and Disease. *Biochem. Soc. Trans.* 45, 805–812. doi:10.1042/bst20160376

Lai, M., Chandrasekera, P. C., and Barnard, N. D. (2014). You Are what You Eat, or Are You? The Challenges of Translating High-Fat-Fed Rodents to Human Obesity and Diabetes. *Nutr. Diabetes* 4, e135. doi:10.1038/nutd.2014.30

Liang, Y., Yu, B., Wang, Y., Qiao, Z., Cao, T., and Zhang, P. (2017). Duodenal Long Noncoding RNAs Are Associated with Glycemic Control after Bariatric Surgery in High-Fat Diet-Induced Diabetic Mice. *Surg. Obes. Relat. Dis.* 13, 1212–1226. doi:10.1016/j.soard.2017.02.010

Liang, Y., Yu, B., Wang, Y., Qiao, Z., Cao, T., and Zhang, P. (2018). Jejunal Long Noncoding RNAs Are Associated with Glycemic Control via Gut-Brain Axis after Bariatric Surgery in Diabetic Mice. *Surg. Obes. Relat. Dis.* 14, 821–832. doi:10.1016/j.soard.2018.03.006

Liu, R., Hong, J., Xu, X., Feng, Q., Zhang, D., Gu, Y., et al. (2017). Gut Microbiome and Serum Metabolome Alterations in Obesity and after Weight-Loss Intervention. *Nat. Med.* 23, 859–868. doi:10.1038/nm.4358

Lynch, C. J., and Adams, S. H. (2014). Branched-Chain Amino Acids in Metabolic Signalling and Insulin Resistance. *Nat. Rev. Endocrinol.* 10, 723–736. doi:10.1038/nrendo.2014.171

Magkos, F., Bradley, D., Schweitzer, G. G., Finck, B. N., Eagon, J. C., Ilkayeva, O., et al. (2013). Effect of Roux-En-Y Gastric Bypass and Laparoscopic Adjustable Gastric Banding on Branched-Chain Amino Acid Metabolism. *Diabetes* 62, 2757–2761. doi:10.2337/db13-0185

Matsumoto, Y., Mochizuki, W., Akiyama, S., Matsumoto, T., Nozaki, K., Watanabe, M., et al. (2017). Distinct Intestinal Adaptation for Vitamin B12 and Bile Acid Absorption Revealed in a New Mouse Model of Massive Ileocecal Resection. *Biol. Open* 6, 1364–1374. doi:10.1242/bio.024927

Mercer, T. R., and Mattick, J. S. (2013). Structure and Function of Long Noncoding RNAs in Epigenetic Regulation. *Nat. Struct. Mol. Biol.* 20, 300–307. doi:10.1038/nsmb.2480

Mingrone, G., Panunzi, S., De Gaetano, A., Guidone, C., Iaconelli, A., Leccesi, L., et al. (2012). Bariatric Surgery Versus Conventional Medical Therapy for Type 2 Diabetes. *N. Engl. J. Med.* 366, 1577–1585. doi:10.1056/NEJMoa1200111

Mintziori, G., Nigdelis, M. P., Mathew, H., Mousiolis, A., Goulis, D. G., and Mantzoros, C. S. (2020). The Effect of Excess Body Fat on Female and Male Reproduction. *Metabolism* 107, 154193. doi:10.1016/j.metabol.2020.154193

Newsholme, P., Brennan, L., Rubi, B., and Maechler, P. (2005). New Insights into Amino Acid Metabolism, β-Cell Function and Diabetes. *Clin. Sci. (Lond).* 108, 185–194. doi:10.1042/cs20040290

Ogurtsova, K., da Rocha Fernandes, J. D., Huang, Y., Linnenkamp, U., Guariguata, L., Cho, N. H., et al. (2017). IDF Diabetes Atlas: Global Estimates for the Prevalence of Diabetes for 2015 and 2040. *Diabetes Res. Clin. Pract.* 128, 40–50. doi:10.1016/j.diabres.2017.03.024

Pareek, M., Schauer, P. R., Kaplan, L. M., Leiter, L. A., Rubino, F., and Bhatt, D. L. (2018). Metabolic Surgery: Weight Loss, Diabetes, and beyond. *J. Am. Coll. Cardiol.* 71, 670–687. doi:10.1016/j.jacc.2017.12.014

Reddy, M. A., Chen, Z., Park, J. T., Wang, M., Lanting, L., Zhang, Q., et al. (2014). Regulation of Inflammatory Phenotype in Macrophages by a Diabetes-Induced Long Noncoding RNA. *Diabetes* 63, 4249–4261. doi:10.2337/db14-0298

Sjöström, L., Narbro, K., Sjöström, C. D., Karason, K., Larsson, B., Wedel, H., et al. (2007). Effects of Bariatric Surgery on Mortality in Swedish Obese Subjects. *N. Engl. J. Med.* 357, 741–752. doi:10.1056/NEJMoa066254

Sjöström, L., Peltonen, M., Jacobson, P., Sjöström, C. D., Karason, K., Wedel, H., et al. (2012). Bariatric Surgery and Long-Term Cardiovascular Events. *Jama* 307, 56–65. doi:10.1001/jama.2011.1914

Wahlström, A., Sayin, S. I., Marschall, H.-U., and Bäckhed, F. (2016). Intestinal Crosstalk between Bile Acids and Microbiota and its Impact on Host Metabolism. *Cel Metab.* 24, 41–50. doi:10.1016/j.cmet.2016.05.005

Williams, B. L., Hornig, M., Buie, T., Bauman, M. L., Cho Paik, M., Wick, I., et al. (2011). Impaired Carbohydrate Digestion and Transport and Mucosal Dysbiosis in the Intestines of Children with Autism and Gastrointestinal Disturbances. *PLoS One* 6, e24585. doi:10.1371/journal.pone.0024585

Zhang, X., Yu, B., Yang, D., Qiao, Z., Cao, T., and Zhang, P. (2016). Gastric Volume Reduction Is Essential for the Remission of Type 2 Diabetes Mellitus after Bariatric Surgery in Nonobese Rats. *Surg. Obes. Relat. Dis.* 12, 1569–1576. [Epub ahead of print]. doi:10.1016/j.soard.2016.04.018

Zhu, X., Wu, Y.-B., Zhou, J., and Kang, D.-M. (2016). Upregulation of lncRNA MEG3 Promotes Hepatic Insulin Resistance via Increasing FoxO1 Expression. *Biochem. Biophysical Res. Commun.* 469, 319–325. doi:10.1016/j.bbrc.2015.11.048

Conflict of Interest: The authors declare that the research was conducted in the absence of any commercial or financial relationships that could be construed as a potential conflict of interest.

Advantages of publishing in Frontiers

OPEN ACCESS
Articles are free to read for greatest visibility and readership

FAST PUBLICATION
Around 90 days from submission to decision

HIGH QUALITY PEER-REVIEW
Rigorous, collaborative, and constructive peer-review

TRANSPARENT PEER-REVIEW
Editors and reviewers acknowledged by name on published articles

Frontiers
Avenue du Tribunal-Fédéral 34
1005 Lausanne | Switzerland

Visit us: www.frontiersin.org
Contact us: frontiersin.org/about/contact

REPRODUCIBILITY OF RESEARCH
Support open data and methods to enhance research reproducibility

DIGITAL PUBLISHING
Articles designed for optimal readership across devices

FOLLOW US
@frontiersin

IMPACT METRICS
Advanced article metrics track visibility across digital media

EXTENSIVE PROMOTION
Marketing and promotion of impactful research

LOOP RESEARCH NETWORK
Our network increases your article's readership